UNIVERSITY OF NAIROBI

CHARACTERIZATION AND APPLICATION OF NANOZEOLITIC MATERIALS AS SMART DELIVERY SYSTEMS FOR UREA FERTILIZER AND LAMBDA CYHALOTHRIN PESTICIDE

BY

GABRIEL ANDATI WASWA

I80/50037/2015

A Thesis Submitted for examination in the Fulfillment of the Requirements for Award of the Doctor of Philosophy Degree in Chemistry of the University of Nairobi

2020

DECLARATION

I declare that this Thesis is my original work and has not been submitted for the award of degree to this university or any institution of higher learning. Where other people's work or my own has been used, this has properly been acknowledged and referenced in accordance with the University of Nairobi's requirements.

Signature: …….. …….. Date:……

Gabriel Andati Waswa
I80/50037/2015
Department of Chemistry
School of Physical Sciences
University of Nairobi

The thesis has been submitted for examination with our approval as supervisors:

	Signature	Date
Dr. Immaculate N. Michira Department of Chemistry University of Nairobi P.O Box 30197-00100 Nairobi Kenya imichira@uonbi.ac.ke	……...……..	……
Dr. Deborah A. Abong'o Department of Chemistry University of Nairobi P.O Box 30197-00100 Nairobi Kenya dabongo@uonbi.ac.ke	……...……..	……
Prof. Dickson M. Andala Department of Chemistry Multimedia University of Kenya P.O BOX 15653-00503 Nairobi Kenya andalad@gmail.com	……...……..	……
Dr. Austin O. Aluoch Department of Chemical Science and Technology Technical University of Kenya P.O BOX 52428-00200 Nairobi Kenya austin.ochieng@gmail.com	……...……..	……

DEDICATION

To the Late Prof. Geoffrey N. Kamau, my senior supervisor for both MSc and PhD. Though you left us so unexpectedly, your vision and belief in me never died. You were such an exceptional human being. May the Almighty Lord forever rest your soul in eternal peace.

ACKNOWLEDGEMENT

To the University of Nairobi, College of Biological and Physical Sciences, School of Physical Sciences, Chemistry Department, I appreciated the chance offered to me to undertake my postgraduate studies, having done my undergraduate course in the same institution. I am incredibly obligated to my supervisors; Dr. Immaculate Michira (UoN), Dr. Deborah A. Abong'o (UoN), Prof. Dickson. Andala (MMU) and Dr. Austin. Aluoch (TUK) for their guidance throughout the study period. Greatly, my sincere gratitude to Prof. Andala for being understanding, congenial and empowering; his trustworthiness and dependability will forever be appreciated for helping me keep up certainty and inspiration all through this venture despite the challenges encountered. I would like to acknowledge the National Commission for Science, Technology, and Innovation (NACOSTI) and the National Research Fund (NRF) for their Endowment Funds for this Project. I might likewise want to recognize the accompanying organizations for availing instruments for various analysis: State Department of Infrastructure Material Testing and Research Division in Kenya, Mines and Geology Department in Kenya, Kenya Agricultural and Livestock Research Organization, University of Nairobi College of Biological and Physical Sciences and St. Austin's Academy Chemistry Laboratory. I would also like to recognize the following people for their special support in helping me attain the project objectives: Dr. A. K. Waswa from Department of Geology, UoN for your insights on zeolites, Mr. J. K. Mbugua PhD student from Department of Chemistry UoN for being part of my research team and hosting my field work studies, Mr. J. Njoroge from Infrastructure Material Testing and Research Division for facilitating some of our laboratory works and all other people involved in this research work that I may have not mentioned. I would also like to thank my family for their patience and support. I would not be where I am today without them having been by my side throughout the years. Finally, to God of whom I acknowledge His Lordship, I am everlastingly appreciative for His unending love, favor, and mercies over my life.

ABSTRACT

Natural zeolites could be applied as smart delivery system for controlled release of agricultural inputs resulting in enhanced productivity and reduced environmental pollution caused by excessive use of fertilizer and pesticides. This is because zeolites have nano porous voids and channels that can be loaded with quest molecules like urea fertilizer and pesticides. The formulated zeolite composites can then be applied as carrier agent for target and slow delivery of the fertilizer or pesticide to the intended part of the plants, thus improving the efficiency and effectiveness of the agricultural inputs. Besides, these zeolites being natural are meant to be more cost effective and pose less harm to the environment. This research work aimed at sampling natural zeolites from different parts in Kenya and characterizing them in comparison with the commercial zeolites applied as the standard. Kinetics studies were then conducted to determine their fertilizer and pesticide loading properties. After which formulation, modelling, and agronomic simulation studies were done using urea and lambda cyhalothrin pesticide on tomatoes and spinach. Sample collection was done, guided by Kenya's geological and mineralogical mapping in five selected places named as Eburru volcanic crater, Lake Magadi, Lake Baringo, Ebulbul-Ngong, and Kitum caves-Mt. Elgon. The collected samples transported to the laboratory were mechanically grinded and sieved to obtain homogeneous fine particles. The powdered samples were then calcined at 550 ^{o}C for 2 hours to remove some of the organic and amorphous components. The samples were then packed in airtight plastic bags labelled EB-GA-02, MG-GA-03, BG-GA-04, NG-GA-05, and EL-GA-06 respectively as per their selected sampling places. Commercial zeolites (CPZ,from Sigma Aldrich) labelled ZT-GA-01 were applied as the standard sample for the study. Sample characterization was done using X-ray diffractometer (XRD, D2 Phaser from Bruker), Energy dispersive spectrophotometer (EDS, Shimadzu EDX-720), Fourier Transform Infrared (FT-IR, Tracer 100 Shimadzu), X-ray Fluorescence spectrometer (XRF TITAN 600) and Scanning Electron microscope (SEM, Hitachi S4800). XRD patterns of the standard sample ZT-GA-01 showed that it was zeolitic A artificial, abbreviated as Linde Type A (LTA), having a chemical composition of $[Na_{96}(H_2O)_{216}][Si_{96}Al_{96}O_{384}]$, crystal data of: a = 24.61 Å, b = 24.61 Å, c = 24.61 Å, $\alpha = 90^{o}$, $\beta = 90^{o}$, $\gamma = 90^{o}$ and X-ray single refinement (Rw) = 0.04. Sample EL-GA-06 was found to be mainly Phillipsite natural zeolites deposits with some mixtures of nitrolites, though its low availability quantity limited its application. IR Spectroscopy for ZT-GA-01 and EB-GA-02 showed similar peaks between 3420 – 3480 cm^{-1}, 2350 – 2360 cm^{-1} ,1630 – 1660 cm^{-1} and 440 – 670 cm^{-1}. Besides comparable EDX characterized silica to alumina composition of sample EB-GA-02 and the artificial zeolite A applied as the standard, determined as 37.4 % to 18.8 % and 43.6 % to 56.4 % respectfully, its physical properties like porosity and morphology as determined by Scanning Electron Microscopy indicated higher zeolitic similarity, hence they were applied as the main natural zeolitic materials for nanozeolitic formulations. Physical properties of samples ZT-GA-01 and EB-GA-02 in terms of BET surface area, BJH pore volume and pore sizes were obtained as; 0.6716 m^2/g, 0.002333 cm^3/g, 151.519 Å and 0.7099 m^2/g, 0.006767 cm^3/g, 389.846 Å respectively. Urea loaded samples EB-GA-02 indicated a 39.844 % reduction in pore sizes after successful loading of urea fertilizer into the nano-spaces, while pesticide loading indicated a reduction in pore volumes and pore sizes by 19.15 % and 32.74 % respectively. The simulated release process of urea-loaded zeolitic materials and pesticide loaded zeolitic materials in water and soil indicated a sustained slow release profile. About 82.8 % of stacked urea fertilizer was discharged in water and 74.2 % loaded urea released in soil over the 18 days monitoring duration. Similarly, 34.4 % and 40.1 % lambda cyhalothrin pesticide amounts were released by pesticide loaded zeolitic sample EB-GA-02 in water and soil respectively over the 18 days monitoring duration. Application of zeolitic sample EB-GA-02 as smart delivery systems demonstrated a sustained slow release of both urea and Lambda cyhalothrin pesticide on tomato and spinach growing and monitoring experiments for the 60 days' period. For urea loaded nanozeolitic sample EB-GA-02, a higher concentration difference in the

soil of almost 17.00 % and 16.00 % was recorded between the 25^{th} and 35^{th} day for tomato and spinach respectively, while similar monitoring experiments for Lambda cyhalothrin pesticide gave higher concentration difference in the soil of almost 70.00 % and 67.00 % for tomato and spinach respectfully between the 15^{th} and 35^{th} day. In summary, this thesis work showed that the sample natural zeolites EB-GA-02 could be loaded with urea and lambda cyhalothrin pesticide molecules and then be effectively applied as carrier agent for smart delivery systems. Improved sampling approach and purification processes could enhance the quality of the formulated materials. This may result in scaled-up production of these smart delivery systems that could complement in the smart farming practices and sustainable agriculture.

TABLE OF CONTENTS

LIST OF TABLES

Appendices

LIST OF FIGURES

Appendices

LIST OF PUBLICATIONS:

i. G. A. Waswa, D. Andala, A. O. Aluoch, G. N. Kamau,I. Michira and J. K. Mbugua. Kinetics and Isothermal studies of Lambda Cyhalothrin sorption on Eburru soil in Kenya. **Journal of the Kenya Chemical Society 10-1 (2017), 24-34**

ii. Gabriel A. Waswa, Immaculate N. Michira, Debora A. Abong'o, Dickson Andala, Austin O. Aluoch. Characterization; Formulation and Application of Natural Nano Zeolitic Materials from Kenya as Smart Delivery Systems for Fertilizers and Pesticides. **International Journal of Scientific Research in Science, Engineering and Technology, 2020, 7 (3), 38-349**

iii. Waswa, G. A., I. Michira, O. Abong, J. K. Mbugua, and D. Andala. "Dissipation and Sorption of Urea on Eburru Soils in Kenya." **Journal of Physical Chemistry & Biophysics, 7, no. 271 (2018): 2161-0398.**

iv. Waswa G. A., Andala D., Aluoch A. O., Kamau G. N. and Michira I. Application of Eburru Rocks from Kenya as Urea Carrier Agents**. International Journal of Recent Advances in Multidisciplinary Research, 2017, 04(4), 2532-2541**

LIST OF ABBREVIATIONS:

AAS	-	Atomic Absorption Spectroscopy
ANOVA	-	Analysis of variance
ASAL	-	Arid and Semi-Arid land
ASS	-	Agricultural Sector Strategy
BET	-	Brunauer-Emmett-Teller
CAADFP	-	Comprehensive Africa Agricultural Development Program
CAFO	-	Concentrated Animal Feed Operation
CEC	-	Cations Exchange Capacity
DDT	-	Dichlorodiphenyltrichloroethane
EDS	-	Energy Dispersive X-ray Spectroscopy
FAO	-	Food and Agricultural Organization
FT-IR	-	Fourier-Transform Infrared Spectroscopy
GDP	-	Gross Domestic Product
GoK	-	Government of Kenya
HPLC	-	High Performance Liquid Chromatography
IZA	-	International Zeolite Association
KALRO	-	Kenya Agricultural and Livestock Research Organization
MDG	-	Millennium Development Goals
MS	-	Mass Spectroscopy
MTIP	-	Medium Term Investment Plan

NHL	-	Non-Hodgkin’s Lymhoma
NMR	-	Nuclear Magnetic Resonance
NNI	-	National Nanotechnology Initiative
NSDS	-	Nanozeolitic Smart Delivery Systems
pH	-	Potential of Hydrogen
PRSP	-	Poverty Reduction Strategy Paper
PSA	-	Particle Size Analyzer
RS	-	Raman Spectroscopy
SBU	-	Secondary Building Units
SDS	-	Smart Delivery Systems
SEM	-	Scanning Electron Microscopy
SOM	-	Soil Organic Matter
SPM	-	Scanning Probe Microscopy
TEM	-	Transmission Electron Microscopy
USEPA	-	United State Environmental Protection Agency
USGS	-	US Geological Survey
UV	-	Ultraviolet Visible Spectroscopy
WFP	-	World Food Program
WHO	-	World Health Organization
XRD	-	X-ray Diffraction

CHAPTER 1: INTRODUCTION

1.1: Background

Most developing countries, like Kenya and other countries in Sub-Saharan Africa, have almost 60 % of their GDP anchored on agriculture (Brock *et al*., 2011). As the population of such countries increase, coupled with other factors that affect the agricultural sector such as climate change, diminishing arable land and depleting water sources; subsistence agricultural practices are insufficiently meeting the expected increase in productivity. To enhance productivity for many decades, uses of fertilizer and pesticides have been applied in the agricultural sector as a measure for sustainable livelihood.

Current agricultural practices put strain both on environment and aquatic ecosystem through increased pollution from fertilizers and pesticides used to enhance food productivity. Aspects such as imbalanced fertilization, decreasing soil organic matter, increasing environmental pollution through processes that includes leaching, eutrophication and bioaccumulation, have an impact on the type and amount of fertilizer and pesticides introduced to the environment. These are factors that could hamper the intended increased productivity in the long run. Besides, a number of researchers (Shaviv, 2000; Chinnamuthu and Boopathi, 2009), have indicated that averagely only 35 % for nitrogen and 20 % for phosphorous fertilizers are actually utilized efficiently by plants. This raised concerns, because it seemed that a significant percentage of fertilizer applied was actually not utilized by plants, meaning that an increase in fertilizer loading applied does not translate to higher yields. Furthermore, increased fertilizer loading is also associated with increased pollution as more chemicals are released to the environment.

Having looked at all these decade-long challenges, the greatest concerns would be on exploring modern approaches to agriproduction, with a keen focus on environmental conservation alongside improved productivity. To mitigate these dynamics, modern practices are being adopted, many of which integrate the latest line of technological innovations such as nanotechnology inventions in agriproduction. Naderi *et al*., (2013) argued that the development of the agricultural sector could be realized more through the compelling utilization of current advances which roots least harm to the production bed and as well lead to reduced environmental pollution. By applying nanotechnology, there will be a great focus on nanostructured formulations of fertilizer and pesticides. These utilize new mechanisms that focuses on target delivery and regulated discharge, through carrier agents such as zeolitic materials (materials which contain some percentage of zeolites or having zeolite like properties) that could serve as one of the approaches of increased nutrients use efficiency, reduced soil toxicity and environmental pollution. It is the unique properties of these zeolitic materials, whether natural or synthetic, that enhances their applicability in nanoformulations. Usually, they contain crystalline aluminosilicates (Manikandan and Subramanian, 2013) with a series of microporous, mesoporous and nanoporous structures. Ions or molecules can be immobilized within these pores for example by ion exchange and chemisorption mechanisms. This could be a way of loading or encapsulating fertilizer or pesticides to be delivered to plants, while acting as slow/ controlled release process (Chinnamuthu and Boopathi, 2009).

In addition, the porosity of zeolites enables them to be applied in many other areas such as nanoparticle filters for detoxification or remediation of harmful pollutants (Karn *et al*., 2009; Gilman, 2006), as well as activated catalytic features. When applied as nanoparticle filters for water purification, they serve as low cost alternative material sorbents for ion exchange on heavy metal ions like Pb^{2+}, Cu^{2+}, Fe^{3+} and Cr^{3+}, commonly found in industrial water discharges and which tend to accumulate in organisms (Inglezakis *et al*., 2002 and 2003; Lin *et al*., 2002). This

is in comparison to processes such as precipitation, reverse osmosis, phytoextraction, electrodialysis and ultrafiltration (Geselbarcht, 1996; Schnoor, 1997; Senguptal *et al*., 1980) that could be used to mitigate heavy metal ions contamination, may not be very cost-effective. Besides, zeolites can act as potential sorbents for organic pollutants like pesticides introduced purposefully through agriproduction or accidentally by spillage or their disposal. Hence, they may contribute in remediating the environment by decreasing contamination and persistence of these compound's active ingredients or their metabolites.

Evidently, Substantial level of research has been commenced on different zeolites, to characterize their surface, chemical and ion-exchange properties, particularly with interest on their application as adsorbents and water purifiers (Hafez *et al*., 1978; Galli *et al*., 1983; Mondela *et al*., 1995; Semmens *et al*., 1976; Zamzow *et al*., 1969; Joshi *et al*., 1983; Blanchard *et al*., 1984; Bailey *et al*., 1999; Truong et al., 2007).

1.1.1: The fate of Organic pollutants in the soil

Once introduced into the environment, organic compounds like pesticides could undergo a number of processes, besides performing their intended purpose of application. These compounds can undergo degradation (either biotically or abiotically) while others could volatize or leach, yet some could be adsorbed on soil organic matter or still undergo bioaccumulation (Semple *et al*., 2003; Schwarzenbach *et al*., 1993). Numerous dynamics affect the fate of these organic pollutants once they are introduced into the environment. This includes their individual properties like molecular structures, polarity, solubility, and hydrophobicity. Others include environmental aspects like weather and climate or other factors like biological diversity, nature of soil minerals and organic matter content (Semple *et al*., 2003; Reid *et al*., 2000; Doick *et al*., 2005). Depending on the type of organic pollutant introduced into the environment, their pollution effects and levels of toxicities would vary. However, it's due to these reasons that concerns are raised, particularly

when its known that toxic effects, either acute or chronic as shown by the dosage levels (Helfrich *et al*., 1996), could result in varied medical and health problems to both humans and animals. These may include neurobehavioral disorder, carcinogenicity, and disruption of biological processes like the immune, reproductive, and endocrine systems (Helfrich *et al*., 1996).

1.1.2: Environmental impact of agrochemicals

Although fertilizer and pesticides are vital inputs to increased agri-production and food security, their intensive and extensive application and introduction to the environment components like soil, water and air could result in pollution effects as discussed below.

1.1.2.1: Fertilizer

In Kenya and generally Sub-Saharan Africa, utilization rates of fertilizers vary with regions and crops cultivated. For example, it is estimated that of the 70 % Kenya's cultivated land by subsistence farmers, maize plantation consumes 40 % of the applied fertilizer (Ariga *et al.*, 2008). Comparatively, cereals (which includes sorghum, maize, wheat, rice and millet) accounts for 75 %, tea accounts for 13 %, while 16 % is for coffee (Ariga *et al.*, 2008).

With reference to the subject of discussion, one would want to explore the environmental impact of excessive fertilizer application. Most fertilizers contain nitrogen or nitrates, which makes them very soluble in water. This poses a higher likelihood of polluting water sources and bodies, either through surface run-off, leaching, percolation, or infiltration. The extent of ground water contamination arising from fertilizer usage has been a common phenomenon in many regions (Oenema *et al.*, 1998; Agrawal *et al*., 1999), which poses to be a serious problem since it can be hardly reversed (Van Lanen and Dijksma, 1999). For example, even in the US where there has been a tremendous increase in the amount of fertilizer consumed, about 15 % of their ground

water is estimated to have exceeded the 10 ppm World Health Organization supreme standard for benign drinking water (Mallin, 2000; Howarth *et al*., 2002).

Among the various potential negative impacts of expanded nitrate levels in ground water incorporates; conceptive issues (Kramer et al., 1996), Methemoglobinemia and malignant growth (Gupta et al., 2000; Van Mannen et al., 2001; Weyer et al., 2001) and high dangers for Non-Hodgkin's Lymhoma (NHL) (Ward *et al*., 1996). Besides ground water pollution, eutrophication of water sources has and remains one of the greatest challenges when it comes to excessive use of fertilizer as documented by various studies (Howorth, 1988; NRC, 1993; Nixon *et al*., 1996; Nixon, 1995; Justic *et al.*, 1995; Boynton *et al.*, 1982; Howarth, 1995; D'Elia *et al*., 1986). Eutrophication in tropical lagoons could be attributed to a higher concentration of phosphorous adsorbed on carbonaceous sand, while Nitrogen is the major cause for temperate estuaries (Howarth *et al*., 1995). Among the substantial effects of eutrophication to the ecosystem includes lack or reduction of oxygen in estuaries and coastal seas (NRC, 1993), which could result in significant loses in fish and other marine life (Lein and Ivanov 1992; Larsson *et al*., 1985; Officer *et al*., 1984; Baden *et al*., 1990; Hansson and Rudstan, 1990; Parker and O'Reilly, 1991). In addition, there could be interference in aquatic organisms (Howarth, 1991), within the sub-tidal beds of macro-algae and in the corals (NRC, 1993). Increase in algal bloom in creeks and shorelines (Smayda, 1989), which could be lethal to fish and other marine life such as dinoflagellates (Burkholder *et al*., 1992; Anderson, 1989) and of brown-tide organisms (Cosper *et al*., 1987) is also of concern.

Lastly, without necessarily exhausting all the environmental impacts of excessive use of fertilizer, researchers have linked increased emission, transportation, deposition and reaction of nitrogen trace gases such as ammonia, NH_3 and nitrous oxide, NO to increased fixation and mobilization of nitrogen. This could be through atmospheric emission of NO generated during combustion of

fossil fuels, agrarian preparation that builds the centralization of unstable NH_3, as well as spray drifts (Schlesinger and Hartley, 1992; Eichner, 1990). These gases are vastly reactive in the atmosphere; like nitric oxide would affect the concentration of hydroxyl radicals (Logan, 1985) and could add to photochemical reaction (Chameides *et al*., 1994; Jacob and Wefsy, 1990; William *et al*., 1992; Reich and Amundson, 1985). On the other hand, ammonia acts as an acid neutralizing agent, influencing the pH of rainfall and cloud water, of which it's increased emission could lead to increased concentration of nitrogen in soil and waters (Schlesinger and Hartley, 1992; Denmead, 1990; Fenn and Hossner, 1985).

In this study, urea, $(NH_2)_2CO$, was chosen as a fertilizer sample applied because of its essential component as a nitrogenous fertilizer, and its high solubility. Also, it's among the most depended upon fertilizer for horticultural production of two crops of interest namely tomatoes and spinach. Essentially, urea organic compounds, also called carbamide, is applied as a nitrogenous fertilizer and for industrial use as analytical reagents and binders (IRPTC data profile). According to Friedrich (1828) and Meessen (2005), urea was first manufactured from ammonia and carbon dioxide and 90% of subsequent industrial production went to agricultural use. In living organisms' oxidation of amino acids or ammonia in the urea cycle forms urea (Sakami, 1963). Urea is customarily an odorless, colorless, and greatly soluble crystalline organic compound. Table 1.1 (IRPTC data profile) below summarizes some of the properties of urea. Urea hydrolyses when reacting with water in soil to form ammonium ions that discharges ammonia as illustrated below:

$$(NH_2)_2CO_{(aq)} + 2H_2O_{(l)} \rightarrow (NH_4)_2CO_{3\,(aq)} \; \ldots \ldots \text{(Equation 1.1)}$$

$$(NH_4)_2CO_{3(aq)} + 2H^+_{(aq)} \rightarrow 2NH_4^+{}_{(aq)} + CO_{2(g)} + H_2O_{(l)} \ldots \text{(Equation 1.2)}$$

$$NH_4^+{}_{(aq)} + OH^-_{(aq)} \rightarrow NH_{3(aq)} + H_2O_{(l)} \; \ldots \ldots \text{(Equation 1.3)}$$

The proportion of ammonia loss in this process is favored by great temperature, high pH and low soil cation exchange capacity. Thermolysis studies on urea indicate its initial vaporization occurring at around 133 ˚C to 250 °C, followed by decomposition as shown by the equation below:

$$(NH_2)_2CO \rightarrow NH_3 + HNCO \text{ ……..……..(Equation 1.4)}$$

Much higher temperatures could cause production of biuret, isocyanic acid or formation of ammelide or melanine (Koebel et al., 2000; Schaber et al., 2004).

The HNCO formed could still decompose further in presence of water as shown below (Martyn, 2006).

$$HNCO + H_2O \rightarrow CO_2 + NH_3\text{……...…..(Equation 1.5)}$$

The volatilization procedure for ammonia is favored by high pH, high temperature and low CEC value of soil (Clain *et al.*, 2013).

Table 1.1 Summary of some selected properties of urea

Properties	Description
Molecular Formula	CH_4N_2O
Molecular Weight	60.06
Melting Point	133 ^{O}C
Boiling Point	135 ^{O}C decomposition
State	Crystal prismatic or powder
Density	1323 kg/m3 at 20-24 ^{O}C
Vapour Pressure	80 Pa (0.6 mmHg) at 20C CAL
Octanol/Water Partition: Coefficient	log Pow =-1.59 at 20-25 ^{O}C experimental
Water Solubility	1080 g/L at 20 ^{O}C
Solubility in other Solvents	10 g/L in 95% alcohol, 167 g/L in methanol, 500 g/L in glycerol
Colour	Colourless to white
Additives	Urea-formaldehyde binder can be used in some prilling processes.
Impurities	Biuret 0.3 - 2 wt%; cyanates. Analysis of technical urea gave the followings: water (as moisture) 0.4 wt%; free ammonia 0.4 wt%; Fe 2+ <0.0002 wt%; ash content < 0.02 wt%. Degree of purity 98-99 wt%.

1.1.2.2: Pesticides

As already highlighted, the varied range of pesticides can be classified depending on their functions and properties. Normally, the primary role of pesticide use in agriculture is to improve productivity through pest control. However, the sustained use of pesticide has been known to cause environmental pollution directly or indirectly.

Many researchers have shown that consumption of pesticides directly affects people, posing potential risk on people's health (Abong'o *et al.,* 2014, Forget 1993, Jeyaratham 1981, Igbedioh 1991). Among the categories of high-risk exposure include production workers, formulators, mixers, sprayers, farm workers and product consumers for retained pesticide molecules. Some effects such as reproduction abnormalities, cancer, disruption of hormone and immune suppression on human health have been associated with endocrine disruption chemicals which mimic or antagonize natural hormone systems in the body (Hurley *et al*., 1998, Brouwer *et al*., 1999, Crisp *et al*., 1998). For example, Frumkin (2003) noted that almost 3 million Americans serving in the Vietnam War, dubbed "Operation Ranch Hand", from 1962 to 1971, were exposed to defoliant mixtures which included Agent Orange. It's argued that the military squirted nearly 19 million gallons of herbicide blends of Phenoxy herbicide 2,4,5-dichlorophenoxyacetic acid (2,4-D) and 2,4,5-trichlorophenoxyacetic acid (2,4,5-T) on roughly 3.6 million acres of Vietnamese land to create their base by removing forest cover, clear vegetation and destroy crop. Consequently, there was evidence of cancer risks among some militants, workers, and Vietnamese population.

Due to pesticide contamination in food stuffs, many countries carry out monitoring of pesticide residues in import and export products to control their dietary intake, ensuring that each product meets the minimum requirement limit. For example, since 1996, the European Commission (2001) started a program called "Monitoring of pesticide residues in Products of plant origin in the European Union", since which an analysis of averagely 9,700 samples has been done for groups like benomyl and maneb in products like fruits and horticulture. Results show that 5.2 %

of the trials contained deposits, out of which 0.31% exceeded the minimum requirement levels, the highest being 118 mg/Kg of mancozeb residue in lettuce. 6,000 samples were analyzed in 1997 for 13 pesticides (DDT, chloropyrihos, diazimon, acephate, carbendazin, endosulfan, chlorothalonil, methamidophos, metalaxy, iprodione, thiabendazole, triazophos and methidathion) in five commodities (beans, potatoes, pears, mandarins and apples) of which pesticide residues were found in 34% of them at or below the minimum requirement levels, while about 1 % exceeded (European Commission, 1998).

Pesticide poisoning and resulting death is also another cause of worry. In 2000 alone, for example, it is estimated that in Asia and West Pacific, over half a million people died from self-harm linked to pesticides (WHO, 2001), while among the Sri Lankan's and young Chinese women, the commonest cause of death is suicide involving pesticides (Murray and Lopez, 1996; WHO, 2001; Sri Lankan Ministry of Health, 1995).

With environmental focus, several studies have been done to determine the extent of environmental contamination and pollution associated with pesticides. The US Geological Survey (USGS) carried out a major survey on main river basins transversely the U.S that revealed that more than 90 % of water and fish tests from just all streams contained a couple of pesticides (Kole et al., 2001; Bortleson and Davis, 1987-1995), of which 2,4-D was the most frequently detected, while diazinon insecticide, dichlobenil, diuron, glyphosate and triclopyr weed-killers were mostly detected in Puget Sound basin streams. Besides surface water, ground water contamination has also been on the widespread. Waskom (1994) noted that almost 43 states had pesticides detected, to a range of at least 143 diverse pesticides and almost 21 metabolites. 58 % of consumption water samples from Bhopal India had organ chlorine pesticides contamination above EPA standards. The challenge with ground water contamination is that it may take decades for the contaminant

to dissipate or clean up, besides the process being intricate and very exorbitant (Waskom, 1994; US EPA, 2001; O'Neil, 1998).

The extend of soil contamination by pesticides is still a wide topic of research, particularly when one puts in mind the spread, distribution channels, applications, sources, as well as origin. Not many of all pesticides have been documented with regard to soil pollution, though as concern grows, a number of researchers have explored this area (Robern and Hutson, 1999; Barcelo' and Hennion, 1997; Roberts, 1998). When dealing with soil contamination, pesticides and their transformational products could be classified into hydrophobic, persistent, bioaccumulative and polar species.

Half-life in soil (DT_{50}), soil-sorption constant (K_{oc}), water solubility and octanol/water partition coefficient (K_{ow}) are among factors that define persistency and movement of pesticides and their transformational products in the soil. Once introduced, these pesticides could follow several metabolic pathways like ring cleavage, hydrolysis and methylation to produce their transformational products and residues which could be retained in the soil at different extends depending on among factors like soil organic matter content, as will be discussed later (Andreu and Pico', 2004).

At this point, it is also imperative to note that substantial management of soil with pesticides could also affect the soil advantageous micro-organisms, like; trichloropyr constrains soil bacteria that transmute ammonia into nitrates (Pell *et al*., 1998), the development and action of nitrogen fixing microscopic organisms in the soil is abridged by glyphosates (Santos and Flores, 1995) and bacteria nitrogen fixation on roots of bean plants is reduced by 2,4-D (Fabra *et al*., 1997; Arias and Fabra, 1993). Progression and action of nitrogen fixing blue-green algae as well as the conversion of nitrates from ammonia by soil bacteria are reduced and inhibited by 2,4-D respectively (Martens and Bremmer, 1993; Singh and Singh, 1989; Frankenberger et al., 1991 Tozum-Calgan and Sivaci-Guner, 1993;).

Lastly, one would likewise need to investigate the effect of pesticides on non-target living beings, vegetation and environmental components like air and soil, which mainly arises due to drifting and volatilization during and dependent on the conditions of application. Almost about 25 % of applied pesticides undergoes drift spreading, while nearly 90 % undergo volatilization (Majewski, 1995), of which could be detected in the atmosphere, rain, fog or even snow (Savonen, 1997; U.S Geological Survey, 1999). For example, samples from Arctic environment like air and water have shown a positive test for pesticides like: dacthal, chloropyrifos, chlorothalonil, metaclor, trifluralin and terbufos (Garbarino *et al*., 2002; Rice and Cherniak, 1997).

Cases of toxicity on aquatic animals have also been reported. These includes chloropyrifos on fish in urban streams (U.S EPA, 2000; U.S Geological Survey, 1999), as well as trifluralin and weed killers (Ronstar and Round up) (U.S EPA, 1996; Koyama, 1996; Shafiei and Costa, 1990; Folmar et al., 1979). Poisoning cases of animals like dolphins have also been recorded widely, mostly contributed due to their great tropic level in the nutrition chain, comparatively lower undertakings of drug metabolizing enzymes, their habitats including riverine and estuaries that could pose proximal point of source pollution (Reeves *et al*., 1991; Tanabe *et al*., 1988; Perrin *et al*., 1989; Reeves and Chaudhry, 1998). Hostile effects on reproduction and immunological functions have been shown to occur in fish and other marine or fresh water animals and mammals arising from contact with more amounts of persistent, bio-accumulative and toxic contaminants like 1,1,1-trichloro-2,2-bis[p-chlorophenyl] ethane (DDT) and PCBs (Helle *et al*., 1976; Reijnders, 1986; Ross et all., 1995, Kannan *et al*., 1993 Martineau *et al*., 1987; Colborn and Smolen, 1996).

Lastly, a few studies on bats have related their decline in population to pesticides like p, p'-dichlorophenyldichloroethene (P, P'-DDE), oxychlordanes (OCs), PCBs (Altenbach *et al*., 1979; Clark, 1976, 1981, 1983; Thie and McBee, 1994; Becker, 1989; Cade *et al*., 1989; Bernardz *et al*., 1990; Castillo *et al*., 1994; Mora, 1996, 1997; Senthilkumar *et al*., 2000; Jefferies, 1976; Geluso *et al*., 1976).

The pesticide chosen for this study was Lambda-cyhalothrin, which is an active ingredient in common commercial pesticide brands applied in horticulture practice, even in Kenya. Lambda-cyhalothrin is a pyrethroid pesticide active constituent found in numerous trademark label products like scimitar, warrior, matador, and icon, applied in agriculture to aphids, pests, as well as in community well-being to control mosquitoes, cockroaches, flies and ticks. In Kenya, some of the common market brands registered by the Pest Control and Product Board (PCPB, 2010) include Duduthrin 1.7EC, PCPB(CR)0486 manufactured by Syngenta UK Ltd and distributed by Twiga Chemicals Industries. Duduthrin is applied as emulsified concentrate and acts as a contact pesticide for control of diamond black and aphids in cabbages, kales, and other horticultural crops. The other common brand is Karate, PCPB(CR)0297, distributed by Syngenta E. A Ltd. Karate is applied as water dispersible granules for control of aphid, thrips, caterpillar, and whiteflies on vegetables.

This compound, was initial recounted by Robson and Crosby (1984), is synthesized from pyrethrum chrysanthemum flowers and photostabilized by substitution reactions (Spurlock, 2006; Syngenta, 2007).

The structure of Lambda-cyhalothrin (Figure 1.1 and Figure 1.2) is a 1:1 combination of two isomers: (*S*)-α-cyano-3-phenoxybenzyl-(*Z*)-(1*R*,3*R*)-3-(2-chloro-3,3,3-trifluoroprop-1-enyl)-2,2-dimethylcyclopropanecarboxylate and (*R*)-α-cyano-3-phenoxybenzyl-(*Z*) -(1*S*,3*S*)- 3-(2-chloro-3, 3,3-trifluoroprop-1-enyl)-2,2-dimethylcyclopropanecarboxylate respectively (Li-Ming *et al.*, 2008).

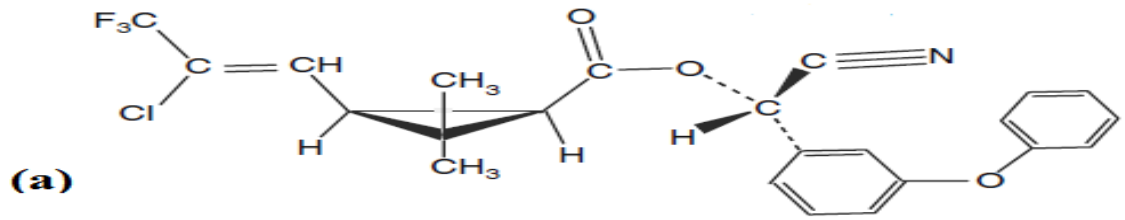

Figure 1. 1 Structures of Lambda-cyhalothrin; (a) (S)-alcohol (Z)-(1R)-cis-acid

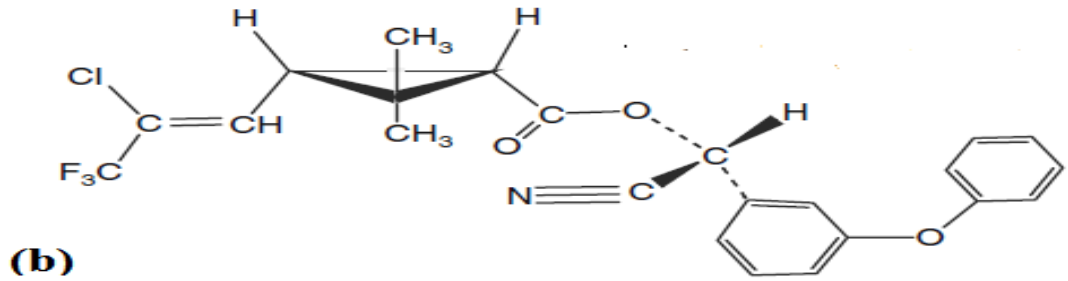

Figure 1. 2 Structures of Lambda-cyhalothrin; (b) (R) - alcohol (Z) - (1S) - cis – acid

Li-Ming *et al*., (2008) gave some summary properties of Lambda-cyhalothrin (Table 1.2). It's low Henry's law constant and vapor pressure shows that it has a very low volatility. The high Kow (octanol-water partition coefficient) indicates greater lipid partitions. The high Koc (mean water-soil organic carbon partition coefficient) suggest more attraction to soil organic matter and higher adsorption rates to particles (sediments). These are aspect that may reduce its degradation rate due to unavailability to micro-organisms and sunlight when introduced in streams and rivers; but also may form the mechanisms of sediment sorption removal and mitigation of toxicity in water. Lambda-cyhalothrin is a nonsystemic pesticide, that has a brisk wreck and repellant impact through contact, stomach action and consequently halting vermin harm in crops. The compound acts as a pesticide by complexing to a protein that normalizes the voltage-gated sodium passage of the nervous system, preventing them from normal closing causing uncontrolled nerve

stimulation and tremors that paralyze and kills (Shafer and Meyer, 2004; Burr and Ray, 2004; Bradbury and Coats, 1989).

Fernandez-Alvarez *et al*., (2007) proposed that Lambda-cyhalothrin photodegradation observed the first-order kinetics with an ostensible first-order rate constant (Kap) of 0.163 min^{-1} and half-life ($t_{1/2}$) of 4.26 min, with pathways identified as reductive dehalogenation, decarboxylation and ester bond cleavages. Gupta *et al*., (1998) proposed the hydrolysis of Lambda-cyhalothrin under basic conditions. Wang *et al*., (1997) studied the dissipation of Lambda-cyhalothrin (European Commission, 2001).

In soil and sediment, Lambda-cyhalothrin undergoes strong adsorption due to its high Koc value. Freundlich isotherm has mostly been applied in this data analysis, where sorption rates dependent soil type and as well as contact time (Ali and Baugh, 2003; Oudou and Hansen, 2002; Zhou *et al*., 1995; Bandareko *et al*., 2006; Wang *et al*., 1997). In water, Lambda-cyhalothrin also dissipates (Farmer *et al*., 1995; Roessink *et al*., 2005; Hadfield *et al*., 1993).

Ecotoxicity studies of Lambda-cyhalothrin reveals it's slight to high toxicity levels to terrestrial and aquatic animals, while for fish, the LC_{50} (96 hrs) is 210 ng/L for blue gill sunfish and 0.8 ng/L for sheep head minnow (Roessink et al., 2005; USDA, 2007; USEPA, 2007). Weston et al., (2004) studied Lambda-cyhalothrin sediment toxicity, with the median lethal concentration LC_{50} residue being 0.45 µg/g which corresponds to 1.4 ng/L for pore water concentration (Amweg *et al.*, 2006). Hence, there is need to mitigate the ecological contamination allied with the wide range consumption of this pesticide.

In conclusion, this research focused on exploring availability of natural zeolites deposits in Kenya, characterization and utilization of these zeolitic nanoporous materials for controlled release of urea fertilizer and lambda cyhalothrin pesticide as carrier agents for target delivery or slow/controlled release on spinach and tomato vegetable production with the intention of enhanced productivity alongside reduced ecological contamination.

Table 1.2 Physicochemical properties of Lambda-cyhalothrin

Properties	Description
Molecular formula	$C_{23}H_{19}ClF_3NO_3$
Molecular weight (g/mol)	449.9
Density (g/mL at 25°C)	1.33
Melting point (°C)	49.2
Boiling point (°C at 0.2 mmHg)	187–190
Water solubility (mg/L at 20°C)	0.005
Octanol–water partitioning (log *K*ow at 20°C)	7.00
Hydrolysis half-life (d): pH 5 pH 7 pH 9	 Stable Stable 8.66
Photolysis half-life (d): Water at pH 5 and 25°C Soil	 24.5 53.7
Bioconcentration factor (BCF) (fish)	2,240
Soil adsorption *K*oc (cm3/g)	247,000–330,000
Soil degradation half-life (d) Aerobic soil	 42.6
Aquatic degradation half-life (d) aerobic aquatic 21.9	 21.9
State at room temperature	solid
Colour: Solid solution	 Colourless yellow
CAS number	91465-08-6
US EPA PC Code	128897

1.2: Statement of the problem

Increasing reliance on fertilizer and pesticide as agriproduction inputs to improve yield is significantly contributing to increased environmental pollution through aspects like eutrophication and accumulation of pesticide active ingredients or their metabolites. Despite extensive research in the medical field novel and target delivery systems to improve efficiency and effectiveness in administering medicine, minimum focus has been given to novel or smart/target delivery system based on nanotechnology that can increase efficiency and effectiveness in application of agriproduction inputs like fertilizer and pesticides, which would in turn improve productivity and minimize environmental pollution.

1.3: Objectives

1.3.1: Main objective

To sample, characterize and formulate natural nanoporous zeolitic materials and apply them as smart delivery systems for urea fertilizer and lambda cyhalothrin pesticide.

1.3.2: Specific objectives.

The specific objectives were to:

i) To collect samples of natural zeolites deposits in Eburru volcanic crater, Lake Magadi, Lake Baringo, Ebul bul-Ngong, and Kitum caves-Mt.Elgon regions in Kenya.

ii) Characterize chemical and physical properties of natural zeolitic materials relative to synthetic zeolites.

iii) Determine fertilizer and pesticide loading and release properties of the zeolitic materials.

iv) Determine the efficiency of nanozeolite loaded urea fertilizer delivery systems in tomatoes and spinach crops production.

v) Determine the efficiency of nanozeolite loaded pesticide delivery systems in tomatoes and

spinach crops production.

1.4: Justification and significance

The increasing pollution effects like eutrophication and pesticide persistence due to perennial excessive application of fertilizer and pesticides as agriproduction inputs meant to increase yield and productivity are in essence posing a greater risk on the environment, food sustainability and general human existence. It is therefore paramount that continued research be conducted to address these global challenges, particularly focusing on novel and slow/controlled release technologies which are cost effective. In as much as polymer coating technologies for fertilizer and pesticides have been explored, such technologies have not yielded much in achieving ideal goals due to aspects like; high cost factors, introduction of polymer components in environment on disintegration and complexity in their formulation. The use of nanoporous zeolitic materials could prove to be a milestone, particularly in formulation of smart delivery systems for fertilizer and pesticides. Modeled on nanopore properties of zeolites, whereby guest molecules could be loaded in their nanopore structures and applied as carrier agents for smart delivery systems, zeolitic material could transform the utilization of these agriproduction inputs. These zeolitic materials are quite cheap and non-toxic since they are formed naturally in the earth as part of soil.

1.5: Scope and Limitations

This research was fixated on utilization of the selected zeolitic materials as smart delivery systems by formulating urea fertilizer and Lambda-cyhalothrin pesticide into their nanopore spaces through simple immersion techniques, as well as by ion exchange process for the nutrient delivery through adsorption-desorption studies. The zeolitic materials applied were used as obtained in their natural form without further purification. Calcination process done at 550 $^{\circ}$C was only able to remove some organic and amorphous components. Synthesis of the zeolites were beyond the scope of research objectives, so no attempts were made in the same. The capacity and efficiency of the zeolitic materials loaded with fertilizers and pesticides on nutrients release pattern was

monitored using adsorption-desorption modelling studies and on tomato and spinach crops grown on a simulated farm in Kikuyu area of Kiambu County, Kenya. The research work was limited by the variations in types of natural zeolitic materials, both in their structure and composition depending on sample origin, as well as their process of formation, hence analysis and discussions was determined by the data obtained from these samples in their natural condition under the stated methodologies. The simulated farm crops only involved a selected variety of tomatoes and spinach vegetables as representative crops that are used commonly by many households and are easier to cultivate and study, grown outside the greenhouse and determined by the ecological conditions as per the study duration and crop management practices applied to meet the research objectives, not necessarily under ideal agronomic expert opinions and practices.

CHAPTER 2: LITERATURE REVIEW

2.1: Zeolites

Zeolites are a cluster of aluminosilicate minerals occurring naturally as part of volcanic sedimentary rock deposits or can be synthesized using different silicates and aluminium precursors. According to Mumpton (1984), there are about fifty different species of natural zeolites, of which the common eight are: Clinoptilolite, Modernite, Analcime, Erionite, Chabazite, Ferrierite, Phillipsite and Laumonite. These minerals have useful chemical and physical properties which includes; large open 'channels' or pores in their crystalline structures ideal for adsorption and cation exchange capacities due to their large void space, low density (2.1 – 2.2 gcm^{-3}), high cation exchange capacity (150-250 $cmol^{-1}kg^{-1}$) and excellent molecular sieve properties (Mumpton, 1984; Wieslaw *et al.*, 2014; Pickering *et al*., 2002; Ayan 2001 and 2002a; Junrungreang *et al*., 2002).

Extensive research on zeolites has expanded to cover areas like agriculture, aquaculture, chemical industry, horticulture and waste management is vastly increasing (Mumpton 1984; Parham 1989; Clifton 1987). Advances in agriculture technologies have seen zeolites being applied as smart delivery systems of pesticides and herbicides, animal feed additives, soil and compost additives etc., owing to their uniqueness in properties like large porosity and high cation exchange capacities. For example, solubilization of phosphate minerals has been tested to increase when mixed with ammonium charged zeolites (Lai and Eberl 1986; Chesworth *et al*., 1987) leading to increased yields for Sudan grass due to improved phosphorous uptake (Barbarick *et al*., 1990), while Eberl and Lai (1992) advanced chips, which can act as slow release of nitrogen based fertilizer, from urea-impregnated zeolites. Natural zeolites have vast varieties, hence extensive mineralogical studies and characterization during selection could improve their applicability. For this reason, it's important to note also that some researchers like

Barbarick and Pierela (1984) had pointed out that certain sodium exchangeable cations zeolites could actually decrease plant growth, while Suzuki and Kohyama (1988) alluded that erionites could cause harm to human and animals when inhaled.

2.1.1: Structure and naming of zeolites

Zeolites structures contain $[AlO_4]^{5-}$ and $[SiO_4]^{4-}$ tetrahedrally connected by shared oxygen atoms in three-dimensional network (Breck, 1974); whose chemical structure can be demonstrated by Figure 2.1 below.

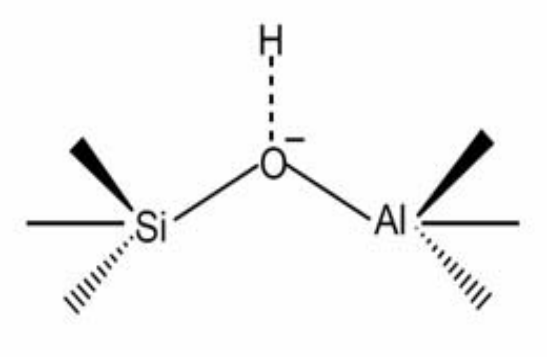

Figure 2. 1 Chemical structure of zeolite (Breck, 1974)

These structures have a typical bond length of 1.6Å, 3.07 Å and 2.63 Å for Si-O, O-O and Si-Si respectively, as exemplified by Figure 2.2 below.

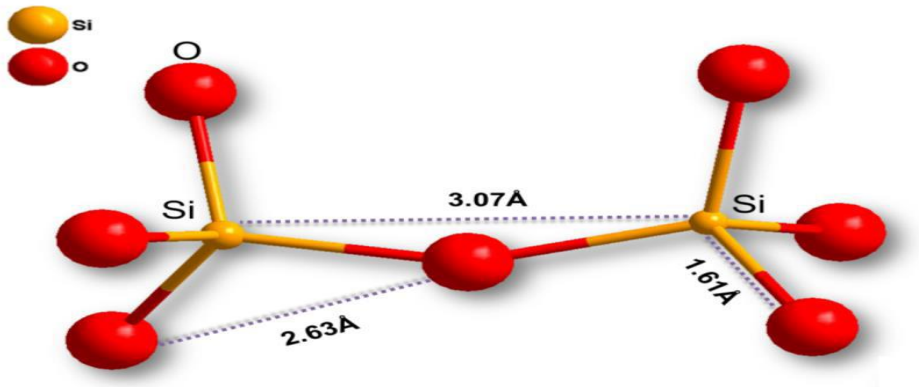

Figure 2. 2 Illustration of average bond length in zeolite structures (Breck, 1974)

When considered as an inorganic polymer, its building blocks would be (Bekkum *et al*., 1991):

$M^{n+}[(AlO_2)_x(SiO_2)_y].wH_2O$ ……..……..……(Equation 2.1)

Where: n- is the cationic valence

M- is the alkali metal cation

w- is the unit cell water molecules number

x and y- are the tetrahedral total number per unit cell.

(The ratio of x/y ranges 1 - 5, though can be 10-100 for silica zeolites).

The framework structure of zeolites consists of Primary Building Units (which are the tetrahedrons) as shown by Figure 2.3 below and Secondary Building Units (SBU) (formed from the geometric arrangements of the tetrahedral) which could be the simple polyhedral e.g. cubo-octahedra, cubes or hexagonal prisms (Bekkum *et al*., 1991).

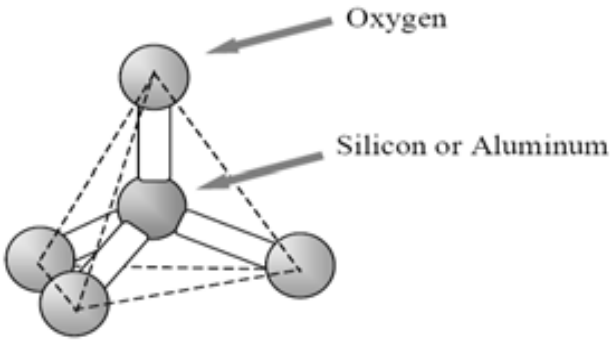

Figure 2. 3 Zeolite structure Primary building unit

Classification of zeolite structures depends on the repeating SBU, forming simple arrangements of tetrahedral membered rings e.g. of 3, 4, 6, 8, 10, etc. as illustrated in Table 2.1 below (Dimitar *et al*., 2009).

Table 2. 1 Zeolite structures classifications

Number of linked tetrahedral	SBU created (Oxygen rings)	Shorthand description
4	4	S4R
5	5	S5R
6	6	S6R
8	8	S8R
8	4-4	D4R
12	6-6	D6R
16	8-8	D8R

(S = single, R = ring, D = double)

For example, the scheme in Figure 2.4 (Pauling, 1930) below elucidates the complete formation from 4-4 SBUs which could form closely related structures of different zeolites, with all codes referred from Atlas of zeolite framework types.

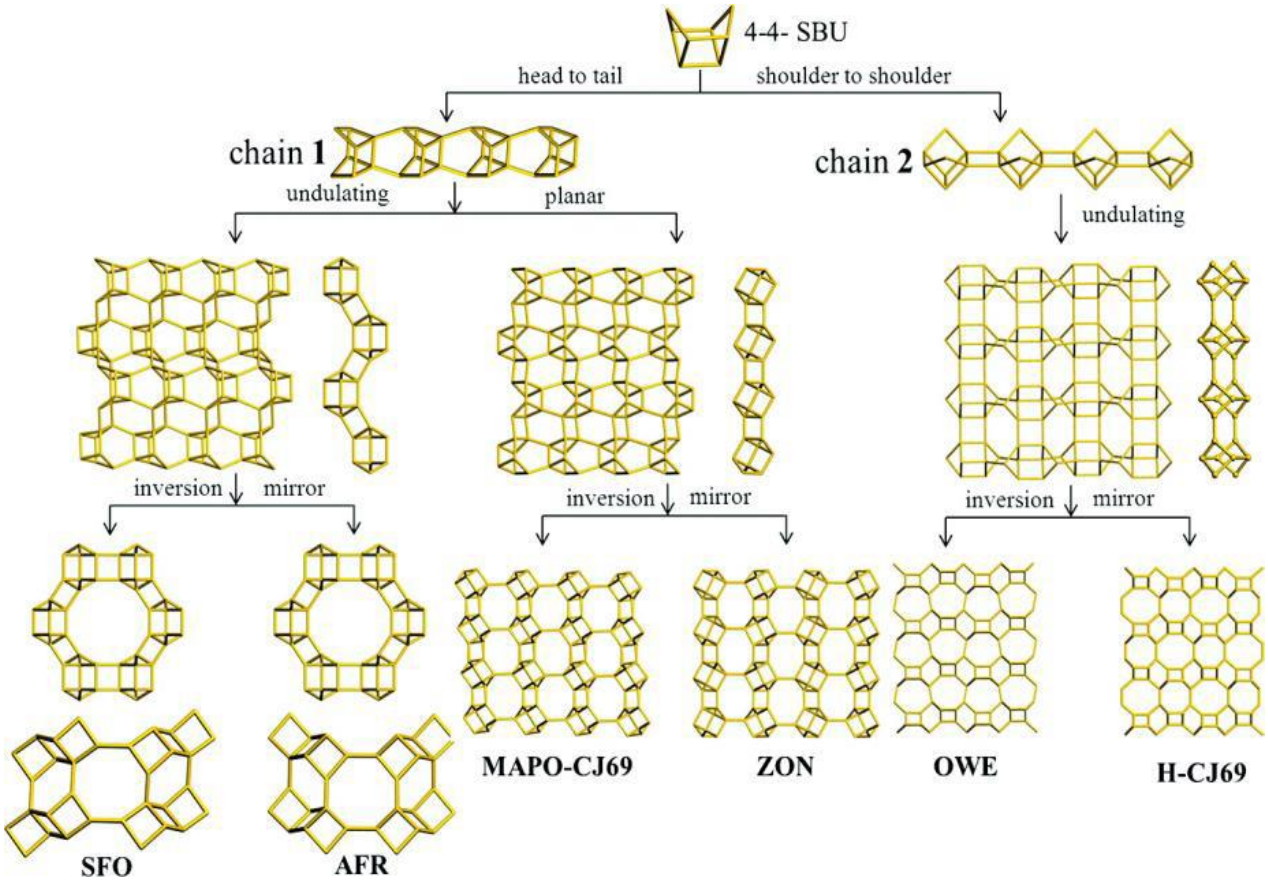

Figure 2. 4 Zeolites formation from 4-4 SBUs (Pauling, 1930)

These frameworks have many interconnected voids/channels (whose diameter could range from 0.3 - 20Å), containing water molecules and cations which can undergo ion exchange. These cations balance the negative charges on AlO_4^{1-} tetrahedrons. Pore sizes on zeolite structures can be influenced by the type of cation exchanged or the extra framework cation's size and location. The International Zeolite Association (IZA) determines and assigns the naming and coding, (as shown in Table 2.2) (Dimitar *et al*., 2009) for synthetic zeolites and Table 2.3 (Inglezakis, 2005) for some natural zeolites, given to different zeolite structures formed due to multiple linking ways between SBU and the polyhedral to generate varied framework topologies as shown in Figure 2.5 below.

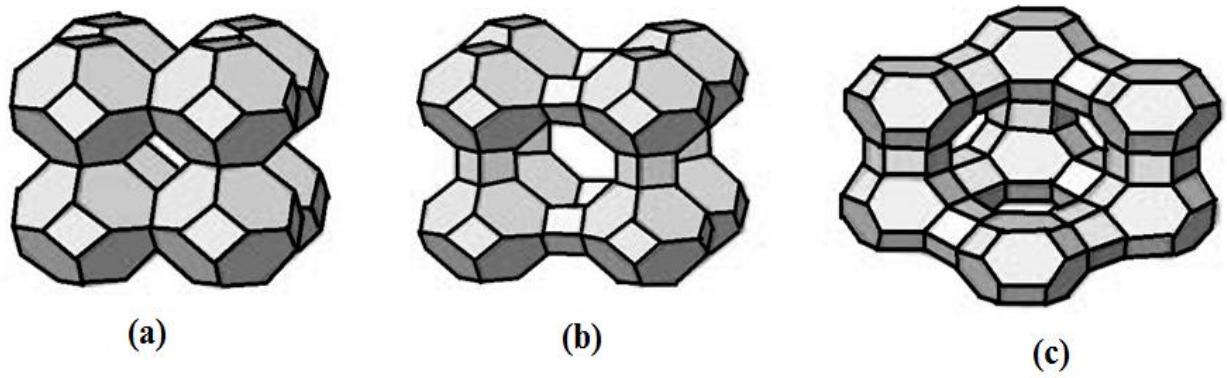

Figure 2. 5 Zeolites structure displays.

(a – Sodalite; b - Zeolite A/ZK-4; c – Zeolites X/Y) (Peng, 2016)

Additional diagrams of some of these rings and resultant structures discussed above are also presented in Figure 2.6 below (Peng, 2016).

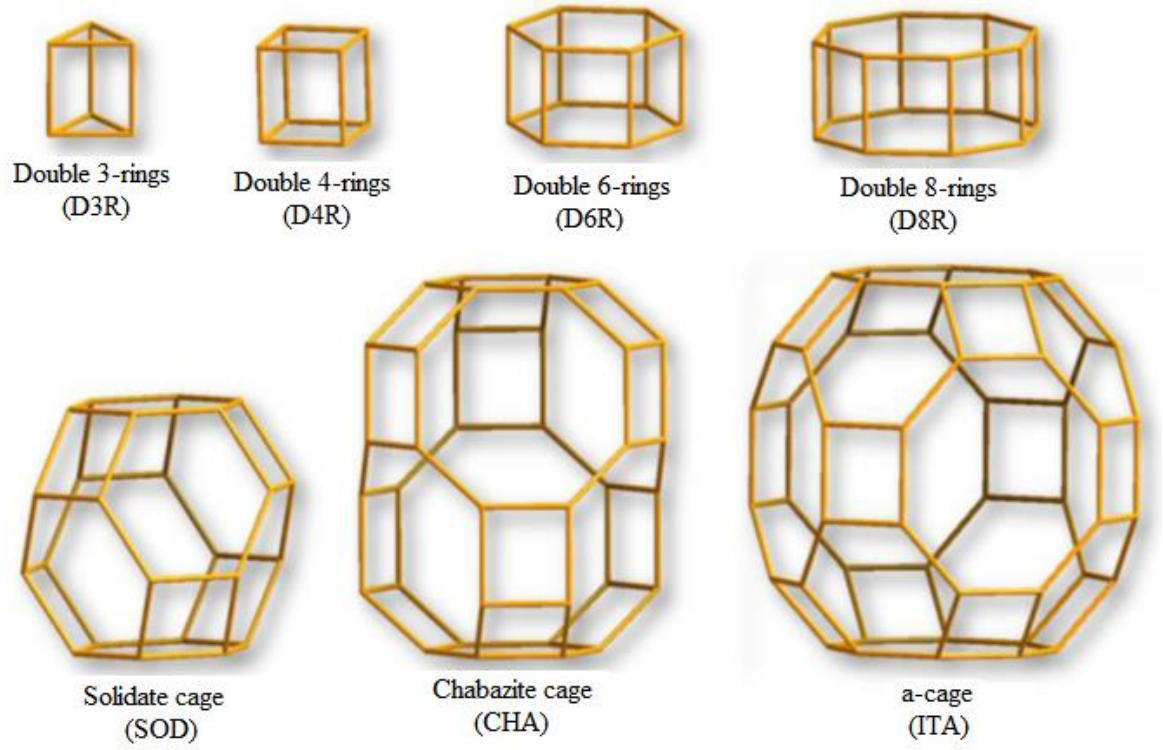

Figure 2. 6 Rings and cage assembly for some zeolite frameworks (Peng, 2016)

For instance, the solidate cage is mainly a truncated octahedral, consisting of 24 connected tetrahedral that undergo auxiliary linkages generating varied zeolites having specific unique uniform pore, as illustrated by zeolite A structure (Truong *et al*., 2007) (Figure 2.7).

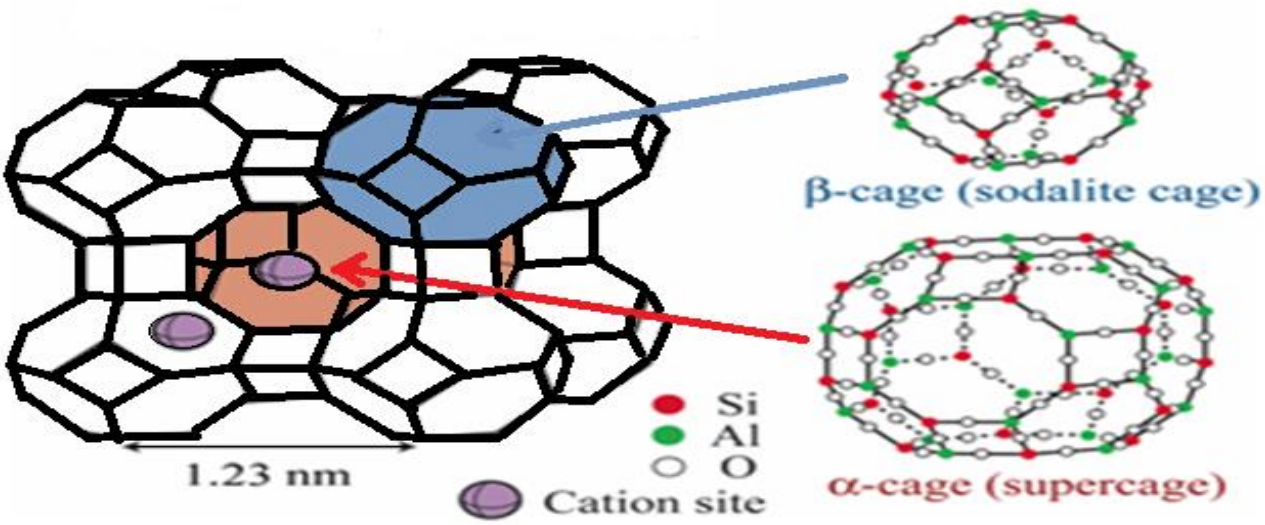

Figure 2. 7 Structure of zeolite A (Truong *et al*., 2007)

Table 2. 2 Characteristic oxide formulae of formulated zeolites

Zeolite notation	Oxide formula
A	$Na_2O.Al_2O_3.2SiO_2.5H_2O$
N-A	$(Na, TMA)_2$ O. $Al_2O_3.4,8SiO_2.7H_2O$ TMA – $(CH_3)_4N^+$
H	$K_2O.Al_2O_3.2SiO_2.4H_2O$
L	$(K_2Na_2)O.Al_2O_3.6SiO_2.5H_2O$
X	$Na_2O.Al_2O_3.2,5SiO_2.6H_2O$
Y	$Na_2O.Al_2O_3.4.8SiO_2.8,9H_2O$
P	$Na_2O.Al_2O_3.2 - 5SiO_2.5H_2O$
O	$(Na_2,K_2,TMA_2)O.Al_2O_3.7SiO_2.3,5H_2O$;TMA – $(CH_3)_4N^+$
Ω	$(Na,TMA)_2O.Al_2O_3.7SiO_2.5H_2O$; TMA – $(CH_3)_4N^+$
ZK-4	$0.85Na_2O.0.15\ (TMA)_2O.\ Al_2O_3.3,3SiO_2.6H_2O$

Table 2. 3 Examples of some natural zeolites and their respective formulae

Zeolite	Chemical formula
Chabazite	$(Ca0.5,Na,K)_4[Al_4Si_8O_{24}]\cdot 12H_2O$
Clinoptilolite	$(Na,K)_6\,[Al_6Si_30\ O72]\cdot 20H_2O$
Erionite	$K_2(Na,Ca0.5)_8[Al_{10}Si_{26}O_{72}]\cdot 28H_2O$
Ferrierite	$(Na,K)_2Mg(Si,Al)_{18}O_{36}(OH).9H_2O$
Heulandite	$(Na,K)Ca_4[Al_9Si_{27}O_{72}]\cdot 24H_2O$
Laumontite	$Ca_4[Al_8Si_{16}O_{48}]\cdot 18H_2O$
Mordenite	$(Ca,Na_2,K_2)Al_2Si_{10}O_{24}.7H_2O$
Phillipsite	$(Ca,Na_2,K_2)_3Al_6Si_{10}O_{32}.12H_2O$
Faujasite	$(Na_2Ca)Al_2Si_4O_{12}.6H_2O$

2.1.2: Formation of zeolites

Zeolite minerals are mostly of fine crystalline nature originating from geodes and fissures of eruptive sedimentary rocks (Glauco and Ermanno, 1985). These minerals could form naturally or can be synthetically made.

2.1.2.1: Natural zeolites

Hay (1978, 1981) identified some of the major zeolite formation environments like saline alkaline lakes, open hydrological structures, deep-sea hydrological sediments, weathered zones, hydrothermal hot springs and metamorphic settings of sedimentary origin. There are many different species of zeolites as already presented by Mumpton (1984), of which modernite, clinoptilolite, chabazite, erionite, phillipsite, laumonite, ferrierite and analcite can be exploited commercially (Hanson, 1995).

Existence of authigenic natrolite, analcime and heulandite-Na formed from diagenesis of marine sediments of arc-source terrains exposed on the western Vizcaino Peninsula, Califonia and Mexico were reported by Banes *et al*., (1984). Within those volcaniclastic rocks, the zeolites replaced plagioclase and glassy vitric fragments. Diagenesis and metamorphism of lava flow rocks like basalts within cavities and veins have been found to facilitate formation of natural zeolites in places like; Iceland, where fibrous zeolites are known to form (Walker, 1960); in the Table Mountains, Colorado (Kile and Modreski, 1988); at Neubauerberg, Bohemia, Czech Republic, where fine fibers of natrolite in vesicular basalt form and as extended crystals in Pune, India (Currier, 1976).

Diagenesis of marine pyroclastic and volcanistic sequences like deposition and accumulation of flow, fall-out tuffs and sand within shallow marine basins resulted in the deposition of zeolite minerals constrained by neighborhood geography and liquid sources like of marine water heated by hot pyroclastic rocks or simply the geothermal gradient of the active volcanic areas, resulting in forming zeolitic mineral zoning like clinoptilolite and analcime within the northeast Rhodope Mountains of Southern Bulgaria (Aleksieve and Djourova, 1975; Vanev *et al*., 2006). In hydrologically open systems, there could be the replacement of rhyolitic pyroclastic rocks, an alteration process occurring by percolation of meteoric water that hydrates, dissolves and crystallizes the zeolites, which often produces lateral variations in their authigenic mineralogy (Hay, 1963; Broxton *et al*., 1987).

Besides, it is also possible to form zeolite deposits in deep marine sediments (Murray and Renard, 1891; Boles, 1977; Iijima, 1978; Kastner and Stoneciphor, 1978; Boles and Wise, 1978). Zeolites minerals easily crystallize in water of closed basin arid lakes which tend to be highly saline. For example, altered tuff beds arising from big sandy formations have been reported to contain analcime zeolites in places like Wikieup, Arizona (Sheppard and Gude, 1973; Ross, 1928),

Anatolia basin in Turkey (Echle, 1975; Whateley *et al*., 1996; Gundogdu *et al*., 1996; Ataman and Beseme, 1972) and in Ankara area (Ataman and Gundogdu, 1982). The zeolite forming reactions, particularly analcine, appear to involve aluminium and silicon sources such as kaolinites or smectite, sodium rich water and high pH. Other regions reported include Lake Natron in Tanzania (Hay, 1970), Lake Bogoria, Kenya (Renaut, 1993), Unita Basin, USA (Remy and Ferrell, 1989), the Carboniferous Rocky Brook Formations of western New found land in Canada (Gall and Hyde, 1989) and in New Jersey, Newark Basin that contains Triassic Lockatong formation, (Van Houten, 1960, 1962, 1965). Quite a number of researchers have also linked occurrence of zeolites as intrusive rocks, phenocrysts and in ground mass of some alkaline lava (Goble *et al*., 1993; Harker, 1954; Pearce, 1970, 1993; Roux and Hamilton, 1976; Saha, 1959; Gupta and Fyfe, 1975; Wilkison, 1965, 1968; Cundari and Graziani, 1964; Luhr and Giannetti, 1987). Table 2.4 below shows a summary of the secondary minerals in volcanic caves in Kenya.

Table 2. 4 The secondary minerals in volcanic caves of Kenya

Mineral	Chemical Formula	Crystal System	Habit or mode of occurrence	References
Apophyllite	$KCa_4[Si_8O_{20}(F, Na, OH)].8H_2O$	Hexagonal	Prismatic crystal	Udluft (1928)
Aragonite	$CaCO_3$	orthorhombic	Small clusters of flowers	Simons (1998)
Bobierrite	$Mg_3(PO_4)_2.8H_2O$	monoclinic	Small radiating acicular crystals	Simons (1974, 1976)
Brushite	$CaH(PO_4).2H_2O$	monoclinic	*Radial aggregates of thin needles*	
Calcite	$Ca\,CO_3$	trigonal	*Rhombohedral crystals*, stalactites, stalagmites	Udluft (1928), Jérémine (1934), Sutcliffe (1973)
Celestine	$Sr\,SO_4$	orthorhombic	*Small zig-zag shaped coating*	
Collophane	$Ca_5(PO_4)_3(OH, F, Cl)$	amorphous	Secondary stalactites	Simons (1998)
Gypsum	$Ca\,SO_4.2H_2O$	monoclinic	*Bladed or acicular curved crystals*	Simons (1974) Kashima & Ogawa (1998)
Halite	NaCl	cubic	*Small spots or cubic crystals*	
Hannayite	$Mg_3(NH_4)_2H_4(PO_4)_4.8H_2O$	triclinic	*Transparent prismatic crystals*	
Hydroxyapophyllite	$KCa_4Si_8O_{20}(OH).8H_2O$	tetragonal	*Tetragonal prismatic crystal*	
Hydroxylapatite	$Ca_5(PO_4)_3(OH)$	hexagonal	*Small plate-like masses*	
Kogarkoite	Na_3FSO_4	monoclinic	*Aggregates of small bladed crystals*	
Mesolite	$Na_2Ca_2[Al_6Si_9O_{30}].8H_2O$	orthorhombic	Prismatic crystals	Udluft (1928)
Mesotype (natrolite)	$Na_2[Al_2Si_3O_{10}].2H_2O$	orthorhombic		Jérémine (1934)
Mirabilite	$Na_2SO_4.10H_2O$	monoclinc	Cuved crystals, efflorescences	Sutcliffe (1973) Simons (1998)
Mendozite	$Na\,Al(SO_4)_2.16H_2O$	monoclinc	Blisters	Sutcliffe(1973)
Natrolite	$Na_2[Al_2Si_3O_{10}].2H_2O$	orthorhombic	*Prismatic crystals*	Udluft (1928), Sutcliffe(1973)
Newberyite	$Mg\,HPO_4.3H_2O$	orthorombic	*Plate-like masses of fractured crystals*	
Opale	$Si\,O_2.nH2O$	amorphous	*Stalactites, Stalagmites*	Simons (1974,1998)
Phillipsite	$K_2(Ca_{0.5},Na)_4[Al_6Si_{10}O_{32}].12H_2O$	monoclinic	*Pseudo-tetragonal* pseudo-orthorhombic *twinned crystals*	
Sodium Alum	$Na\,Al(SO_4).12H_2O$	cubic	Efflorescences	Simons (1998)
Taranakite	$H_6K_3Al_5(PO_4)_8.18H_2O$	trigonal	*Nodule of prismatic bladed crystals*	
Tetranatrolite	$(Na,Ca)_{16}[Al_{19}Si_{21}O_{80}).16H_2O$	tetragonal	White acicular frostwork	Kashima & Ogawa (1998)
Thermonatrite	$Na_2CO_3.H_2O$	orthorhombic	*Thin crusts of prismatic crystals*	
Thenardite	Na_2SO_4	orthorhombic	Pale yellowish soft cave powder	Kashima & Ogawa (1998)
Trona	$Na_2CO_3{\cdot}NaHCO_3{\cdot}2H_2O$	monoclinic	*Thin blade-shaped laths*	

2.1.2.2: Synthetic zeolites

Synthetic zeolites could be prepared by either solid state reactions synthesis routes where the reaction depends on reactants diffusing at the interface of the solid phase or hydro-thermal synthesis routes, whereby reactions happen between individual molecules in liquids. Comparatively, hydrothermal synthesis routes could have varied reaction mechanisms like hydrolysis, ion exchange, agglomeration and redox, which uses similar starting materials to form different structures. Hydrothermal synthetic routes are preferred since they can be used to synthesize compounds with extreme properties like low melting point, low thermal stability and high vapour pressure (Ruren Xu *et al*., 2007).

2.2: Nanotechnology

Nanotechnology is defined as the knowledge and application of material at 1-100 nanometers scale through science, engineering and technology related (Alan *et al*., 2008). The definition considers nanotechnology as an interdisciplinary field for research, development, and inventions of novel application properties at nanoscale sizes (PCAST, 2005).

Nanotechnology approach tends to utilize properties of materials at miniature levels, which tend to be superior compared to bulk sizes, hence when suitably controlled, could give new nanometer-scaled discoveries (Rao and Cheetham, 2001).

Nanostructure synthesis could take the bottom-up and/or top-down approaches, which include: Template directed synthesis methods, Self-assembly synthesis methods, Soft lithography synthesis methods, integrated chemical synthesis methods and Size dimension reduction methods (Shakeel *et al*., 2015; Jiyun, 2003; Brust *et al*., 2002; Whitesides *et al*., 1991 and 2002; Lindsey, 1991; Martin *et al*., 1995 and 1996 and Changdeuck *et al*., 2008).

Nanotechnology deployment is quite varied; like in the medical field, nutrition and wrapping business, electronics, biochemistry, catalysis, agricultural production and environmental science (Martin *et al*., 2003; Lee *et al*., 2002; Park *et al*., 2006; Uchida *et al*., 2002; Alan et al., 2008;

Changdeuck *et al*., 2008). In this study, focus is drawn on application of nanotechnology as nanodelivery systems for smart release of agricultural chemicals to enhance efficiency and effectiveness in the production process (Chuprova, 2004; Jinghua, 2004; Baptista-Filho *et al*., 2008; Bernardi et al., 2011; Campona *et al*., 2015; Chi-fai *et al*., 2007; Chen *et al*., 2006; Maynard, 2006; Raco and Bainbridge, 2005; Roco et al. 2005).

2.3: Slow/controlled release nanotechnology based smart delivery systems

The microporous framework channels of zeolitic materials can be applied as carrier agent of molecules/ materials like fertilizer and pesticides, which can be done by encapsulating these molecules inside the nano-porous materials, coating the zeolitic materials with thin polymer films or using the zeolitic materials to deliver their content as emulsions or nanoscale dimension (Rai *et al*., 2012). Either of these processes could involve primary synthesis methods in which reaction aspects like chemical treatment, calcination, extraction assisted routes are used to modify the zeolite structures and load the quest molecules. On the other hand, secondary synthesis approaches such as surfactant modification of the zeolitic framework, ion exchange or isomorphous heteroatom substitution could be applied (Ruren Xu *et al*., 2007).

The mechanisms of formulation could involve solvent impregnation where the quest molecules are incubated in a solvent with the carrier materials at a suitable temperature or through solid-state methods which involve fusion of the materials. This is applied to compounds with low solubility and high thermal instability, where normally no solvent or catalysts are applied (Popova *et al*., 2014).

Nanoformulated fertilizers are fundamental in agriproduction and environmental protection initiatives. Studies have shown that nanobased fertilizers, also referred to as ‘smart fertilizers’, enhances nutrients use adeptness and reduces budgets of ecological fortification (Cui *et al*., 2006; Martin, 1997; Liu, 2006; Jighua, 2004; Chinnamuthu and Boopathi, 2009; Al-Amin Sadek and

Jayasuriya, 2007). In addition, smart fertilizer can be combined with nanodevices that are able to synchronize N and P nutrient release with crops uptake. This is critical because it prevents undesirable nutrients losses to (and interaction with) the environment (soil, water or air) (DeRosa *et al*., 2010). Cui (2006) stated some recompenses linked to altered formulation of conformist fertilizer expanding nanotechnology to include: Regulated discharge as per crop uptake pattern, augmented fertilizer efficacy and uptake ratio, extended availability of fertilizers nutrients into soil and reduced leaching nutrients loss.

Nano formulation of pesticides (herbicides, insecticides, and fungicides) increases their stability and solubility in water, hence optimizing their effectiveness. Besides, this new discovery has increased the ability to moderate active ingredients release dependent on the conditions, implying that wastages such as through run-off could be minimized, protecting the environment (Chinnamuthu and Boopathi, 2009). This also reduces direct contact of active ingredients with the agricultural workers, minimizing their associated risks.

Once formulated, the adsorption-desorption processes of these nanocarriers can be attributed to varied number of mechanisms. Calvet (1989) argued that only hypothesis is ascribed to given mechanisms when describing retention of pesticides. In addition, DiVenzo and Sparks (2001) suggested that only spectroscopic, thermodynamic, and kinetic studies can actually result to mechanistic interpretation, while the soil heterogeneous nature make spectroscopic non vital. These mechanisms include: Ionic exchange that arises from non-specific electrostatic interactions. They could involve cationic species undergoing cation exchange due to the negatively clay and soil organic matter or exchange of ions between the positive sites and soil surface (Haper, 1994). Cation bridging, which occurs when pesticide or fertilizer ionic functional groups and exchangeable cations form inner sphere complex, which usually is with displacement of water or from a reaction caused by the organic functional group. Hydrophobic sorptions, for solutes from water considered as solvent and nonspecific surface partitioning (Senesi, 1992). Charge transfer, occurring when electron rich moieties and electron deficient structures of humic

substances undergo electron donar-acceptor mechanism (Senesi, 1992). Van der Waals interactions, which according to Calvet (1989), physical adsorption of organic matter constitutes Van der Waals interactions. There could be organic matter and water solute partitioning, which is depends on the solvent and affected by entropy or solute adsorption, which depends on the sorbent and is enthalpy driven. Bound residues which happens when adsorbed organic chemicals react to covalently bind into the soil matrix (Kosken and Harper, 1990). Usually, stable, and irreversible pesticide humic complex is formed (Happer, 1994; Scribner *et al*., 1992; Senesi, 1992). Ligand exchange, which involves replacement of polyvalent cation ligands by apposite adsorbed molecules such as hydration water with s-triazines and anionic pesticides. Lastly, hydrogen bonding, which is the interaction between electronegative atoms (N and O), having electron withdrawing properties, with electropositive hydrogen nucleus covalently bonded to the same atoms.

2.4: Physisorption Isotherms

2.4.1: Adsorption kinetics

Regularly, sorption isotherms are normally logical reproductions that endeavor to articulate the appropriation adsorbate species among the fluid or strong solid phases. These isotherms depend on various assumptive elements like the class of inclusion, heterogeneity/homogeneity of the strong surface and the collaboration conceivable outcomes between adsorbate species (Shahmohammadi et al., 2011). They are intended to give significant data about the physicochemical procedures of sorption.

Among the considered models in this study include Langmuir, Freundlich, Redlich-Perterson and Temkin. The choice on these models is based on their aptitude to provide a noble correlation to the data, in addition to the consideration on the number of fitted parameters, as well as their physical meaning.

2.4.1.1: Langmuir model

This model proposes that adsorption of sorbate molecules happens on a homogeneous surface to form a monolayer having no relations amongst the adsorbed particles (Langmuir, 1918).

The Langmuir equation is represented by Equation 2.2 as:

$$q_e = \frac{q_m K_L C_e}{1+K_L C_e} \quad \text{(Equation 2.2)}$$

Linearized as:

$$\frac{C_e}{q_e} = \frac{1}{q_m K_L} + \frac{C_e}{q_m} \quad \text{(Equation 2.3)}$$

Where: q_e (mg/g) is the amount adsorbed, C_e (mg/L) is the concentration of sorbate molecules, q_m (mg/g) is the maximum amount of adsorbed sorbate molecules per unit mass of sorbent corresponding to complete coverage of the adsorptive sites and K_L (L/mg) is the Langmuir constant related to the energy of adsorption.

2.4.1.2: Freundlich model

The Freundlich (Freundlich, 1906) model is an experiential equivalence centered on assorted surface sorption. This is generally exemplified as presented in Equation (2.4).

$$q_e = K_F C_e^{1/n} \quad \text{(Equation 2.4)}$$

This can be rearranged linearly by Equation 2.5.

$$\ln q_e = \ln K_F + \frac{1}{n} \ln C_e \quad \text{(Equation 2.5)}$$

Where C_e (mg/L) is the equilibrium concentration and q_e (mg/g) is the amount of adsorbed pesticide per unit mass of the adsorbent. The constant *n* is the Freundlich equation exponent that represents the parameter characterizing quasi-Gaussian energetic heterogeneity of the adsorption surface (Bansal and Goyal, 2005). K_F (L/g) is the Freundlich constant indicative of the relative

adsorption capacity of the adsorbent.

According to Chantawong (2003), *n* should be between 1-10 for classification as better adsorption.

2.4.1.3: Quasi-Langmuir Model

Quasi-Langmuir isotherm is utilized as a Freundlich – Langmuir compromise models, which is given in equation (2.6) (Redlich and Peterson, 1959):

$$q_e = \frac{K_C C_e}{1+ \alpha_C C_e^{\beta}} \quad \text{.....(Equation 2.6)}$$

This can be linearized as:

$$\frac{1}{q_e} = \frac{1}{K_C C_e} + \frac{\alpha_C}{K_C} \quad \text{.....(Equation 2.7)}$$

Where K_c (L/g), α_c (L/mol) and β are Quasi-Langmuir coefficients, with β values 0 to 1. Hence plots of $1/q_e$ versus $1/C_e$ from equation 2.7 are linear.

2.4.1.4: Temkin model

From Temkin and Pyzhev (1940), adsorbent-adsorbate interactions of all molecules in a layer resulted into undeviating diminish in the enthalpy of adsorption and of which unvarying dispersal of bonding energies characterize the adsorption. This model is exemplified by Equation (2.8).

$$q_e = \frac{RT}{b} \ln(K_T C_e) \quad \text{.....(Equation 2.8)}$$

Taking $B_T = RT/b$, this can be rearranged linearly as:

$$q_e = B_T \ln K_T + B_T \ln C_e \quad \text{.....(Equation 2.9)}$$

Where T is the total temperature (K), R is the widespread gas steady (8.314J/mol. K), KT is the harmony restricting consistent (L/mg), b is the variety of adsorption vitality (kJ/mol) and BT is

Temkin steady, which is identified with the Heat of adsorption (kJ/mol). Therefore, plots of q_e against lnC_e from equation 2.9 should be linear.

2.4.2: Adsorption kinetics

Sorption process involving most sorbate and their sorption medium phases are usually time-dependent. Hence, the kinetics of these processes could help in understanding the dynamics of interactions of inorganic/organic pollutants with the environment, hence understanding their effects in the environment (Spark and Suarez, 1991; Spark, 1989).

Among the various kinetic models already known, this study only focuses on Pseudo-first-order and Pseudo-second-order.

2.4.2.1: *Pseudo*-first order kinetic model

Pseudo-first-order Kinetic model of Lagergren (Lagergren, 1898) is founded on the solid capability for sorption analysis, illustrated by Equation 2.10.

$$\frac{dq_t}{dt} = k_f(q_e - q_t) \quad \text{.....(Equation 2.10)}$$

where q_t is the measure of adsorbate adsorbed at time t (mg/g), k_f is the rate steady of pseudo-first-order energy (min) and t is the time (min). The mix of equation 2.10 with the underlying condition, $q_t = 0$ at $t = 0$ prompts the pseudo-first-order rate equation:

$$\ln(q_e - q_t) = lnq_e - k_f t \quad \text{.....(Equation 2.11)}$$

Plots of ln(qe −qt) versus t are utilized to decide the Pseudo-first-request rate consistent (*kf*) (min^{1-}).

2.4.2.2: *Pseudo*-second order model

The pseudo-second order rate kinetic model dependent on the sorption balance limit can be illustrated by equation 2.12 (Ho, 2006),

$$\frac{dq_t}{dt} = k_s(q_e - q_t)^2 \quad \text{.....(Equation 2.12)}$$

Which linearized as:

$$\frac{t}{q_t} = \frac{1}{k_s q_e^2} + \left(\frac{1}{q_e}\right) t \quad \text{.....(Equation 2.14)}$$

Where K_s (g/mg.min) – is the Pseudo-second order rate constant and q_t (mg/g) – is the measure of adsorbate adsorbed per unit of adsorbent at time *t*. The Initial adsorption rate *h* (mg/g.min) at *t*-0 is expressed as:

$$h = k_s q_e^2 \quad \text{.....(Equation 2.15)}$$

h, q_e and K_s are generated from plots of t/q_t against *t.*

2.5: Theory of analytical techniques

Numerous analytical systems can be applied in characterization of zeolites and related materials. These includes X-Ray Diffraction, Fourier-Transform Infrared Spectroscopy, Energy Dispersive X-Ray Spectroscopy, X-Ray Fluorescence Spectroscopy and Scanning Electron Microscopy, among others. Only some techniques applied in this research work will be examined as beneath.

2.5.1: X-Ray Diffraction (XRD)

XRD is commonly used for crystallinity characterization in which unit cell parameters and phase identification of samples are done (Kulprathipanja, 2010). The sample is subjected to X-Ray beams like Cu Kα radiation in which the force of the rising rays is recorded as a parameter of the deflection angle 2θ based on Bragg's law given as: $\eta\lambda = 2d_{hkl} \sin\theta$; η is the order for diffraction, λ is the frequency, d_{hkl} is the grid dividing and θ is the redirection point as represented in Figure 2.8 underneath.

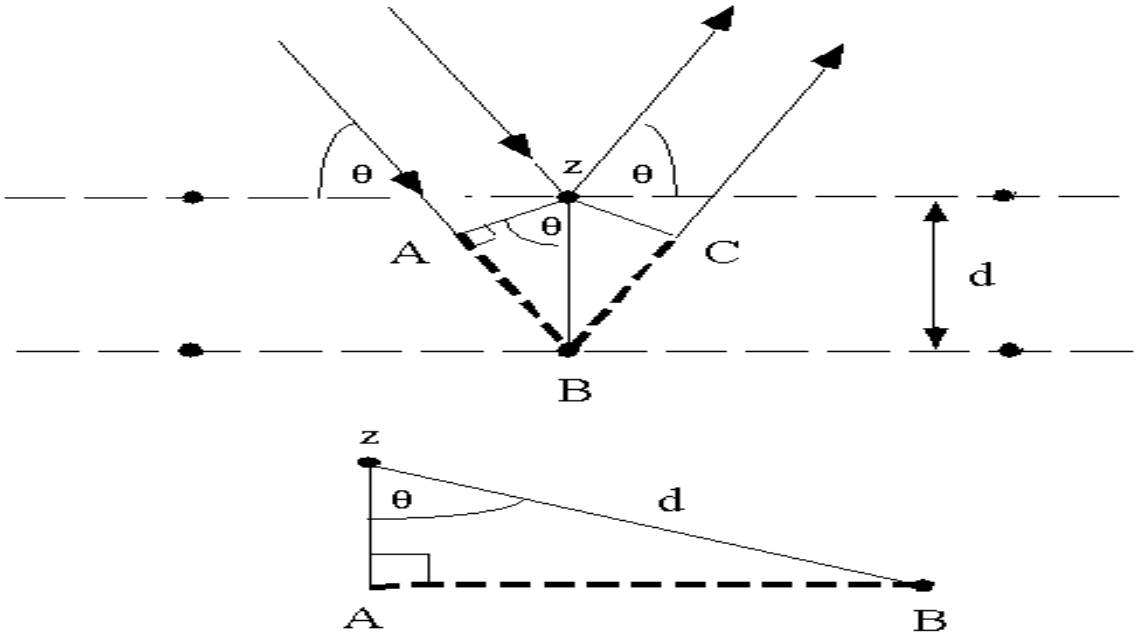

Figure 2. 8 XRD diffraction

The unit cubicle size a_0 could be determined from the angular positions of the reflection within the lattice spacing (d_{hkl}) as:

$$a_0 = \frac{\lambda\sqrt{h^2+k^2+l^2}}{2Sin\theta} \quad \text{……(Equation .2.16)}$$

; in which 'h' 'k' 'l' are orientations indicated by the Miller's indices (Bruker AXS, 2001)

2.5.2: Energy Dispersive X-Ray Spectroscopy (EDX)

EDX analysis indicates the sample structure as elemental or corresponding oxides present.

EDX works by subjecting a sample to an electric beam which excites the existing atoms, producing X-rays of characteristic energy recorded as spectra of intensity against energy (keV) (John *et al*., 2015). When incident high energy electron beams eject an electron leaving a vacant inner shell, it loses corresponding energy conveyed to the ejected electron. Hence, an external shell electron fills the gap creating energy as X-rays normal for the atomic number from which it is inferred (John *et al*., 2015).

2.5.3: Fourier-Transform Infrared Spectroscopy (FTIR)

FT-IR examines the samples functional groups dependent on the recurrence of the vibrations inside the bonds between various elements. The sample is exposed to IR light of which if it's frequency compares to the frequency of band vibrations; IR light is assimilated. The various kinds of functional groups present on the outside of the material are controlled by looking over a scope of frequencies like 400-4000cm^{-1} while recording the measure of transmitted light (Breck, 1974). Ordinarily, the vibration vitality relies upon the majority and substance condition of particular atoms framing the functional groups, just as the particular kind of vibrations.

2.5.4: X- Ray Fluorescence Spectroscopy (XRF)

XRF is an investigative method for determination of chemical composition of samples, widely used for elemental analysis. Ideally, when X-ray is irradiated on a target sample, there is usually transmittance, absorbance (which produces fluorescent radiation) and scattering back (as either Compton or Rayleigh) (Peter, 2003). These resultant fluorescent radiations and X-rays are emitted at energies characteristic of each element, which are deduced by measuring their energetics and intensities by the detector (Redus, 2008).

2.5.5: Scanning Electron Microscopy (SEM)

SEM is applied in the analysis of surface structure and morphology. Usually, electron beam generated from a cathode or filament collide with inner atomic shell electrons of the target sample, generating backscattered and secondary electrons escaping from the sample that are collected by suitable detectors, producing emission current that modulates the brightness of a cathode ray tube display generating suitable images (Robson, 2001; Ohrman, 2000).

2.5.6: Ultraviolet Visible Spectrophotometry (UV-Vis)

It is applied in concentration determination studies of amount of solute in given solvent.

When the analyte interacts with ultraviolet and visible radiation, there is electronic transition due to photon absorption, which can be related to it's concentration through the Beer's law expressed as:

$$A = \varepsilon bc \quad \text{.....(Equation .2.17)}$$

where; ε is the absorptivity ($Lmol^{-1}cm^{-1}$), *b* is the path length and *c* is the analyte concentration ($molL^{-1}$).

2.5.7: Sorption techniques

These are applied on porous material characterization in determination of explicit exterior area, aperture capacity and sizes (Sing *et al.*, 1985). Among some of the techniques applied include the Brunauer-Emmett-Teller (BET) gas adsorption (Brunauer *et al*., 1938) for determination of the surface area and Barrett-Joyner-Halenda (BJH) for aperture capacity dispersal (Barrett *et al*., 1951). The sorption data obtained is presented and interpreted in the form of sorption isotherms classified according to the IUPAC. Capillary condensation in mesopores as illustrated by isotherm is a phenomenon whereby a gas condenses to a liquid-like phase in pores at a pressure *p* less than saturation pressure p^0 of the bulk liquid. Varied pore volumes and distributions results in differences in pore condensation steps that causes hysteresis loops on the isotherms (Trunschke, 2015).

2.5.7.1: Specific surface area

This is commonly determined by Brunauer-Emmett-Teller (BET) gas sorption technique (Brunauer *et al*., 1938) that evolved from the Langmuir theory with multilayer correction, with assumptions that:

i. The adsorbent exterior is identical, and all adsorption destinations are equal

ii. Adsorbed particles do not relate

iii. All adsorption takes place via similar steps

iv. Monolayer formed with no interactions

The linearized BET is expressed as:

$$\frac{p}{n^a.(p^0-p)} = \frac{1}{n_m^a.C} + \frac{(C-1)P}{n_m^a C P^0} \quad \text{..... (Equation 2.18)}$$

Where:

n^a -is the adsorbed amount at pressure p/p^0

n_m^a-is the maximum monolayer amount adsorbed

C -is a system dependent constant

p- is the gas pressure at equilibrium

p^0- is the gas pressure at saturation

This is a type II isotherm, with a higher value of C indicating greater adsorbent-adsorbate interaction, often signifying a sharp point B on the isotherm.

Calculating BET surface area is then done by:

$$a_s\,(BET) = A_s\,(BET)/m \quad \text{..... (Equation 2.19)}$$

And

$$A_s\,(BET) = n_m^a.L.a_m \quad \text{..... (Equation 2.20)}$$

Where:

$a_s(BET)$ -is the surface area specific

$A_s(BET)$ -is the surface area total

m – is the sample mass

L -Avogadro's number and

a_m - is the sub-atomic cross-sectional zone involved by the adsorbate particle in the total monolayer (Sing *et al*., 1985).

2.5.6.2: Mesopore size analysis

According to Sing *et al.*, (1985), duct buildup and the Kelvin equation underneath forms the main principle for calculating the pore size.

$$\ln \frac{p}{p^0} = -\frac{2\gamma V_l}{RT}\left(\frac{\cos\theta}{r_k}\right) \quad \text{(Equation 2.21)}$$

Where:

γ -is the adsorptive liquid surface tension

V_L-is the liquid molar volume

θ – is the solid and the condensed phase contact angle

r_k – is the liquid meniscus mean radius

Pore condensation occurs at critical pressure determined by pore radius. This often results in the hysteresis loops discussed earlier (Sing *et al*., 1985).

The BJH method (Barrett *et al*., 1951) is then useful for the calculations, communicating Kelvin span as capacity of relative weight as:

$$r_k\left(\frac{P}{P^0}\right) = \frac{2\gamma V_L}{RT\ln\frac{P}{P^0}} \quad \text{(Equation 2.22)}$$

Then obtaining pore size r_p by:

$$r_p = 2(r_k + t) \quad \text{(Equation 2.23)}$$

Where:

t – is the adsorbed layer thickness

r_p- is the pore width/radius

r_k - is the liquid meniscus mean radius

The total length of pores with r_p radius is then calculated, which is applied to find area of pores, stepwise in the model to determine the overall PSD by considering all differences in amounts of adsorptive.

BJH calculation method is applied based on the following assumptions (Sing *et al*., 1985):

i. All apertures have a tubular profile

ii. The applicability of the Kelvin equation

iii. Hemispherical meniscus formed with θ = 0

iv. Multilayer correction is valid

Finally, porosity is determined by:

$$Porosity = \frac{Total\ pore\ volume, V_P}{Volume\ of\ the\ material} \quad \text{(Equation 2.24)}$$

V_P Is taken to be the adsorbed liquid volume.

CHAPTER 3: MATERIALS AND METHODS

3.1: Materials and reagents

The following materials were used: commercial zeolites (CPZ, from Sigma-Aldrich, P-Code: 101554254, Lot # BCBM 9330V and CAS:1318-02-1, purchased and used without further purification) labeled as sample ZT-GA-01(used as standard), natural zeolitic rock samples labeled: EB-GA-02, MG-GA-03, BG-GA-04, NG-GA-05, EL-GA-06, Urea (analytical standard 99 % pure from IOBA Chemie), Lambda cyhalothrin (analytical standard 99 % pure from IOBA Chemie), Potassium dichromate, Barium chloride, Concentrated Sulfuric acid, Potassium sulfate, Copper sulfate, Selenium sulfate, Concentrated hydrochloric acid, Ammonium acetate, Potassium chloride, Potassium bromide (all analytical standards 99 % pure from IOBA Chemie) and soil sample KIK-GA-01(used as control).

3.2: Instrumentation

The following equipment's were used in characterization of materials: UV-Visible spectrometer, X-ray diffractometer (XRD, D2 Phaser SSD160 A26-X1-A2DOB2B1, 2nd Gen. from Bruker), Fourier Transform Infrared (FTIR, IR Tracer-100 from Shimadzu), Energy dispersive spectrophotometer (EDS, Shimadzu EDX-720), Analytical balance (Fischer A-160), Orbital shaker (Fischer G-18), Atomic absorbance spectrophotometer (AAS, Perkin Elmer 2100), X-ray fluorescence spectrometer (XRF, TITAN 600), Scanning Electron Microscope (SEM, Hitachi S4800), ASAP 2020 Micromeritics equipment, Flame photometer (Sherwood scientific 410) and Calcinator (N3A Simon Muller 220V Berlin).

3.3: Procedures

3.3.1: Samples collection

From their different sampling sites guided by geological mineral deposit map, some rocks were collected bare, while others had to be excavated. About 2.0 -3.0 Kg of these zeolitic rocks were ferried to the laboratory; sun dried for three days and packed in airtight plastic bags for further preparation and analysis. Soil applied in the modelling and simulation process (Sample KIK-GA-0l) was collected in Kikuyu area (1.26921^{o} S, 36.6713^{o} E), Kiambu County, at a depth not exceeding 20.0 cm in arable land, previously having maize and vegetables intergrown. It represented the actual soil and location where the monitoring was done. This was applied as the control sample in this research work.

3.3.1.1: Sample ZT-GA-01

This was commercial zeolitic material samples (ZT-GA-01) procured from Sigma Aldrich and was applied as purchased devoid of supplementary refining. This was the standard sample for research work.

3.3.1.2: Sample EB-GA-02

This sample (Figure 3.1) was collected from Eburru volcanic crater (0.63^{o} S, 36.23^{o} E), which is located about 8 Km North-West of Lake Naivasha within the Kenyan Rift Valley. The sample was taken from the base of a quarry, about 10 feet deep, excavated by the Kenya Electricity Generating Company that was exploiting geothermal energy in the area.

Figure 3. 1 Sample EB-GA-02

3.3.1.3: Sample MG-GA-03

This sample (Figure 3.2) was collected along the shores of Lake Magadi (1.9010° S, 36.2468° E), as relatively homogeneous bare surface deposits spatially extending 200 m by 10 m. The collected sample mainly consisted of exposed surface rock crusts, no efforts were made to explore samples under the water, lakebed or deep in the ground due to the limitations of the sampling equipment availed for this work.

Figure 3. 2 Sample MG-GA-03

3.3.1.4: Sample BG-GA-04

The sample (Figure 3.3) was collected from Ol Arabel and Endao seasonal riverbeds near their entry to Lake Baringo (0.6321° N, 36.0567° E). Due to increased water levels in the lake, the shores of this lake were flooded as at the time when sampling was being carried out. Some structures of the existing facilities established on the shore had actually flooded, like those of Soi Country Lodge. Deposition on the lake is of debris and rocks carried by flash floods from these seasonal rivers, so the samples collected were taken to be a fair replica of the lake sediments deposits. Challenges of lake flooding and excavation equipment did not allow for underwater and deep excavation sampling.

Figure 3. 3 Sample BG-GA-04

3.3.1.5: Sample NG-GA-05

The sample (Figure 3.4) was collected from a quarry excavated site done by The China Road and Railway Construction Company at Ebul bul (1^0 22'S, $36^0$38'E) near Ngong town in Kajiado

County. Only samples at the base of the quarry, about 15 feet deep, were collected for further analysis.

Figure 3. 4 Sample NG-GA-05

3.3.1.6: Sample EL-GA-06

The sample (Figure 3.5) was collected from Kitum caves found at the foot of Mt. Elgon (1.1493° N, 34.5418° E), accessed through the Mt. Elgon National Park.

Figure 3. 5 Sample EL-GA-06

3.3.2: Sample preparation

The preparation of the natural zeolitic rock samples labeled as EB-GA-02, MG-GA-03, BG-GA-04, NG-GA-05 and EL-GA-06 involved mechanical grinding and sieving using 0.85 mm sieve to obtain very fine homogeneous particle sizes powder. The powdered samples were then calcined at 550 °C for 2 hours to remove some of the organic and amorphous components. Commercial zeolitic material samples (ZT-GA-01) were used as received in all the experiments as the standard sample, without further preparation.

3.3.3: Characterization methods

3.3.3.1: X-Ray Diffraction (XRD)

For XRD, 0.3 - 0.5 g of the grounded and homogeneously sieved sample was compressed on aluminium sample holder. The sample was then subjected to x-ray beam rays using Cu-Kα radiations (k = 1.54184 Å, 40 kV, 40 mA) with stepwise increase of 0.02° sec^{-1} over 1°-8° and 2° min^{-1} over 8°- 90° for small angle and wide angles respectively. The diffractometer was equipped with Ni-fitted Cu-Kα radiation source (8978 Ev). The spectrum was recorded as intensity against 2θ on the computer equipped with a PC-APD diffraction software and saved in Microsoft Excel 2010 format for analysis (Toyara, 1986 and Burton, 2009).

3.3.3.2: Energy Dispersive X-Ray Spectroscopy (EDX)

Shimadzu EDX-720 instrument was used for the SEM analysis. 100.0 mg of sample was uniformly ground and spread on a sample holder of approximately 25 mm diameter and then subjected to x-rays of accelerating voltage up to 40 keV. The spectrums were recorded as intensity (cps/μA) against energy (keV), with identification of individual lines on the accompanied table of energies or wavelengths (Kliewer, 2009).

3.3.3.3: Fourier-Transform Infrared Spectroscopy (FT-IR)

About 0.3 mg of fine powdered sample were homogenized with KBr (0.1 wt %) in the ratio of

1:15 and pressed into pellets. The pellets were scanned by infrared radiation using attenuated total reflectance technique (ATR) in the wavenumber range of 400 - 4000 cm^{-1} by collecting 140 scans at a resolution of $4cm^{-1}$. This generated spectrum of percentage transmittance (% T) against wavenumbers (cm^{-1}) (Liu, 2009).

3.3.3.4: X- Ray Fluorescence Spectroscopy (XRF)

The samples were homogeneously grounded to less than 60 µm. The sample was then pressed into pellets with chromatographic cellulose as the binder in a proportion 1:10 by weight to give 150 mg pellets. X-rays were irradiated onto the samples, that subsequently emitted fluorescence recorded in the form of Energy (keV) and Intensity counts corresponding to the diverse elements existing in the samples.

3.3.3.5: Scanning Electron Microscopy (SEM)

A 12 mm double-sided carbon tape was used to cover a 40.0 mm by 20.4 mm Aluminium stub. The carbon tape was then attached to a transparency paper that was cut into 12 mm by 3 mm pieces. The pieces were then dipped into the finely powdered sample to attach. The samples were then scanned with a beam of incident electrons operated 15 – 20 kV to form SEM images on the detector (Kliewer, 2009).

3.3.3.6: Nitrogen adsorption - desorption isotherms

The bulk rock samples had first been mechanically grinded and sieved to obtain homogeneous powder that was calcined at 550 ^{o}C for 2 hours. ASAP 2020 Micromeritics equipment was then used to collect isotherms of nitrogen adsorption – desorption on 0.2 g powdered samples at 77 K, which had been initially outgassed at 673 K for 6 hours in a vacuum. This was to ensure that the water inside the sample was completely removed and subsequently cooled at room temperature. The standard BET method (Brunauer *et al.*, 1938) was used in determining the specific surface area. BJH method (Barrett *et al.*, 1951) was applied to find the pore size distributions as

determined from sorption isotherms of N_2 at -196 °C at relative pressure (P/P_o) in the range of 0.00 – 0.99.

3.3.4: Soil content analysis for KIK-GA-01

Control sample KIK-GA-01 were set up for investigation via air drying in regular daylight at room temperature for four days to forestall supplement change, crashed, sieved utilizing 0.85 mm sifter size and put away in hermetically sealed examining sacks in readiness for the following analysis:

i) The dried soil tests were investigated for Na, Ca and K utilizing a flame photometer. First, the standard solutions were prepared by serial dilution as 2, 4,6,8 and 10 ppm which were scanned to produce calibration charts. Then 0.05 g of each powdered sample weighed in a platinum crucible was mixed with 2 ml of hydrofluoric-sulfuric acid mixture, heated and 10 ml of deionized water added and then diluted further to a 50 ml volumetric flask. The samples were then aspirated, and readings recorded.

ii) P, Mg and Mn were investigated colorimetrically, utilizing the Mehlich Double Acid Method (Mehlich, 1953; Tran and Simard, 1993). 5.0 g of the soil sample was mixed 20 ml Mehlich extracting solution (0.05 N HCl mixed with 0.025 N H_2SO_4). The mixture was shaken on an orbital shaker at 180 rpm for 10 minutes and filtered. Mg and Mn were analyzed using AAS, while P was done using ascorbic-ammonium molybdate and intensity of the blue coloration measured by UV-Vis. Spectroscopy.

iii)Trace components like Fe, Zn, and Cu were analyzed by Atomic Absorbance Spectrophotometer (Yang and Chang, 2005). 5.0 g of air-dried, grinded, and sieved samples in an Erlenmeyer flask was mixed with 20 ml of an extracting solution (0.05 N HCl and 0.025 N H_2SO_4) and shaken for 15 minutes, then sieved. The elutes were analyzed on AAS for the elements.

iv)Total organic carbon (C) was determined by calorimetric method. All-natural C in the soil sample was oxidized by acidified dichromate at 150 °C for 30 minutes to guarantee total oxidation. Barium chloride was added to the cool reviews. In the wake of blending completely, processes were permitted to stand overnight. The C amount was determined on the spectrophotometer at 600 nm (Gislason et al., 2005).

v) Aggregate sum of nitrogen was studied by Kjeldahl technique (Jan-Åke et al., 2008). A bout 5.0 g of the homogeneous soil was placed in a digestion flask and two Kjeldahl tablets of 5 g Missouri catalyst with 20 ml sulfuric acid added. The content was placed into a digestion unit and heated at 380 ^{o}C for 200 minutes. The sample was cooled to room temperature and 100 ml distilled water added and then distillation done, followed by titration with 0.25 mol/L HCl until the solution had a slight violet color.

vi) Soil pH was measured in a 1:1 (w/v) soil – water suspension with pH – meter. 10.0 g of air dried and finely sieved soil sample was mixed 10 ml distilled water and shaken for 1 hour. The mixture was immediately analyzed in the digital PH meter and readings taken when the instrument had stabilized.

vii) To determine Cation Exchange Capacity (CEC) at pH 7.0 and Exchangeable Ca, Mg, K, Na, the sample was drained with 1 M ammonium acetate buffered at pH 7. The leachate was examined for replaceable Ca, Mg, K and Na. The sample was additionally drained with 1M KCl, and afterward the leachate utilized for the analysis of the CEC. Components, for example, Na and K were resolved with a flame photometer, while Ca and Mg were assessed with AAS (Atomic Absorption Spectrophotometer). CEC was done by distillation, followed by titration with 0.01 moldm^{-3} HCl (Carroll et al., 1959; Turner et al., 1966).

3.3.5: Kinetics of fertilizer adsorption on zeolitic materials sample EB-GA-02

Standard concentrations of urea fertilizer were prepared through serial dilutions by varying concentrations from 1:2, 1:4, 1:10, 1:20, 1:40, 1:60, 1:80, 1:100 and 1:200 w/v in aqueous medium. They were scanned in triplicates between 200 - 900 nm wavelength on the UV-Visible Spectrophotometer to determine the maximum wavelength of urea and subsequently generate the calibration curves at obtained wavelength of 203 nm, that was used to determine concentrations of other urea solutions.

Sorption studies on effect of concentration variation was done by treating 5.0036 g of EB-GA-02 with 10 ml aqueous solutions each containing 1:2, 1:4, 1:6, 1:8, 1:10, 1:20, 1:40, 1:60, 1:80 and 1:100 w/v concentrations of urea solutions. The mediums were shaken at room temperature for 24 hours each, then centrifuged at 10,000 rpm for 10 minutes. The supernatants were then filtered using 0.22 µm whatman papers and equilibrium concentration determined in triplicates by UV-Visible Spectrophotometer at 203 nm.

Sorption studies on varying shaking times were conducted using 1.00 g of EB-GA-02 suspended in 10 ml urea solution of concentration 1:100 w/v. The mediums were stirred at 300 rpm at room temperature for 15, 30, 45, 60, 75, 90, 100, 120, 140 and 160 minutes each, then centrifuged at 10,000 rpm for 10 minutes after each time interval. The supernatants were then filtered using 0.22 µm whatman papers and equilibrium concentration determined in triplicates by UV-Visible Spectrophotometer at 203 nm. These sorption study methods were modified from Zaranyika and Mandihza, (1999).

3.3.6: Quantitative determination of adsorbed fertilizer

Quantitative determination of equilibrium amount of loaded urea was done by suspending 1.00 g of EB-GA-02 in 10 ml of 1:60 w/v urea solutions. The mediums were shaken at room temperature for varied contact times of 3, 10, 20, 24, 40, 48 and 96 hours, then centrifuged at 10,000 rpm for 10 minutes after each time interval. The supernatant was then filtered using 0.22 µm whatman papers and equilibrium concentration of the remaining urea determined in triplicates by UV-Visible Spectrophotometer at 203 nm. The difference between initial concentration and equilibrium concentration gave the amount loaded in the samples. This step was used in determination of maximum equilibration time to adsorb the most urea into the nanopre spaces.

3.3.7: Loading of fertilizer into zeolitic materials

Done by suspending 20.00 g of EB-GA-02 in 35 ml of 1:60 w/v urea solution. The mediums were shaken using a magnetic stirrer at 300 rpm at room temperature for 24 hours, then centrifuged at 10,000 rpm for 10 minutes. The supernatant was then filtered using 0.22 µm whatman papers and equilibrium concentration of the remaining urea determined in triplicates by UV-Visible Spectrophotometer at 203 nm. These procedures are modified from simple liquid immersion hydrothermal techniques (Chang, 1997). The difference between initial concentration and equilibrium concentration gave the amount of urea loaded in the samples. The resulting urea loaded samples were dried at 60 °C for 3 hours. Similar procedures were repeated for KIK-GA-01, applied as control experiment.

3.3.8: Modelling studies of fertilizer loaded zeolitic materials in water

Done by placing 20.00 g of urea loaded EB-GA-02 in 250 ml separating funnels and 50 ml distilled water infiltrated through at an approximate flow rate of 0.1667 ml/min. 50 ml distilled water was refilled every 24 hours to infiltrate the same samples for 18 days. The filtrates/elutes

were collected daily prior to refilling, filtered using 0.22 µm whatman papers and equilibrium concentration determined in triplicates by UV-Visible Spectrophotometer at 203 nm (Banswal et al., 2006). Blank experiment was conducted using 20.00 g of EB-GA-02, while the control experiments were done using urea treated KIK-GA-01 mixed with untreated EB-GA-02 following similar procedures.

3.3.9: Modelling studies of fertilizer loaded zeolitic materials in soil

20.00 g of urea loaded EB-GA-02 were homogenized with 20.00 g of KIK-GA-01, placed in 250 ml separating funnels and 50 ml distilled water infiltrated through at an approximate flow rate of 0.1667 ml/min. 50 ml distilled water was refilled every 24 hours to infiltrate the same samples for 18 days. The filtrates/elutes were collected daily prior to refilling, filtered using 0.22 µm whatman papers and equilibrium concentration determined in triplicates by UV-Visible Spectrophotometer at 203 nm (Bansiwal et al., 2006). Control experiment was done using 20.00 g of KIK-GA-01 placed in 250 ml separating funnel, followed by similar procedures above.

3.3.10: Agronomic simulation of urea-zeolitic-soil composites

The procedures involved growing the spinach and tomato seeds in their beds to develop seedlings for the actual research work. The seedbeds had well prepared soil incorporated with well-composed organic manure. Spinach seeds were planted about 0.5-inch-deep in separation lines of about 3-4 inches. Transplanting was done after 4-5 weeks when the transplants had about 4-6 mature leaves and well-developed root systems at a spacing of about 3 inches. Similar seedbed planting and transplanting procedures were applied for tomato crops. Individual spinach leaves were harvested at intervals, starting with when they were about 2 inches off the ground. For tomato crops, support staking was done at 3-4 weeks after transplanting, with the first harvest done at 45-55 days after flowering. The research work was conducted in the form of blank experiments, control experiments and actual monitoring experimental set-ups for growing the

spinach and tomatoes separately in pot-setups of about 40 cm diameter and 60 cm depth capacity. The blank set-up had 5000 g soil alone. The control set-up had 5000 g soil and 100 g of urea fertilizer uniformly added to the surface as top-dressing, while the actual monitoring experimental set-up had 5000 g of soil and sample EB-GA-02 loaded with 100 g of urea uniformly top-dressed on the surface. All the crops were grown under prevailing environmental conditions and general practiced crop husbandry, not in a greenhouse.

Data collection involved determination of the concentration of urea in the leachate from the soil at a depth of 30 cm over a two months' period, at 5, 20, 30, 45 and 60 days' intervals. Leachate concentration determinations in triplicates were conducted using UV-Spectrophotometry studies.

3.3.11: Sorption/desorption of Lambda cyhalothrin pesticide on sample EB-GA-02

Standard concentrations of Lambda-cyhalothrin pesticide were prepared through serial dilutions by varying concentrations from 2.0, 4.0, 6.0, 8.0, 10.0, 20.0, 40.0, 60.0, 80.0 and 100.0 ppm in 10 ml aqueous medium dissolved by sonication for 15 minutes. They were scanned between 200-900 nm wavelengths on the UV-Visible Spectrophotometer in triplicates to determine the maximum absorption wavelength of the pesticide, which was obtained at 218 nm. Calibration curves at 218 nm were used to determine concentrations of other pesticide solutions.

Studies on variation of time and concentrations were done by treating 1.00 g of sample EB-GA-02 with 10 ml aqueous solutions each containing 10.0, 20.0, 30.0, 40.0 and 50.0 ppm concentrations of Lambda-cyhalothrin pesticide. The media were shaken using a magnetic stirrer at 300 rpm at room temperature for 15, 30, 45 and 60 minutes each, and then centrifuged at 10,000 rpm for 10 minutes. The supernatants were then filtered using 0.22 µm whatman papers and equilibrium concentration determined in triplicates.

Sorption effects on variation of masses was conducted using 0.10, 0.20, 0.50, 1.0, 1.5, and 2.0 g of sample EB-GA-02 suspended in 10 ml pesticide solution of concentration 50 ppm, shaken for 24 hours and then centrifuged at 10,000 rpm for 10 minutes before determining equilibrium concentrations in triplicates. These procedures modified from Manikandan *et al*., 2014 and Zaranyika *et al*., 1999.

3.3.12: Loading of pesticides into sample EB-GA-02

To load the pesticide into the zeolitic pores, 15 g of sample EB-GA-02 was spiked with 25 ml of 100 ppm Lambda- cyhalothrin pesticide solution, shaken using a magnetic stirrer at 300 rpm at room temperature for 24 hours, then equilibrium concentration of the remaining pesticide determined in triplicates. The difference between initial concentration and equilibrium concentration gave the amount loaded in the samples. The solvent was then slowly evaporated under reduced pressure (0.085 mPa) in water bath at 50 °C for 2 hours using a rotary evaporator. The resulting pesticide loaded sample EB-GA-02 was dried at 100 °C for 24 hours to obtain the pesticide smart delivery samples. Similar procedures were repeated for KIK-GA-01, applied as control experiment.

3.3.13: Batch release kinetics of pesticide loaded zeolitic sample EB-GA-02 in water

Desorption studies were conducted by placing 15 g of pesticide loaded sample EB-GA-02 in 250 ml separating funnels and 50 ml distilled water infiltrated through at an approximate flow rate of 0.1667 ml/min. The 50 ml distilled water was refilled every 24 hours to infiltrate the same samples for 18 days. Modified from Bansiwal *et al*., (2006). The filtrates/elutes were collected daily prior to refilling, filtered using 0.22 µm what man papers and equilibrium concentration determined in triplicates.

3.3.14: Modelling studies of pesticide loaded zeolitic materials in soil

This was done by homogenizing 15 g of pesticide loaded zeolitic materials with 25 g of soil, placed in 250 ml separating funnels and 50 ml distilled water infiltrated through at an approximate

flow rate of 0.1667 ml/min. 50 ml distilled water was refilled every 24 hours to infiltrate the same samples for 18 days, as illustrated in figure 3.6 below. The filtrates/elutes were collected daily prior to refilling, filtered using 0.22 µm whatman papers and equilibrium concentration determined in triplicates by UV-Visible Spectrophotometer at 218 nm. Similar procedures were conducted using pesticide loaded soils samples obtained from Kikuyu area, applied as control experiment.

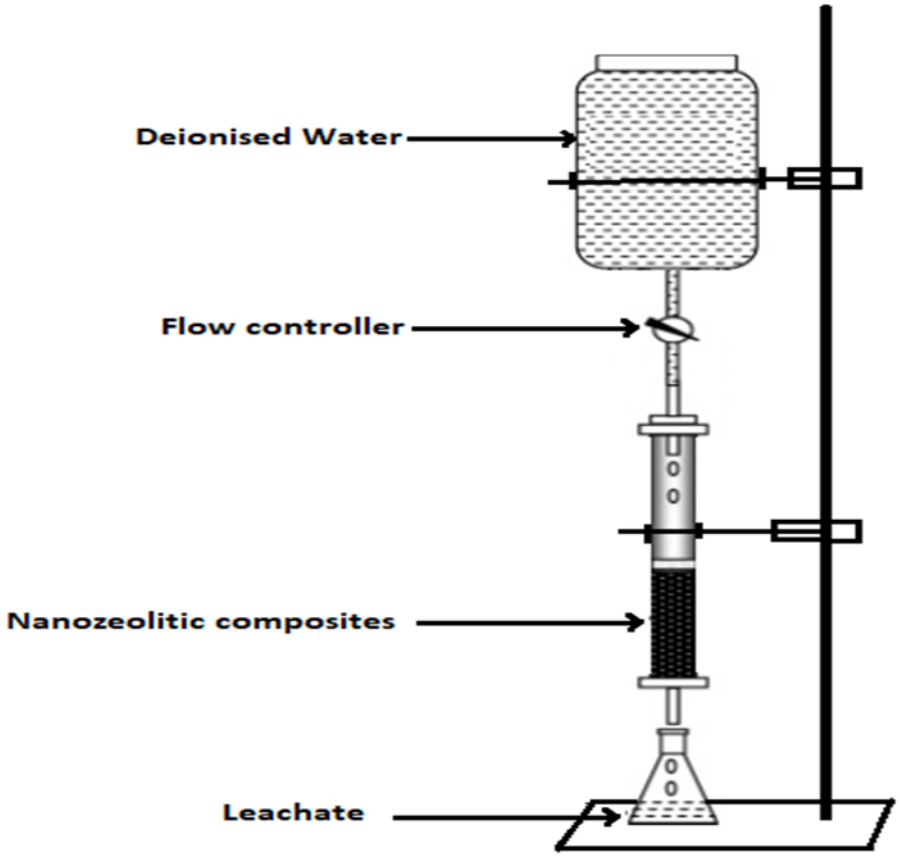

Figure 3.6 Nanozeolitic composite modelling studies illustration

3.3.15: Agronomic simulation of pesticide-zeolitic-soil composites

The initial procedure involved growing the spinach and tomato seeds in their beds to develop seedlings for the actual research work. The seedbeds had well prepared soil incorporated with well-composed organic manure. Spinach seeds were planted about 0.5-inch-deep in separation lines of about 3-4 inches. Transplanting was done after 4-5 weeks when the transplants had about

4-6 mature leaves and well-developed root systems at a spacing of about 3 inches. Similar seedbed planting and transplanting procedures were applied for tomato crops. Individual spinach leaves were harvested at intervals before flowering, starting with when they were about 2 inches off the ground. For tomato crops, support staking was done at 3-4 weeks after transplanting, with the first harvest done at 45-55 days after flowering.

The research work (as illustrated in figure 3.7 below) was conducted in the form of blank experiments, control experiments and actual monitoring experimental set-ups for growing the spinach and tomatoes separately in pot-set-ups of about 40 cm diameter and 60 cm depth capacity. The blank set-up had 5000 g soil alone. The control set-up had 5000 g soil and 100 g of pesticide uniformly added to the surface as top-dressing, while the actual monitoring experimental set-up had 5000 g of soil and sample EB-GA-02 loaded with 100 g of pesticide uniformly spread on the surface. All the crops were grown under prevailing environmental conditions and general practiced crop husbandry, not in a greenhouse. Data collection involved determination of the concentration of the pesticide in the soil at a depth of 30 cm over a two months' period, at 5, 20, 30, 45 and 60 days' intervals. Concentration determinations were conducted in triplicates using UV-Spectrophotometry studies.

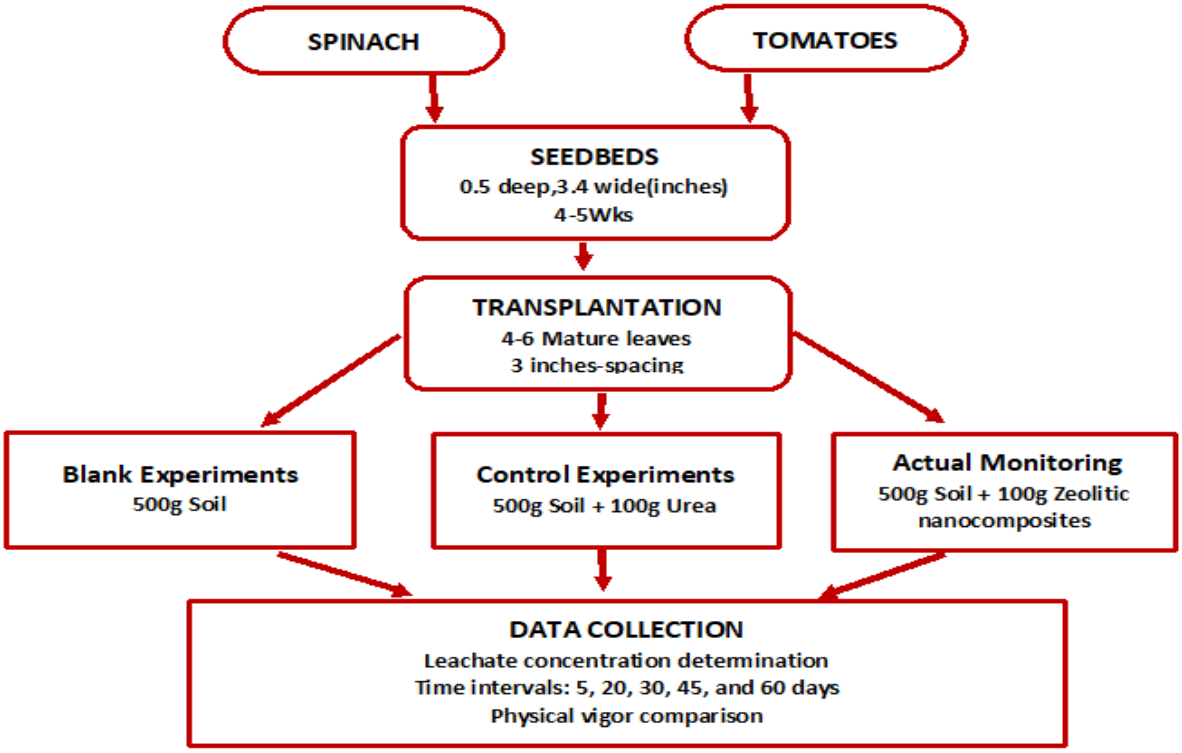

Figure 3.7 Illustration of agronomic zeolitic composite simulation process on spinach and tomatoes

3.3.16: Integrated comparative study of zeolitic smart delivery system

This was carried out alongside the other studies above, in similar two pot-set ups, each having 5000 g of soil, urea loaded samples EB-GA-02 applied as top dressing and pesticide loaded samples EB-GA-02 applied for pest control. Spinach and tomato crops were grown separately in these pots. The other procedures, experimental conditions and data collection methodologies were similar to 3.3.10 to 3.3.15 above.

3.4: Data analysis

This was done through Analysis Of Variance (ANOVA) model using Mitab 19 statistical software.

CHAPTER 4: RESULTS AND DISCUSSION

4.1: Sample characterization

The characterization of samples; ZT-GA-01, EB-GA-02, MG-GA-03, BG-GA-04, NG-GA-05 and EL-GA-06 was done to ascertain their properties and identity relative to the standard commercial zeolites. This would determine their suitability for formulation and application as smart delivery system for urea fertilizer and lambda cyhalothrin pesticide.

4.1.1: X-Ray Diffraction (XRD)

X-ray diffraction analysis of sample ZT-GA-01(commercial zeolites) (Figure 4.1) shows distinct peaks comparable to the ones informed by Treacy *et al*., (2001), having 2θ values of characteristic artificial zeolite A at 7.2°, 10.3°, 12.6°, 16.2°, 21.8°, 24°, 26.2°, 27.2°, 30°, 30.9°, 31.1°, 32.6°, 33.4° and 34.3°.

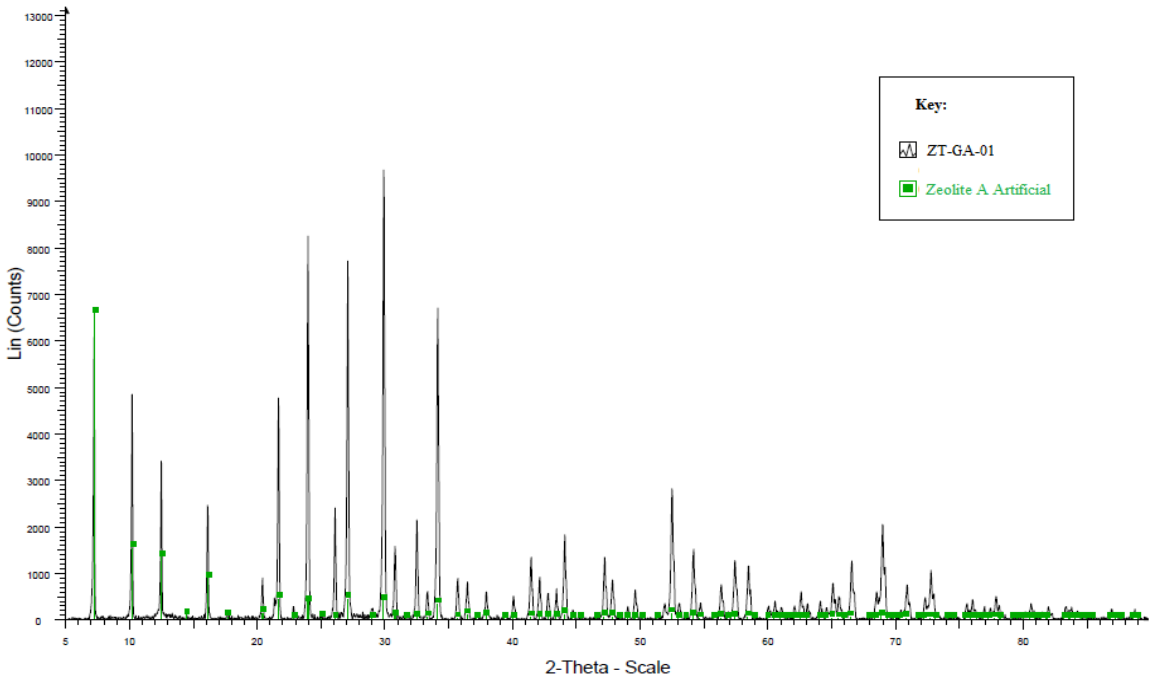

Figure 4. 1 XRD spectra of ZT-GA-01

According to Treacy and Higgins (2001), in their assortment of mimicked XRD powder designs for zeolites, zeolite A Artificial is abbreviated as Linde Type A (LTA), having a chemical composition of $[Na_{96}(H_2O)_{216}][Si_{96}Al_{96}O_{384}]$, crystal data of: a = 24.61Å, b = 24.61Å, c = 24.61Å, α=90º, β=90º, γ=90º and X-ray single refinement (Rw) = 0.04. Other crystal structure parameters of similar 2θ values as those of sample ZT-GA-01 from Figure 4.1 above are summarized in table T4.1 (shown in the appendix), hence the commercial zeolite sample ZT-GA-01 are classified as Zeolite A, with microcrystalline particle diffraction pattern.

The other natural rock samples EB-GA-02, MG-GA-03, BG-GA-04 and NG-GA-05 were analyzed to determine their similarity with sample ZT-GA-01 above. These rocks were characterized while in their natural state after calcination, without any advanced purification process, hence this explains the presence of nonuniform peaks and additional mineral peaks detected.

XRD characterization of zeolitic sample EB-GA-02 gave the characteristic spectrum shown by Figure 4.2 below, the corresponding diffraction parameter data summarized in Table 4.1.

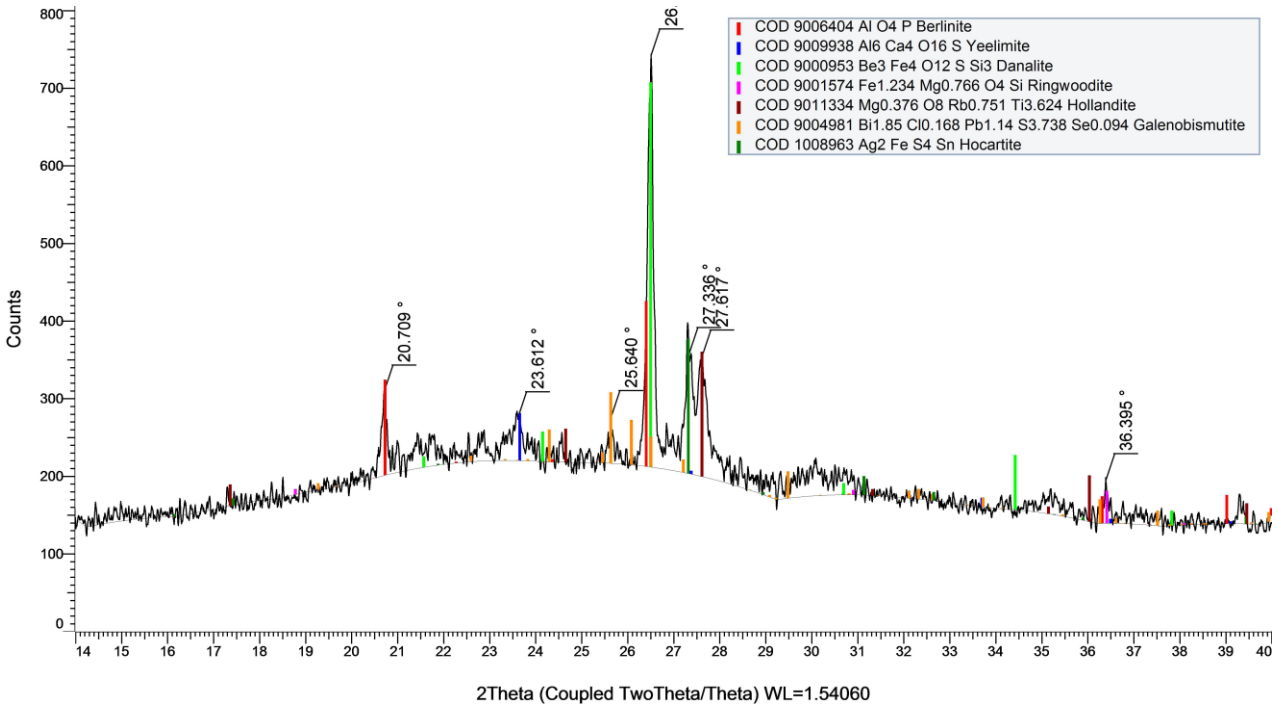

Figure 4. 2 XRD spectra of EB-GA-02

Table 4. 1 Diffraction parameter data for EB-GA-02

Index	Angle	d Value	Rel. Intensity
2	23.612 °	3.76492 Å	10.3 %
7	36.395 °	2.46657 Å	10.6 %
3	25.640 °	3.47156 Å	11.3 %
1	20.709 °	4.28560 Å	20.4 %
5	27.336 °	3.25990 Å	29.1 %
6	27.617 °	3.22740 Å	29.2 %
4	26.512 °	3.35935 Å	100.0 %

Donalite, Hollandite and Berlinite minerals were found to be the most predominant in this sample at 41.2 %, 21.6 % and 14.3 % respectively. For each of the minerals present, their chemical formulae were determined as recorded in Table 4.2 below.

Table 4. 2 Formula and percentage composition

Index	Compound Name	Formula	Pattern Number	I/Ic DB	S-Q
5	Hollandite	$Mg_{0.376}O_8Rb_{0.751}Ti_{3.624}$	COD 9011334	3.190	21.6 %
4	Ringwoodite	$Fe_{1.234}Mg_{0.766}O_4Si$	COD 9001574	3.610	5.0 %
6	Galenobismutite	$Bi_{1.85}Cl_{0.168}Pb_{1.14}S_{3.738}Se_{0.094}$	COD 9004981	7.580	5.2 %
3	Danalite	$Be_3Fe_4O_{12}SSi_3$	COD 9000953	5.170	41.2 %
2	Yeelimite	$Al_6Ca_4O_{16}S$	COD 9009938	3.630	7.2 %
1	Berlinite	AlO_4P	COD 9006404	6.390	14.3 %
7	Hocartite	Ag_2FeS_4Sn	COD 1008963	13.790	5.4 %

Figure 4.3 and Table 4.3 below indicates XRD information generated by sample MG-GA-03.

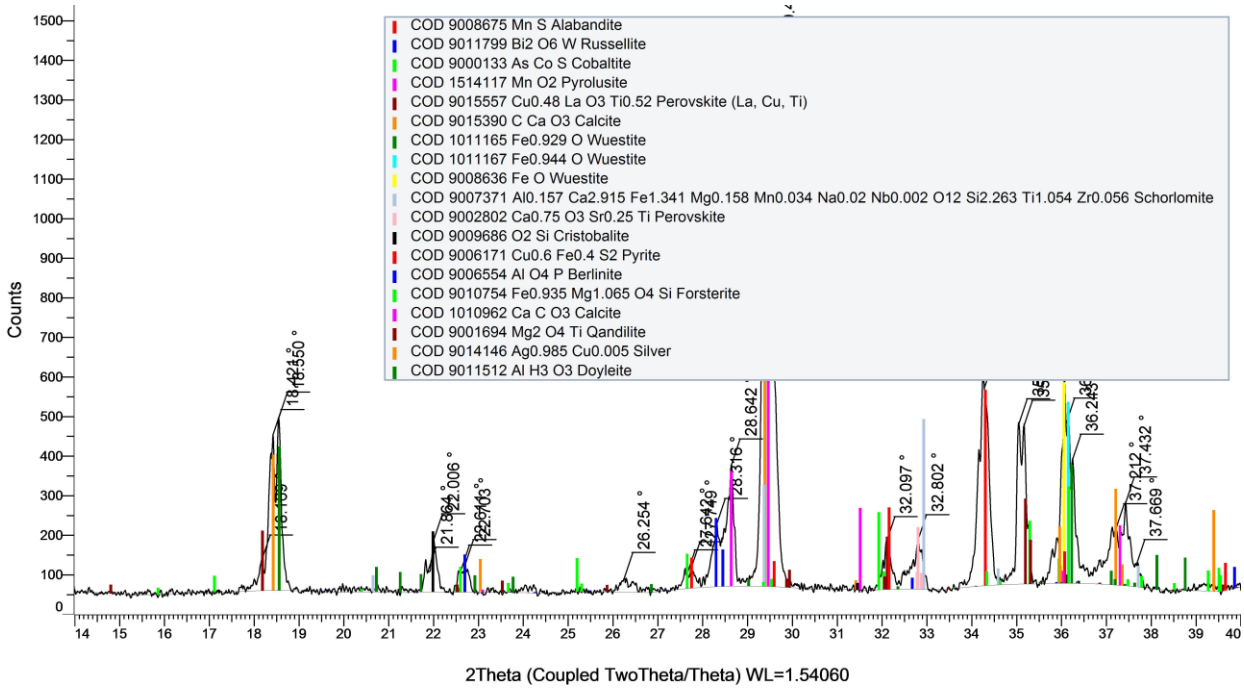

Figure 4. 3 XRD spectra of MG-GA-03

Table 4. 3 Diffraction parameter data for MG-GA-03

Index	Angle	d Value	Rel. Intensity
9	27.642 °	3.22445 Å	2.5 %
8	26.254 °	3.39178 Å	2.6 %
4	21.864 °	4.06184 Å	3.6 %
10	27.749 °	3.21234 Å	4.0 %
6	22.611 °	3.92925 Å	4.1 %
23	37.669 °	2.38604 Å	4.1 %
7	22.703 °	3.91353 Å	5.1 %
1	18.169 °	4.87861 Å	5.7 %
14	32.097 °	2.78635 Å	9.0 %
15	32.802 °	2.72811 Å	9.3 %
5	22.006 °	4.03586 Å	10.0 %
21	37.212 °	2.41427 Å	10.6 %
11	28.316 °	3.14932 Å	11.9 %
22	37.432 °	2.40060 Å	15.8 %
12	28.642 °	3.11411 Å	23.1 %
20	36.243 °	2.47656 Å	23.5 %
2	18.421 °	4.81249 Å	29.5 %
18	35.163 °	2.55015 Å	30.0 %
19	36.102 °	2.48596 Å	30.3 %
17	35.049 °	2.55814 Å	30.4 %
3	18.550 °	4.77923 Å	32.8 %
16	34.282 °	2.61362 Å	37.5 %
13	29.484°	3.02711 Å	100.0 %

This sample was mainly of trona origin composed of mineral salt calcite. Table 4.4 below gives the proportional minerals found with their respective formulae.

Table 4. 4 Formula and percentage composition

Index	Compound Name	Formula	Pattern Number	I/Ic DB	S-Q
12	Cristobalite	SiO_2	COD 9009686	5.510	1.4 %
1	Alabandite	MnS	COD 9008675	7.300	3.4 %
4	Pyrolusite	MnO_2	COD 1514117	4.740	3.1 %
17	Qandilite	Mg_2O_4Ti	COD 9001694	1.670	6.5 %
8	Wuestite	$Fe_{0.944}O$	COD 1011167	5.750	6.3 %
15	Forsterite	$Fe_{0.935}Mg_{1.065}O_4Si$	COD 9010754	1.250	9.9 %
7	Wuestite	$Fe_{0.929}O$	COD 1011165	5.670	4.2 %
9	Wuestite	FeO	COD 9008636	6.030	6.2 %
13	Pyrite	$Cu_{0.6}Fe_{0.4}S_2$	COD 9006171	3.920	2.7 %
5	Perovskite	$Cu_{0.48}LaO_3Ti_{0.52}$	COD 9015557	9.330	0.7 %
11	Perovskite	$Ca_{0.75}O_3Sr_{0.25}Ti$	COD 9002802	3.700	2.1 %
16	Calcite	$CaCO_3$	COD 1010962	3.820	15.4 %
2	Russellite	Bi_2O_6W	COD 9011799	25.290	0.3 %
3	Cobaltite	AsCoS	COD 9000133	3.430	1.3 %
10	Schorlomite	$Al_{0.157}Ca_{2.915}Fe_{1.341}Mg_{0.158}Mn_{0.034}$ $Na_{0.02}Nb_{0.002}O_{12}Si_{2.263}Ti_{1.054}Zr_{0.056}$	COD 9007371	2.470	8.8 %
14	Berlinite	AlO_4P	COD 9006554	2.540	1.9 %
19	Doyleite	AlH_3O_3	COD 9011512	1.890	9.7 %
18	Silver	$Ag_{0.985}Cu_{0.005}$	COD 9014146	15.930	1.1 %

For zeolitic sample BG-GA-04, it's XRD characterization spectrum is shown by Figure 4.4 and the equivalent index considerations recorded in Table 4.5 below.

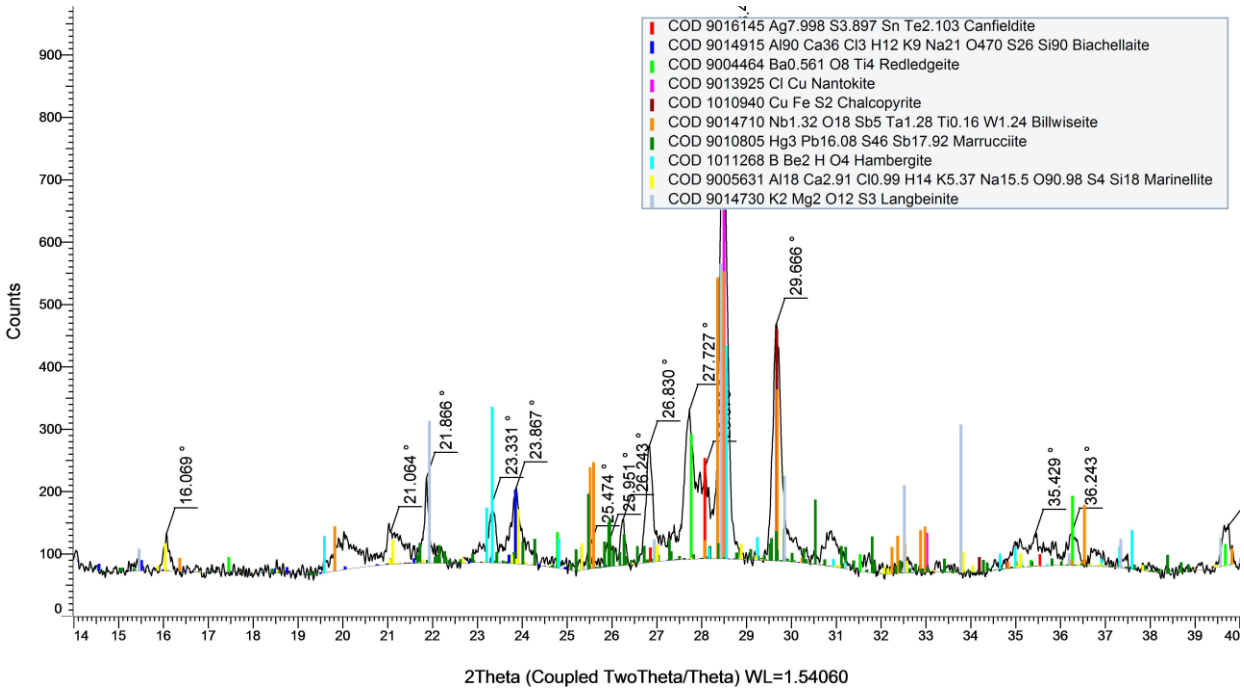

Figure 4. 4 XRD spectra of BG-GA-04

Table 4. 5 Diffraction parameter data for BG-GA-04

Index	Angle	d Value	Rel. Intensity
6	25.474 °	3.49375 Å	3.6 %
7	25.951 °	3.43064 Å	5.4 %
14	35.429 °	2.53163 Å	6.4 %
15	36.243 °	2.47657 Å	6.4 %
2	21.064 °	4.21417 Å	6.5 %
16	39.696 °	2.26875 Å	7.5 %
1	16.069 °	5.51115 Å	7.5 %
8	26.243 °	3.39313 Å	9.1 %
4	23.331 °	3.80965 Å	12.0 %
5	23.867 °	3.72528 Å	15.4 %
3	21.866 °	4.06139 Å	17.1 %
11	28.079 °	3.17531 Å	18.5 %
9	26.830 °	3.32025 Å	23.3 %
10	27.728 °	3.21476 Å	30.0 %
13	29.666 °	3.00895 Å	47.7 %
12	28.490 °	3.13040 Å	100.0 %

This sample was mainly found to contain Hambergite and Langbeinite minerals at 42.5% and 12.3% respectfully, which are accessory minerals in granite pegmatites.

Formulae and composition of all the other minerals characterized in this sample are recorded in Table 4.6 below.

Table 4. 6 Formula and percentage composition

Index	Compound Name	Formula	Pattern Number	I/Ic DB	S-Q
6	Billwiseite	$Nb_{1.32}O_{18}Sb_5Ta_{1.28}Ti_{0.16}W_{1.24}$	COD 9014710	5.380	6.8 %
10	Langbeinite	$K_2Mg_2O_{12}S_3$	COD 9014730	3.050	12.3 %
7	Marrucciite	$Hg_3Pb_{16.08}S_{46}Sb_{17.92}$	COD 9010805	1.730	5.6 %
5	Chalcopyrite	$CuFeS_2$	COD 1010940	9.270	3.2 %
4	Nantokite	ClCu	COD 9013925	9.110	6.9 %
3	Redledgeite	$Ba_{0.561}O_8Ti_4$	COD 9004464	3.430	4.7 %
8	Hambergite	BBe_2HO_4	COD 1011268	0.640	42.5 %
2	Biachellaite	$Al_{90}Ca_{36}Cl_3H_{12}K_9Na_{21}O_{470}S_{26}Si_{90}$	COD 9014915	3.760	6.3 %
9	Marinellite	$Al_{18}Ca_{2.91}Cl_{0.99}H_{14}K_{5.37}Na_{15.5}O_{90.98}S_4Si_{18}$	COD 9005631	0.720	9.7 %
1	Canfieldite	$Ag_{7.998}S_{3.897}SnTe_{2.103}$	COD 9016145	6.490	2.0 %

Analysis of zeolitic sample NG-GA-05 gave the spectrum in Figure 4.5 and parameters recorded in Table 4.7 respectfully

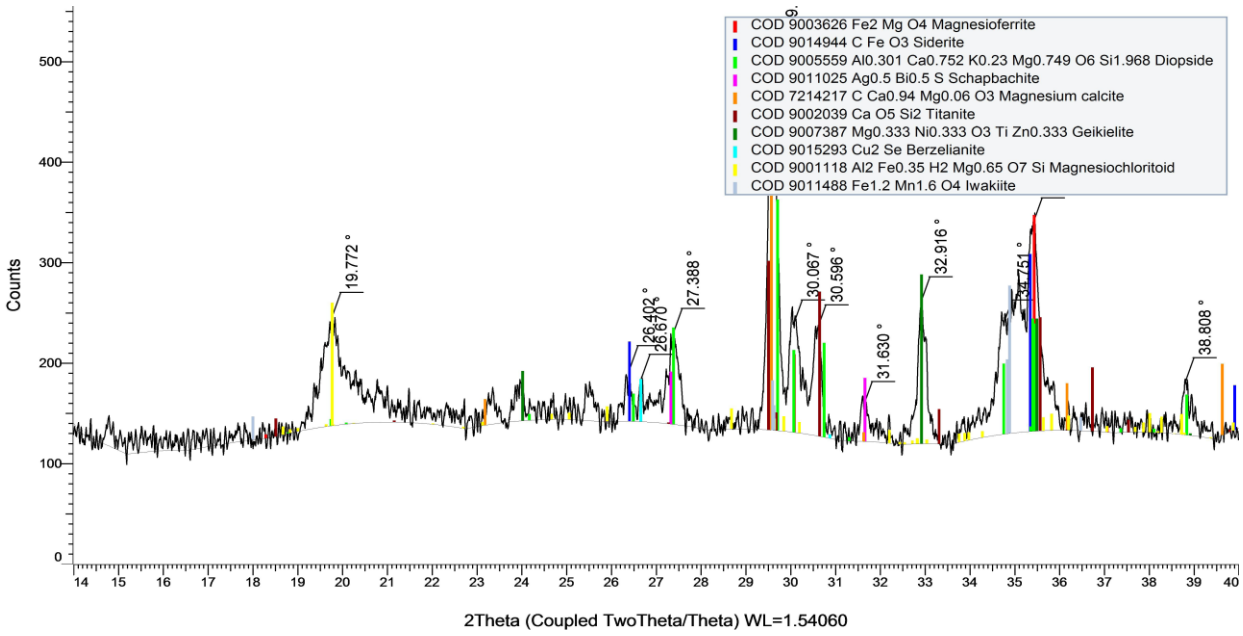

Figure 4. 5 XRD spectra of NG-GA-05

Table 4. 7 Diffraction parameter data for NG-GA-05

Index	Angle	d Value	Rel. Intensity
8	31.630 °	2.82646 Å	9.5 %
3	26.670 °	3.33975 Å	11.5 %
2	26.402 °	3.37305 Å	13.7 %
12	38.808 °	2.31857 Å	14.1 %
4	27.388 °	3.25379 Å	24.3 %
7	30.596 °	2.91955 Å	28.4 %
6	30.067 °	2.96974 Å	28.7 %
1	19.772 °	4.48661 Å	28.9 %
10	34.751 °	2.57940 Å	29.2 %
9	32.916 °	2.71887 Å	37.9 %
11	35.421 °	2.53217 Å	55.4 %
5	29.588 °	3.01673 Å	100.0 %

This sample was found to contain Diopside and Titanite minerals in larger quantities. The formula and percentage composition of each mineral present is recorded in Table 4.8 below.

Table 4. 8 Minerals and data for NG-GA-05

Index	Compound Name	Formula	Pattern Number	I/Ic DB	S-Q
7	Geikielite	$Mg_{0.333}Ni_{0.333}O_3Ti$	COD 9007387	3.240 6	6.8 %
1	Magnesioferrite	Fe_2MgO_4	COD 9003626	5.130	5.5 %
10	Iwakiite	$Fe_{1.2}Mn_{1.6}O_4$	COD 9011488	3.400	5.7 %
8	Berzelianite	Cu_2Se	COD 9015293	6.080	1.4 %
6	Titanite	CaO_5Si_2	COD 9002039	1.130	19.6 %
2	Siderite	$CFeO_3$	COD 9014944	3.820	6.1 %
5	Magnesium calcite	$CCa_{0.94}Mg_{0.06}O_3$	COD 7214217	3.420	13.3 %
9	Magnesiochloritoi	$Al_2Fe_{0.35}H_2Mg_{0.65}O_7$	COD 9001118	1.140	14.1 %
3	Diopside	$Al_{0.301}Ca_{0.752}K_{0.23}$	COD 9005559	1.130	26.8 %
4	Schapbachite	$Ag_{0.5}Bi_{0.5}S$	COD 9011025	15.420	0.5 %

XRD characterization of zeolitic sample EL-GA-06 generated the spectrum and diffraction parameters recorded in Figure 4.6 and Table 4.9 below.

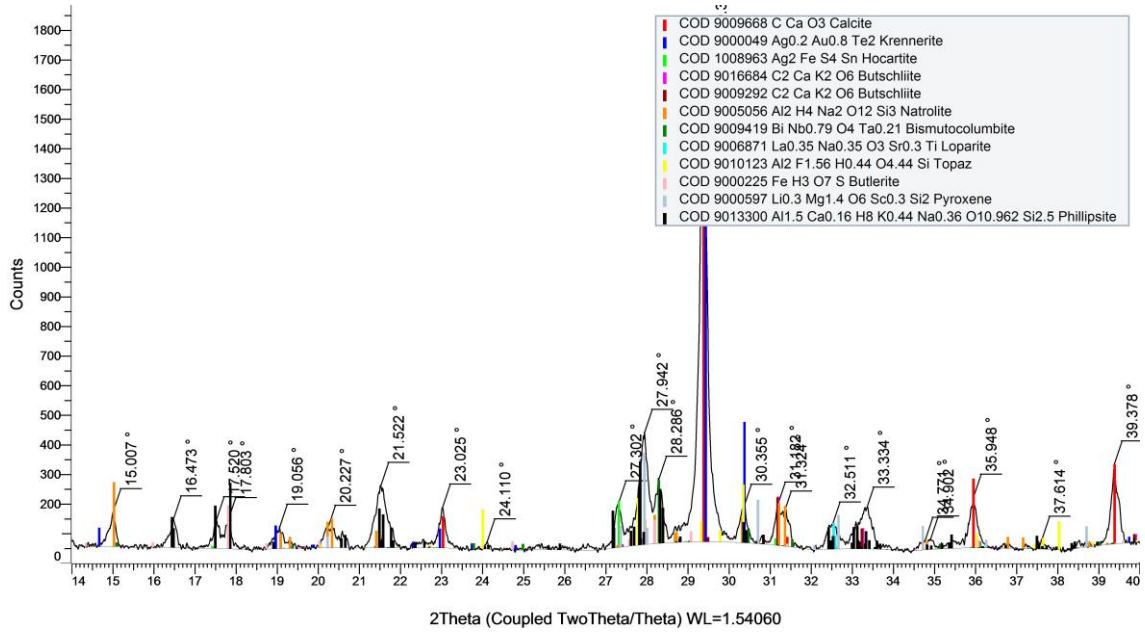

Figure 4. 6 XRD spectra of EL-GA-06

Table 4. 9 Diffraction parameter data for EL-GA-06

Index	Angle	d Value	Rel. Intensity
9	24.110 °	3.68834 Å	1.4 %
19	34.771 °	2.57795 Å	1.9 %
22	37.614 °	2.38942 Å	2.0 %
20	34.902 °	2.56864 Å	2.1 %
6	20.227 °	4.38665 Å	3.9 %
5	19.056 °	4.65366 Å	4.3 %
17	32.511 °	2.75183 Å	4.9 %
4	17.803 °	4.97802 Å	5.7 %
2	16.473 °	5.37702 Å	5.8 %
3	17.520 °	5.05795 Å	5.8 %
16	31.324 °	2.85333 Å	6.5 %
1	15.007 °	5.89877 Å	7.1 %
14	30.355 °	2.94225 Å	7.2 %
18	33.334 °	2.68575 Å	7.9 %
15	31.182 °	2.86603 Å	8.2 %
8	23.025 °	3.85961 Å	8.3 %
10	27.302 °	3.26389 Å	8.9 %
21	35.948 °	2.49625 Å	10.4 %
7	21.522 °	4.12562 Å	12.8 %
12	28.286 °	3.15253 Å	13.2 %
23	39.378 °	2.28632 Å	16.4 %
11	27.942 °	3.19061 Å	23.1 %
13	29.374 °	3.03822 Å	100.0 %

Mineral composition of this sample indicated presence of natural zeolites like Phillipsite, Natrolite and Krennerite.

Sample EL-GA-06 was found to be natural zeolites of Phillipsite nature. There was presence of other mineral impurities like calcite and topaz as specified in Table 4.10 beneath.

Table 4. 10 Formula and percentage composition

Compound Name	Formula	Pattern Number	S-Q
Phillipsite	$Al_{1.5}Ca_{0.16}H_8K_{0.44}Na_{0.36}O_{10.962}Si_{2.5}$	COD9013300	31.7%
Natrolite	$Al_2H_4Na_2O_{12}Si_3$	COD9005056	11.0%
Bismutocolumbit	$BiNb_{0.79}O_4Ta_{0.21}$	COD9009419	0.6%
Loparite	$La_{0.35}O_3Sr_{0.3}tI$	COD9006871	0.8%
Topaz	$Al_2F_{1.56}H_{0.44}O_{4.44}Si$	COD9010123	12.2%
Butlerite	FeH_3O_7S	COD9000225	2.3%
Pyroxene	$Li_{0.3}Mg_{1.4}O_6Sc_{0.3}Si_2$	COD9000597	10.8%
Butschliite	$C_2CaK_2O_6$	COD9009292	2.5%
Hocartite	Ag_2FeS_4Sn	COD1008963	0.5%
Krennerite	$Ag_{0.2}Au_{0.8}Te_2$	COD9000049	3.6%
Calcite	$CCaO_3$	COD9009668	21.2%

Generally, X-ray diffraction patterns obtained for zeolites were affected by a number of factors. These included phase purity, trepidations in the framework assembly, sparkler morphology, further framework materials, setting and occupation of cation sites, as well as crystallite size (Kokotailo *et al*., 1995). Patterns produced by commercial zeolite samples showed very distinct peaks. This was due to its high level of purity. Natural zeolitic materials or such rocks contained amorphous materials and less stable components (Kokotailo *et al*., 1995) like organic matter and other impurities; hence their patterns produced indicated broader and masked peaks. Purification of such samples by calcination and alkali hydrothermal treatment (Mousa *et al*., 2014), may improve the distinctiveness and intensity of their peaks.

4.1.2: Energy Dispersive X-Ray Spectroscopy (EDX)

This was done to characterize the samples in terms of elemental oxides composition. Zeolite A which was commercially acquired contained mainly oxides of Aluminium and Silicon at 56.0 % and 44.0 % respectively, as shown by Table 4.11, with its corresponding spectrum (Figure 4.7)

below. This was used as standard reference in Energy Dispersive characterization of the other samples.

Table 4. 11 EDX quantitative results of sample ZT-GA-01

Analyte	Result %	Standard Deviation	Line	Intensity (cps/uA)
Al_2O_3	56.368	1.335	AlKα	0.0721
SiO_2	43.632	0.398	SiKα	0.4315

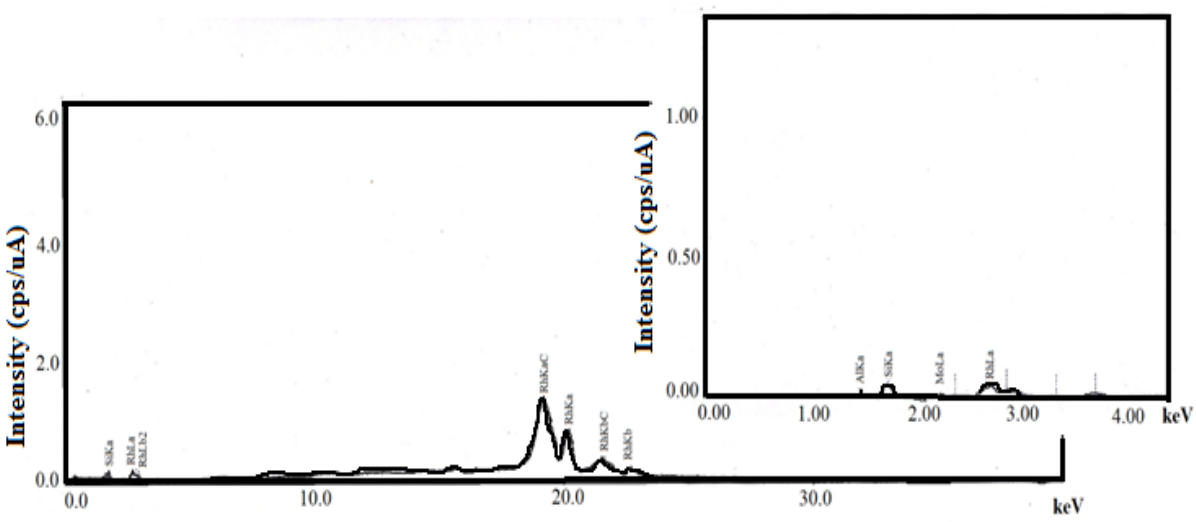

Figure 4. 7 EDX Spectra of sample ZT-GA-01

Characterization of sample EB-GA-02 indicated oxides of Aluminium and Silicon at 18.8 % and 37.4 % respectively, alongside other oxides like of Fe and K as indicated in Table 4.12 below. Multiple peaks corresponding to the present elements are illustrated by the spectrum in Figure 4.8 below.

Table 4. 12 EDX quantitative results of sample EB-GA-02

Analyte	Result %	Standard Deviation	Line	Intensity (cps/ uA)
SiO_2	37.410	0.433	SiKα	0.7178
Fe_2O_3	21.389	0.069	FeKα	116.996
K_2O	20.671	0.149	K Kα	1.8806
Al_2O_3	18.764	1.649	AlKα	0.0294
ZrO_2	0.609	0.004	ZrKa	29.8216
MnO	0.585	0.014	MnKα	2.8732
CaO	0.194	0.033	CaKα	0.2792
NbO	0.100	0.002	NbKα	5.9555
SO_3	0.075	0.004	S Kα	0.0746
Y_2O_3	0.074	0.002	Y Kα	3.6852
ZnO	0.074	0.003	ZnKα	1.6514
Rb_2O	0.057	0.002	RbKα	2.8905

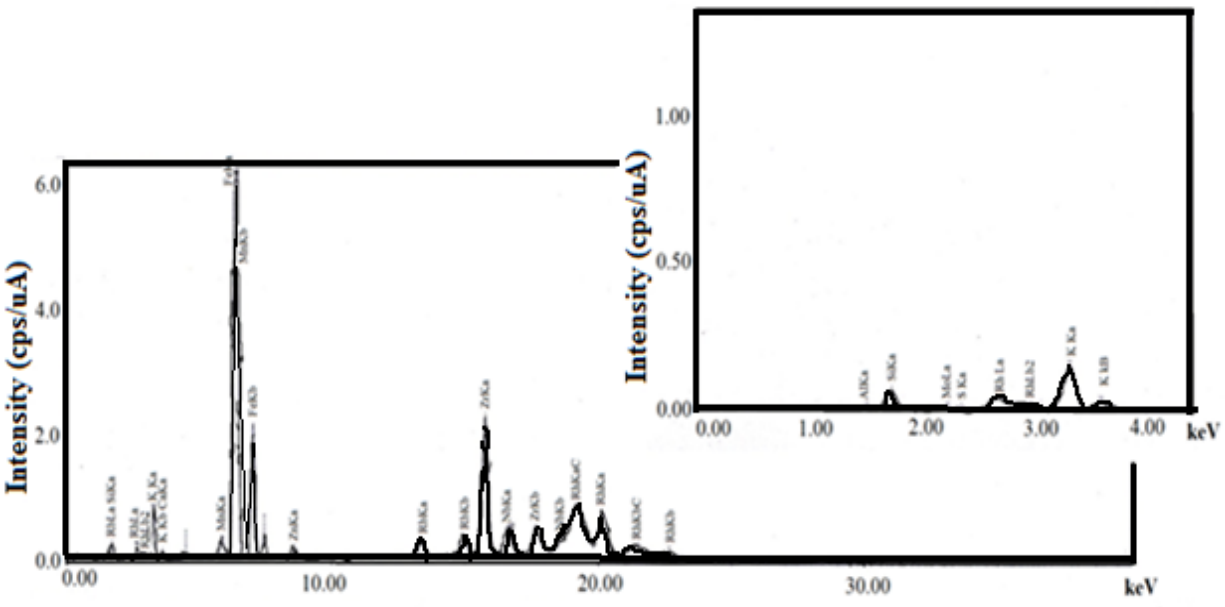

Figure 4. 8 EDX Spectra of sample EB-GA-02

Sample MG-GA-03 lacked Aluminium composition, only having 34.8 % silicon oxide and the rest as oxides of K and Fe. This is shown in Table 4.13, alongside its continuum in Figure 4.9 below.

Table 4. 13 EDX quantitative results of sample MG-GA-03

Analyte	Result %	Standard Deviation	Line	Intensity (cps/ uA)
K_2O	34.999	2.807	KKα	0.4880
SiO_2	34.770	1.152	SiKα	0.0419
Fe_2O_3	30.231	0.399	FeKα	7.3434

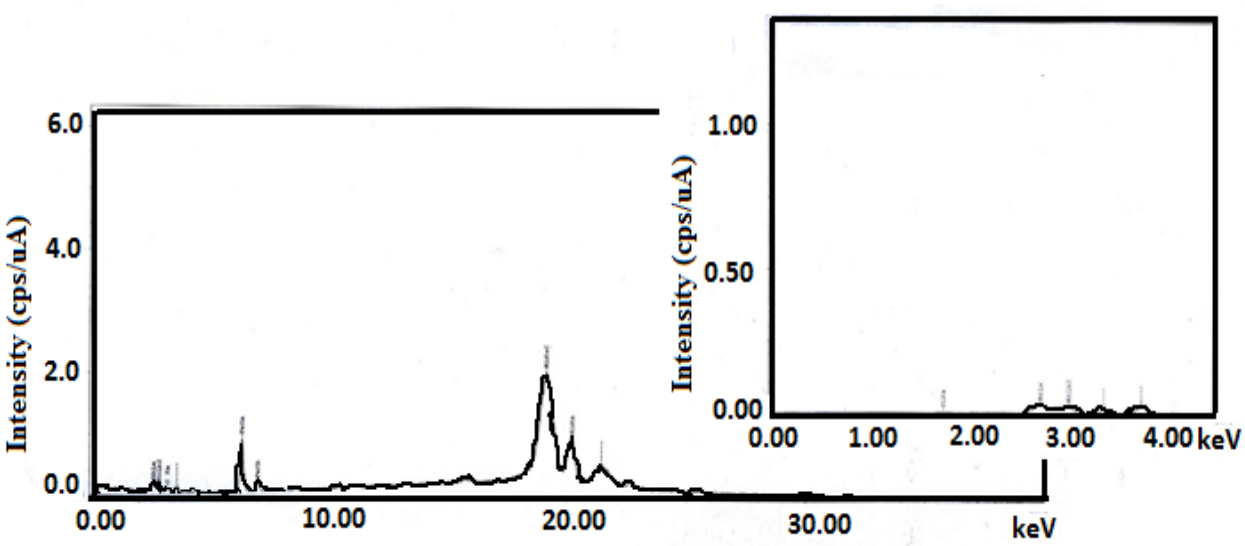

Figure 4. 9 EDX Spectra of sample MG-GA-03

Similarly, sample BG-GA-04 lacked Aluminium composition (Table 4.14) although it had multiple of oxides of other elements like Fe, Ca, K, Mn and Nb, with oxides of silicon forming 22.000 %. The corresponding spectrum obtained for sample BG-GA-04 is shown by Figure 4.10 below.

Table 4. 14 EDX quantitative results of sample BG-GA-04

Analyte	Result %	Standard Deviation	Line	Intensity (cps/ uA)
CaO	35.747	0.092	CaKα	12.7479
Fe_2O_3	23.037	0.092	FeKα	54.5106
SiO_2	22.336	0.388	SiKα	0.3129
K_2O	15.137	0.153	KKα	1.0185
TiO_2	2.461	0.049	TiKα	2.6847
MnO	1.021	0.024	MnKα	2.1520
SrO	0.220	0.003	SrKα	5.2527
NbO	0.040	0.002	NbKα	1.1270

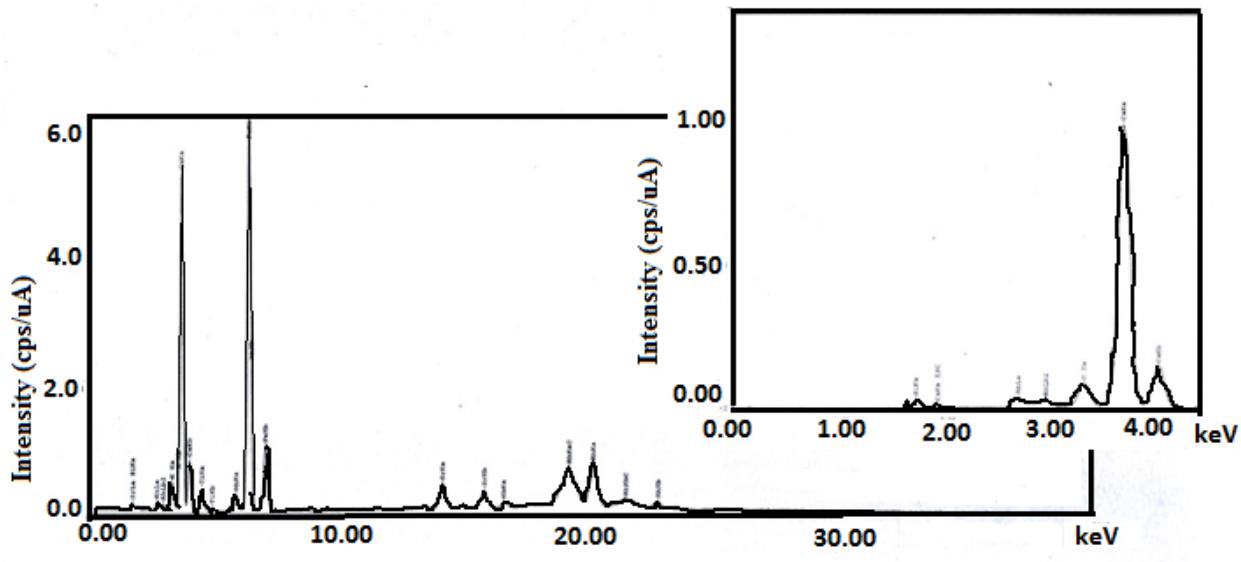

Figure 4. 10 EDX Spectra of sample BG-GA-04

On the hand, EDX characterization of sample NG-GA-05 gave composition of 31.9 % for oxide of Silicon. Other elemental oxides present included Fe, Ca, Ti, K, Mn and V. No oxide of Aluminium was present as shown by Table 4.15 below, alongside its matching spectrum in Figure 4.11 below.

Table 4. 15 EDX quantitative results of sample NG-GA-05

Analyte	Result %	Standard Deviation	Line	Intensity (cps/ uA)
Fe_2O_3	46.765	0.139	FeKα	125.7086
SiO_2	31.884	0.562	SiKα	0.3230
CaO	9.911	0.048	CaKα	3.9287
TiO_2	4.446	0.057	TiKα	7.4052
K_2O	4.239	0.104	KKα	0.2312
MnO	1.558	0.029	MnKα	3.9865
SrO	0.618	0.007	SrKα	10.9825
ZrO_2	0.286	0.006	ZrKα	4.9462
V_2O_5	0.107	0.027	VKα	0.3446
NbO	0.107	0.004	NbKα	2.2200

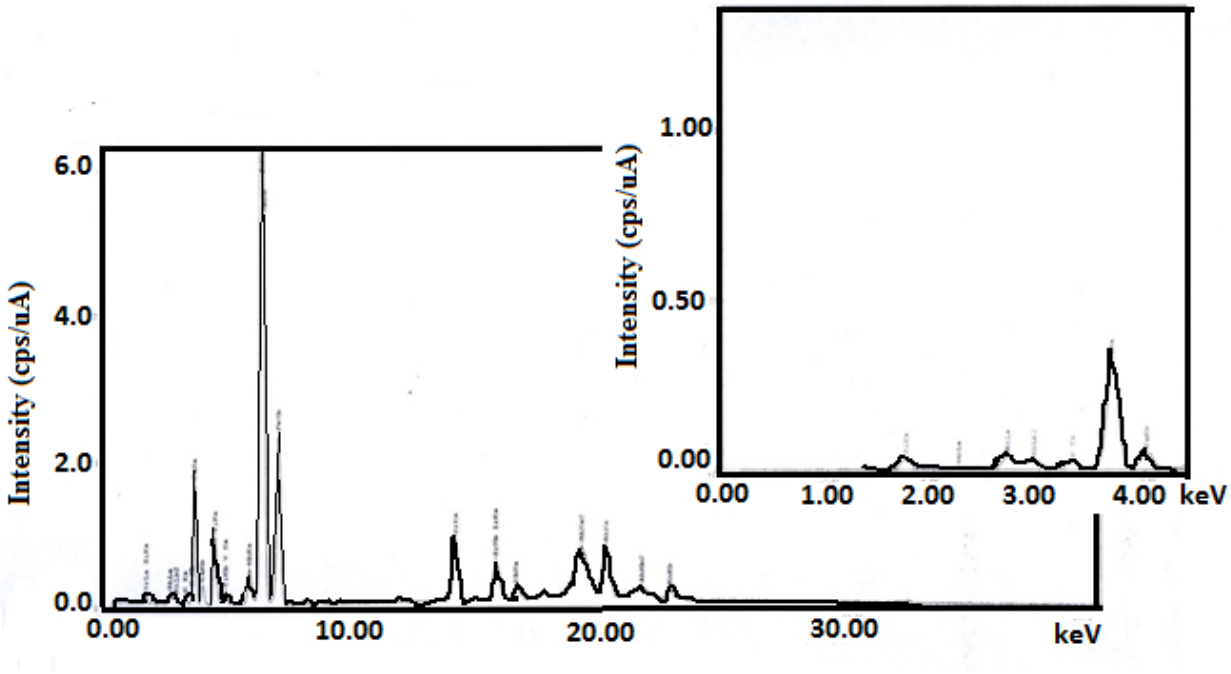

Figure 4. 11 EDX Spectra of sample NG-GA-05

Lastly, analysis of sample EL-GA-06 indicated 15.5% and 35.7% oxides of Aluminium and Silicon respectively (Table 4.16 and Figure 4.12 below). In addition, this sample contained other elemental oxides like K, Fe, Ca, Ti and Mn.

Table 4. 16 DX quantitative results of sample EL-GA-06

Analyte	Result %	Standard Deviation	Line	Intensity (cps/ uA)
SiO_2	35.682	0.372	SiKα	1.0601
K_2O	22.851	0.139	KKα	3.1103
Fe_2O_3	17.026	0.050	FeKα	122.7794
Al_2O_3	15.487	1.338	AlKα	0.0364
CaO	5.429	0.030	CaKα	3.9104
TiO_2	1.670	0.029	TiKα	5.4706
P_2O_5	1.133	0.105	PKα	0.0438
MnO	0.415	0.012	MnKα	2.6528
SrO	0.113	0.002	SrKα	8.4486
V_2O_5	0.087	0.015	VKα	0.3222
CuO	0.056	0.002	CuKα	1.5753
Rb_2O	0.028	0.001	RbKα	2.1151
ZrO_2	0.024	0.001	ZrKα	1.7712

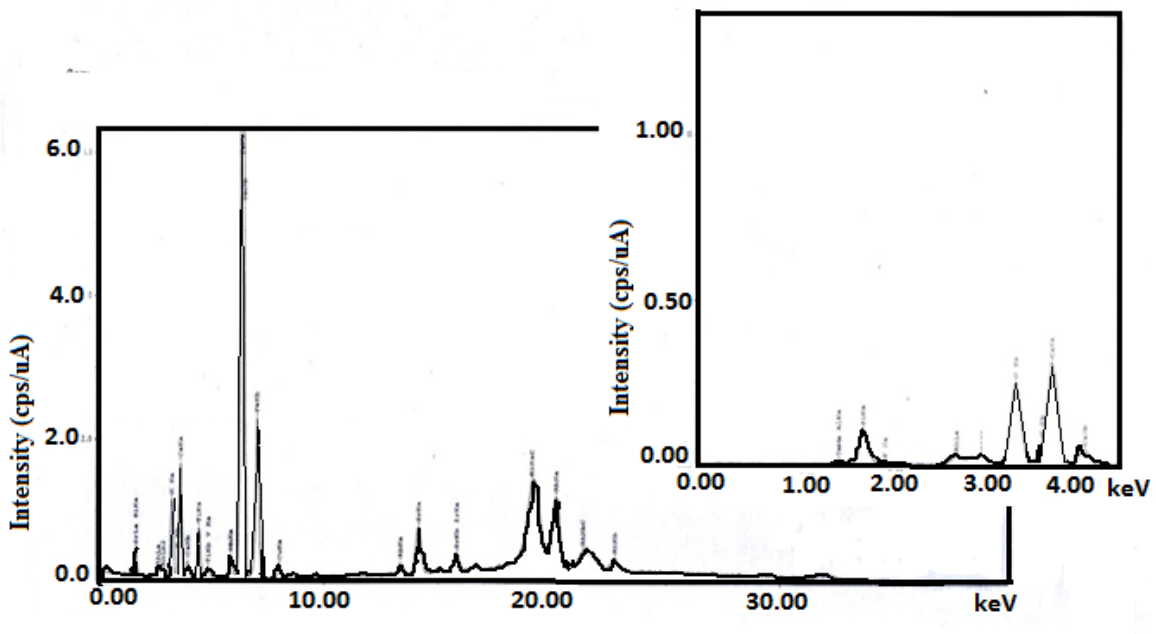

Figure 4. 12 EDX Spectra of sample EL-GA-06

Sample EL-GA-06 compares well to Zeolite A of the commercial type (ZT-GA-01), which was the standard reference, though limited by the accessed deposit quantities as discussed before. Therefore, Energy Dispersive Spectroscopy characterization of the other natural rocks in their raw form indicates a relatively better similarity of sample EB-GA-02, as the second preference, because of its Aluminum and Silicon oxide content which is also found in sample ZT-GA-01. The standard ZT-GA-01 had oxide composition of Al at 56.4 % with Kα at 0.0721 cps/µA intensity and Si at 43.6 % with Kα at 0.4315 cps/µA. Comparatively, EB-GA-02 had oxide

composition of Al at 18.8 % with Kα at 0.0294 cps/µA and Si 37.4 % with Kα at 0.7178 cps/µA. No other remaining natural rock sample had Al Kα composition intensity, besides EL-GA-06. Deposits of sample EB-GA-02 were found in large quantities which could sustain all the research objectives.

4.1.3: Fourier-Transform Infrared Spectroscopy

Results of Infrared spectra of the zeolitic samples ZT-GA-01, EB-GA-02, MG-GA-03, BG-GA-04 and NG-GA-05 showing some of the assigned peaks are presented in Table 4.17 below. Their corresponding distinct spectrums are represented by Figure 4.13 to Figure 4.17 below.

Table 4. 17 Infrared band positions of studied zeolitic materials

Wavenumbers (cm^{-1})					Assignments
ZT-GA-01	EB-GA-02	MG-GA-03	BG-GA-04	NG-GA-05	
3471.87	3421.72	3421.72	3421.72	3444.87	H-O-H Stretching of absorbed water
-	-	2924.09	2924.09	2924.09	C-H Stretching
2357.01	2360.87	2360.87	2360.87	2360.87	H-O-H overtone in plane bending
1654.92	1635.64	1774.51	1774.54	-	H-O-H Bending of water
-	-	1438.90	1438.90	1435.04	C-H Stretching
-	-	1033.85	1033.85	1037.70	Si-O Asymmetric stretch for internal tetrahedral
-	-	875.68	875.68	-	OH Deformation linked to $2Al^{3-}$
-	786.96	702.09	702.09	775.38	Si-O quartz
663.51	-	-	-	-	Si-O-Si Bending
-	447.49	-	-	-	Si-O-Si Bending for internal tetrahedral

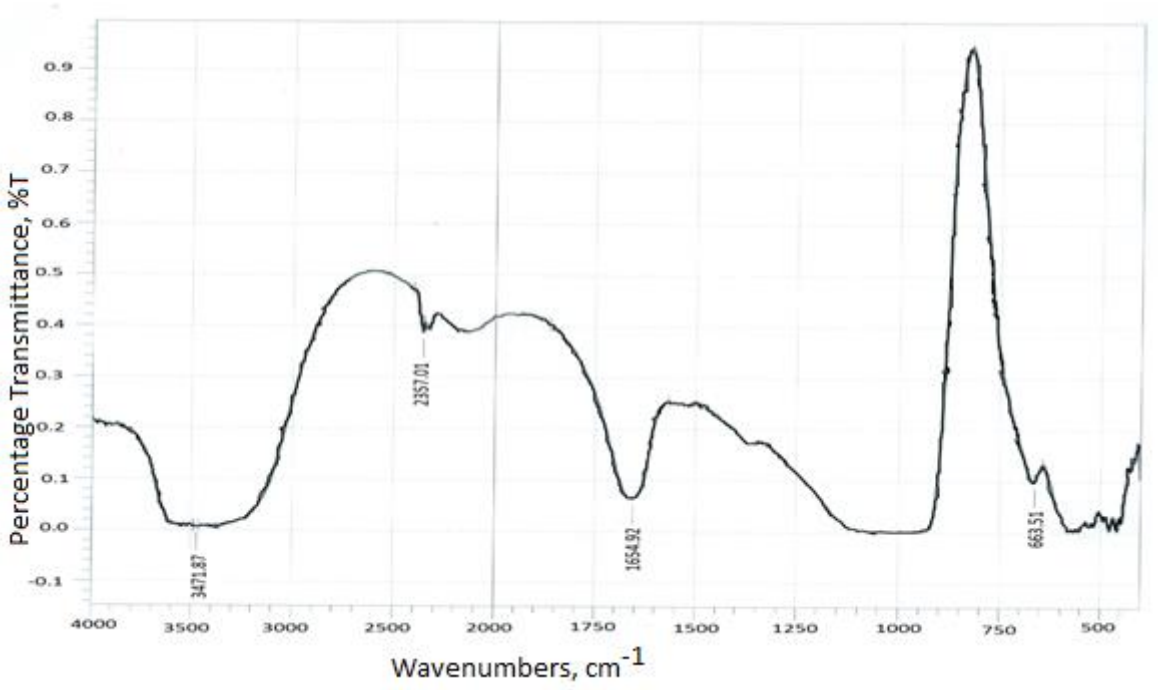

Figure 4. 13 FT-IR spectra of sample ZT-GA-01

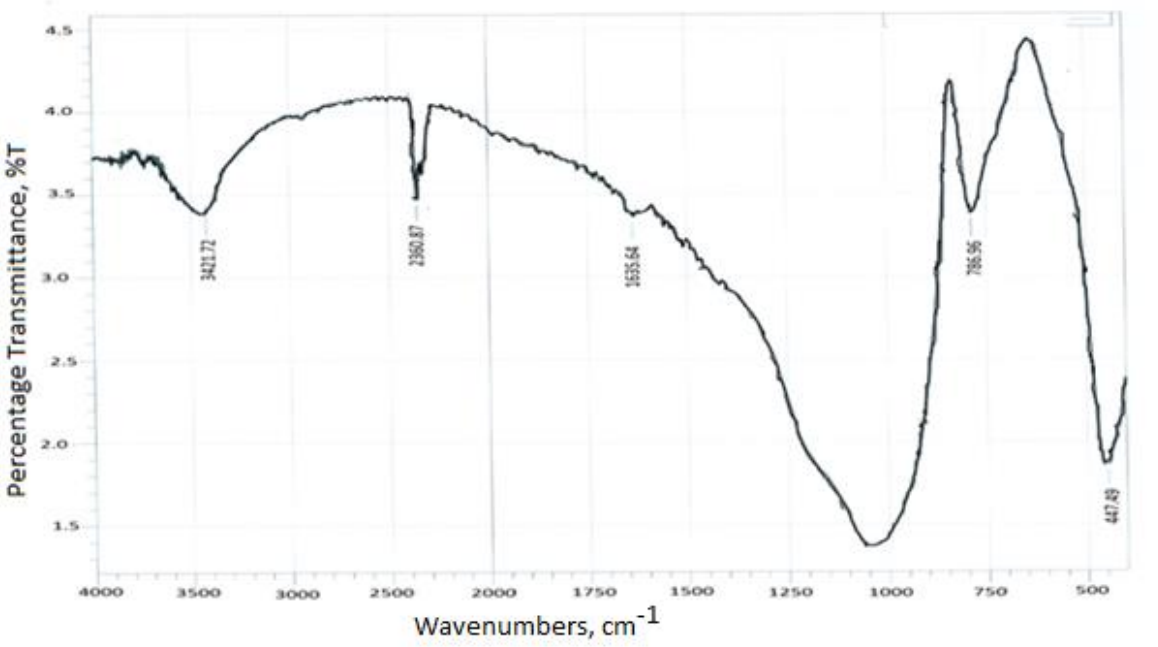

Figure 4. 14 FT-IR spectra of sample EB-GA-02

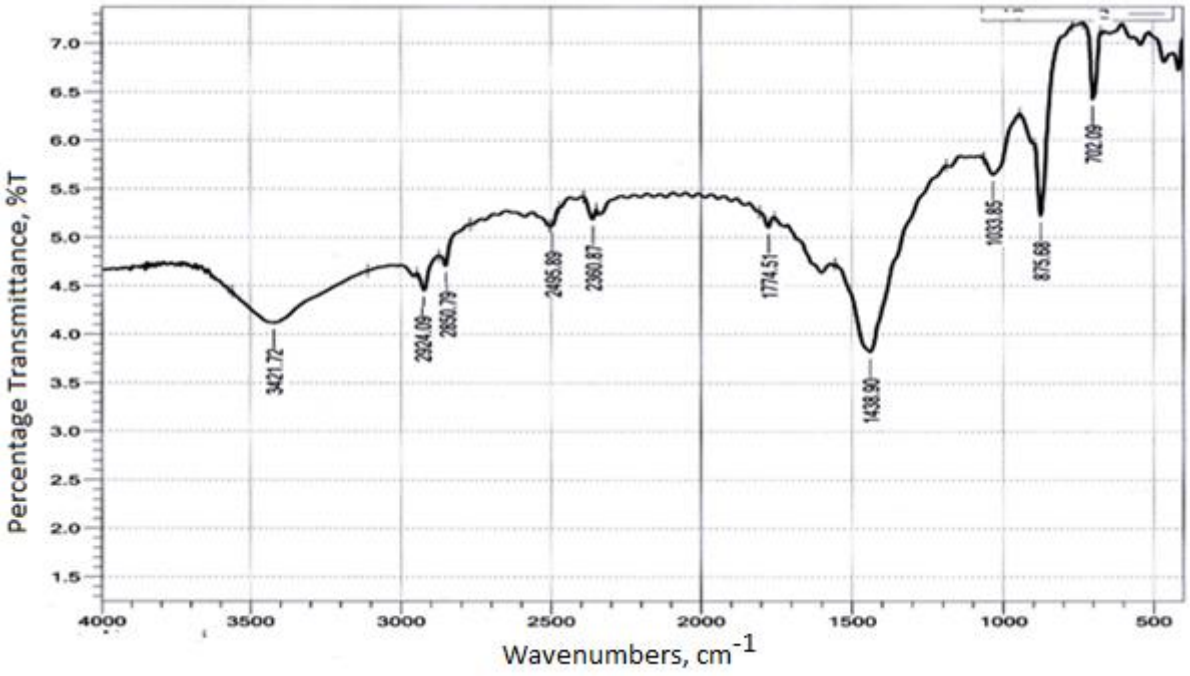

Figure 4. 15 FT-IR spectra of sample MG-GA-03

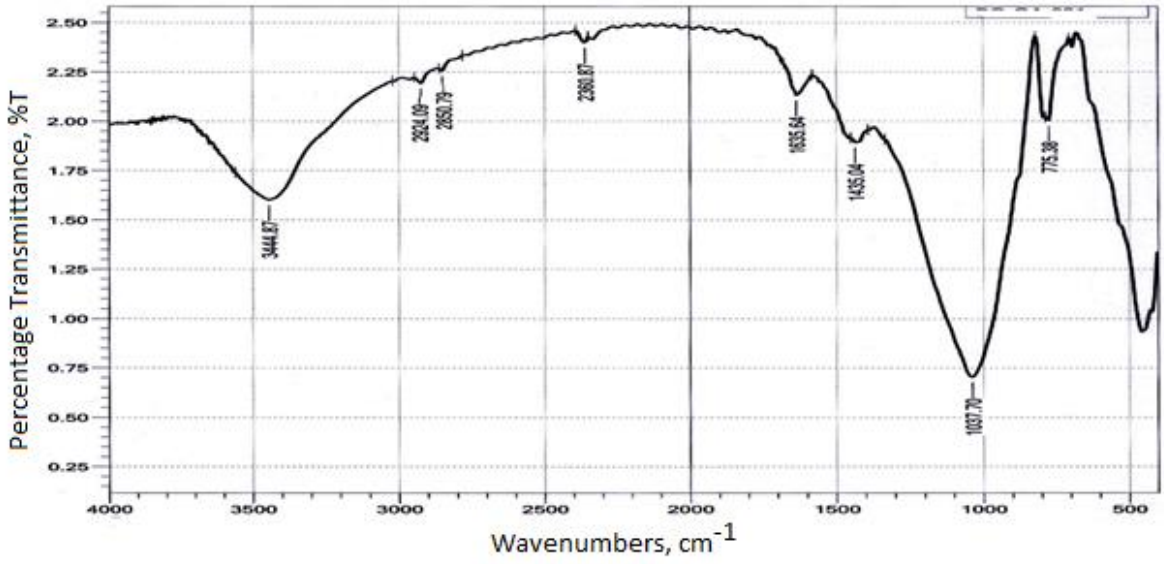

Figure 4. 16 FT-IR spectra of sample BG-GA-04

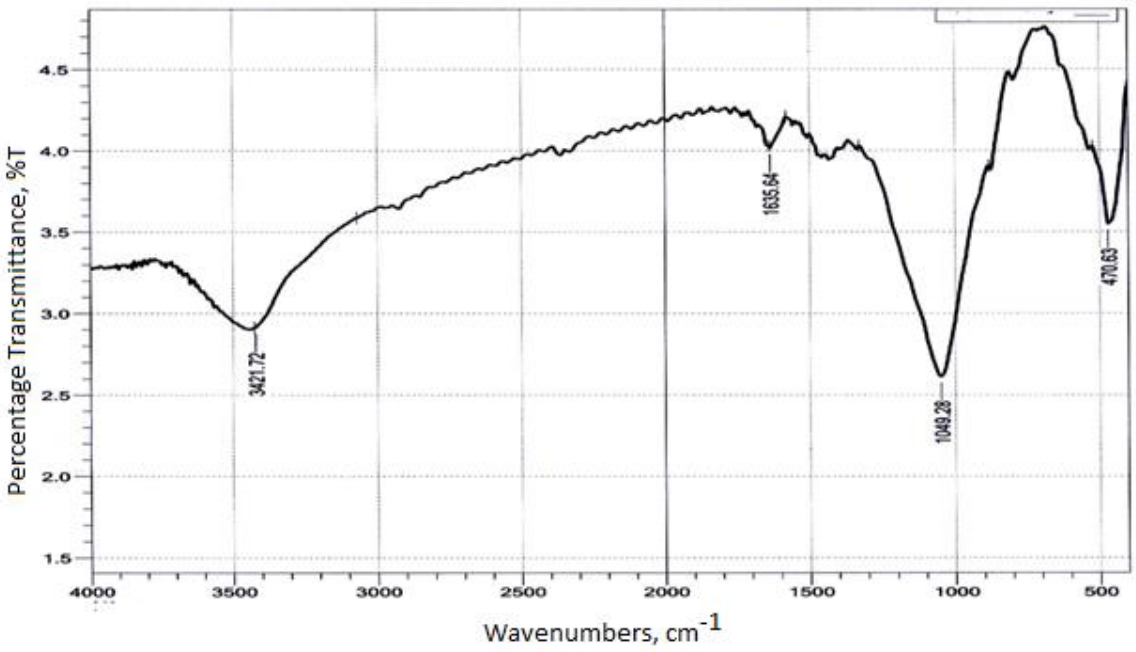

Figure 4. 17 FT-IR spectra of sample NG-GA-05

According to Clark *et al*., 2004, robust essential vibrations of the alumino silicate framework of minerals and glasses, as well as the principal vibration modes of most molecular species like Si-O, C-O, S=O and P-O are located in the mid IR-region. Generally, from these spectra, peaks observed below 900 cm^{-1} could be attributed to symmetric stretching and bending modes within the zeolitic structures (Can *et al*., 2003). A variation of bands is usually a factor of scattering of bond length and angles caused by different conformations of the rings occurring within these structures (Wlodzimier *et al*., 2011). Inferring that peaks between 750 - 820 cm^{-1} could be allocated to four membered ring vibrations due to their relative positions of wavenumbers on the pseudolattice band range, which are theoretically taken to comprised the lowest number of members of all rings happening in the zeolitic structures, according to Sitarz *et al*., 1997, while the lower frequency vibrations of below 620 cm^{-1} could be considered to be for those of six membered ring vibrations.

Mozgawa *et al*., 2005 attributed bond bridge vibration to a range of wavenumbers. Notably, Si-O(Si) and Si-O(Al) could have asymmetric elongating vibrations nearing 1006 cm^{-1}, Si-O-Si

symmetric vibration nears 726 cm^{-1}. On the other hand, Si-O-Al symmetric stretching vibration bridge bonds nears 670 cm^{-1}, vibrations around 550 cm^{-1} could be thought of symmetric stretching of bridge bonds and bending for Si-O-Si and O-Si-O correspondingly, while lower wavenumbers of between 466 cm^{-1} and 250 cm^{-1} could correspond to distinctive bending vibrations occurring in four membered rings (Wlodzimier *et al*,. 2011), of which similar peak was exhibited by sample EB-GA-02 at around 447.49 cm^{-1} suggesting that this particular sample had strong fundamental vibrations of alumino silicate framework composition in comparison to their natural rock samples, informing it's choice as the preferred carrier agent.

4.1.4: X-Ray Fluorescence spectroscopy (XRF)

A summary of the X-Ray Fluorescence data for all the analyzed samples is represented by Table 4.18 below.

Table 4. 18 X-Ray Fluorescence spectroscopy data

Element	ZT-GA-01	±	EB-GA-02	±	MG-GA-03	±	BG-GA-04	±	NG-GA-05	±	Conc'n unit
Potassium (K)	0.070	0.013	3.62	0.36	0.094	0.013	2.82	0.22	0.953	0.132	w %
Calcium (Ca)	0.030	0.004	0.295	0.050	0.099	0.010	21.9	1.1	9.91	0.51	w%
Titanium (Ti)	127	56	2478	306	143	23	9045	599	30600	1500	ppm
Chromium(Cr)	<20	-	288	89	<20	-	130	39	274	41	ppm
Manganese(Mn)	82.1	17.5	2358	205	118	13	2885	106	5530	303	ppm
Iron (Fe)	0.079	0.004	7.04	0.52	0.203	0.010	4.87	0.22	13.1	0.6	w%
Copper (Cu)	148	8	1901	145	95.3	5.7	384	27	618	40	ppm
Zinc (Zn)	10.1	1.5	1262	94	16.9	1.5	115	11	173	14	ppm
Bromine (Br)	<5	-	8.33	0.50	32.9	1.8	<5	-	<5	-	ppm
Rubidium (Rb)	<5	-	326	17	10.1	1.8	89.2	4.2	23.8	3.5	ppm
Strontium (Sr)	3.20	0.42	9.50	1.27	12.2	0.8	593	13	1337	22	ppm
Yttrium (Y)	<5	-	286	13	6.30	0.17	44.0	2.2	39.7	3.3	ppm
Zirconium (Zr)	20.1	2.3	2111	80	48.8	2.9	278	10	454	13	ppm
Niobium (Nb)	5.40	1.27	331	14	11.6	2.6	82.4	2.6	154	7	ppm
Lead (Pb)	1.90	1.15	145	13	<5	-	10.1	2.4	7.43	4.80	ppm

From this table above, all the other actual elemental composition for each sample were determined, beside Aluminium and Silicon, which could likely be due to the instrumental calibration and filters applied. Sample ZT-GA-01, which was used as the standard, being zeolite A obtained commercially had very low concentration units of the listed elements. Cu at 148 ppm was detected as the highest concentration of impurities, followed by Ti at 127 ppm and Mn at 82.1 ppm. Most of the other impurities like Pb, Nb, Y and Rb were below 5ppm. Additionally, this sample had percent by weight of less than 0.08 of K, Ca and Fe elements, which indicates a high level of purity of the commercial zeolites. Comparatively, sample EB-GA-02 had the highest composition of Ti impurities at 2478 ppm, Mn at 2358 ppm, Zr at 2111 ppm and Cu at 1901 ppm, while the other impurities like Pb, Nb, Y and Rb mostly being below 300ppm. This sample had percent by weight between 0.3 – 7.00 of K, Ca and Fe elements. Hence, effective purification process could improve the extent of zeolitic comparability to sample ZT-GA-01, if carried out, a process that was beyond the scope of this current research work. Generally, Ti seemed to be the impurity component detected in highest concentration across the samples characterized, ranging from 30600 ppm highest in sample NG-GA-04 to a lowest of 127 ppm in the standard. This was followed by Mn at high of 5530 ppm to a low of 82.01 in NG-GA-04 and ZT-GA-01 respectively. Bromine was the only halide detected in the samples, besides being the element with the least concentration detected.

4.1.5: Scanning Electron Microscopy (SEM)

SEM images provided evidence on sample external morphology and particle sizes.

Sample ZT-GA-01 which was artificial commercial zeolite A showed aggregated cubical particles of uniformly sized crystals of 10 μm length (Figure 4.18).

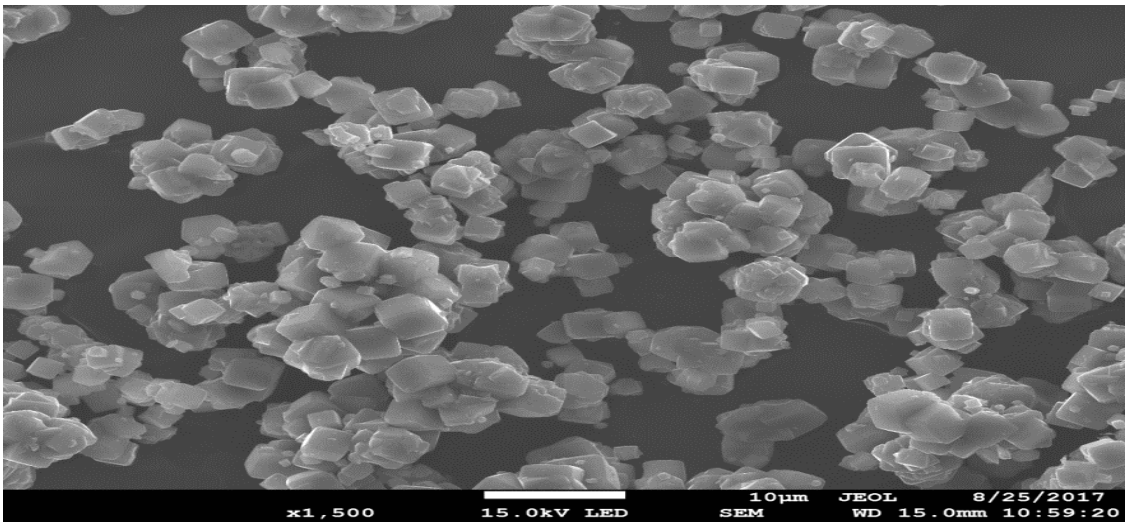

Figure 4. 18 SEM images of sample ZT-GA-01

They had better defined crystals with regular shapes, which seemed to have well-developed structures on surface and converged particles. These are similar observations made by Pereira *et al.* (2012), Bardakci and Bahiceli (2010), Ngoc *et al.* (2013) and Mohanraj (2013). This could probably be due to high levels of crystal purity.

The rest of the samples had nonuniform surface morphologies and particle sizes. These images were from raw natural zeolitic materials which would have probably given more elaborate images on purification and particle reduction processes.

Sample EB-GA-02 showed that the particles were unevenly sized (Figure 4.19). The crystals were dense aggregates of irregular shapes, with not well-developed structures being observed on surface converged particles.

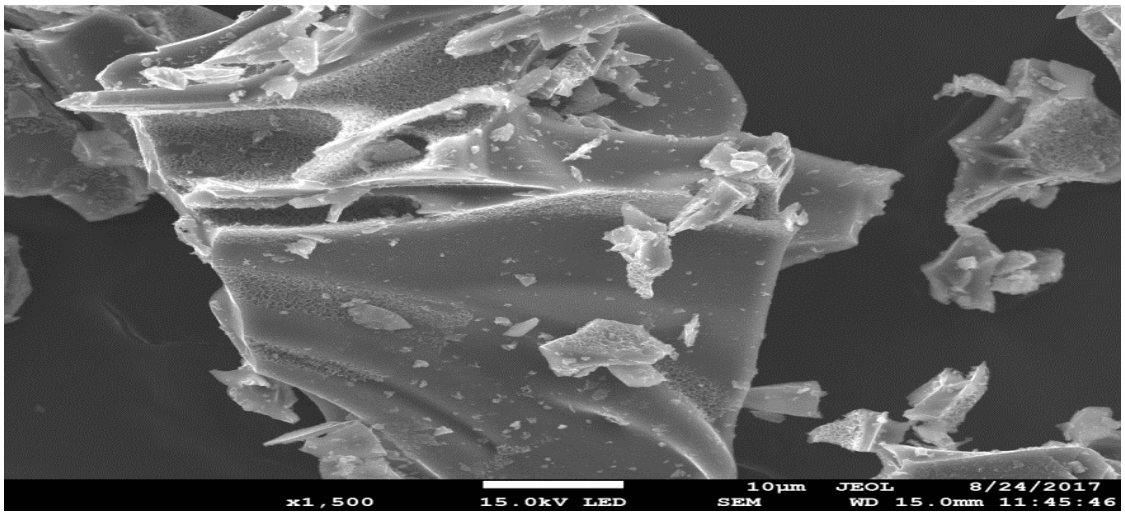

Figure 4. 19 SEM images of Sample EB-GA-02

On the other hand, images of sample MG-GA-03 (Figure 4.20) showed rod like structures, some with cylindrical and others rhombic shapes.

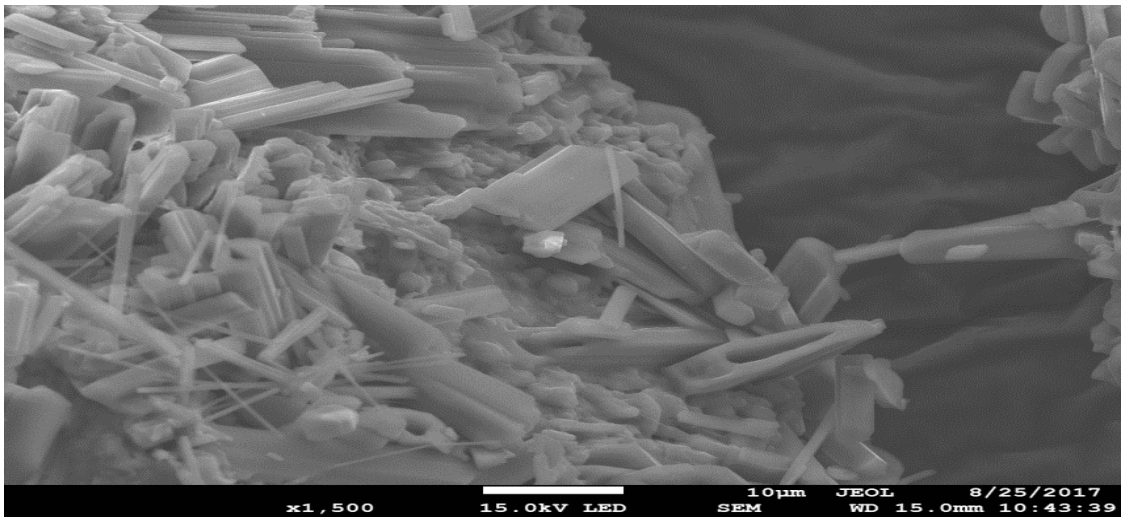

Figure 4. 20 SEM images of Sample MG-GA-03

SEM images of samples BG-GA-04 and NG-GA-05 shown by Figure 4.21 and Figure 4.22 respectfully showed particles agglomerated in different geometries.

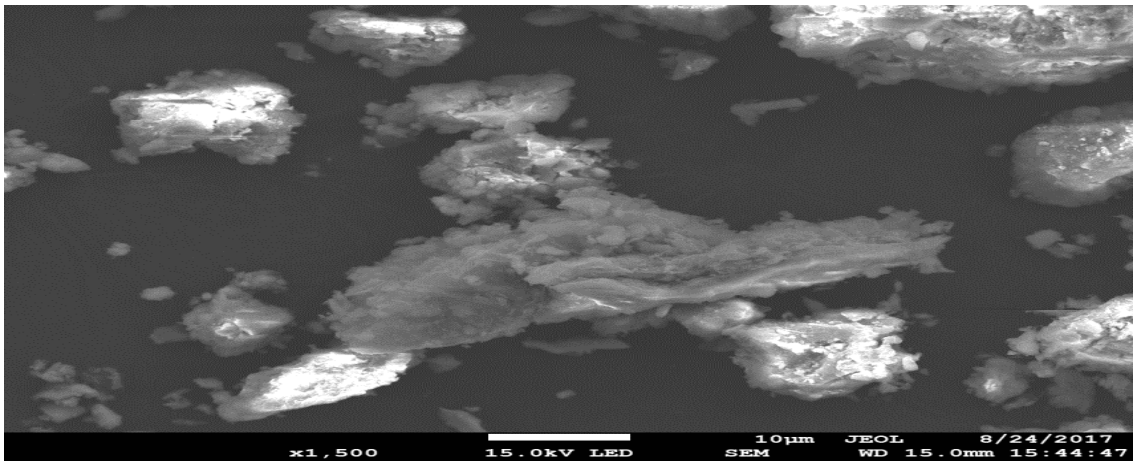

Figure 4. 21 SEM images of Sample BG-GA-04

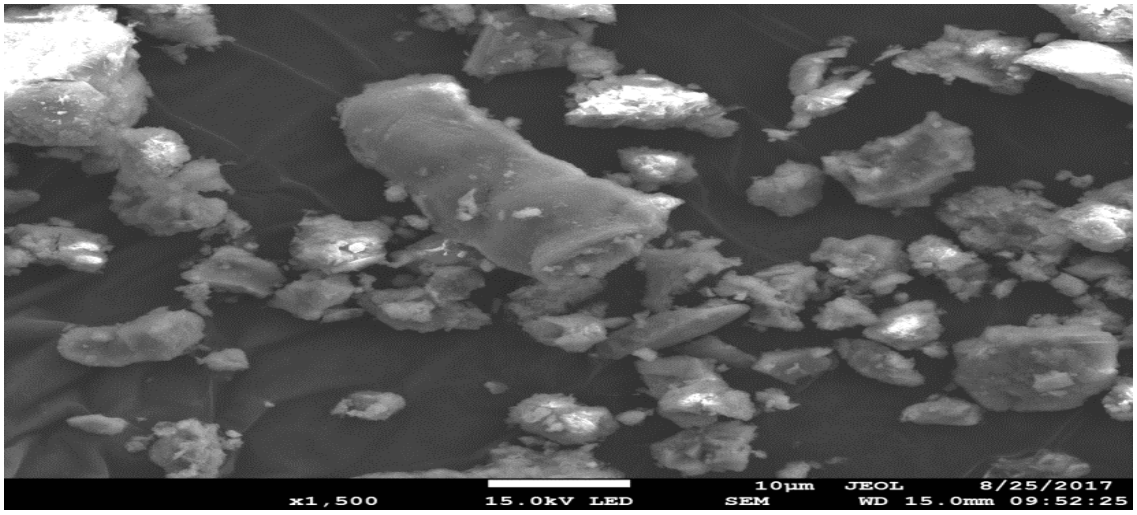

Figure 4. 22 SEM images of Sample NG-GA-05

4.1.6: Nitrogen adsorption - desorption studies

Nitrogen adsorption-desorption isotherm of commercial zeolite sample ZT-GA-01 and natural zeolitic rock sample EB-GA-02 are presented in Figure 4.23 below. These isotherms show variation in adsorption between pressures below 0.2, 0.3 - 0.6 and above 0.8, giving a similarity to type IV isotherm commonly shown by mesoporous materials, a phenomenon of physical adsorption processes (Sing *et al.*, 1985). At relatively higher-pressure desorption levels, there is formation of narrow hysteresis loops which could be associated with mesopore capillary condensation. Pressure zone 0.3 – 0.6 could represent accomplishment of monolayer treatment. This isotherm profile represents a monolayer-multilayer adsorption mechanism of the gas

sorption with a relatively high heat of adsorption forming monolayer coverage. Infection points usually indicates completion of monolayer coverage. This could also explain the variations in the pore volume recorded below as 0.006767 cm^3/g to 0.002333cm^3/g for samples EB-GA-02 and the standard sample ZT-GA-01, respectively. Hence, reversible isotherms are usually a strong indication of physisorption preference in the adsorption phenomenon.

Table 4.19 below gives physical properties of these samples ZT-GA-01 and EB-GA-02 in terms of BET surface area, BJH pore volume and pore sizes. These properties were obtained as; 0.6716 m^2/g, 0.002333 cm^3/g, 151.5 Å and 0.7099 m^2/g, 0.006767 cm^3/g, 389.8 Å respectively for ZT-GA-01 and EB-GA-02. This corresponded to 15.15 nm and 38.98 nm nanopore dimension spaces within ZT-GA-01 and EB-GA-02 respectfully, ascertaining nano channeling within the zeolitic material. Comparative higher surface of EB-GA-02 to ZT-GA-01 could be attributed to increased agglomeration of the particles, often because of low purification. High purity level of commercial zeolite sample ZT-GA-01 could have resulted in the variation in their physical properties recorded. Improved purification methods of natural zeolitic sample EB-GA-02 could result in enhanced physical properties of surface area and porosity.

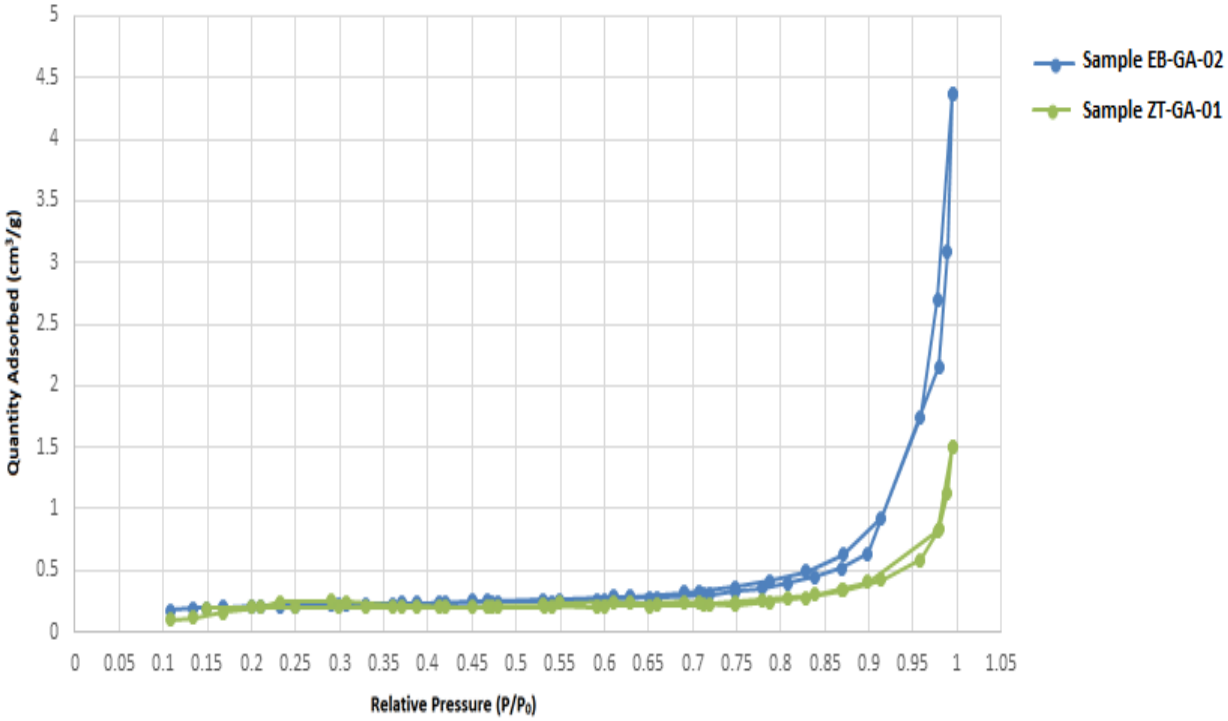

Figure 4. 23 Nitrogen sorption isotherms of samples ZT-GA-01 and EB-GA-02.

Table 4. 19 Physical properties of samples ZT-GA-01 and EB-GA-02.

PROPERTIES	SAMPLE EB-GA-02	SAMPLE ZT-GA-01
1. Surface Area BET Surface Area (m^2/g)	0.7099	0.6716
t-Plot external surface area (m^2/g)	0.7161	0.6683
2. Pore Volume Single point adsorption total pore volume of pores less than 3 553,365 Å diameter at P/Po = 0,994653432 (cm^3/g)	0.006767	0.002333
Single point desorption total pore volume of pores less than 3 553,365 Å diameter at P/Po = 0,994653432 (cm^3/g)	0.006767	0.002333
t-Plot micropore volume (cm^3/g)	-0.000063	-0.000039
3.Pore Size Adsorption average pore diameter (4V/A by BET) (Å)	381.278	138.975
Desorption average pore diameter (4V/A by BET) (Å)	381.278	138.975
BJH Desorption average pore diameter (4V/A) (Å)	389.846	151.519

In concluding this section 4.1 on sample characterization, Table 4.20 below shows a summary of some of the collaborative results. The standard sample ZT-GA-01 was characterized to be zeolite A Artificial, as clearly identified by EDX, FTIR, XRD and SEM results, while sample EB-GA-02 had better comparative characteristics to the standard sample ZT-GA-01 as indicated by the EDX, FTIR and XRD results. As discussed before, EB-GA-02 was identified as the only natural rock that contained both aluminium and silicon oxides at higher composition, besides having specifically Si-O-Si bending vibration for internal tetrahedral characteristics of all zeolites. Further advanced pulverization and purification of the natural rocks could produce XRD peak angles and SEM morphologies. XRF characterization confirmed composition of some similar elements besides Aluminium and Silicon, main constituents of zeolites, like potassium, calicium and iron as characterized by EDX. These elements are present in minerals like danalite, calcite and diopside as characterized by XRD. Hence, this sample characterization confirmed sample EB-GA-02 and EL-GA-06 as natural zeolites as observed from their XRD, EDX, and FT-IR analysis data. The rest of the samples MG-GA-03, BG-GA-04 and NG-GA-05 were lacking Al2O3 in their crystal and oxides, making them not to be classified as natural zeolites.

Table 4. 20 Comparative characterization results

Characterization Technique sampled results		Samples				
		ZT-GA-01	EB-GA-02	MG-GA-03	BG-GA-04	NG-GA-05
XRF -Elemental composition (Concentration in ppm)	Potassium (K)	0.070	3.62	0.094	2.82	0.953
	Calcium (Ca)	0.030	0.295	0.099	21.9	9.91
	Iron (Fe)	0.079	7.04	0.203	4.87	13.1
	Niobium (Nb)	5.40	331	11.6	82.4	154
	Manganese (Mn)	82.1	2358	118	2885	5530
	Zirconium	20.1	2111	48.8	278	454
EDX -Oxide composition (Percentage, %)	Al_2O_3	56.368	18.764	-	-	-
	SiO_2	43.632	37.410	34.77	22.336	31.884
	Fe_2O_3	-	21.389	30.231	23.037	46.765
	K_2O	-	20.671	-	15.137	4.239
	CaO	-	0.194	-	35.747	9.911
	NbO	-	0.100	-	0.040	0.107
FTIR -Peak assignment (Wavenumbers, cm^{-1})	H-O-H Stretching of absorbed water	3471.87	3421.72	3421.72	3421.72	3444.87
	H-O-H overtone in plane bending	2357.01	2360.87	2360.87	2360.87	2360.87
	H-O-H Bending of water	1654.92	1635.64	1774.51	1774.54	-
	Si-O-Si Bending for internal tetrahedral	663.51	447.49	-	-	-
	H-O-H Stretching of absorbed water	3471.87	3421.72	3421.72	3421.72	3444.87
XRD -Main compounds composition (percentage, %)	Zeolite A Artificial	100	-	-	-	-
	Danalite	-	41.2	-	-	-
	Hollandite	-	21.6	-	-	-
	Calcite	-	-	15.4	-	-
	Forsterite	-	-	9.9	-	-
	Hambergite	-	-	-	42.5	-
	Diopside	-	-	-	-	26.8
	Titanite	-	-	-	-	19.6
SEM	Morphology	-Cubical crystalline -Uniform sizes/ regular	-Dense aggregates -Irregular shapes	- Cylindrical - rode-like structures	-Particle agglomeration -Varied geometries	- Varied geometries -Non-symmetrical

4.1.7: Characterization of Sample KIK-GA-01

This was applied as the control sample. Soil content analysis of KIK-GA-01 (Kikuyu soil) revealed a higher organic content, relatively weak acidic pH, with a higher macromineral content (as shown in Table 4.21) ideal for crop sustainability.

Table 4. 21 Composition properties of sample KIK-GA-01

Property	Value
Soil depth cm	Top
Soil pH-H_2O (1:2.5)	6.50
Elect. Cond. mS/cm	0.3
Carbon %	2.7
Sand %	40
Silt %	40
Clay %	20
Cat. Exch. Cap. me%	24.8
Zinc ppm	62.9
Copper ppm	1.22
Calcium milliequivalent(me)%	44.4
Magnesium me%	3.1
Potassium me%	1.5
Sodium me%	3.6
Sum me%	52.6
Base %	100+
ESP	14.4
Total nitrogen %	0.25
Phosphorus ppm	44
Iron ppm	96.2

Electrical conductivity and soil pH parameters are correlated with other soil parameters touching crop production like soil texture and cation exchange capacity, particularly for farmers practicing precision agriculture.

X-Ray diffraction Spectroscopy characterization of sample KIK-GA-01(Figure 4.24) identified other mineral composition present in the soil as quartz, sanidine, paraginite and cristobalite.

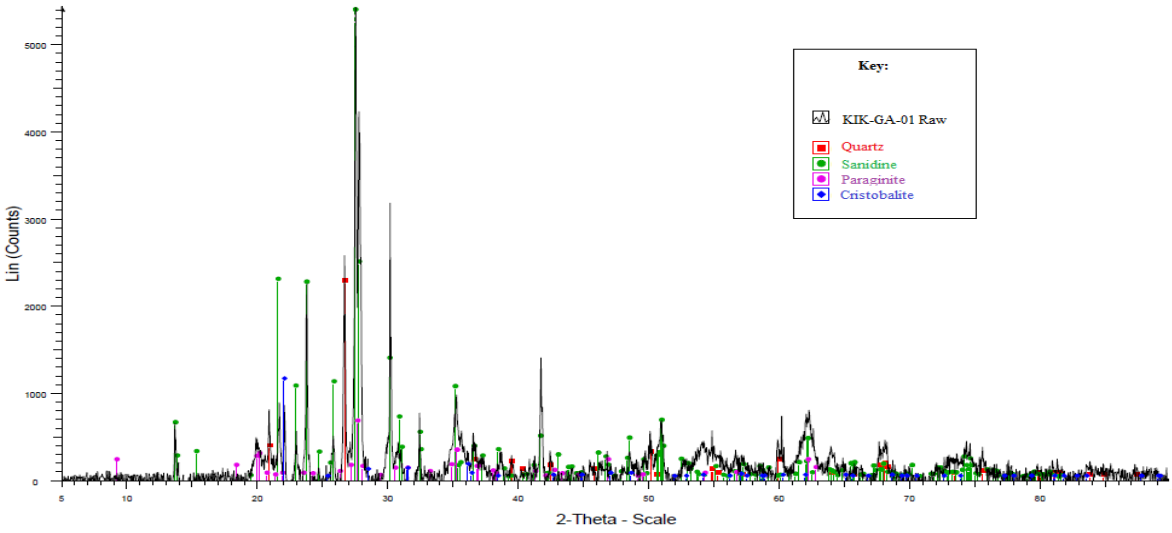

Figure 4. 24 Blank soil from kikuyu KIK-GA-01

Fourier transform infrared analysis of the Kikuyu soil produced the spectrum shown by Figure 4.25 below. Interpretation of the corresponding peaks as indicated by table 4.22 (Bhaskar *et al.*, 2010) revealed varied functional groups as could be found in an arable farm soil. The SEM images recorded for this soil were shown by Figure 4.26, showing the mineral crystals had diameters in the ranges of a few nanometers to many micrometers. It shows the mineralogical composition of this control sample KIK-GA-01 varied significantly from all other samples.

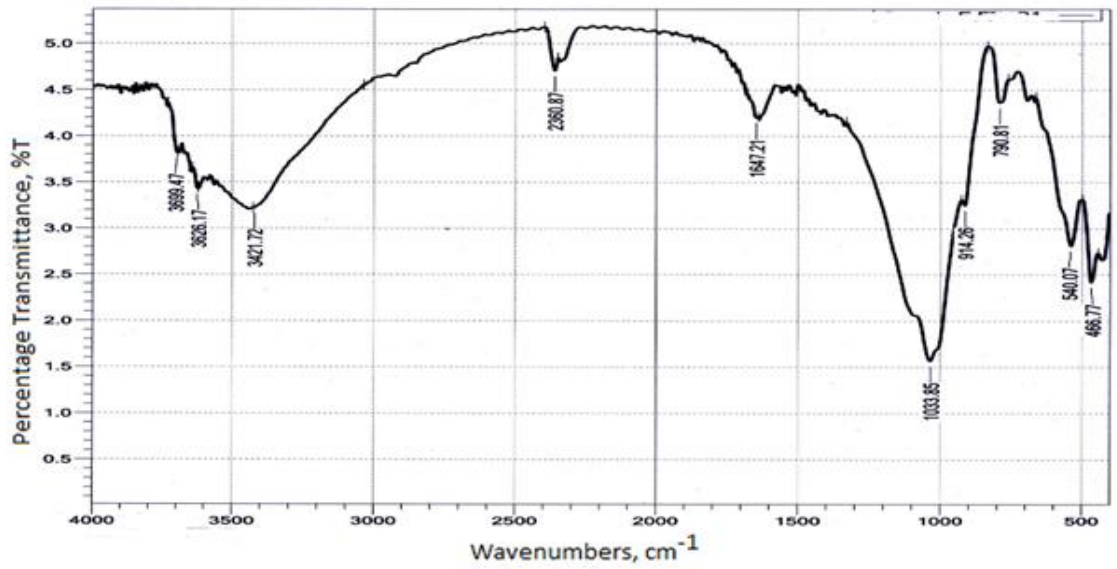

Figure 4. 25 FT-IR spectra of sample KIK-GA-01

Table 4. 22 Infrared band positions in Kikuyu soil

Wavenumbers (cm^{-1})	Assignment
3699.47	O-H Stretching, very weak peak
3626.17	O-H Hydrogen bonded stretching, very weak peak
3421.72	O-H Hydrogen bonded, very broad, could be associated with weak organic acid
2360.87	C≡N Stretching in nitrile related compounds
1647.21	H-O-H Bending of water
1033.85	Si-O Stretching in clay minerals, broad peak
914.26	O-H Deformation linked to Al^{3-}, Mg^{2-}
790.81	Si-O Quartz
540.07	Fe-O Stretching in Fe_2O_3
466.77	Si-O-Si Bending in sand

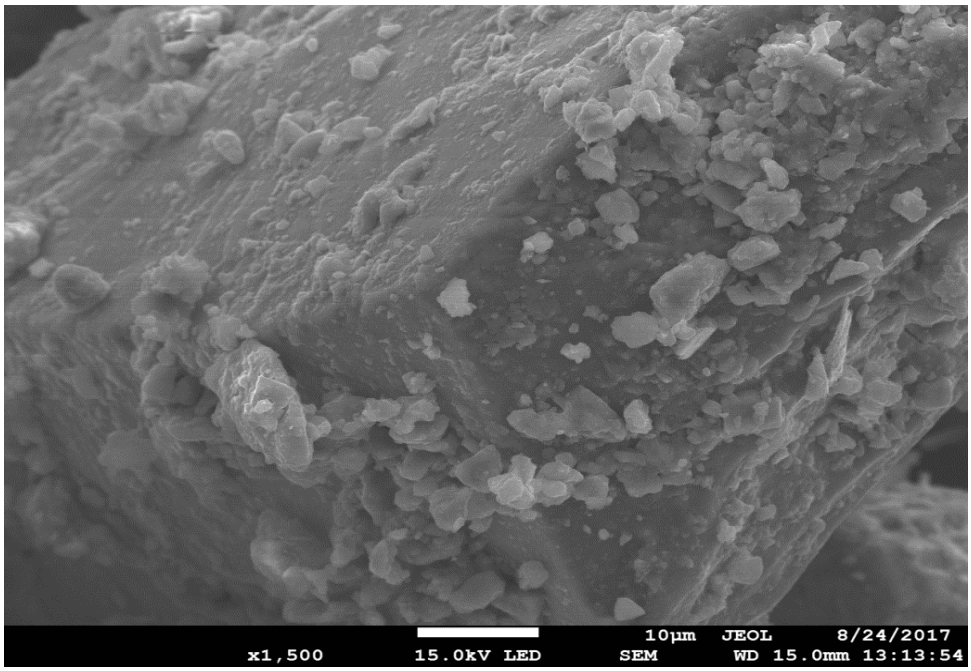

Figure 4. 26 SEM images of sample KIK-GA-01`

4.2: Formulation of smart delivery system for fertilizer

After sample characterization and analysis as discussed in section 4.1 above, sample EB-GA-02, which was the major natural nanozeolitic sample, was applied in fertilizer studies phase of the research work. Urea fertilizer was used as the guest molecules in the nanopores of these materials. These studies included kinetics of urea sorption, urea nanozeolitic material formulation, characterization and their application as smart delivery systems on tomatoes and spinach growing. Comparative experiments were done using sample KIK-GA-01 as the control studies and sample ZT-GA-01 as the standard experiments.

Initially, urea linearized plots according to Beer Lambert's Law were determined. The plot of absorbance against concentration (Figure F4.1 in appendices) generated from the corresponding data (Table T4.2 in appendices) gave linear graph with regression value of 99.5 %.

The plot generated urea linearized graph that adhered to the Beer Lambert's Law, i.e.,

$$A=\acute{\varepsilon}CL$$

where A is absorbance, L is path length, C is concentration and έ is absorption coefficient. This was applied in determination of other concentrations of urea solution from their analyzed absorbances.

4.2.1: Kinetics of fertilizer adsorption on zeolitic materials

Experiments of varying concentration of urea shaken with constant mass of sample EB-GA-02 generated data in Table T4.3 for their absorbance readings and Table T4.4 for their corresponding determined concentrations (displayed in appendices), with an ANOVA P-Value of 0.978 consistent with the null hypothesis under a significance level, $\alpha = 0.05$ (Table T4.30). Generally, there is an increase in amount of urea adsorbed as the spiking concentration increases as illustrated by Figure 4.27 below. This may be attributed to gradual increase in adsorbate molecules in solution as compared to higher initial adsorption active sites of the adsorbent surface.

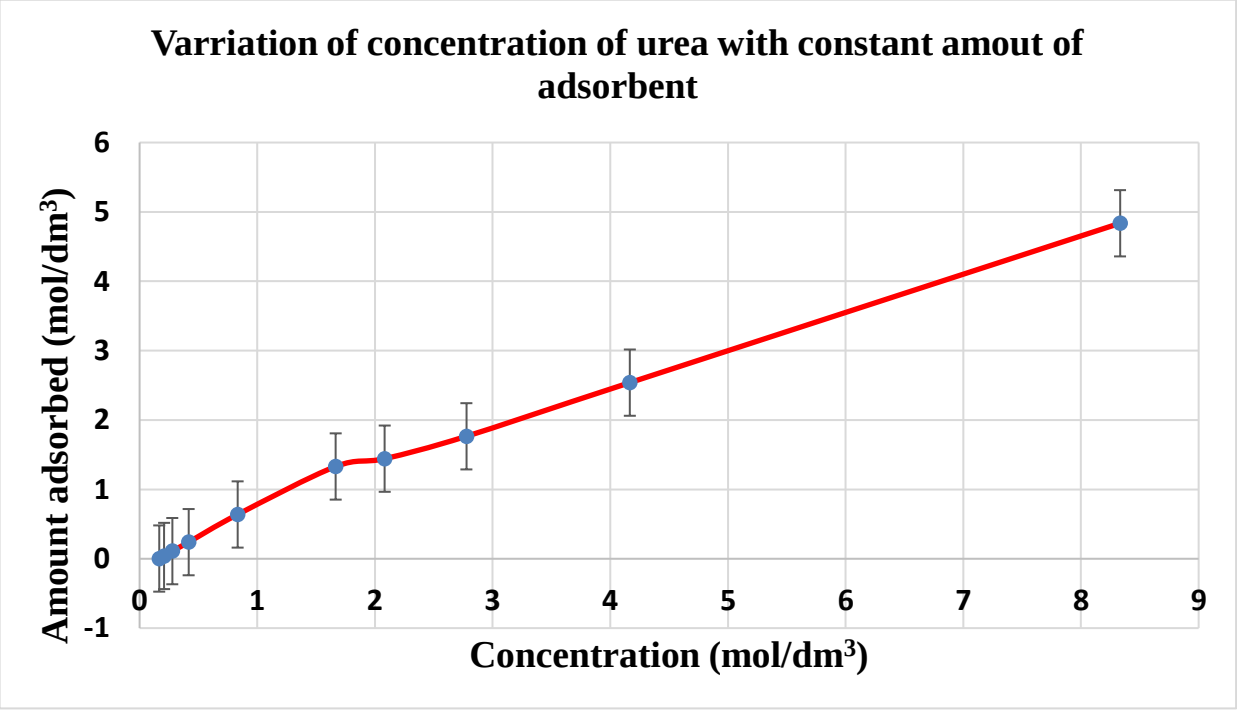

Figure 4. 27 Varying concentration of urea with constant amount of adsorbent

The highest percentage adsorbed was determined to be 80.0 %, with more than 60 % achieved by the 1.00 mol/dm^3 concentration as represented by Figure 4.28 below.

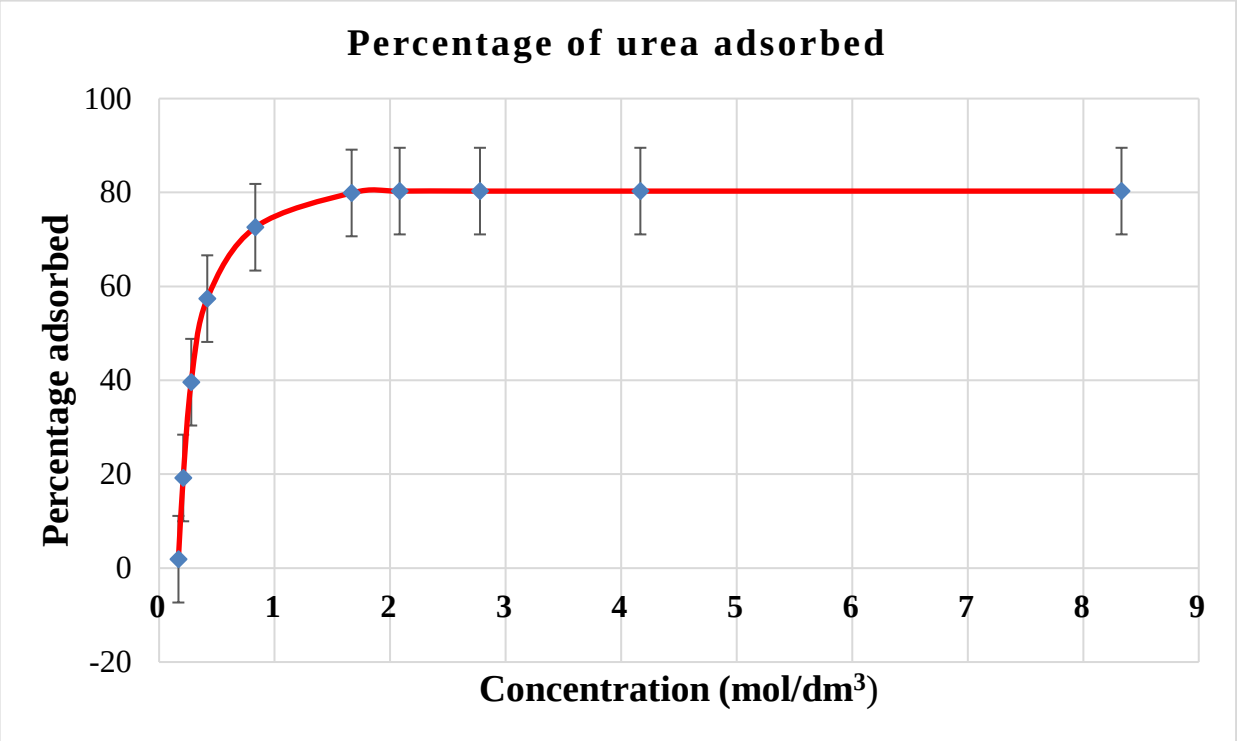

Figure 4. 28 Percentage of urea adsorbed

The initial rapid phase could be due to a high initial sorption gradient between adsorbate in solution and the adsorbent surface of sample EB-GA-02, resultant of initial high number of vacant adsorption sites. Equilibrium sorption rate was attained at the recorded highest percentage above, beyond which desorption also started occurring. Significantly, more amount of urea was adsorbed from the solution initially till equilibration, after which some of the urea molecules could be desorbed back in the solution as illustrated by Figure 4.29 below.

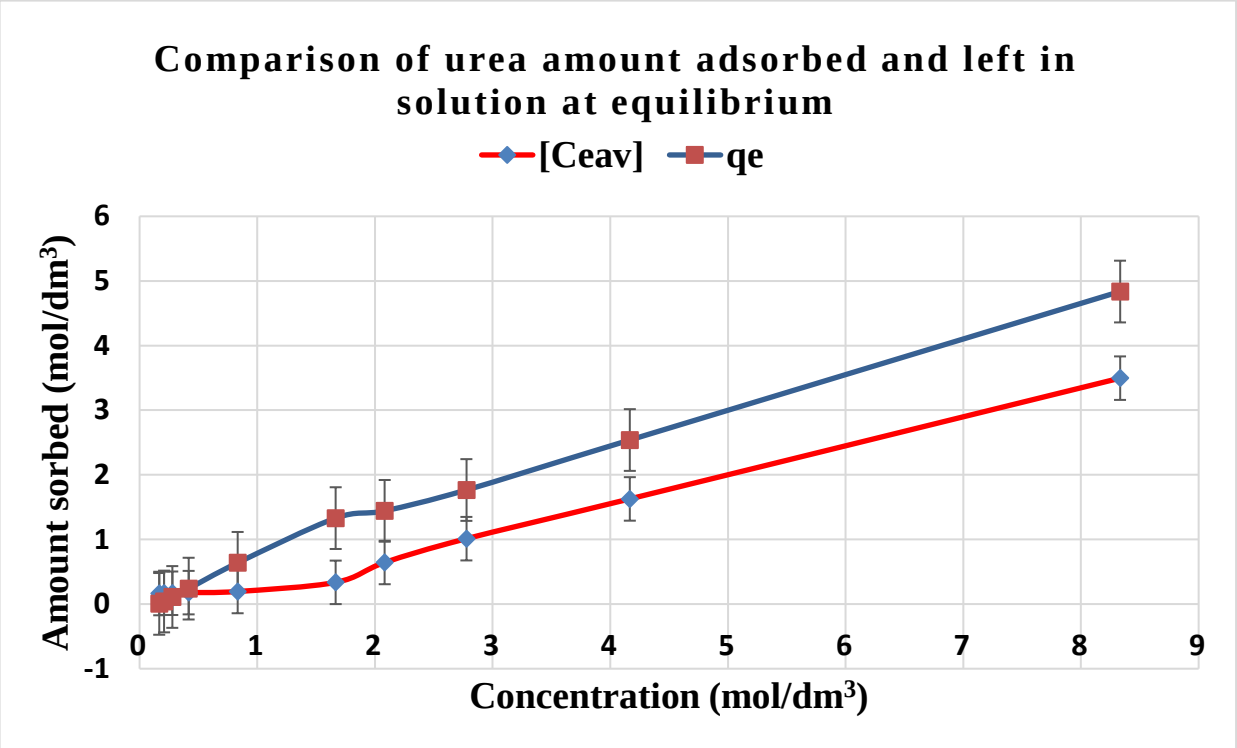

Figure 4. 29 Amount adsorbed (qe) with solution remaining amount (Ce) at equilibrium

Studies of variation of shaking time conducted under constant concentration of urea fertilizer gave absorbance readings recorded in Table T4.5, while their corresponding concentration determined recorded in Table T4.6 (displayed in appendices), with an ANOVA P-Value of 0.832 consistent with the null hypothesis under a significance level, $\alpha = 0.05$ (Table T4.30). Keeping the spiking concentration constant while increasing the shaking time enhances solute sorbate contact that represents more stable equilibration timing with dismal change in amount adsorbed beyond the 30 - 60 minutes as represented by Figure 4.30 below. Better equilibration was recorded at a slightly higher shaking time, though once most of the sorption active sites were used up, further increase in contact time between the urea molecules and sample EB-GA-02 had no significant change of rate of adsorption.

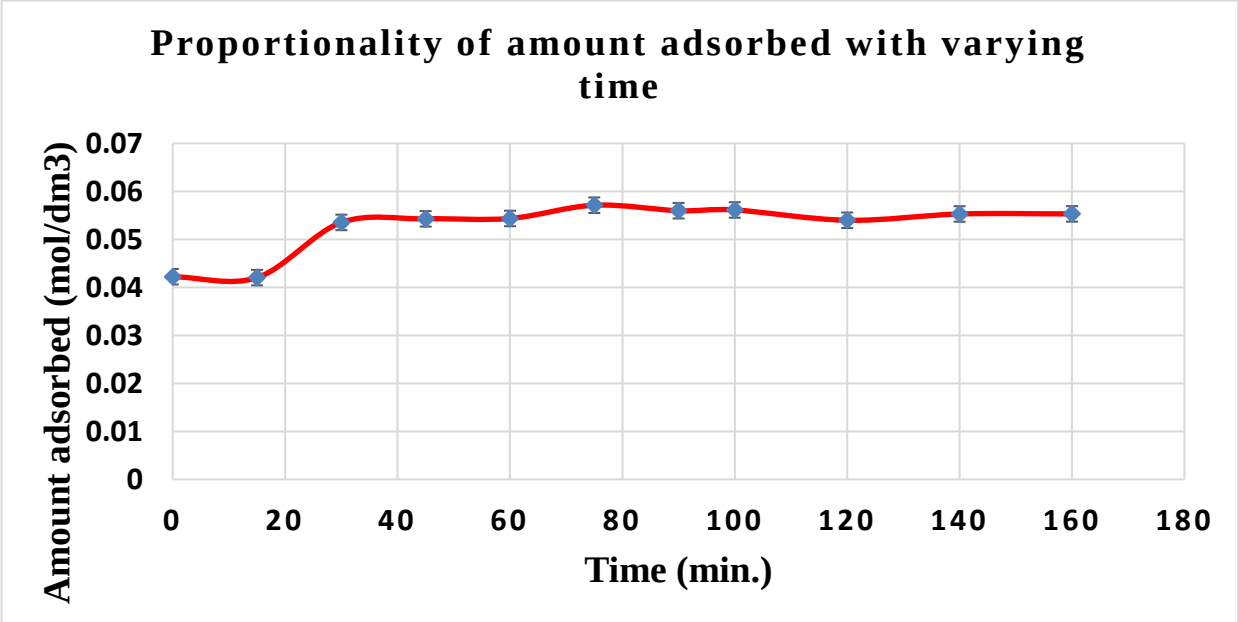

Figure 4. 30 Proportionality of amount adsorbed with varying time

Determination of the percentage of amount of urea adsorbed with increasing shaking time indicated that adsorption rate tended to equilibrate at approximately 33 % for the amount adsorbed, giving near zero gradient at higher shaking time. Generally, the kinetics of urea adsorption on sample EB-GA-02 was determined to be a physisorption process that was affected by parameters like concentration of the adsorbate in solution, contact time and mass of adsorbent surface materials. The increased sorption gradient could be related to the proportionality of the vacant sites within the zeolite matrix as a result of exchangeable cations like Na^{1+}. This process is largely adsorption and could also be affected by other factors such as solubility, pH and ionization.

4.2.2: Quantitative determination of adsorbed fertilizer

Absorbance data analyzed from this particular study was recorded in Table T4.7, while their corresponding determined concentration values recorded in Table T4.8 in the appendices, with an ANOVA P-Value of 0.998 consistent with the null hypothesis under a significance level, $\alpha = 0.05$ (Table T4.30) .

Relatively, higher concentration and longer shaking intervals were used in this study for quantitative determination of adsorbed urea. Higher concentration of sorption solutes exposed to sorption sites for longer durations generated better equilibrations as indicated by Figure 4.31 below, of which the highest column represented maximum sorbed amounts shaken at 24 hours' duration starting with a solution of concentration 0.278 $moldm^{-3}$ corresponding to 1:60 m/v. Similarly, at maximum equilibration, there is an almost equivalent sorption rate on amount of urea molecules binding the sample EB-GA-2 sorption active site within the nanopore spaces as to those released in the aqueous medium. The positive gradient to the maximum could be attributed to more sorption sites and gradual increase in physicochemical binding, while the subsequent decline could be a factor of reverse process of desorption.

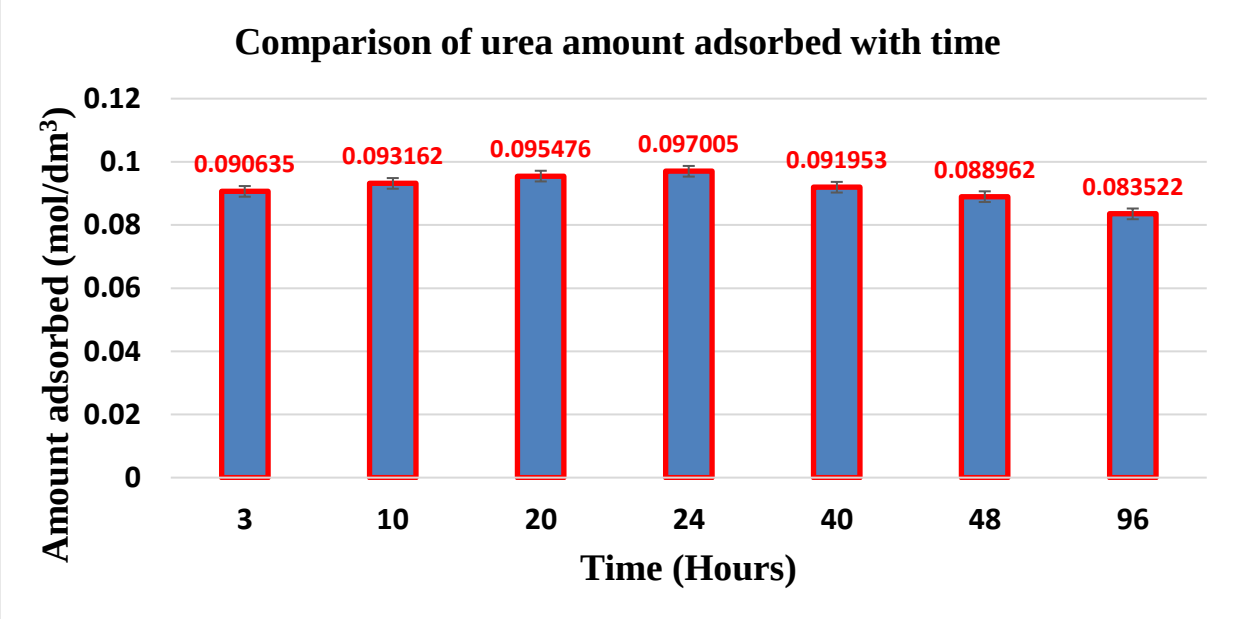

Figure 4. 31 Comparison of urea amount adsorbed with time

Further analysis of variation of percentage of urea adsorption with time as represented by Figure 4.32 below gives the highest index at approximately 35 % when contact shaking time is done for 24 hours. Hence, this experimental finding gave the optimum parameters for loading urea fertilizer in the nanopores of sample EB-GA-02, as was done in the subsequent procedure.

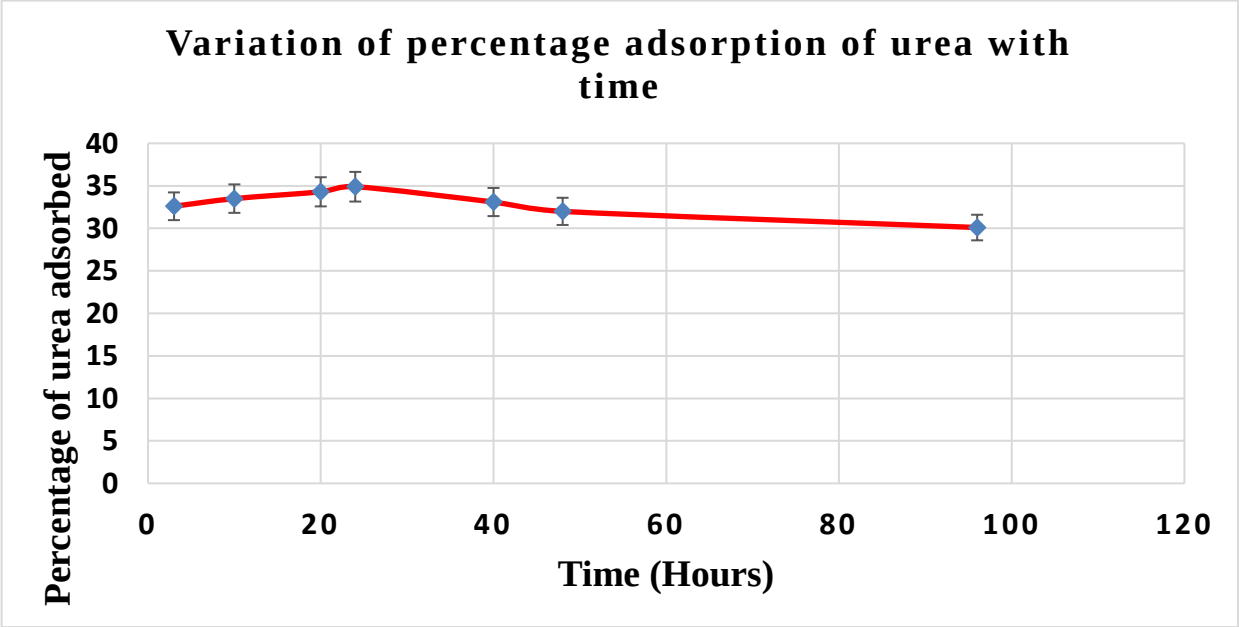

Figure 4. 32 Variation of percentage absorption of urea with time

4.2.3: Loading of fertilizer into zeolitic materials

Table T4.9 in appendices gives the absorbance readings and the corresponding concentrations (Table T4.10) obtained while carrying out the loading of urea into sample EB-GA-02, as a proceeding procedure determined by the immediate previous methodology.

Once formulated, this resultant sample, referred to as urea loaded zeolitic sample EB-GA-02, would then be the one used in the application objectives of the fertilizer smart delivery system.

Confirmation of the loaded urea into the samples was determined by characterization of the urea loaded samples using X-ray diffraction spectroscopy and Fourier transform infra-red spectroscopy as discussed below.

X-Ray diffraction analysis of urea loaded sample EB-GA-02 (Figure 4.33) indicated 2θ peaks values of 22, 24.5, 29.5, 32, 35.5, 37, 38.5, 40.5, 41.5, 45.5 and 55 corresponding to urea peaks.

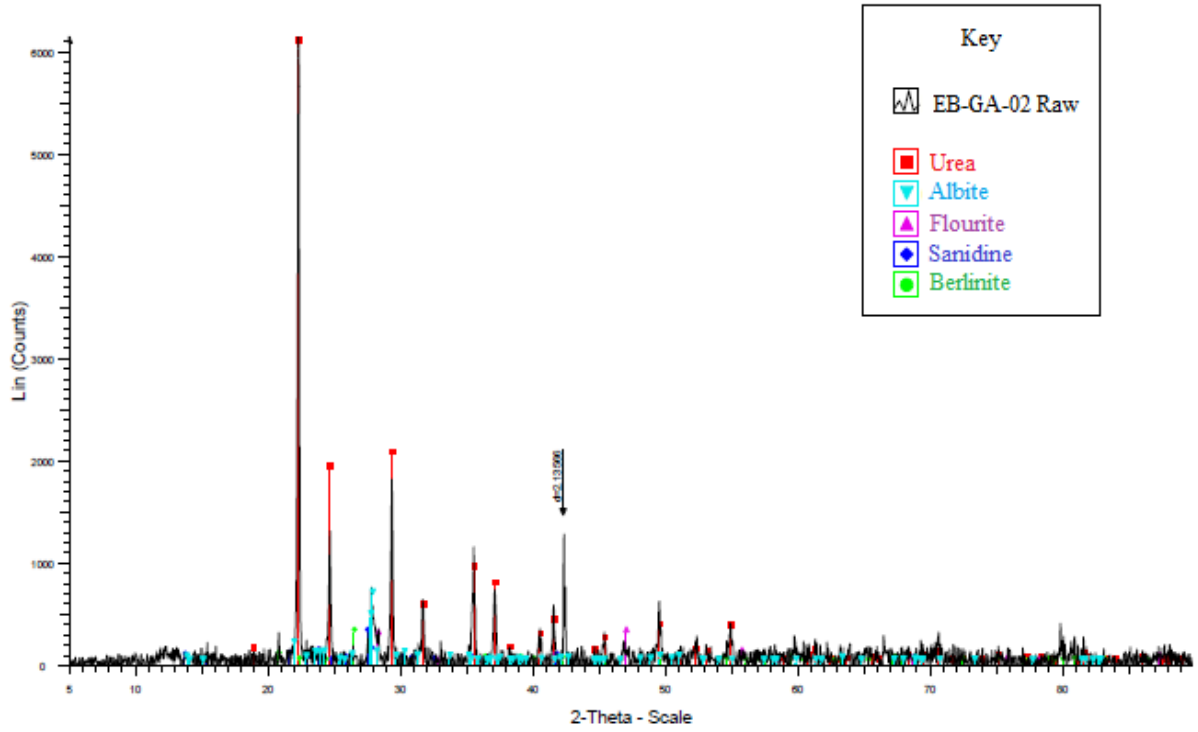

Figure 4. 33 Fertilizer loaded sample EB-GA-02

Fourier Transform Infrared analysis of urea fertilizer (Figure 4.34) showed major peaks at 3348.42-3444.87cm^{-3}, 1624.06-1681.93cm^{-3} and 1465.90cm^{-3} corresponding to N-H, C=O and C-N functional groups respectively (Stuart, 2004). Several researchers have reported that zeolites possess a lot of surface-active sites which exhibit higher ionic selectivity (Shenbagavalli, 2011; Boopathy *et al.*, 2013 and Hollister, 2011). For example, 13.5 – 21.5 mgg^{-1} ammonium ions could be adsorbed by zeolites through ion exchange (Sprynskyy *et al.*, 2005).

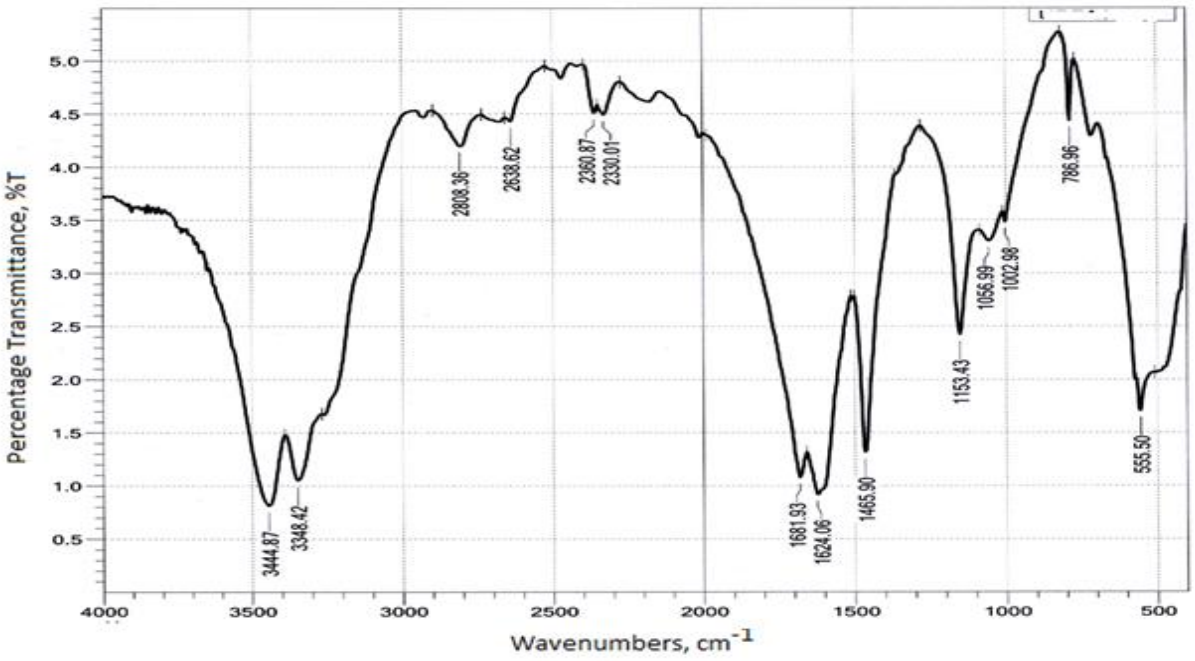

Figure 4. 34 FT-IR spectra of urea

On the other hand, the spectrum of Urea loaded sample EB-GA-02 below (Figure 4.35) contained distinct peaks appearing on the urea spectrum at 3348.42 - 3444.87 cm^{-3}, 1624.06 - 1681.93 cm^{-3} and 1465.90 cm^{-3}, corresponding to N-H, C=O and C-N stretching vibrations for the urea fertilizer functional groups respectively, as appeared in the previous figure above, confirming the loading of urea in the nanopores of the zeolitic materials. The SEM image obtain are shown by Figure 4.36.

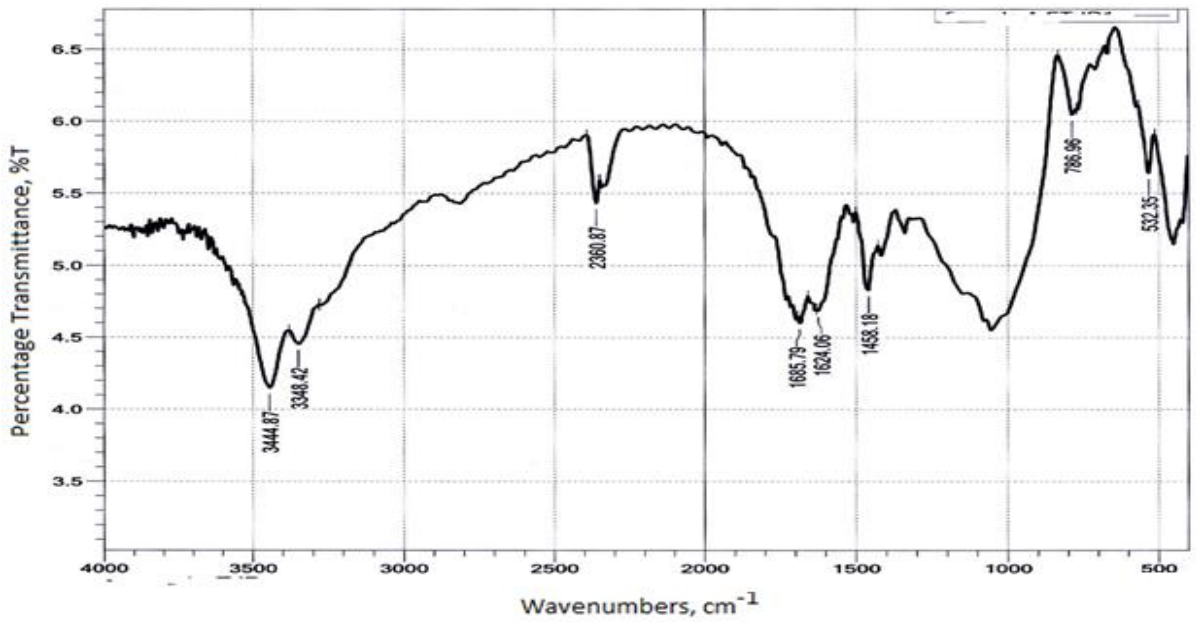

Figure 4. 35 FT-IR spectra of urea loaded sample EB-GA-02

The SEM results below indicate an irregular morphology of the zeolitic samples, with the urea loaded one showing a more granulated surface. Similar results were reported by Mohanraj (2013) and Pereira *et al*., (2013). Difference confirms successful incorporation of the urea fertilizer into the EB-GA-02 adsorbent nanopores.

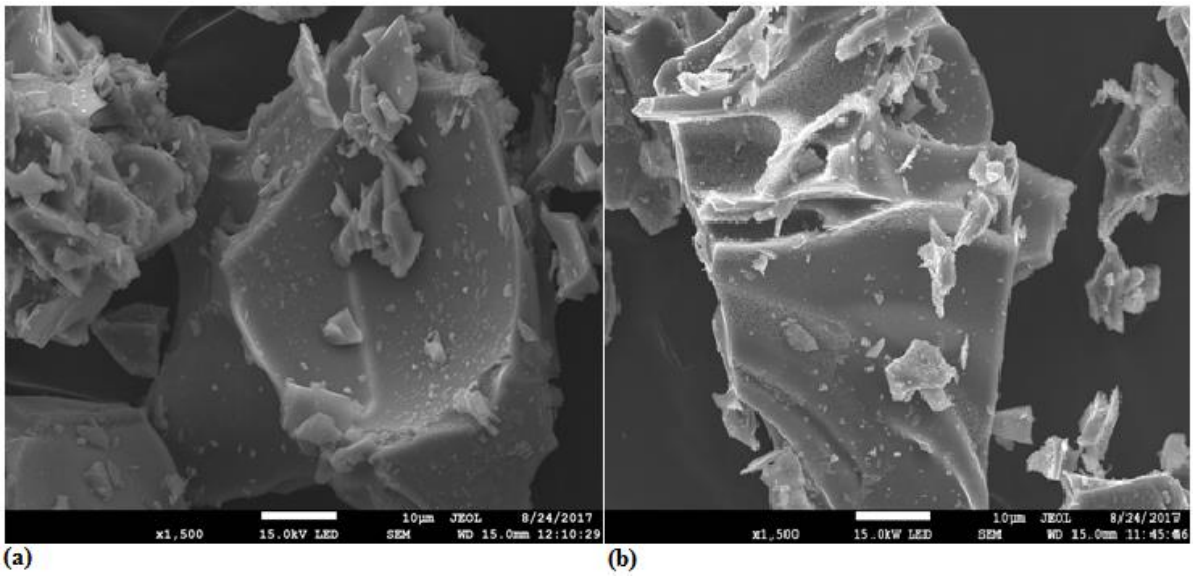

Figure 4. 36 SEM images of EB-GA-02: (a) urea loaded (b) blank

Comparative studies were also conducted on Kikuyu soil (sample KIK-GA-01) for urea loading procedures. The urea loaded soil was also analyzed to confirm the presence urea molecules in their matrix as represented below.

For the X-Ray diffraction analysis of urea loaded Kikuyu soil, indications of urea fertilizer peaks at 2θ values of 22.5, 24.5, 26.5, 29.5, 35.5, 37.0, 41.5, 45.4 and 49.5 degrees were noted as shown in Figure 4.37 below.

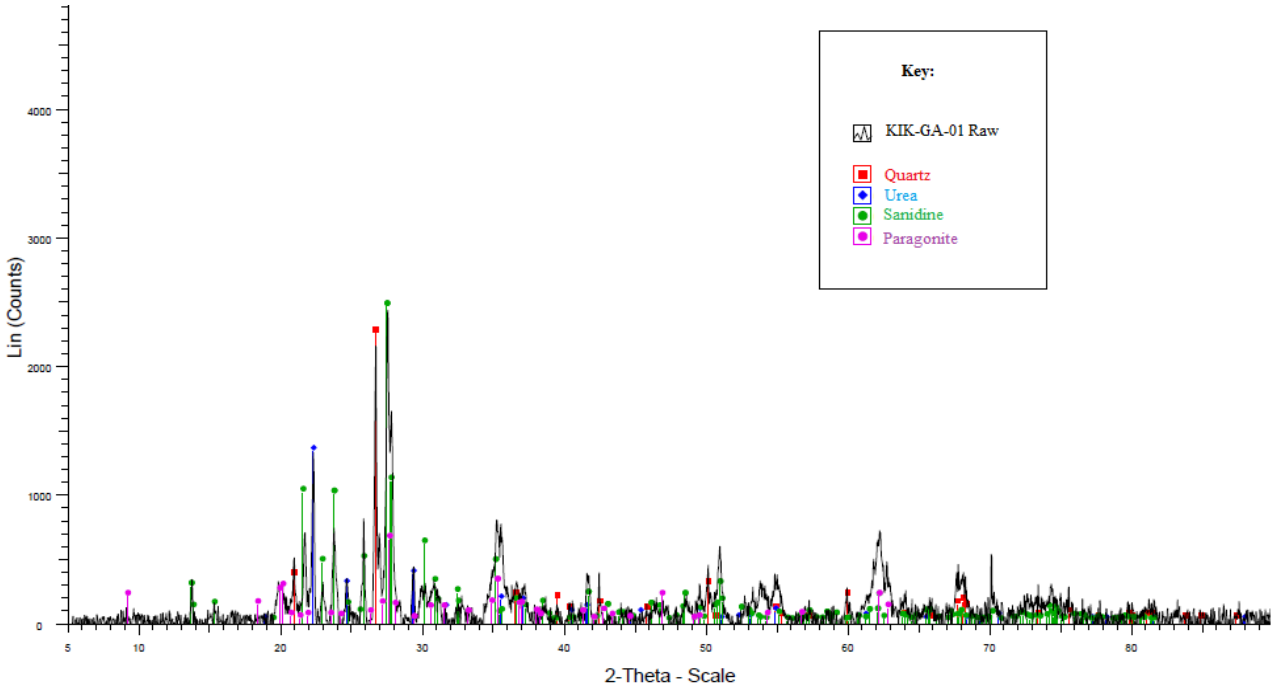

Figure 4. 37 Fertilizer loaded sample KIK-GA-01

Furthermore, the corresponding Infra-red analysis (figure 4.38) of the urea loaded kikuyu soil showed conspicuous peaks of N-H stretching at 3444.87 cm^{-1}, with tiny shoulders at 3618.46 cm^{-1} and 3699.47 cm^{-1}. The C=O stretching peak appears at 1624.06 cm^{-1}, while the C-N stretching peak shifted to 1458.18 cm^{-1}, with their SEM images shown by Figure 4.39 below showing crystal micro-islands compared to the flakey structures in the blank.

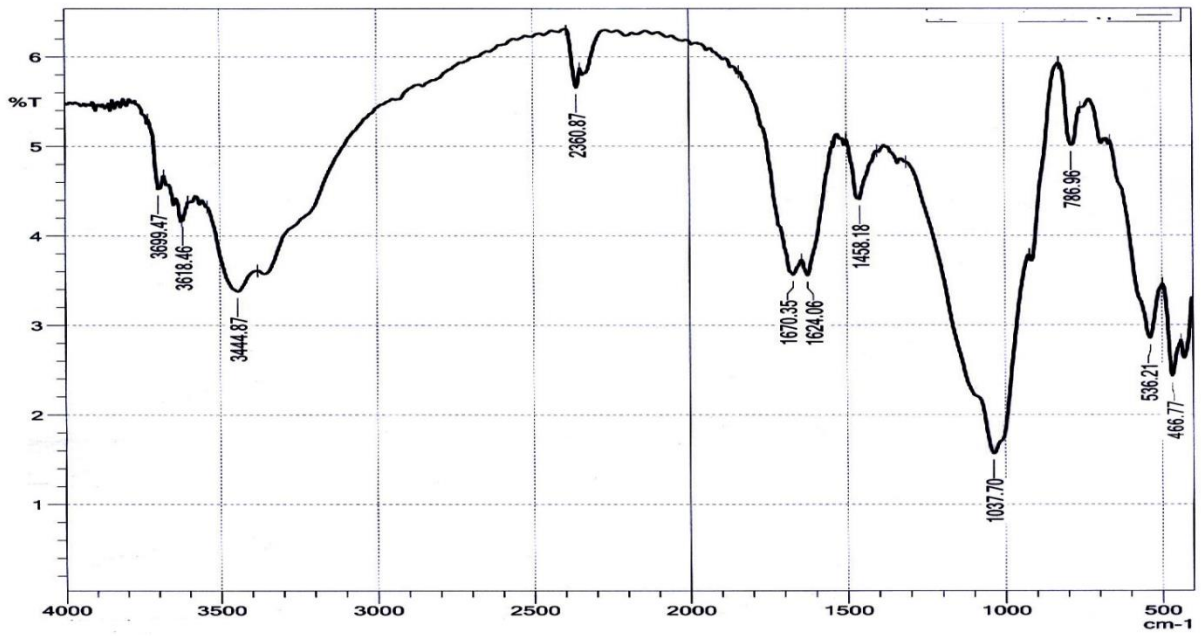

Figure 4. 38 FT-IR spectra of urea loaded sample KIK-GA-01

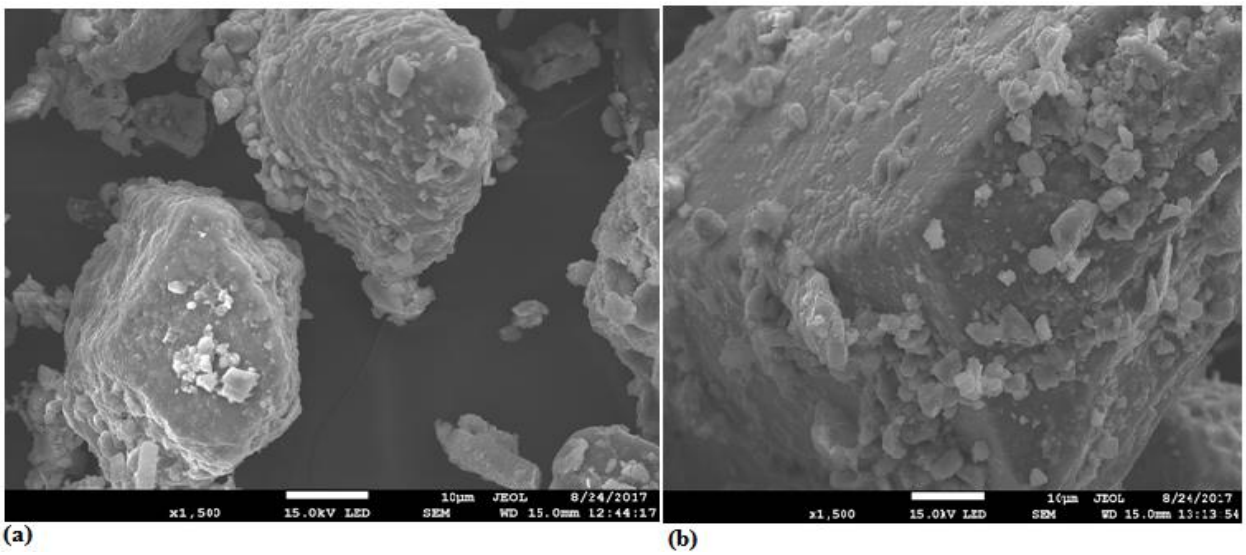

Figure 4. 39 SEM images of KIK-GA-01:(a) urea loaded (b) blank

Nitrogen sorption isotherms of sample EB-GA-02 and their corresponding urea loaded samples UEB-GA-02 are shown in Figure 4.40 below. A summary of some of the physical properties recorded in Table 4.23 indicate a significant reduction in pore sizes after successful loading of urea fertilizer into the nano-spaces by 39.844 %. Intercalation of urea molecules in the

interlamellar spaces of the natural zeolitic material could have led to some expansion of the pore volume sizes by almost 4.68 %. Because of the low purification applied, reduced agglomeration process may have resulted to increased BET surface area after loading the urea molecules.

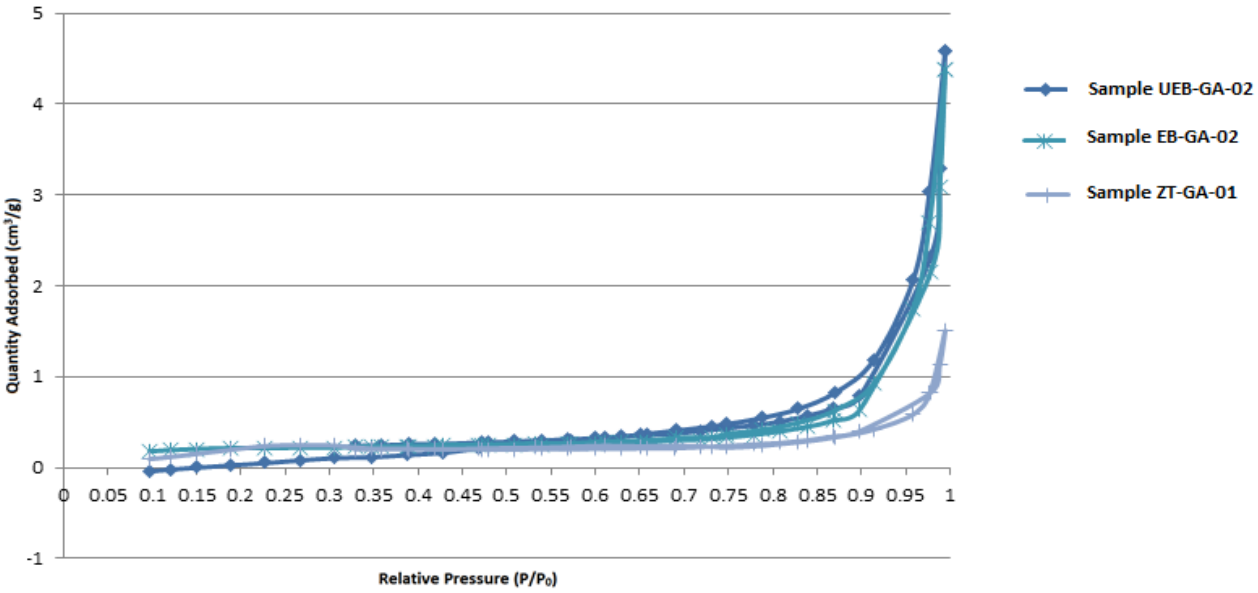

Figure 4. 40 Nitrogen sorption isotherms of ZT-GA-01, EB-GA-02 and UEB-GA-02.

Table 4. 23 Physical properties of samples EB-GA-02 and UEB-GA-02.

PROPERTIES	SAMPLE EB-GA-02	SAMPLE UEB-GA-02
1. Surface Area BET Surface Area (m^2/g)	0.7099	0.7751
t-Plot external surface area (m^2/g)	0.7161	0.9203
2. Pore Volume Single point adsorption total pore volume of pores less than 3 553,365 Å diameter at P/Po = 0,994653432 (cm^3/g)	0.006767	0.007084
Single point desorption total pore volume of pores less than 3 553,365 Å diameter at P/Po = 0,994653432 (cm^3/g)	0.006767	0.007084
t-Plot micropore volume (cm^3/g)	-0.000063	-0.000179
3.Pore Size Adsorption average pore diameter (4V/A by BET) (Å)	381.278	365.588
Desorption average pore diameter (4V/A by BET) (Å)	381.278	365.588
BJH Desorption average pore diameter (4V/A) (Å)	389.846	234.516

4.2.4: Modelling studies of fertilizer loaded zeolitic materials in water

Studies on controlled release behavior of urea loaded sample EB-GA-02 was conducted for 18 days, with urea concentration in the aqueous medium determined daily and recorded as shown in Table T4.11 within the appendices, with an ANOVA P-Value of 0.997 consistent with the null hypothesis under a significance level, $\alpha = 0.05$ (Table T4.30). The total amount of desorbed fertilizer was 0.100254919 mol/dm^3. From this study, it was found that a total of 82.8 % of loaded urea fertilizer was released in water from the carrier material sample EB-GA-02. The rate of discharge was rapid initially, but gradually declined beyond the fifth day till the end of the monitoring period, with steady sustainable release of the fertilizer as represented by Figure 4.41 below.

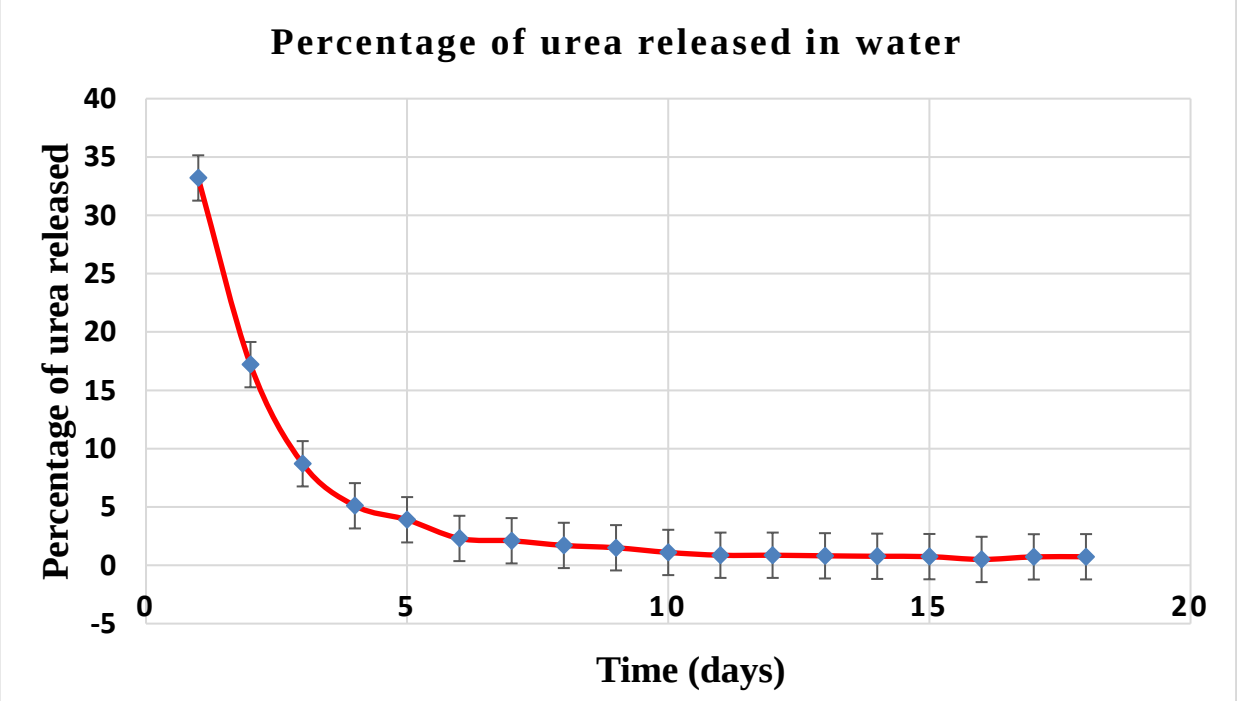

Figure 4. 41 Percentage of urea release in water

Similar research work has been conducted that demonstrate slow release of urea form nanofertilizer based formulations. Rahmat *et al.*, (2015) indicated that urea without zeolites formulation was released up to 100 % limit in just 10 minutes; while urea impregnated with

modified zeolites had a release of up to 100 % at 120 minutes, with a maximum adsorption capacity of 3.668 mg/g.

4.2.5: Modelling studies of fertilizer loaded zeolitic materials in soil

Studies of controlled release behavior of the urea loaded sample EB-GA-02 in Kikuyu soil medium generated data of corresponding concentration values displayed in table T4.12 within the appendices, with an ANOVA P-Value of 0.993 consistent with the null hypothesis under a significance level, $\alpha = 0.05$ (Table T4.30) . The total amount of desorbed fertilizer was determined to be 0.089776702 mol/dm^3, giving a percentage desorption of 74.2 % on the initial amount loaded. Studies conducted by Sharmila (2011) showed that zeolites and montmorillonite were capable of releasing nitrogen for almost over 1000 hours. Graphical representation on the rate of percentage of urea released in Kikuyu soil medium as represented by Figure 4.42 below.

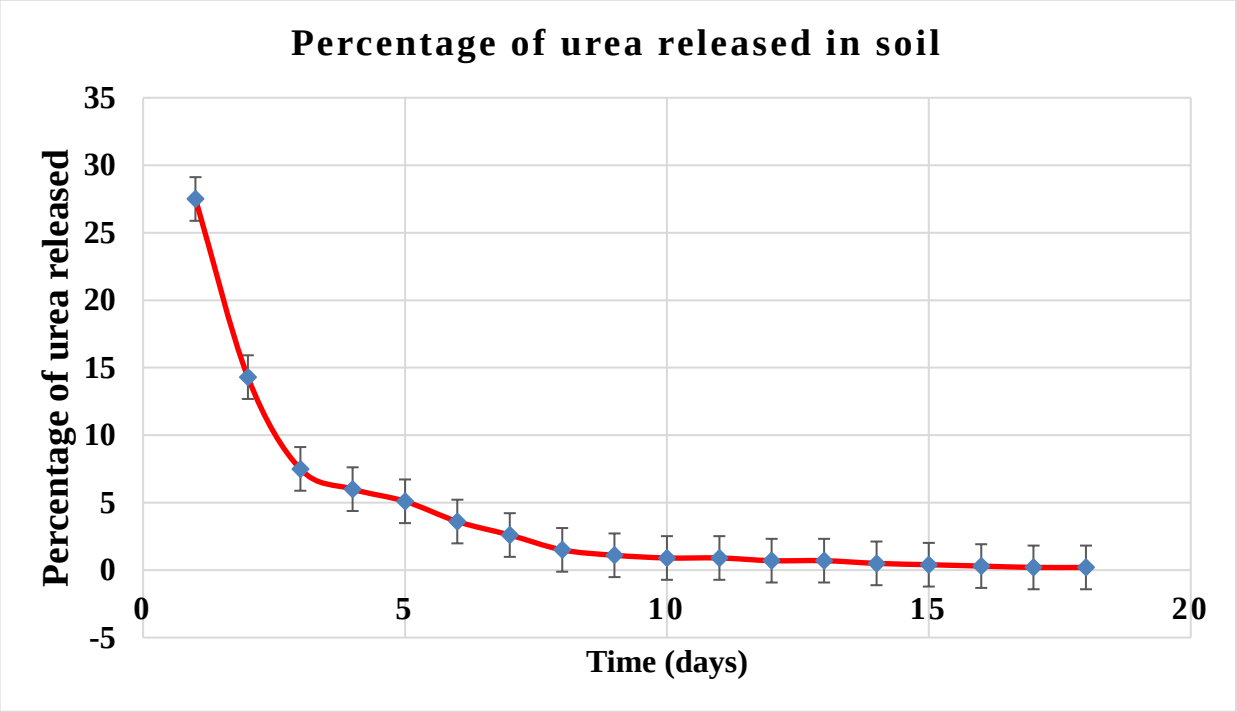

Figure 4. 42 Percentage of urea release in soil

Comparatively, a higher percentage was determined for the discharge of urea loaded sample EB-GA-02 in aqueous medium as compared to discharge on Kikuyu soil medium. As already discussed, natural rock samples of EB-GA-02 had a lower organic carbon content compared to the Kikuyu soil sample KIK-GA-01, a factor that could contribute to low attraction of urea molecules to the sample matrix. Many other factors also affect the adsorption/desorption rates of urea in zeolitic materials and soil matrix. These includes aqueous medium properties like pH and concentration, as well as adsorbate soil properties like particle size, organic carbon content and cationic exchange capacity. Reduction in particle sizes resulted in increased equilibration time and higher adsorption which was also noted at higher contact time.

On the other hand, studies were also conducted on the discharge process of urea loaded Kikuyu soil in aqueous medium and the corresponding data on their determined concentration recorded in Table T4.13 in appendices, with an ANOVA P-Value of 0.990 consistent with the null hypothesis under a significance level, $\alpha = 0.05$ (Table T4.30). Total amount of desorbed fertilizer from urea loaded sample KIK-GA-01 was 0.071309 $moldm^{-3}$ giving a 58.9 % percentage desorption. Previous discussions on this sample KIK-GA-01 which essentially was soil from Kikuyu area indicated a higher organic matter content and proportion of clay. The lower release of loaded urea could then be alluded to stronger binding forces between the urea molecules and the soil matrix, which could be of physicochemical aspect.

Graphical representation of the release process indicates lower percentage changes with a relatively much lower desorption percentage rates as represented by Figure 4.43 below.

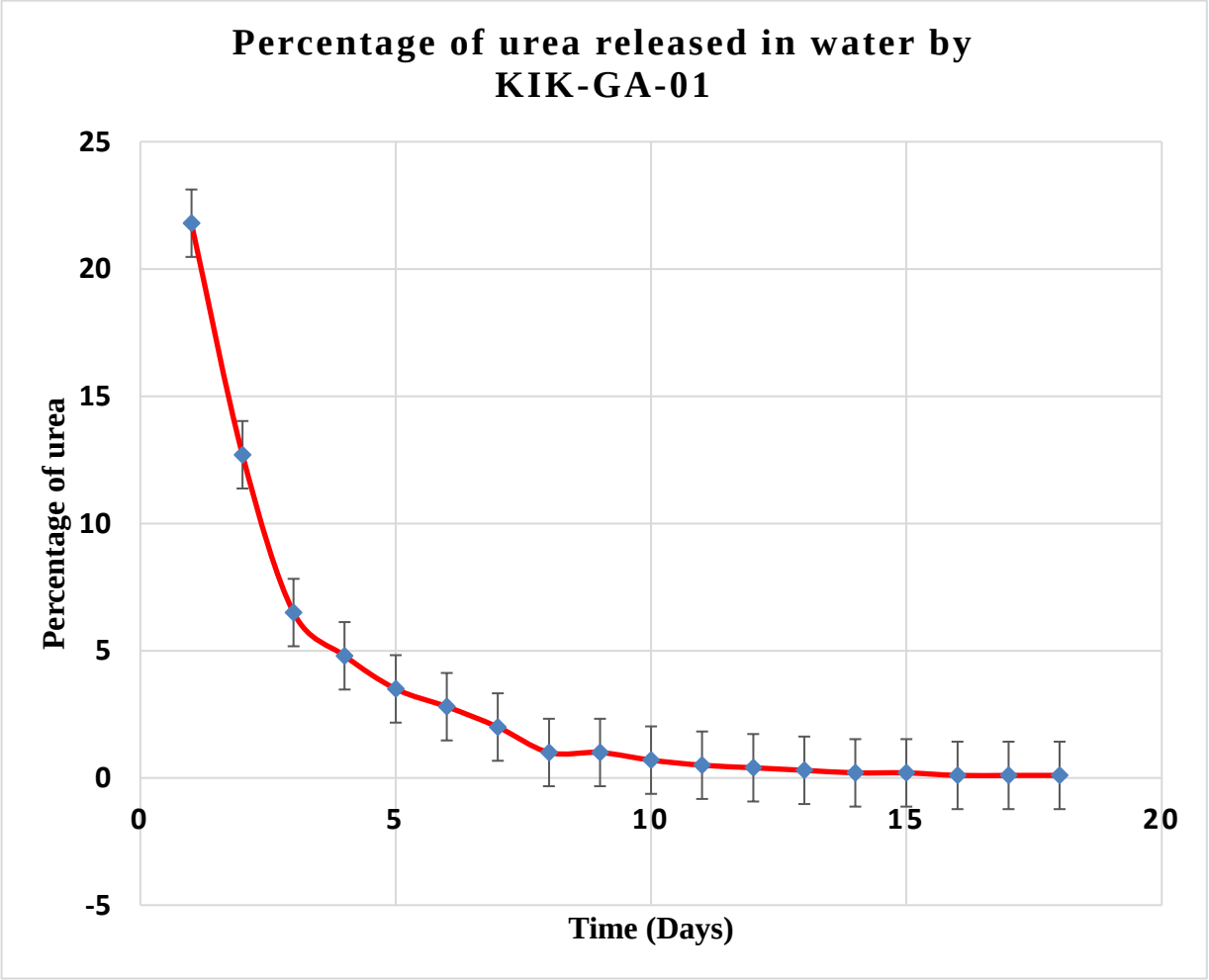

Figure 4. 43 Percentage of urea release in by sample KIK-GA-01

Comparative analysis studies on the urea release for the loaded carrier materials was also conducted for urea loaded sample EB-GA-02 in aqueous medium, urea loaded sample EB-GA-02 in Kikuyu soil and urea loaded sample KIK-GA-01 in aqueous medium represented by ‘a’, ‘b’ and ‘c’ respectively in the ‘key’ for Figure 4.44.

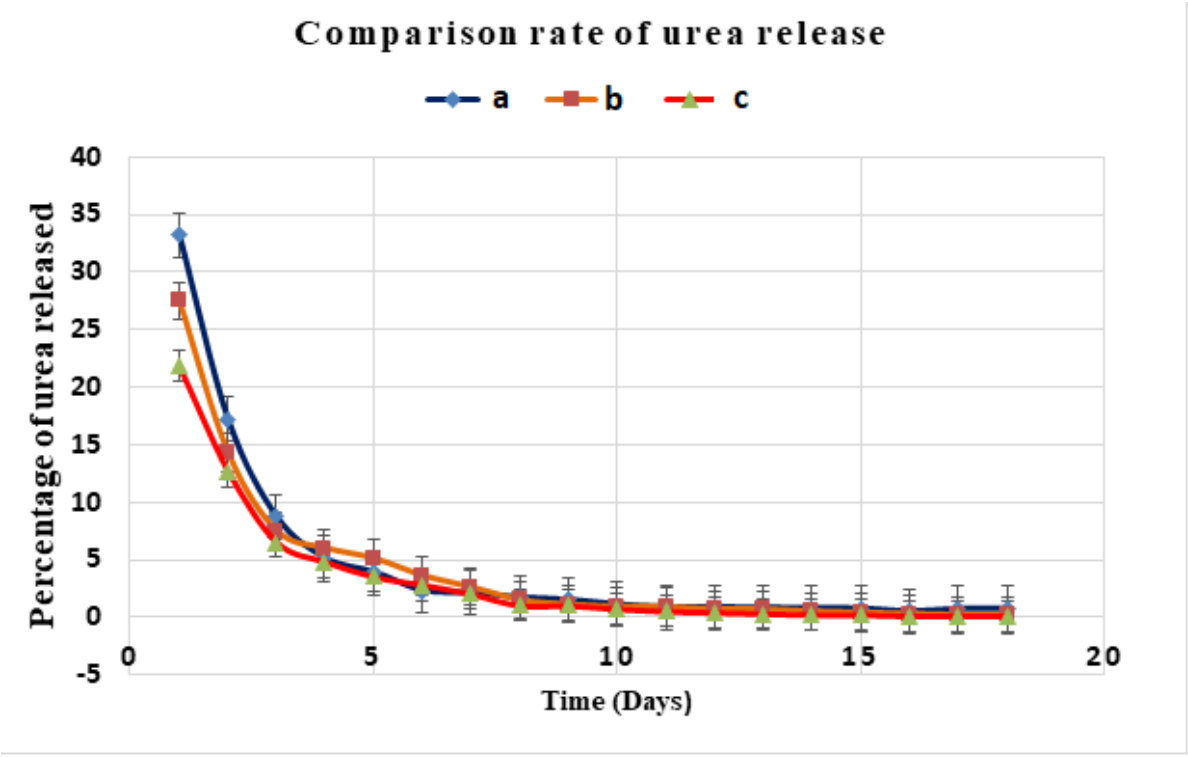

Figure 4. 44 Comparison rate of urea release

Significantly, a higher percentage of urea was discharged in the aqueous medium by the urea loaded sample EB-GA-02 at slower rate on evaluation of the starting point and initial gradient of the three curves in the figure above. Furthermore, this is clearly illustrated by figure 4.45 that represents relative heights of the bars in the graph. Evidently, urea loaded sample KIK-GA-01 had the least discharge amount of urea in aqueous medium as shown by both figures. Beyond the 12 days, the bars of discharge of urea loaded sample EB-GA-02 in aqueous medium was higher proportionally than the others. This implies that loading urea fertilizer into sample EB-GA-02 and applying the same as carrier agents had a better sustained release rate, which could still avail the minimum remaining fertilizer to the crops for slightly longer duration than the direct application.

These findings indicate that when applied as carrier agent, natural zeolites material sample EB-GA-02 could enhance urea utilization by plants. It has been reported that adequate macroelement

fertilization could increase crop yield like green and black gram by 13 % and 38 % respectively over the control (Liu *et al*., 2006). Subramanian et al., (2008) indicated that efficiency and effectiveness of controlled release of nutrients from fertilizer granules can be enhanced by using nanofertilizers and nanocomposite formulations. This has also been proved to reduce pollution effects on the agro-ecosytem, among other benefits attributed to the vast patented products for slow/ controlled release of fertilizers (Ramesh *et al*., 2010; Liu *et al*., 2006; Subramanian *et al*., 2008; De Rosa, 2010 and Selva *et al*., 2017). Manikandan and Subramanian (2014) studied release pattern of nitrogen from urea blended nanoporous zeolites and reported up to 48 days sustained release, while the conventional natural zeolites had 34 days, compared to just 4 days for the same study with no zeolites.

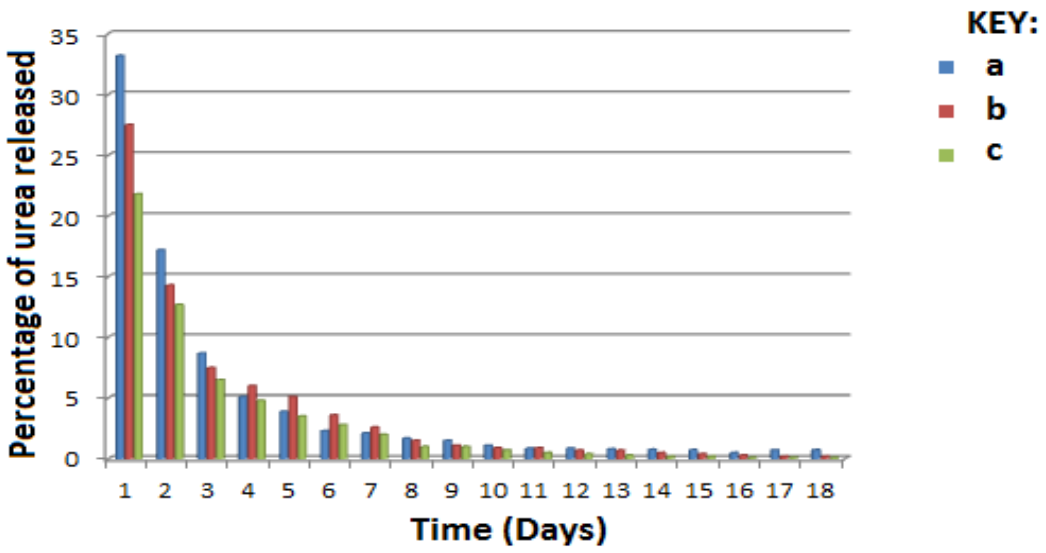

Figure 4. 45 Percentage proportion variation of urea release

4.2.6: Agronomic simulation of urea-zeolitic-soil composites

Urea concentration variations in the soil was determined over 60 days monitoring duration for growing tomatoes and spinach (The generated data was recorded in Table T4.14 in appendices), with an ANOVA P-Value of 0.443 consistent with the null hypothesis under a significance level,

α = 0.05 (Table T4.30). Urea loaded zeolitic sample EB-GA-02 demonstrated a sustained slower but extended releases rate when applied for tomato monitoring (Figure 4.46) and spinach monitoring (Figure 4.48). In both of these figures, it was observed that the graph of urea loaded zeolitic sample EB-GA-02 initially had a lower concentration, but beyond the 25th day, they recorded slightly higher concentration compared to concentration determined by direct fertilizer application.

For tomato studies, urea loaded zeolitic sample EB-GA-02 gave a difference of almost 17.00 % higher concentration, while a difference of about 16.00 % higher concentration was recorded on spinach between the 25th and 35th day as noted in Figure 4.47 and Figure 4.49 below respectfully.

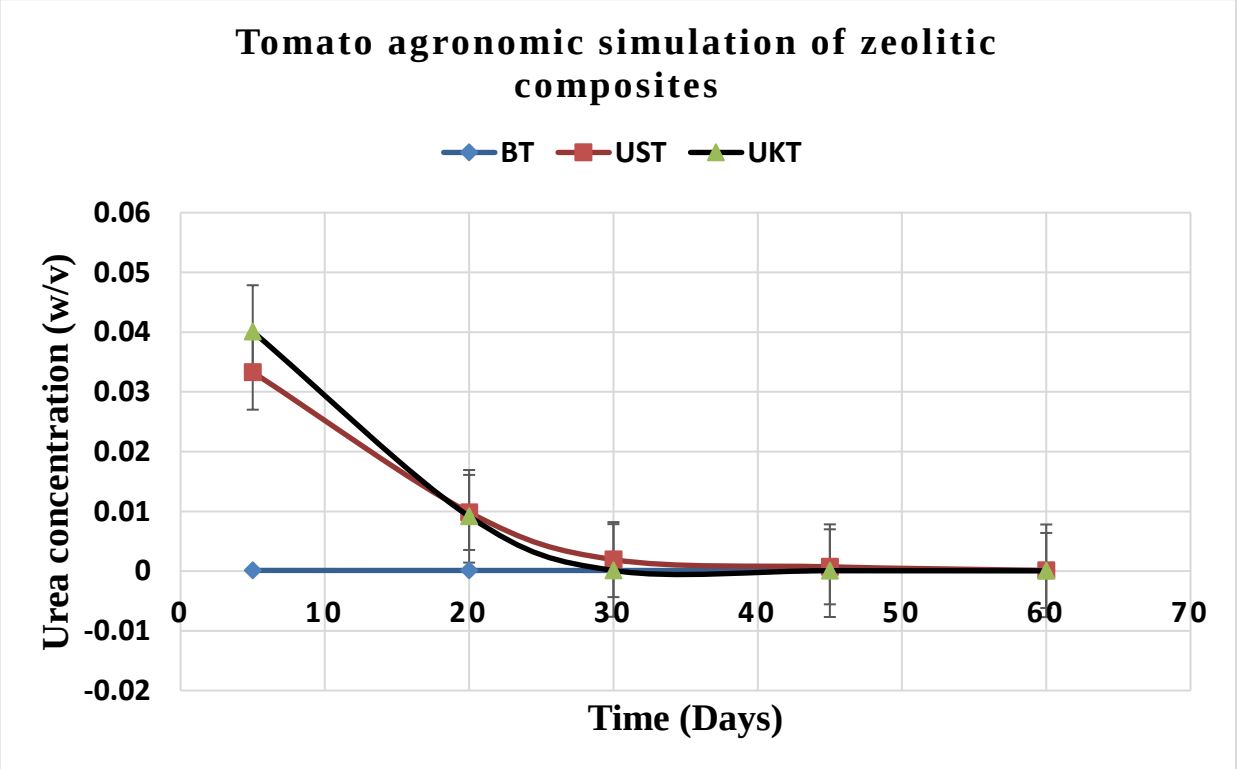

Figure 4. 46 Release rates for urea loaded zeolitic materials in tomatoes studies

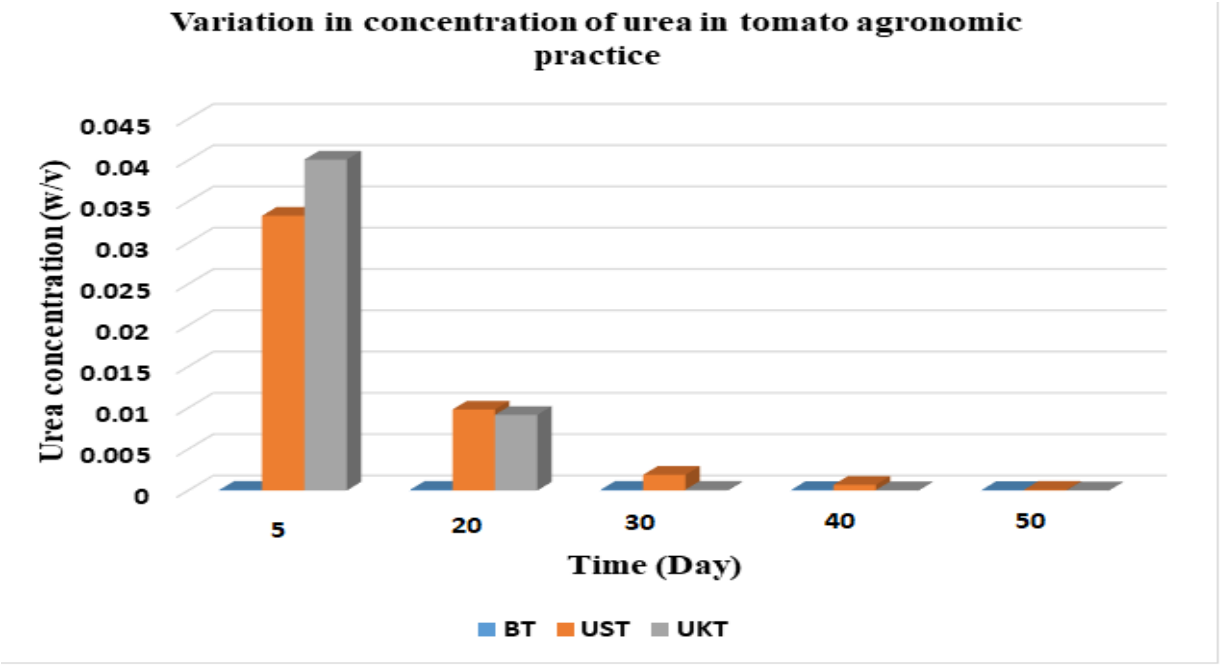

Figure 4. 47 Variations in concentration of urea on tomato studies

Where: BT is Samples taken from a setup of tomatoes grown on blank soil; UST is samples taken from tomato grown using urea loaded sample EB-GA-02 and UKT is samples taken from a set-up of tomatoes grown using commercial urea fertilizer.

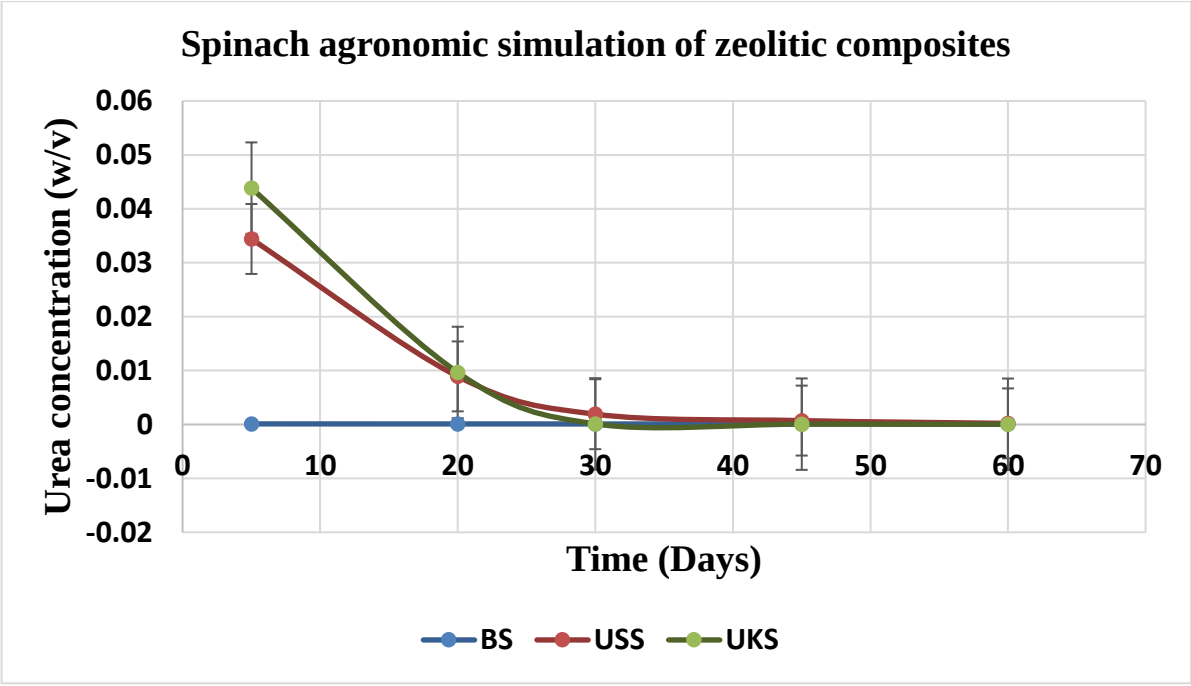

Figure 4. 48 Release rates for urea loaded zeolitic materials in spinach studies

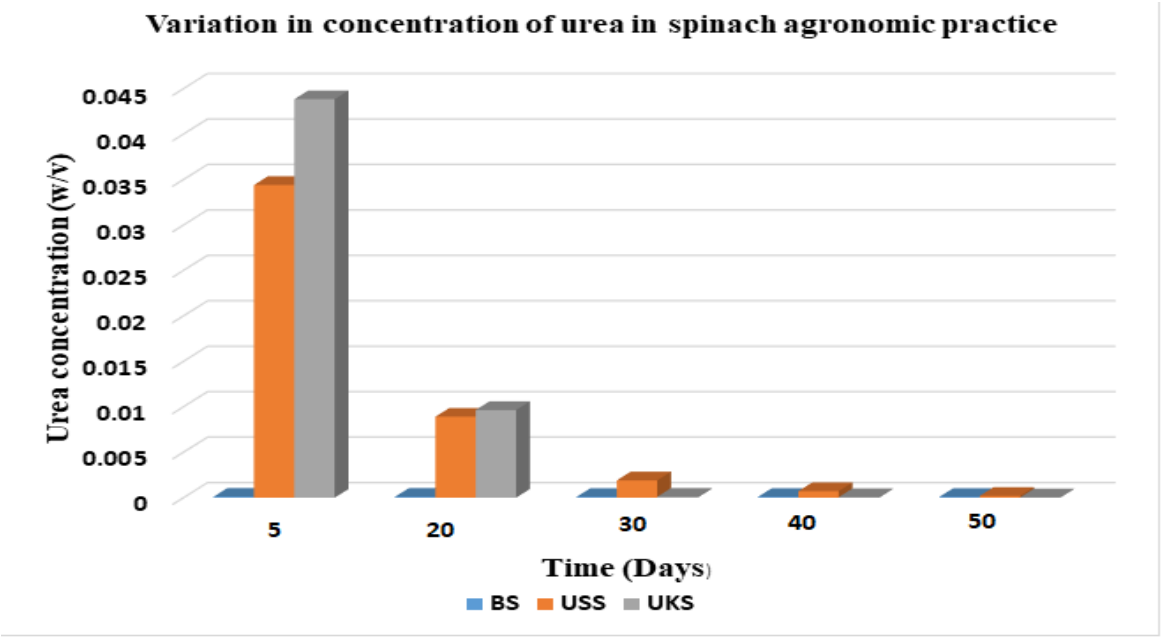

Figure 4. 49 Variations in concentration of urea on spinach studies

Where: BS is Samples taken from a setup of spinach grown on blank soil; USS is samples taken from spinach grown using urea loaded sample EB-GA-02 and UKS is samples taken from a set-up of spinach grown using commercial urea fertilizer.

Therefore, these observations indicate that it is possible to apply urea loaded zeolitic sample EB-GA-02 as carrier agent for urea fertilizer in which the rate of delivery of urea molecules to both tomato and spinach can be monitored. The sustained concentration of urea in the soil over the entire monitoring duration indicated slow delivery process which helps avail the urea nutrients to the plant over a longer duration.

A number of studies have indicated that efficiency and effectiveness in the application of zeolitic material as carrier agents is due to controlled retention of ammonium ions, NH_4^+ which is a product of hydrolysis of urea in soil.

Urea + water → ammonium carbonate

$(NH_2)_2CO + 2H_2O \rightarrow (NH_4)_2CO_3$

ammonium carbonate + hydrogen ions → ammonium ions + carbon dioxide + water

$(NH_4)_2CO_3 + H+ \rightarrow 2NH_4^+ + CO_2 + H_2O$

ammonium ions + hydroxide ions ↔ ammonia + water

$NH_4^+ + OH^- \leftrightarrow NH_3 + H_2O$

High cation exchange capacity of zeolites enables increased ion exchange rate entrapping ammonium ions in the zeolitic matrix structure, hence facilitating partial reduction of ammonia loss through volatilization as well as ground water leaching (Bernadi, 2013; Bartz, 1983 and Fergunson, 1987). Film and particle diffusion have been proposed as the main processes of kinetics in ion exchange of zeolites. This could involve exchangeable ions like Na^+ and K^+ diffusing inside the zeolite framework and the NH_4^+ ions diffusing via the liquid film encompassing the exchangeable cations. The zeolites Si/Al proportion and variety of exchangeable cation could impact the rate of smart delivery process. The channel structure of zeolite like mesopore of around 78 - 115 Å (for clinoptilolite) and great cation exchange capacity of around 2.6 – 3.0 $meq.q^{-1}$ (for stilbite and clinoptilolite respectively) are significant in their effectiveness and efficiency in their application as smart delivery systems (Barros, 2003; Mumpton, 1999; Ming, 2003 and USGS, 2013). Hence, consideration of zeolites as smart delivery system should involve parameters like; size of the molecules to be loaded in the zeolite pores and their hydrophobicity, solvent and methods applied for loading, structure of the zeolites like pore sizes, Si/Al ratio, fertilizer zeolite interactions and related forces or ionic strength and pH of the medium (Spanakis *et al*., 2014; Datt *et al*., 2012; Vilaça *et al*,. 2013 and Datt *et al*., 2012).

4.3: Formulation of smart delivery system for Pesticides

The absorbance curves at wavelength (λ) 218 nm for Lambda-cyhalothrin (derived from data in Table T4.15 of appendices) obeyed Beer's law at lower concentrations (2-10ppm) (as shown in Figure F4.2 of appendices).

4.3.1: Sorption/desorption of pesticide on zeolitic materials

Data obtained for sorption studies for Lambda cyhalothrin pesticide while varying the concentration and contact time on EB-GA-02 was recorded in table T4.16 for absorbance readings and table T4.17 for their corresponding concentrations (displayed in appendices). Figure 4.50 below demonstrates the plots of quantity adsorbed against spiking concentrations generated from the data in table T4.16 above.

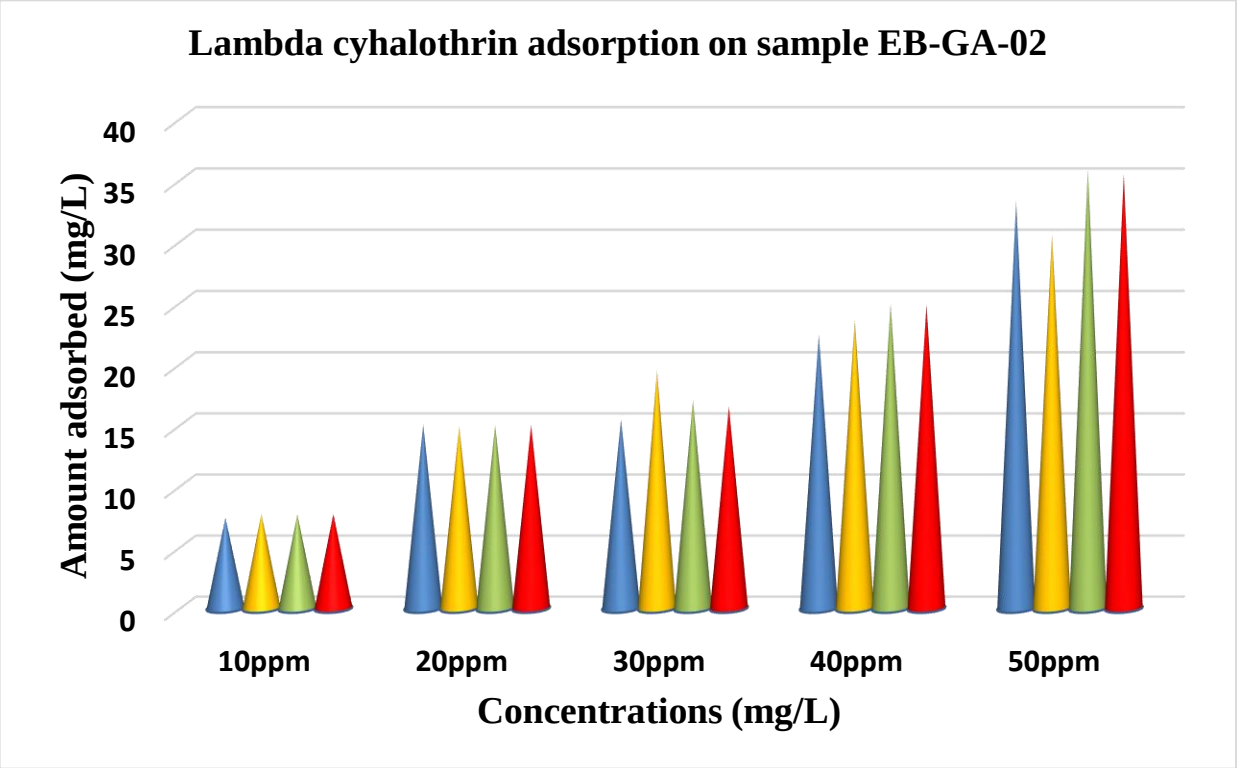

Figure 4. 50 Lambda-cyhalothrin adsorption on samples EB-GA-02

As illustrated from Figure 4.50 and Table T4.17, the quantity of pesticide adsorbed is directly proportional to spiking levels. This was a consequence of higher proportion of unoccupied adsorption destinations, prompting increment in concentration gradient between adsorbate in medium and the adsorbent surface. The equilibration time relied upon the underlying concentration of the pesticide. The lower the amounts, the shorter the time it took to equilibrate due to higher adsorbent surface site ratio to pesticide molecules per unit volume, this explains why the plots are leveled at lower spiking of 10 – 20 ppm despite variation of contact time.

Therefore, increasing the initial pesticide concentration augmented the quantity of pesticide molecules uptake per unit mass of sample EB-GA-02.

Sorption studies for Lambda cyhalothrin pesticide on varying masses of the sorbate generated data in table T4.18 for their absorbance and table T4.19 for their corresponding concentration values (in the appendices), with an ANOVA P-Value of 0.989 consistent with the null hypothesis under a significance level, $\alpha = 0.05$ (Table T4.30). Variation in masses of sample EB-GA-02 reported overall positive gradient on amounts of Lambda-cyhalothrin molecules adsorbed, as shown in Figure 4.51 below. Increase in amount of sample EB-GA-02 increased the concentration of the pesticide adsorbed. Where [Ceav] is the average scan equilibrium concentration in mg/L of the pesticide after shaking with the samples and q_e is the amount of equilibrium adsorbed pesticide in mg/L.

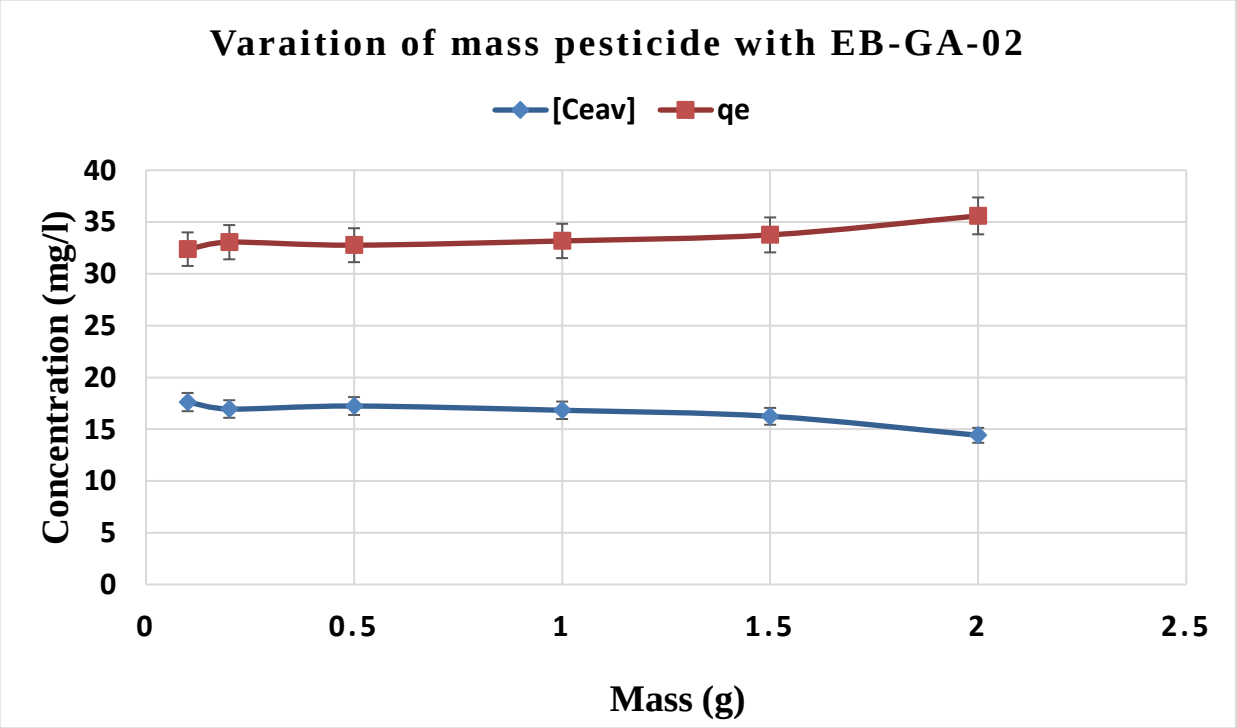

Figure 4. 51 Varying mass of sample EB-GA-02 with concentration of pesticide

Similarly, percentage of pesticide removed from aqueous medium increased from 65 – 70 % when the mass of sample EB-GA-02 increased from about 0.2 – 2.0 g (Figure 4.52). Increasing amounts of sample EB-GA-02 relates to increasing number of adsorption sites which generates higher adsorption gradient.

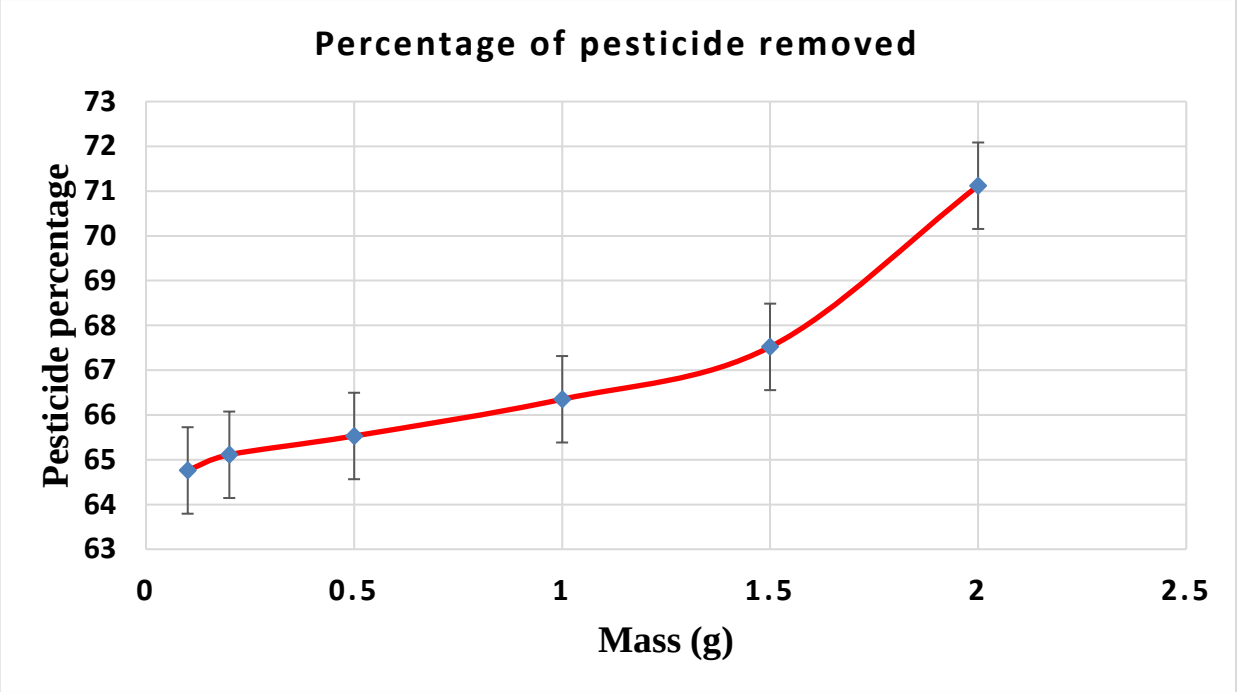

Figure 4. 52 Percentage of pesticide removed

4.3.2: Loading of pesticides into the zeolitic materials

About 15.0 g of soil was spiked with 25 ml of 100 ppm Lambda- cyhalothrin pesticide solution, shaken for 24 hours at room temperature. Equilibration was done in 24 hours, giving the 79.4 % as the amount of Lambda cyhalothrin pesticide removed from the solution. Table T4.20 and Table T4.21 in appendices gives the data obtained in this particular experiment. Hence from this experiment, 79.4 % of Lambda cyhalothrin pesticide was loaded in the weighed mass of the sample EB-GA-02. Confirmation of loading the pesticide molecules into the samples was done using X-Ray diffraction and Fourier Transform Infrared analysis.

X-ray diffraction analysis of Lambda cyhalothrin pesticide loaded sample EB-GA-02 (Figure 4.53) in crystalline form indicates the pesticide 2θ values at 28.5º, 33º, 47º, 56º, 58.5º, 68.5º, 76º, 78º and 87º.

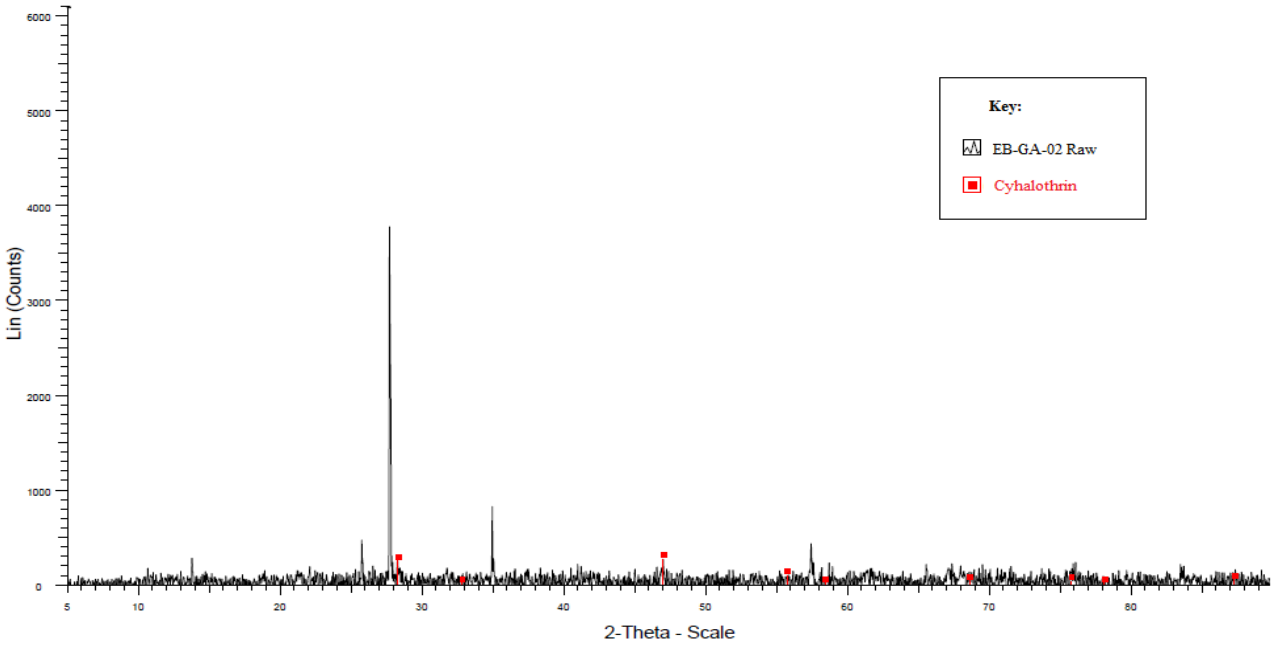

Figure 4. 53 XRD spectra of pesticide loaded sample EB-GA-02

While FT-IR analysis gave the spectrum shown in Figure 4.54 below, with peaks analogous to some of the functional groups present in Lambda cyhalothrin molecule. The corresponding SEM images are shown by Figure 4.55.

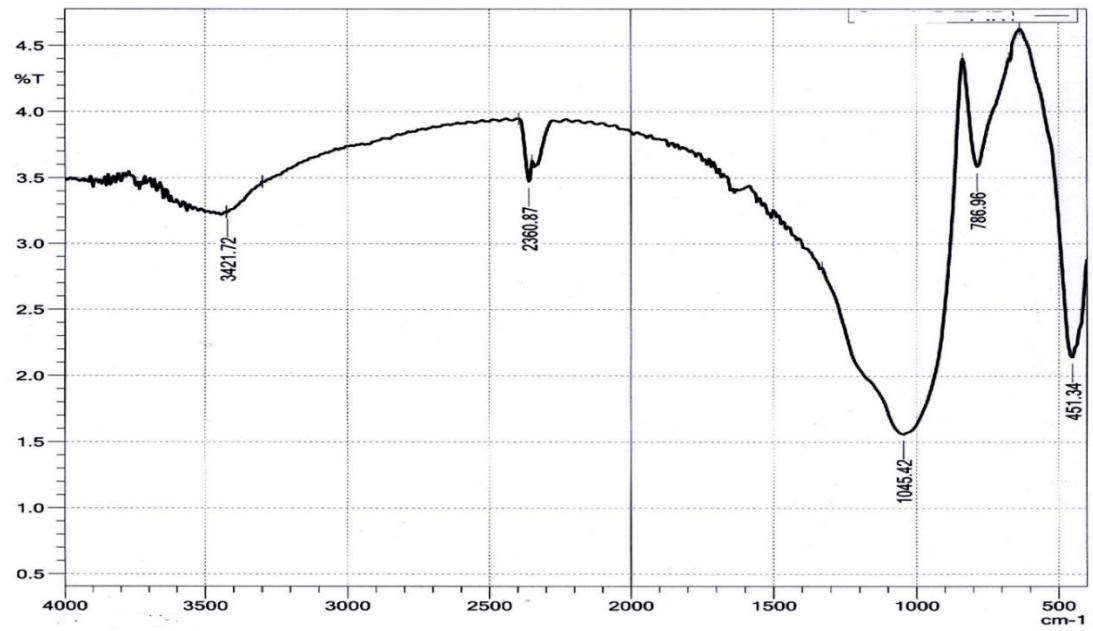

Figure 4. 54 FT-IR spectra of pesticide loaded sample EB-GA-02

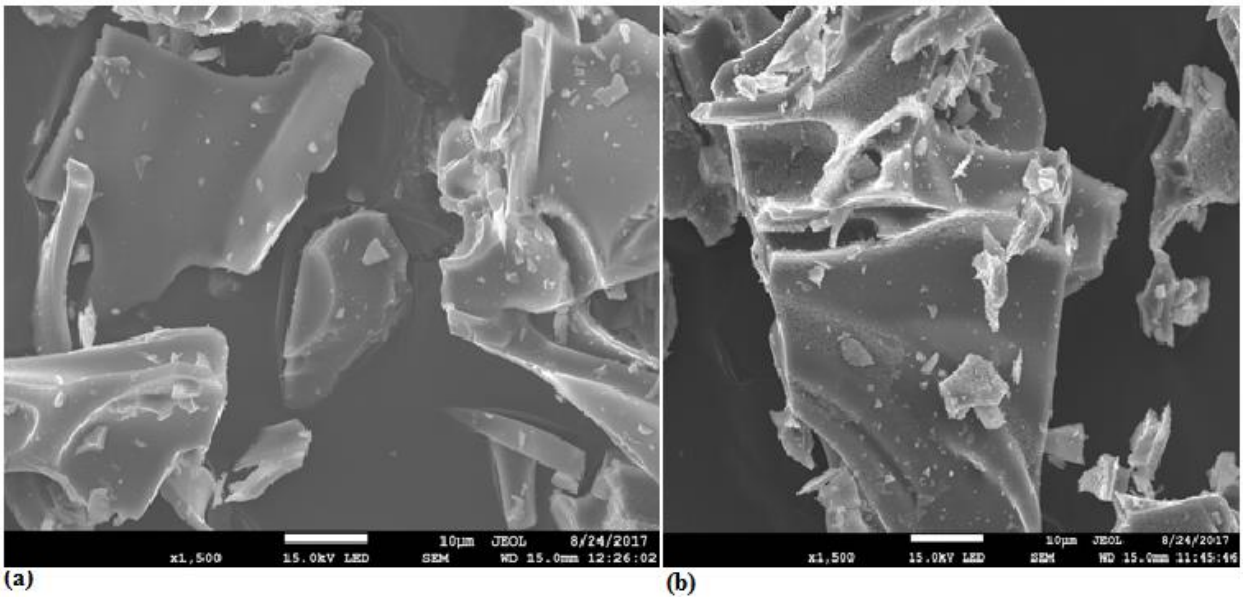

Figure 4. 55 SEM images of EB-GA-02: (a) pesticide loaded (b) blank

Samples KIK-GA-01 was also loaded with Lambda cyhalothrin pesticide under the same procedure as above. Likewise, confirmation of the loaded pesticide was done using XRD and FT-IR characterization.

X-Ray diffraction spectrum of sample KIK-GA-01 (Kikuyu soil) reveals peaks of Lambda cyhalothrin pesticide at 2θ values of 22º, 23º, 23.5º, 24º, 26º, 27.5º, 28º, 28.5º and minor peaks between 30º to 70º as exemplified by Figure 4.56 beneath.

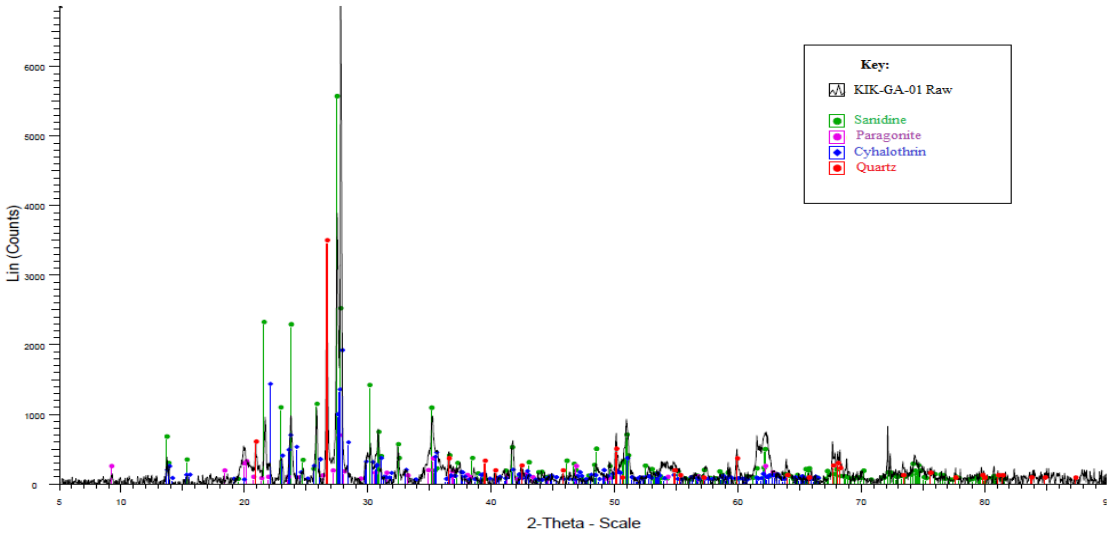

Figure 4. 56 XRD spectra of pesticide loaded sample KIK-GA-01

From the Infrared spectrum in Figure 4.57, some specific peaks associated with some functional groups present in Lambda cyhalothrin structure can be identified. These includes 3695.61 cm^{-1}

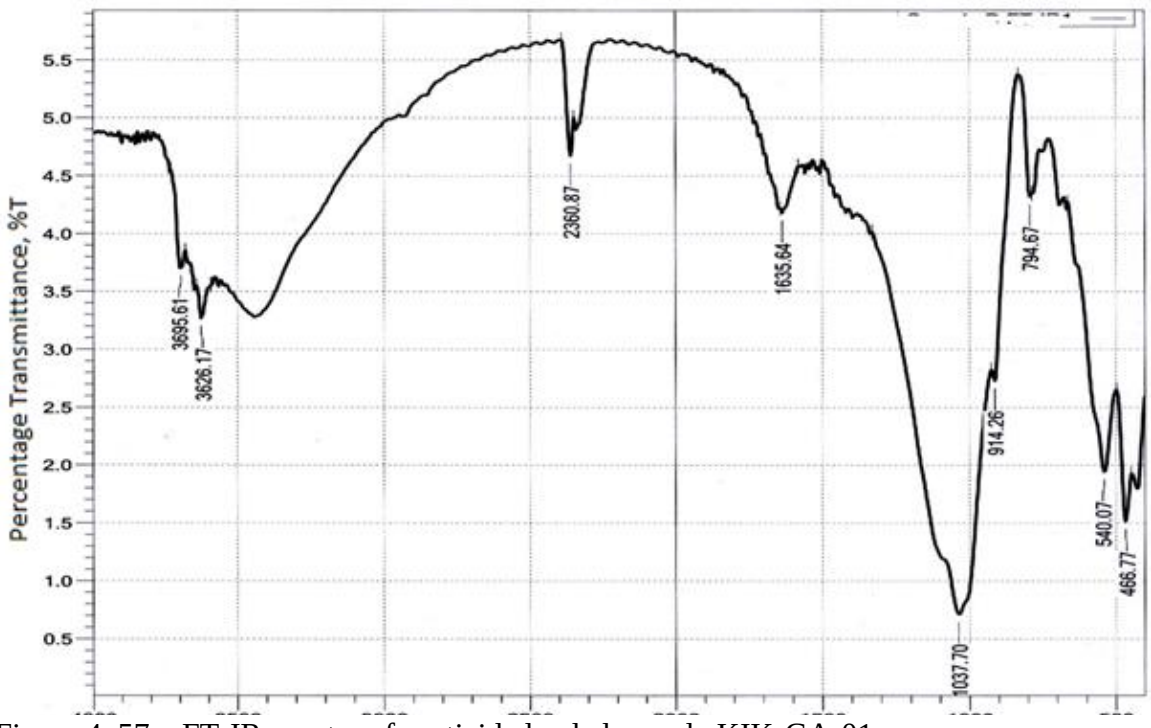

Figure 4. 57 FT-IR spectra of pesticide loaded sample KIK-GA-01

associated with C-H stretching in heterocyclic compounds,1635.64 cm^{-1} for esters, 1037.7 cm^{-1} for C-O stretching in ethers and 794.67 cm^{-1} that could be associated with C-F stretching for halogen substituted organic compounds (Stuart, 2004). The SEM images were shown by Figure 4.58.

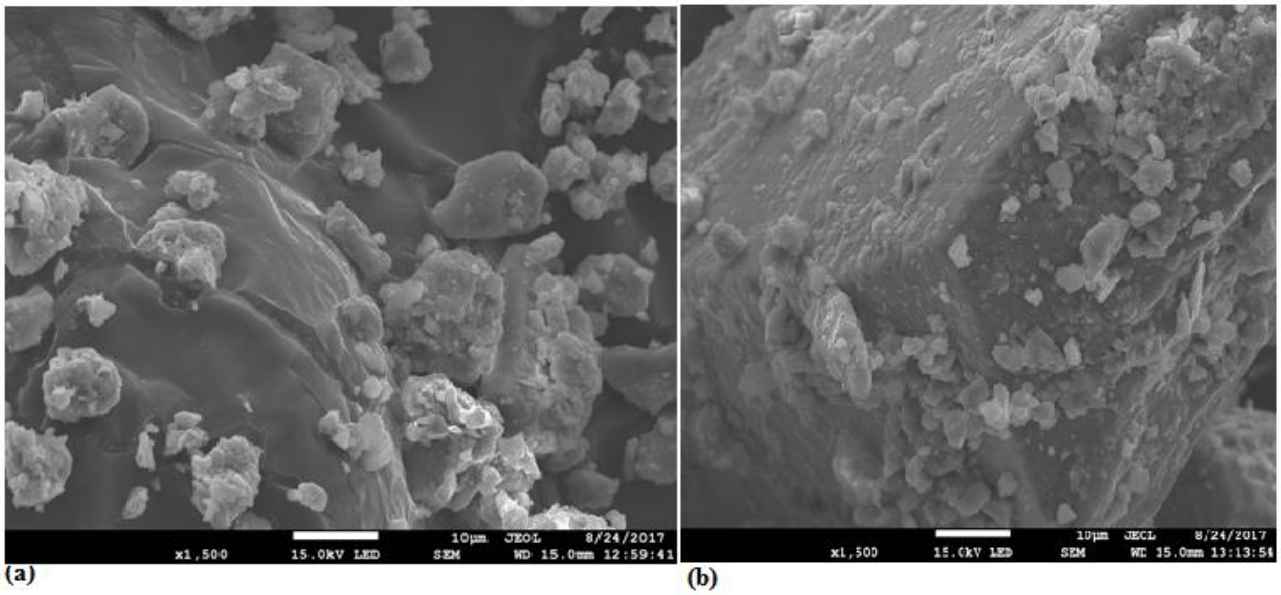

Figure 4. 58 SEM images of KIK-GA-01: (a) pesticide loaded (b) blank

Nitrogen sorption isotherms of sample EB-GA-02 and their corresponding pesticide loaded samples PEB-GA-02 are shown in Figure 4.59 below. A summary of some of the physical properties recorded in Table 4.24 indicate a significant reduction in pore volumes and pore sizes by 19.15 % and 32.74 % respectively. Similarly, low purification applied may have resulted in reduced agglomeration process that increased BET surface area after loading the pesticide molecules.

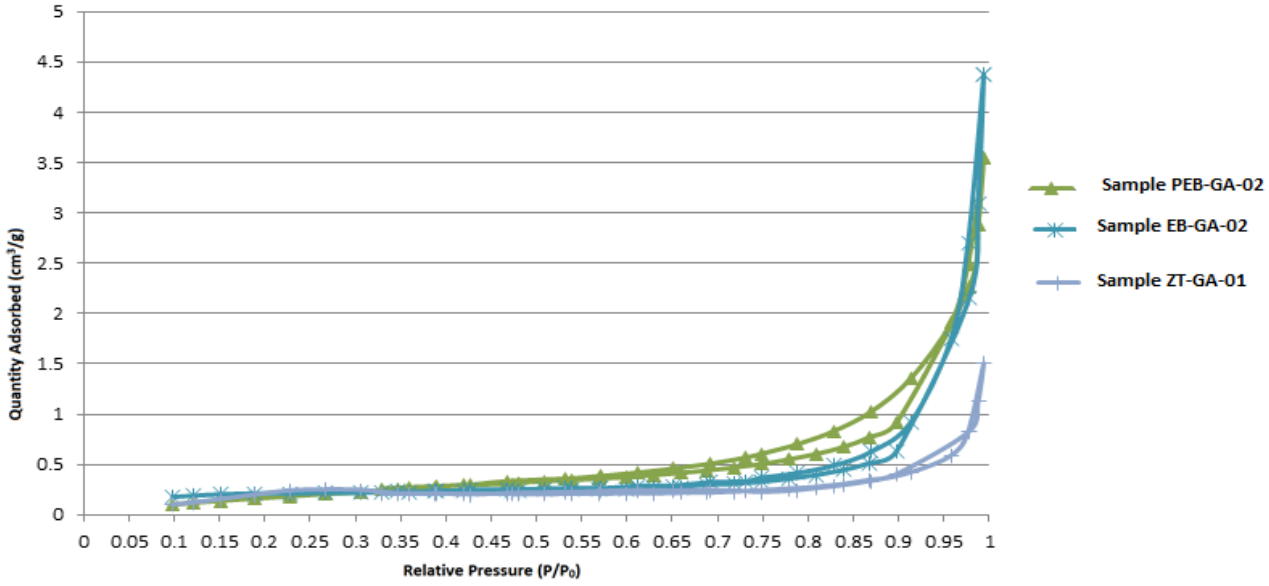

Figure 4. 59 Nitrogen sorption isotherms of EB-GA-02 and PEB-GA-02.

Table 4. 24 Physical properties of samples EB-GA-02 and PEB-GA-02.

PROPERTIES	SAMPLE EB-GA-02	SAMPLE PEB-GA-02
1. Surface Area BET Surface Area (m^2/g)	0.7099	0.8534
t-Plot external surface area (m^2/g)	0.7161	1.0232
2. Pore Volume Single point adsorption total pore volume of pores less than 3 553,365 Å diameter at P/Po = 0,994653432 (cm^3/g)	0.006767	0.005471
Single point desorption total pore volume of pores less than 3 553,365 Å diameter at P/Po = 0,994653432 (cm^3/g)	0.006767	0.005481
t-Plot micropore volume (cm^3/g)	-0.000063	-0.000246
3.Pore Size Adsorption average pore diameter (4V/A by BET) (Å)	381.278	256.455
Desorption average pore diameter (4V/A by BET) (Å)	381.278	256.898
BJH Desorption average pore diameter (4V/A) (Å)	389.846	197.012

4.3.3: Modelling studies of pesticide loaded zeolitic materials in water

The absorbance readings obtained were recorded in Table T4.22, while their corresponding values obtained recorded in Table T4.23 displayed in appendices, with an ANOVA P-Value of 0.999 consistent with the null hypothesis under a significance level, $\alpha = 0.05$ (Table T4.30). The sum of pesticide discharged in water over the 18 experimental days was 27.304 ppm, giving a 34.4 % discharge of the pesticide loaded sample EB-GA-02 in water from the initial loaded amount of 79.36 ppm.

Desorption studies of Lambda cyhalothrin indicated a rapid discharge of pesticide molecules into the aqueous medium (Figure 4.60), with more than 50 % desorbed within the first four days.

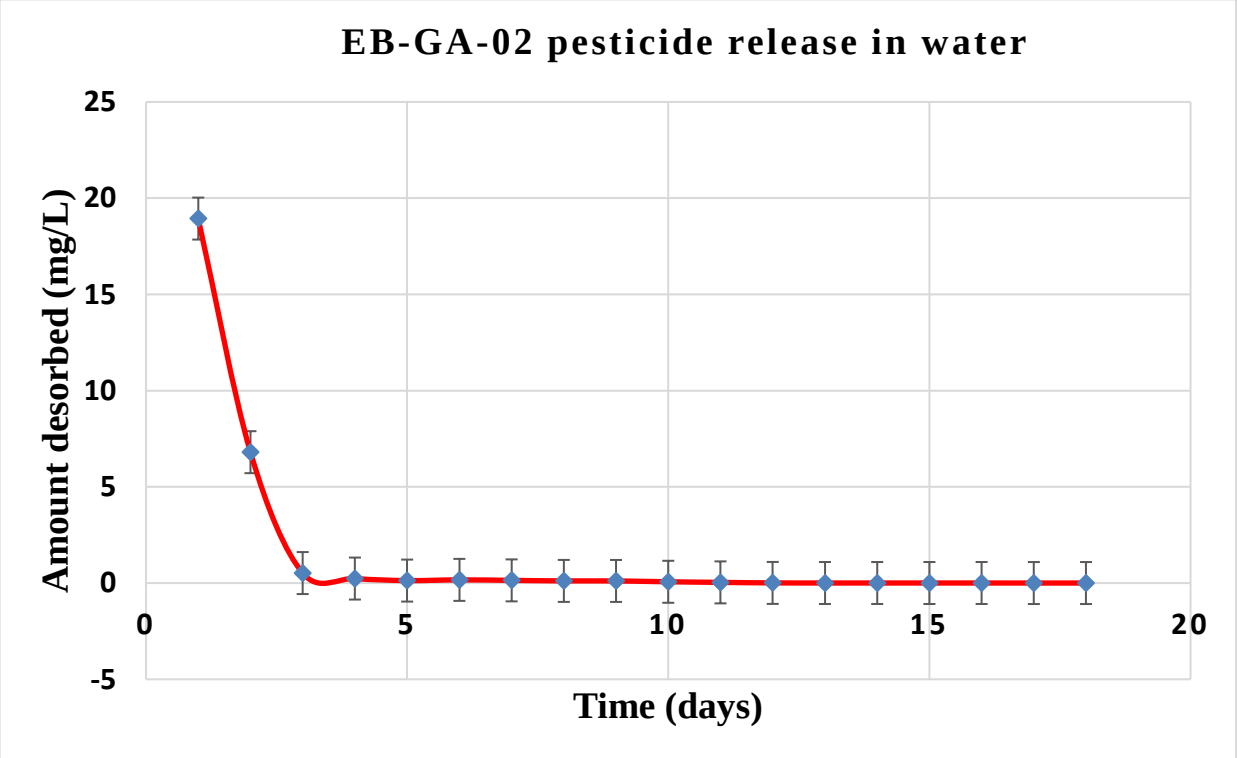

Figure 4. 60 Pesticide released with time by sample EB-GA-02 in water

4.3.4: Modelling studies of pesticide loaded zeolitic materials in soil

Data of release of Lambda cyhalothrin pesticide in soil (Kikuyu soil) was recorded in Table T4.24 for absorbance and the corresponding concentrations in Table T4.25 within the appendices, with an ANOVA P-Value of 1.000 consistent with the null hypothesis under a significance level, α = 0.05 (Table T4.30). This gave 40.1 % as the amount of Lambda cyhalothrin pesticide discharged by pesticide loaded sample EB-GA-02 into the soil over the 18 experimental days.

From Figure 4.61 below, more than 50 % of the above discharged pesticide occurred in the first 5 days. Decreased gradual discharge of the pesticide was recorded in the subsequent days.

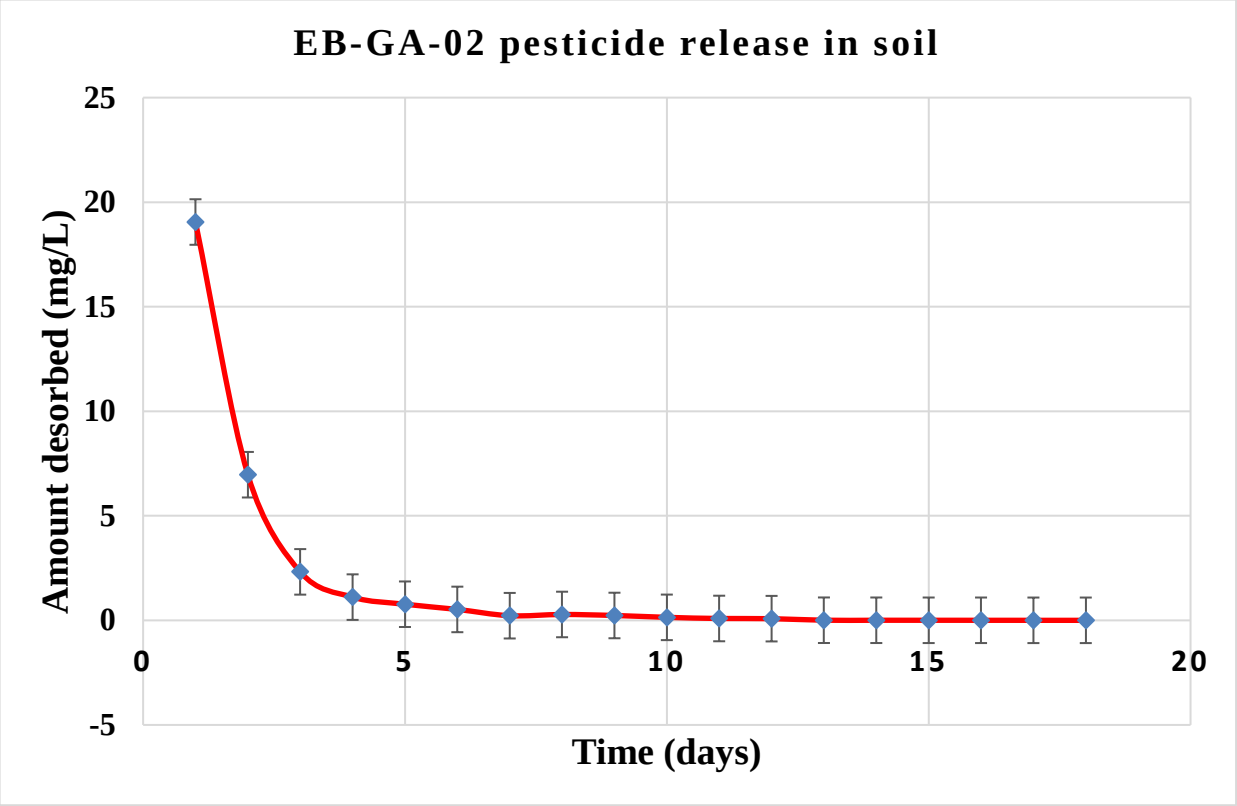

Figure 4. 61 Pesticide released with time by sample EB-GA-02 in soil

Although the literature reported soil adsorption (K_{oc}) for Lambda cyhalothrin (247,000 – 330,000 cm^3g^{-1}) (section 2.14.2.2) is a high value, which is indicative of high preferential affinity to organic matter, only 0.94 % of sample EB-GA-02 was the total organic content. This low organic composition could be strongly attributed to the high initial desorption rates.

Similarly, Lambda cyhalothrin pesticide release by sample KIK-GA-01 was studied and recorded in appendices. Table T4.26 gives the absorbance reading obtained while Table T4.27 gives their corresponding concentration values, with an ANOVA P-Value of 0.999 consistent with the null hypothesis under a significance level, $\alpha = 0.05$ (Table T4.30). Notably, 37.364 % of the pesticide was released by the pesticide loaded sample KIK-GA-01 in aqueous medium. Graphical representation of the amount of pesticide released in water is as shown in Figure 4.62 below.

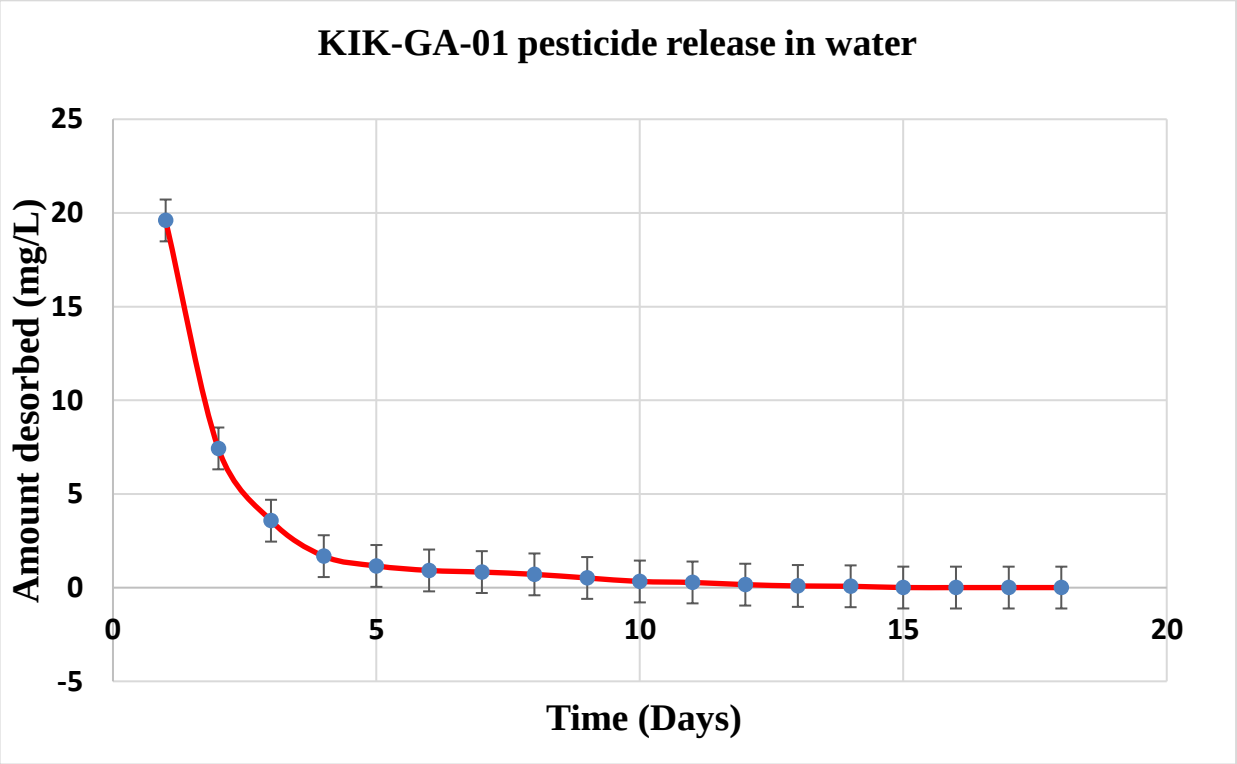

Figure 4. 62 Pesticide released with time by sample KIK-GA-01 in water

Comparative discharge studies were conducted between the pesticide loaded sample EB-GA-02 in aqueous medium, pesticide loaded sample EB-GA-02 in Kikuyu soil and finally pesticide loaded sample KIK-GA-01 in aqueous medium. The results obtained were represented in Figure 4.63 and Figure 4.64 below.

The rate of discharge of the pesticide loaded zeolitic materials in aqueous medium was the highest as seen by graph x in Figure 4.63 having the steepest initial gradient. This could be attributes to very low organic matter content present in these natural rock materials, hence exhibiting low

physicochemical interface amongst the Lambda cyhalothrin particles and the sorption sites of the rock.

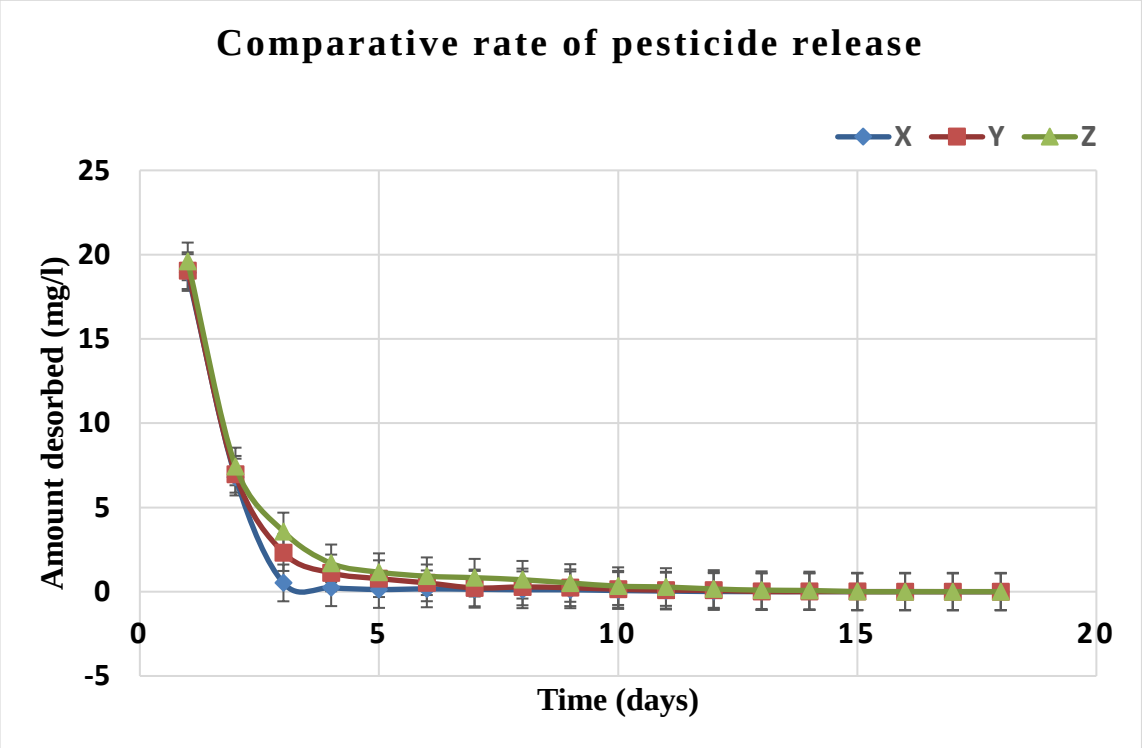

Figure 4. 63 Comparison rate of pesticide release

EB-GA-02 release in aqueous medium, y represents pesticide loaded sample EB-GA-02 mixed with soil from Kikuyu and z represents pesticide loaded sample KIK-GA-01 release in aqueous medium).

Pesticide loaded Kikuyu soil (sample KIK-GA-01) had the least discharge of the loaded pesticide in aqueous medium as represented by 'z' illustrated by plots in Figure 4.63 and the bar chart in figure 4.64. Review of properties of Kikuyu soil indicates that it had higher carbon content at 2.7 %, with more silt and clay medium in it, which could imply a relatively higher physicochemical interaction between the Lambda cyhalothrin molecules and the soil particles. This implies that more pesticide molecules were retained by the soil molecules and matrix.

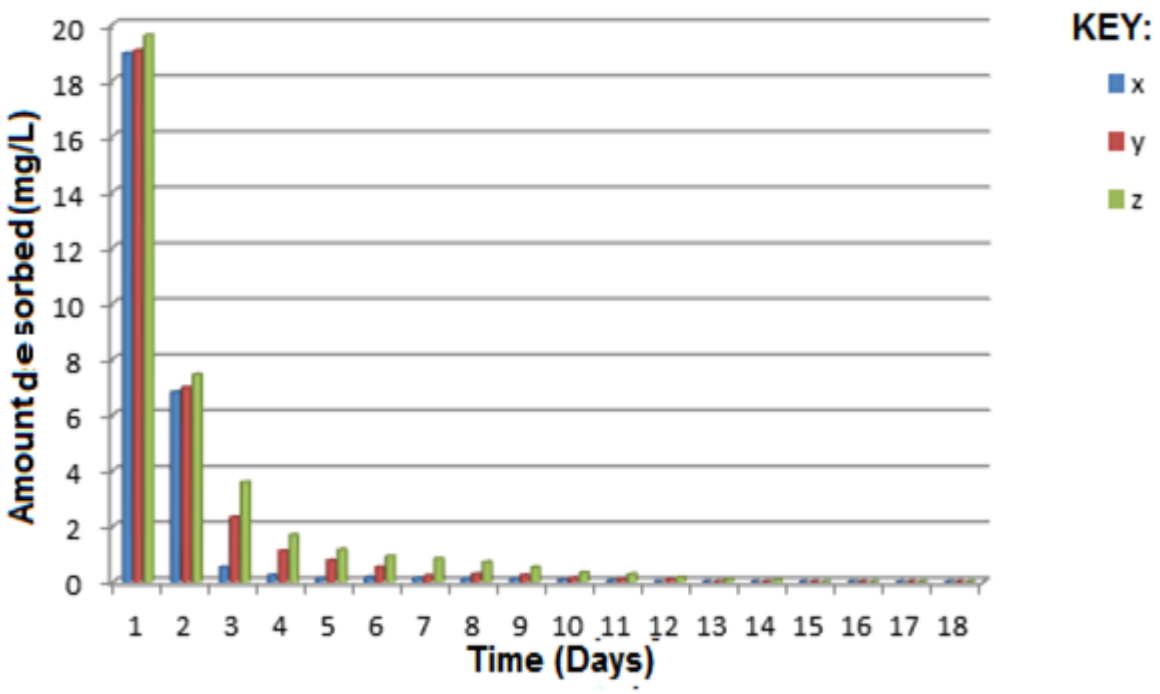

Figure 4. 64 Proportion variation of pesticide release

Where x represents pesticide loaded sample EB-GA-02 release in aqueous medium, y represents pesticide loaded sample EB-GA-02 mixed with soil from Kikuyu and z represents pesticide loaded sample KIK-GA-01release in aqueous medium.

4.3.5: Agronomic simulation of urea-pesticide-soil composites

Concentration data determined from the 60 days monitoring experiments on growing tomatoes and spinach were recorded in Table T4.28 (within the appendices), with an ANOVA P-Value of 0.569 consistent with the null hypothesis under a significance level, $\alpha = 0.05$ (Table T4.30). For tomatoes monitoring studies, the concentration of the pesticide in the soil done over 60 days' duration indicated a sustained slow decrease when pesticide loaded zeolitic sample EB-GA-02 were applied as compared to direct application of the pesticide (Figure 4.65).

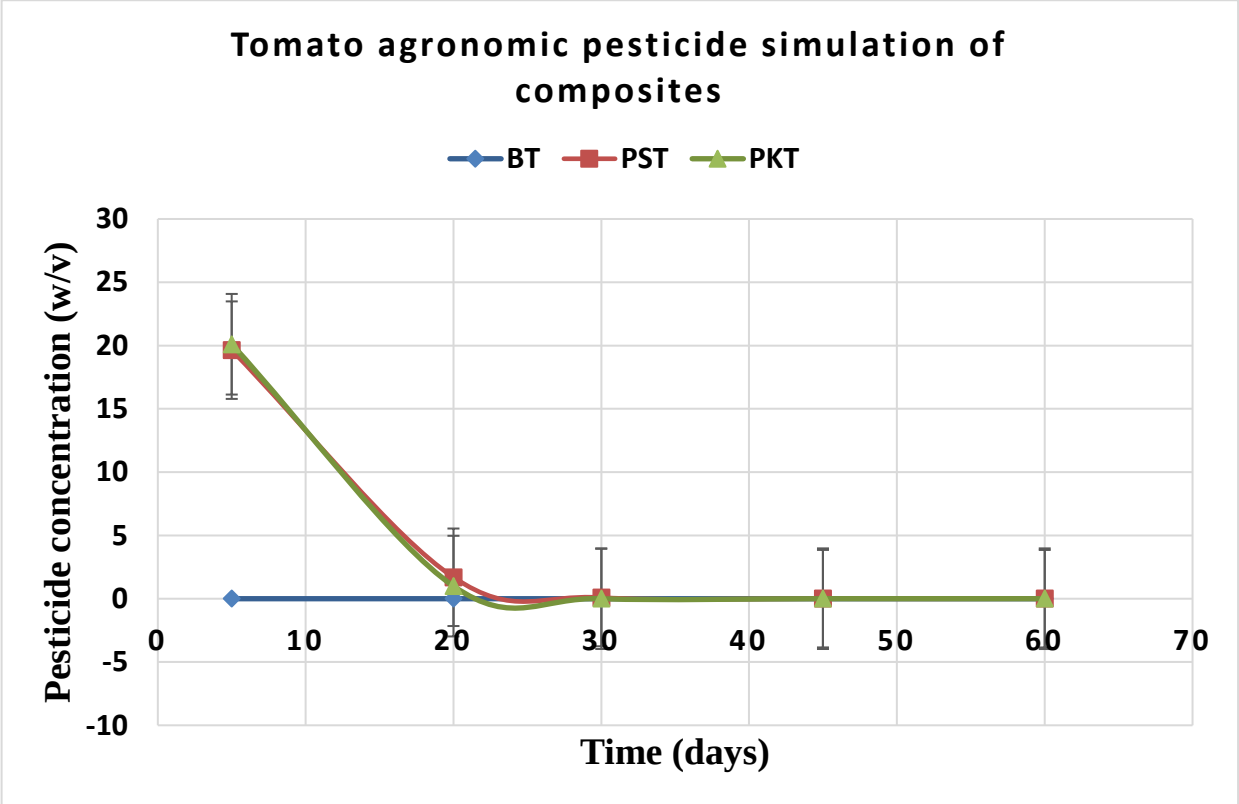

Figure 4. 65 Release rates for pesticide loaded zeolitic materials in tomatoes studies

Initially, there was more pesticide in the soil where direct application was done, mainly over the first 10 days, but around the 20th day, a higher concentration of Lambda cyhalothrin which was more than fivefold, was recorded for the soils in the experiments done using pesticide loaded zeolitic sample EB-GA-02 at almost 70 % difference (Figure 4.66). This indicated a sustained release over the remaining monitoring duration.

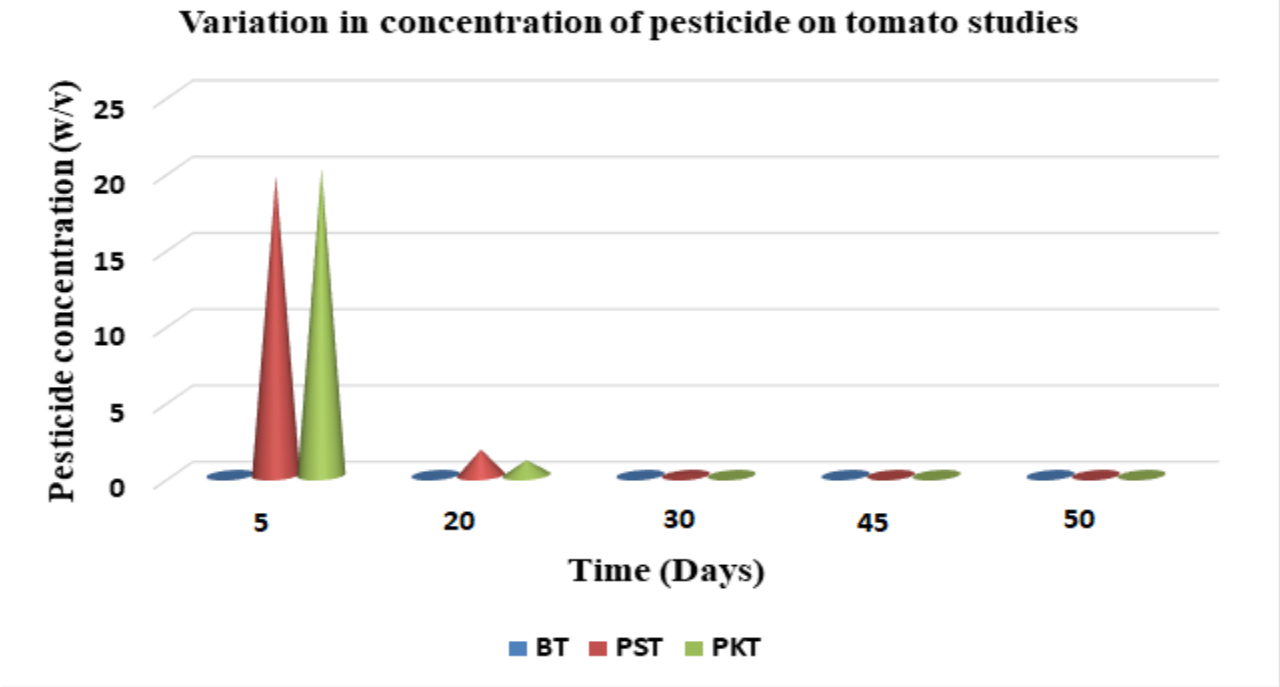

Figure 4. 66 Variations in concentration of pesticide on tomato studies

Where BT were samples taken from a setup of tomatoes grown on blank soil, PST were samples taken from a setup of tomatoes grown using pesticide loaded sample EB-GA-02 and PKT were samples taken from a setup of tomatoes grown using commercial pesticide.

Similar trends were observed when it came to spinach studies. Generally, over the 60 days' duration, there was a more sustained release of Lambda cyhalothrin pesticide into the soil by the pesticide loaded sample EB-GA-02 (Figure 4.67). Higher concentration amounts were noted in the soil, particularly from the 15th day to the 35th day (Figure 4.68), with a 69 % highest value recorded around the 30th day. These findings reinforce the idea of sustained and controlled release of pesticide molecules by the zeolitic loaded samples. Hence, zeolitic samples EB-GA-02 were successfully used as smart delivery systems for lambda cyhalothrin pesticide when applied to both tomatoes and spinach studies.

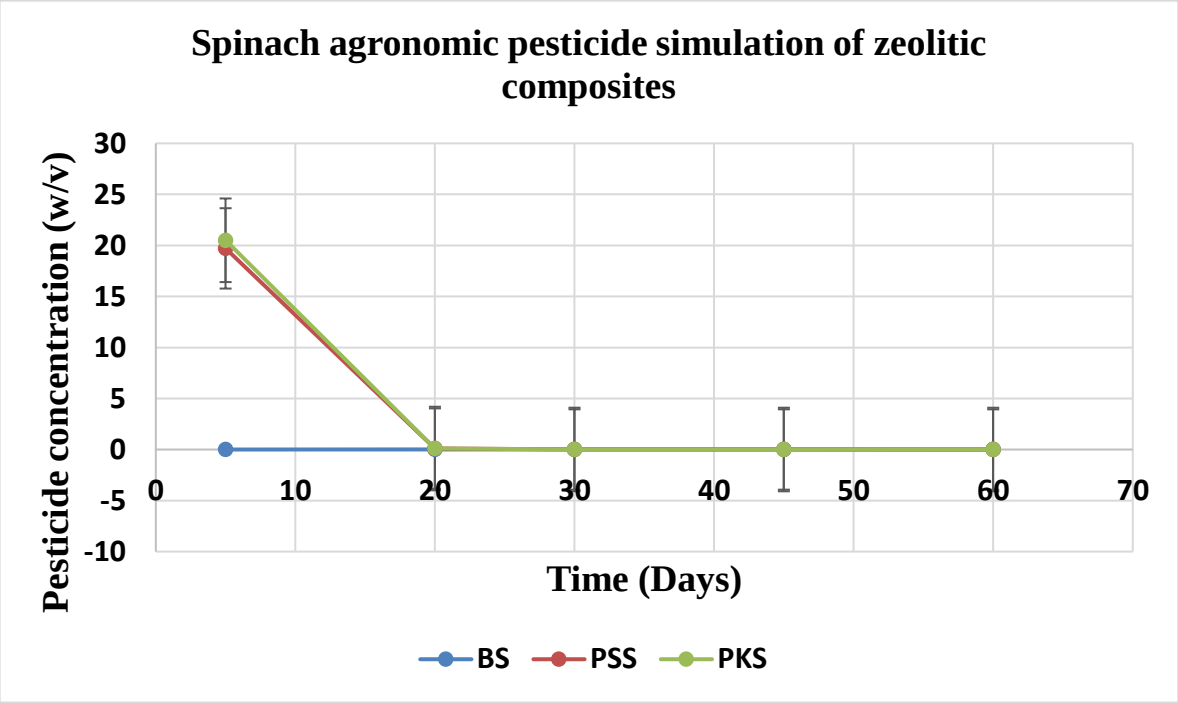

Figure 4. 67 Release rates for pesticide loaded zeolitic materials in spinach studies

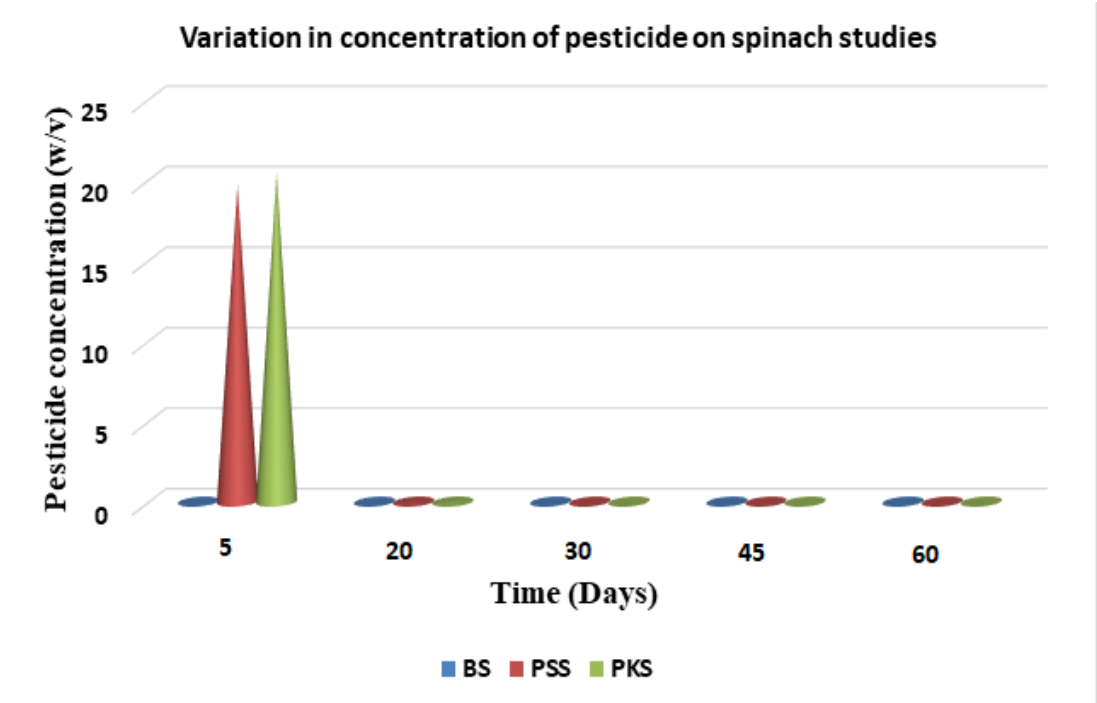

Figure 4. 68 Variations in concentration of pesticide on spinach studies

Where; BS were samples taken from a setup of spinach grown on blank soil, PSS were samples taken from a setup of spinach grown using pesticide loaded sample EB-GA-02 and PKS were samples taken from a setup of spinach grown using commercial pesticide.

4.3.6: Comparative studies

The overlaid plots below in Figure 4.69 shows comparison of X-ray diffraction spectrum for sample EB-GA-02, urea loaded sample EB-GA-02 (A), pesticide loaded sample EB-GA-02(B) and urea loaded sample KIK-GA-02(C).

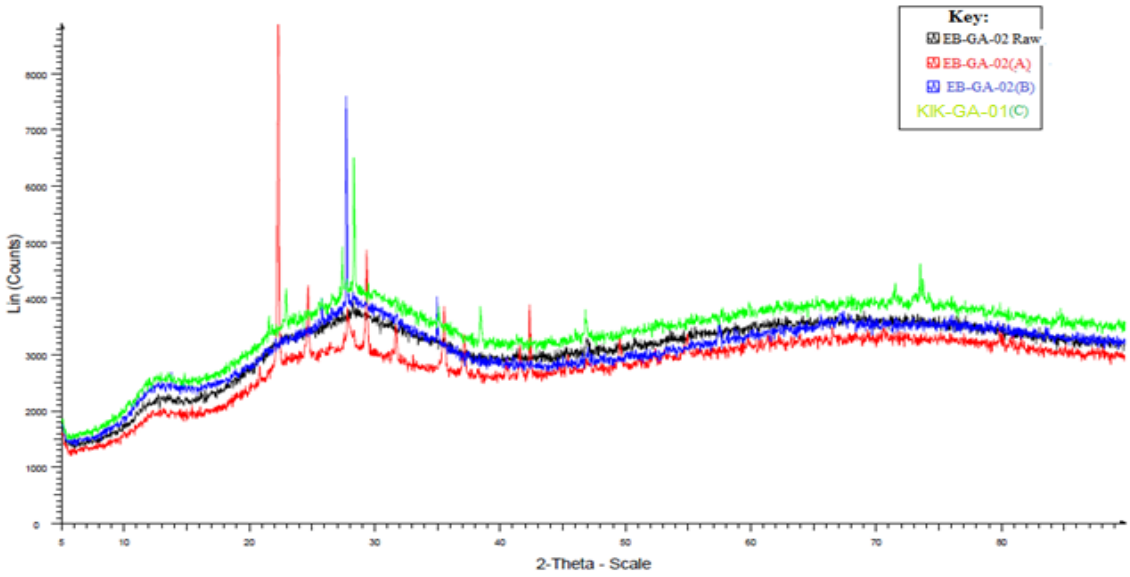

Figure 4. 69 XRD Overlaid spectrums of sample EB-GA-02

On the other hand, Figure 4.70 below shows overlaid X-ray diffraction spectrum for Kikuyu soil (KIK-GA-01), urea loaded Kikuyu soil (KIK-GA-02) and pesticide loaded Kikuyu soil (KIK-GA-03).

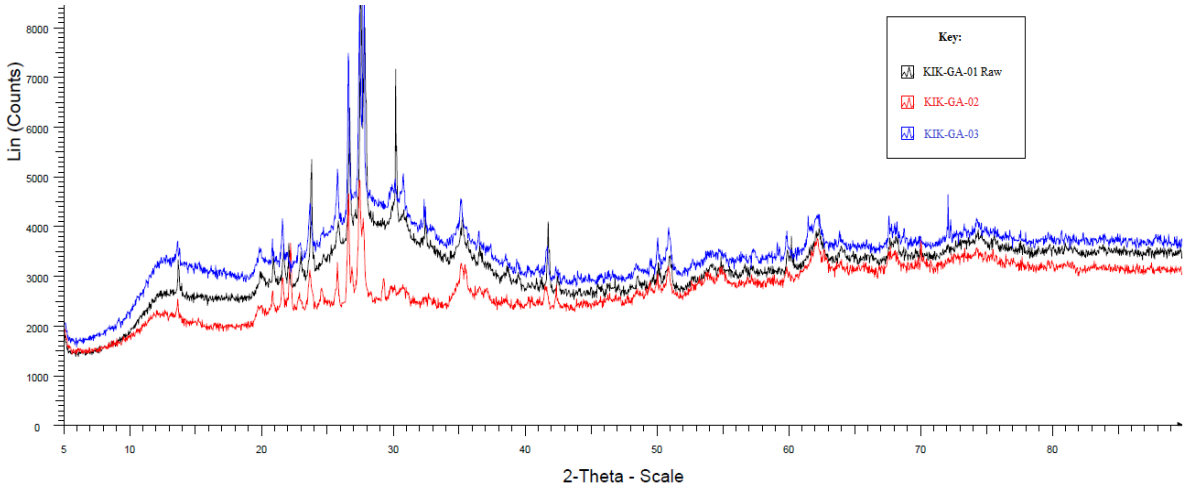

Figure 4. 70 XRD Overlaid spectrums of sample KIK-GA-01

Data from these studies were recorded in Table T4.29 of appendices, with an ANOVA P-Value of 0.966 consistent with the null hypothesis under a significance level, $\alpha = 0.05$ (Table T4.30). Comparing the trends of variation in concentration of urea and the pesticide in soil for spinach and tomato monitoring experiments, a closely uniform rate of reduction in concentration (Figure 4.71 and Figure 4.73) was noted. This could indicate a similarity in the mode of action of the nanozeolitic smart delivery system as already attributed to physical-chemical processes of sorption. Over the entire 60 days monitoring duration, highest concentrations were recorded in the first 20 days, while sustained decreased concentrations were noted during the last 30 days (Figure 4.72 and Figure 4.74).

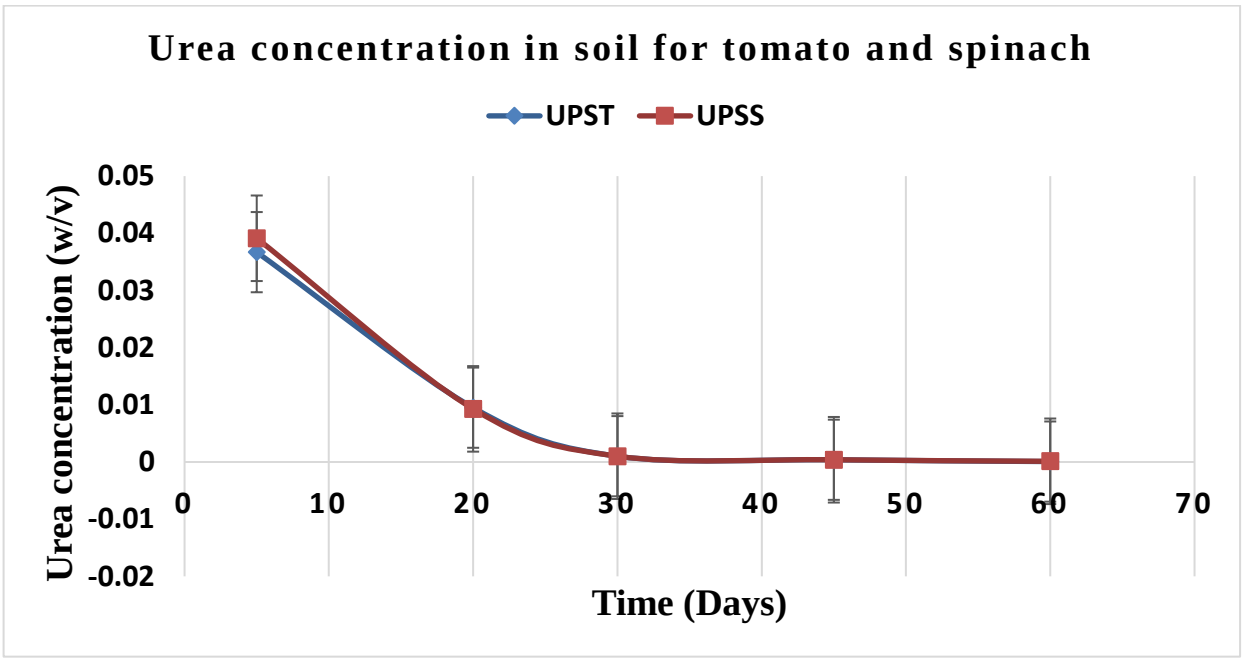

Figure 4. 71 Urea concentration variation in the soil for tomato and spinach

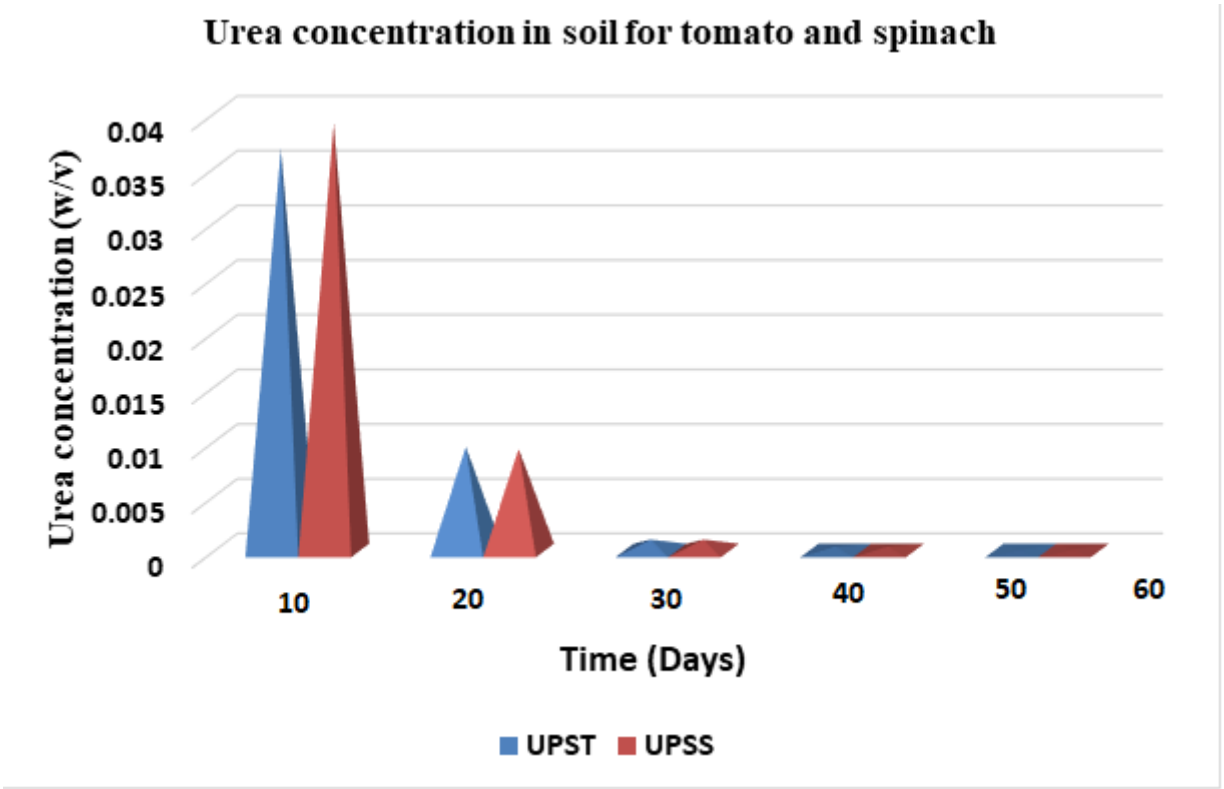

Figure 4. 72 Urea concentration in soil for tomato and spinach

Where UPSS were fertilizer samples taken from a setup of spinach grown using urea loaded sample EB-GA-02 and pesticide loaded sample EB-GA-02 while UPST were fertilizer samples taken from a setup of tomatoes grown using urea loaded sample - EB-GA-02 and pesticide loaded sample EB-GA-02.

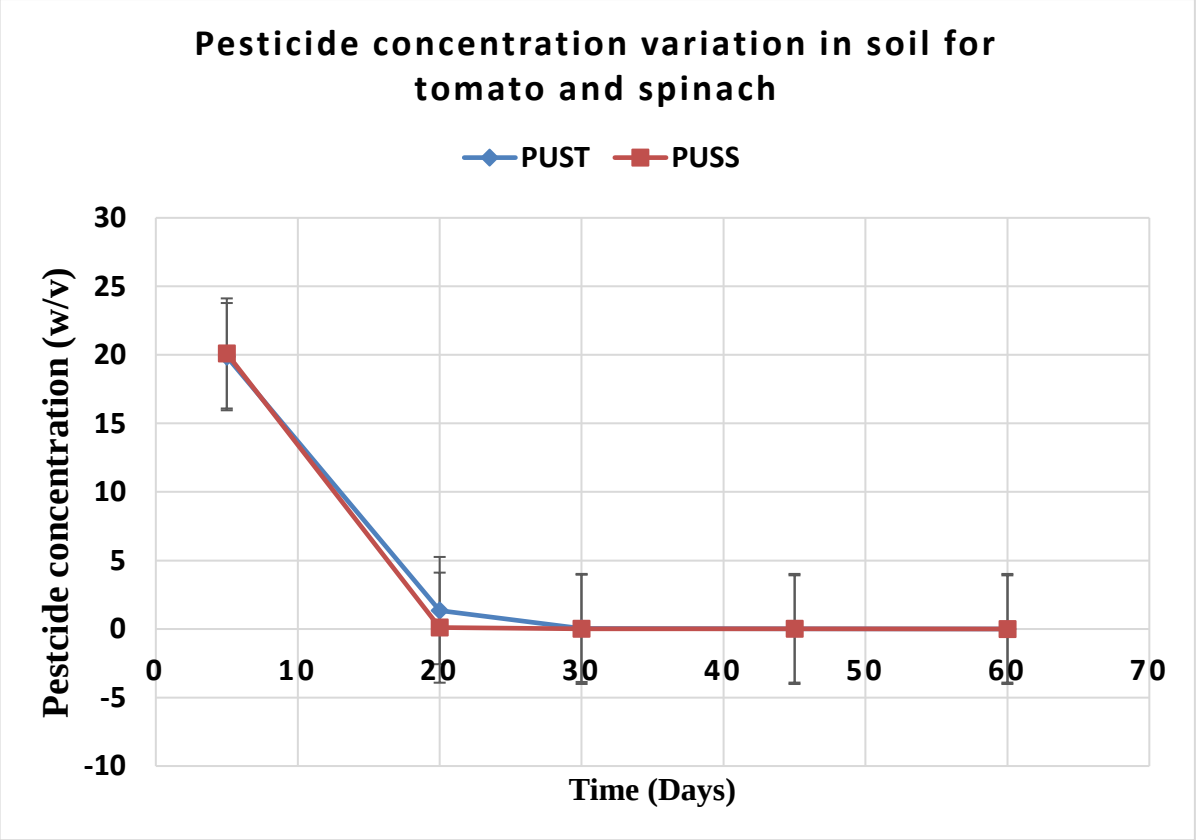

Figure 4. 73 Pesticide concentration variation in the soil for tomato and spinach

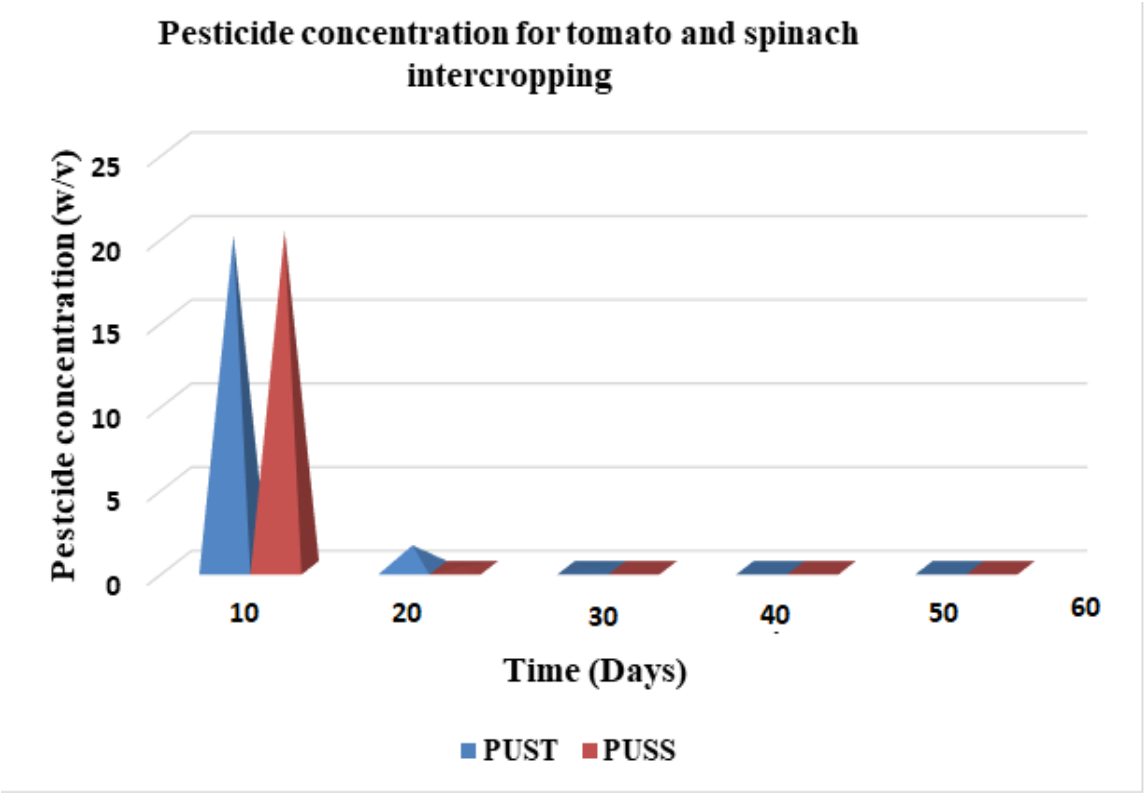

Figure 4. 74 Pesticide concentration in soil for tomato and spinach intercropping

Where PUSS were fertilizer samples taken from a setup of spinach grown using urea loaded sample - EB-GA-02 and pesticide loaded sample EB-GA-02 while PUST were pesticide samples taken from a setup of tomatoes grown using urea loaded sample - EB-GA-02 and pesticide loaded sample EB-GA-02.

4.3.7: Physisorption isotherms

Brunauer-Emmett-Teller (BET) gas adsorption for characterization of the surface area and Barrett-Joyner-Halenda (BJH) for pore size distribution techniques were applied in sorption studies and isotherm interpretation.

Additional models applied in this work includes the Freundlich, Langmuir, Quasi- Langmuir, Temkins and Adsorption kinetics. Where C_e is the average scan equilibrium concentration in mg/L of the pesticide after shaking with the samples and q_e is the amount of equilibrium adsorbed pesticide in mg/L.

4.3.7.1: Freundlich isotherms

The Freundlich model was used to assess the adsorption power of the sorbate on the sorbent surface. The exploratory information from the batch sorption investigation of the Lambda-cyhalothrin pesticide on test EB-GA-02 were plotted logarithmically utilizing the direct Freundlich isotherm condition as appeared in Figure 4.75 beneath.

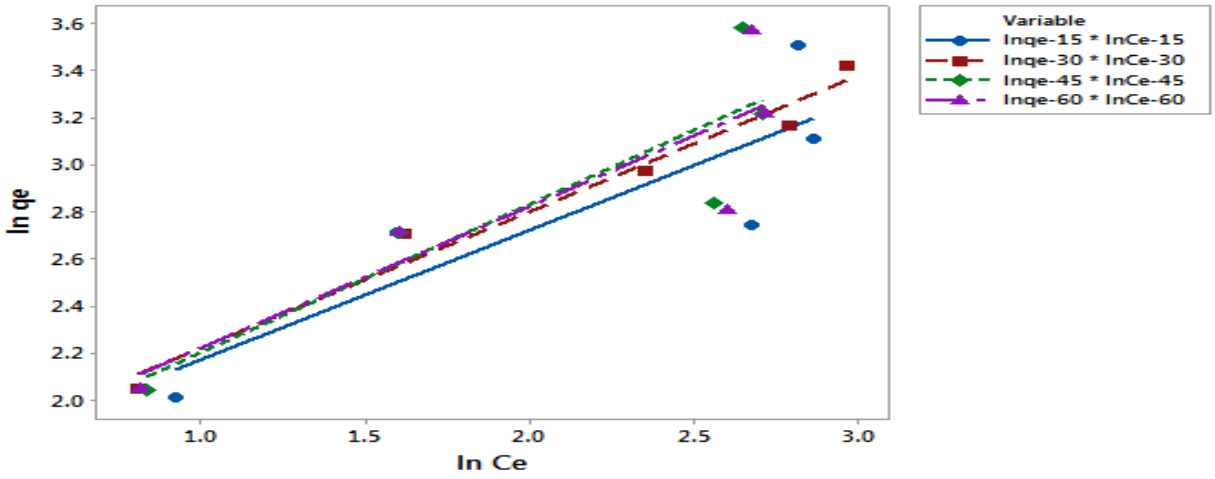

Figure 4. 75 Linear Freundlich isotherm plot

The direct Freundlich isotherm constants for Lambda-cyhalothrin pesticide on test EB-GA-02 are introduced in Table 4.25, where the Gibb's free energy ΔG (kJmol^{-1}) was determined from the conventional equation: $\Delta G = -RTInK_F$, where R was the universal gas constant and T was the room temperature in Kelvins.

Table 4. 25 Freundlich isotherm parameters

Time (min.)	n	K_F (L/g)	R^2	ΔG (kJmol^{-1})
15	1.8089	5.0128	0.753	-3.9938
30	1.7209	5.1397	0.970	-4.0559
45	1.5893	4.8163	0.804	-3.8947
60	1.6606	5.0279	0.786	-4.0013

The average Gibb's free energy of -3.9864 kJmol^{-1} indicates spontaneity in the adsorption process. Adsorption non-linearity parameter (n), which also indicates the quasi-Guassian energetic heterogeneity obtained was an average of 1.6949, while R^2 values ranged from 0.753 to 0.970, comparatively making Freundlich isotherm better definitive of lambda-cyhalothrin adsorption on sample EB-GA-02. This is in line with other studies already done like Ali and Baugh (2003), Bandareko *et al*., (2006) etc. which applied the model on data analysis where sorption rates depended on soil type and contact time. Hence this model authoritatively described the sorption phenomenon of Lambda cyhalothrin pesticide on sample EB-GA-02.

4.3.7.2: Langmuir isotherms

The Langmuir model was used for a homogenous monolayer adsorption with no collaboration between adsorbed atoms and uniform energies of adsorption, whose plots generated Figure 4.76 below.

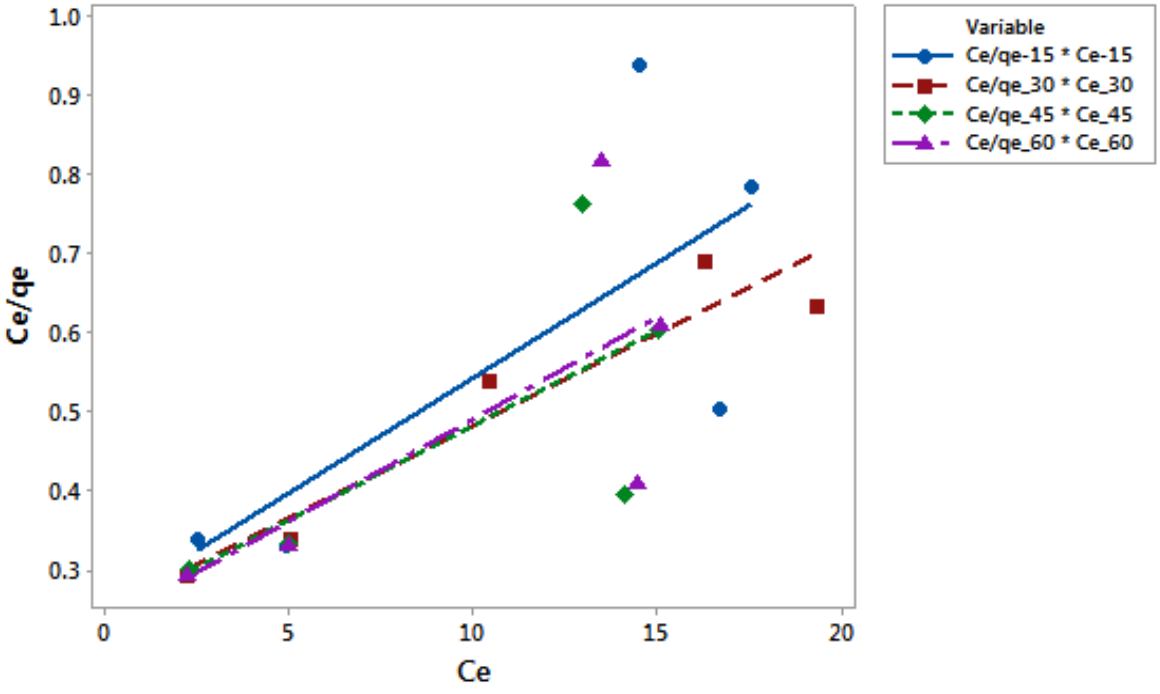

Figure 4. 76 Linear Langmuir isotherm plots

The presumption made is that the adsorbed compound species do not react with each other.

From Figure 4.76 over, the accompanying constants in Table 4.26 were determined.

Table 4. 26 Langmuir isotherm parameters

Time (min.)	$1/q_m$	$1/q_mK_L$	K_L (L/mg)	R^2
15	0.02910	0.2506	0.11610	0.5611
30	0.02325	0.2488	0.09344	0.9110
45	0.02490	0.2475	0.10061	0.9313
60	0.02572	0.2321	0.11081	0.4990

R^2 values extended from 0.4990 to 0.9313, while the average value of K_L constant was 0.1052, as obtained from Table 4.26 above

4.3.7.3: Quasi Langmuir isotherms

This was utilized as a tradeoff among Langmuir and Freundlich models, whose direct plots of $1/q_e$ versus $1/C_e$ obtained are shown below (Figure 4.77).

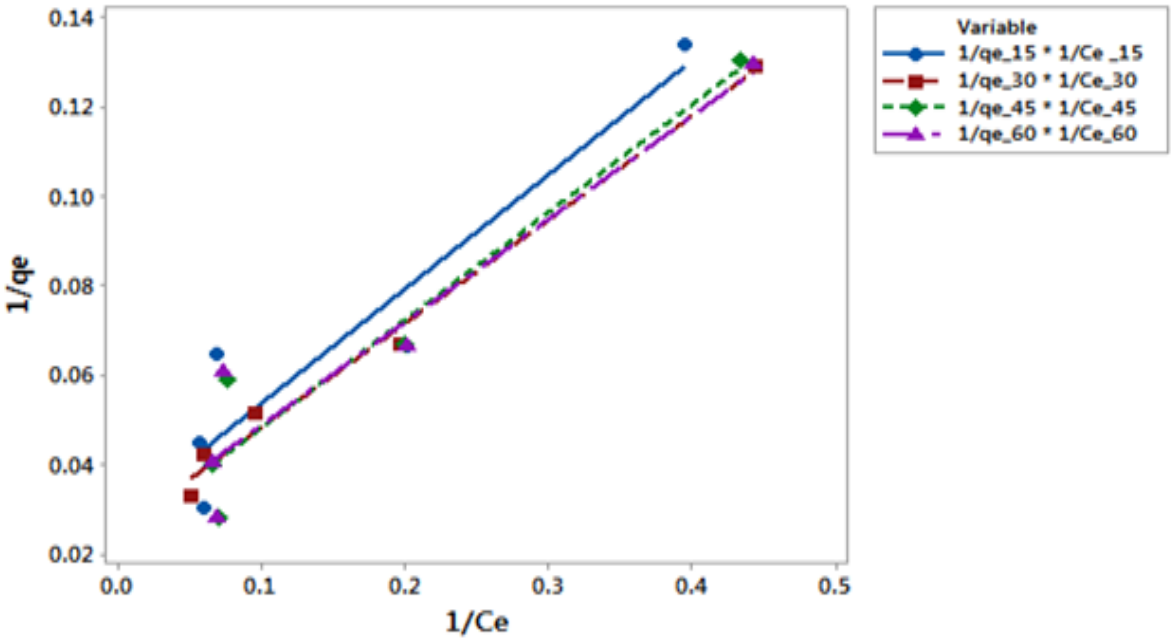

Figure 4. 77 Linear Quasi Langmuir isotherm plots

Table 4.27 shows the Quasi-Langmuir equilibrium constant values from the plots.

Table 4. 27 Quasi-Langmuir isotherm parameters

Time	$1/K_{RP}C_e$	$1/c_e$	K_{RP} (L/g)	R^2
15	0.02910	0.2506	8.6117	0.5611
30	0.02325	0.2488	10.7011	0.9110
45	0.02697	0.2387	8.8506	0.8910
60	0.02572	0.2321	9.0241	0.4990

Quasi-Langmuir average K_c value was 9.2969, while the R^2 values ranged from 0.4990 to 0.9110 as obtained from Table 4.27.

4.3.7.4: Temkin isotherms

This was used to assume the linear decrease in the heat of adsorption of the considerable number of atoms with layer inclusion, and that the adsorption is described by a uniform appropriation of the bonding energies. Plots of q_e against $\ln C_e$ were linear (Figure 4.78).

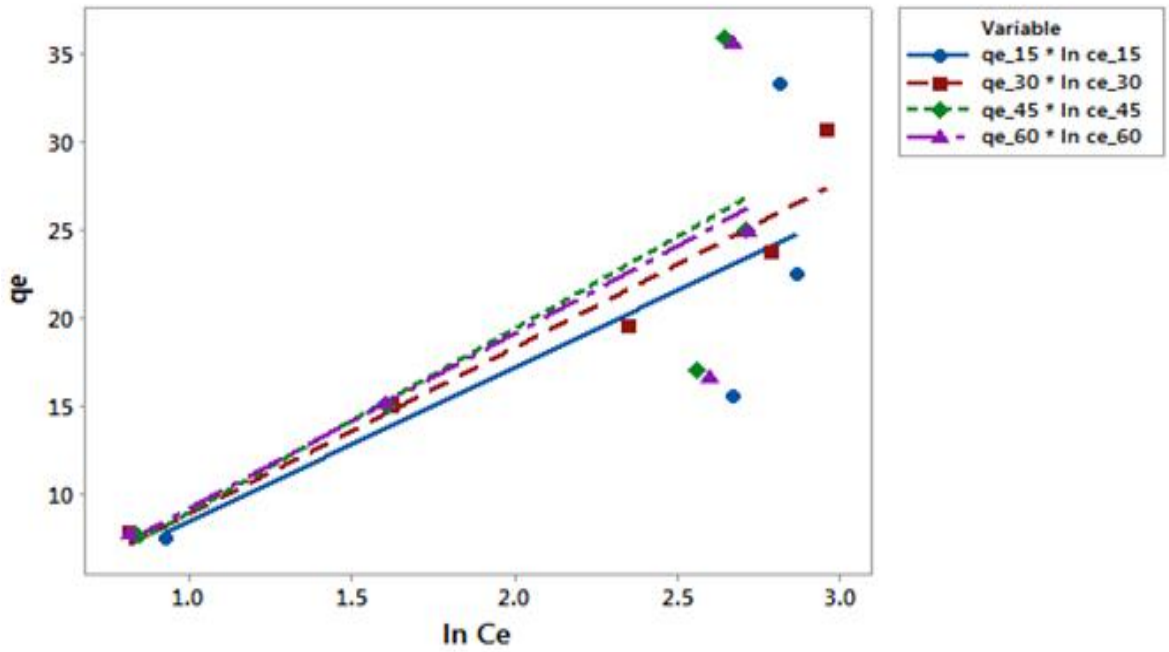

Figure 4. 78 Linear Temkin isotherm plots

The data in table 4.28 shows the Temkin equilibrium constant values from the plots.

Table 4. 28 Temkin isotherm parameters

Time in minutes	B_T (kJ/mol)	$B_T InK_T$	K_T (L/mg)	R^2
15	8.740	0.284	1.033	0.614
30	9.398	0.502	1.059	0.934
45	10.42	1.487	1.153	0.640
60	9.943	0.774	1.081	0.625

The average equilibrium binding constant, K_T, obtained was 1.0815 Lmg^{-1}, while the average Temkin constant, B_T, linked to energy of adsorption was 9.6253 $kJmol^{-1}$.

Comparatively, the Freundlich isotherm model generated the greatest average R^2 value of 0.8285, while Temkin isotherm had the least average R^2 value of 0.70325. With spontaneity of -3.9864 $kJmol^{-1}$ free energy and energetic heterogeneity parameter of 1.7, the Freundlich model illustrated

active sorption process of lambda cyhalothrin on natural zeolitic sample EB-GA-02 in a much better way, hence making it the model that best fitted the adsorption pattern.

4.3.8: Adsorption Kinetics

Kinetic studies were used to analyze sorption dynamics and mechanisms while *pseudo*-first and second orders were utilized to decide the rate constants and orders of sorption processes.

4.3.8.1: *Pseudo*-First-Order Model

A straight line of ln($qe - qt$) versus t proposes the relevance of this dynamic model. Pseudo-first-order rate steady (*kf*) (1/min) can be resolved from the slant of the plot. Table 4.29 shows data generated from plots of the experimental data.

Table 4. 29 Pseudo-first order kinetic parameter

Concentration(ppm)	$\ln q_e$	K_f	Regression
100	0.3872	0.02939	0.996
200	1.240	0.03338	0.831
300	1.828	0.03652	0.746
400	2.162	0.07138	0.957
500	2.929	0.07230	0.980

4.3.8.2: *Pseudo*-second-Order Model

The information produced from plots of this model are demonstrated as follows (Table 4.30). The plot *t/qt* versus *t* gave a straight line of second-order energy, where *qe* and *ks* could be resolved from the slant and intercept, individually. The underlying sorption rate, *h* (mg/g min), as t→0 can be represented as:

$h = ksq_e^2$ ……(4.1)

Table 4. 30 Pseudo-second-order kinetic parameter

Concentration(ppm)	$1/k_sq_e$	$1/q_e$	k_s (g/mg min)	*h*(mg/g min)	R^2
100	0.06786	0.1281	1.8877	115.0363	0.999
200	0.03781	0.0665	1.7588	397.7161	0.997
300	0.0782	0.06061	0.7751	210.9935	0.984
400	0.09594	0.03846	0.4009	271.0301	0.999
500	0.09525	0.026682	0.2801	393.4380	0.987

The straight line plot for the pseudo-first-order sorption dynamic model between ln(*qe*−*qt*) versus *t* was plotted for sorption of Lambda cyhalothrin. The estimation of the rate steady determined from the incline of plots ran from 0.02939 to 0.07230 min^{-1}. The direct plots of pseudo-second-order kinetic model was likewise plotted between *t/qt*. versus *t,* and sorption limit and pseudo-second-order rate constants *qe* and *ks* were determined from the incline and intercept of the plot. The pseudo-second-order kinetic steady *ks* and sorption limit *qe* extended from 1.8877 to 0.280 $gmg^{-1}min^{-1}$ and 7.8064 to 37.47845 mgg^{-1} between 100 to 500 ppm respectively. Coefficient of determination values ranged from 0.984 to 0.999, a good illustration of the pesticide adsorption having followed *pseudo*-second-order rate expression. Additionally, initial sorption rates, *h*, increased from 115.0363 to 393.438 $mgg^{-1}min^{-1}$ between 100 to 500ppm respectively, as shown in Table 4.30.

4.3.8.3: Intraparticle Diffusion Model

The intra-particle diffusion was determined using the intra-particle diffusion model given in equation (4.2).

$q_t = k_{id}t^{\frac{1}{2}} + I$ ……....(4.2)

where k_{id} is the intra-molecule dispersion rate constant. As per equation 4.2, a plot of *qt* versus $t^{1/2}$ ought to be a straight line with a slant of k_{id} and intercept *I* when adsorption instrument follows the intra-particle dispersion process solely. The data derived from the plots are summarized in Table 4.31.

Table 4. 31 Intra-particle diffusion model parameters

Concentration(ppm)	*I*	k_{id}	R^2
100	6.386	0.1770	0.995
200	11.32	0.5458	0.796
300	12.90	0.5357	0.787
400	19.84	0.6953	0.953
500	25.37	1.4200	0.961

Lower regression values were acquired with the plots not passing the origin. The qualities for k_{id} and *I* were in a scope of 0.177 – 1.42 and 6.386 – 25.37 separately. *'I'* values gives understanding on thickness of the limit layer, whereby, bigger intercepts propose more noteworthy limit layer impact (Anirudhan and Suchithra, 2012). Deviation of the lines from the origin is ascribed to the distinctions in the rate of mass exchange in the underlying and last phases of adsorption, demonstrating that pore dispersion may not be the main rate controlling step (Kannan and Sundaram, 2001).

CHAPTER 5: CONCLUSIONS AND RECOMMENDATIONS

5.1: CONCLUSIONS

Sampling for zeolites was done in the five selected places in Kenya, namely Eburru volcanic crater, Lake Magadi, Lake Baringo, Ebulbul-Ngong, and Kitum cave-Mt. Elgon. The collected samples were labelled EB-GA-02, MG-GA-03, BG-GA-04, NG-GA-05, and EL-GA-06 respectively and characterized using XRD, EDX,FT-IR, XRF, and SEM in comparison with the standard sample ZT-GA-01 which was zeolite A artificial. Samples EB-GA-02 and EL-GA-06 were found to contain Aluminosilicate composition similar to the standard sample, therefore being classified as natural zeolites. Samples MG-GA-03, BG-GA-04, and NG-GA-05 lacked the aluminium composition in their crystalline oxide composition, implying that they were not zeolites.

Natural zeolites sample EB-GA-02 was applied in the kinetic, formulation, modelling, and simulation studies for urea fertilizer and lambda cyhalothrin pesticide. Fertilizer and pesticide loading and release properties indicated that 35.00 % of urea and 79.40 % of lambda cyhalothrin were able to be loaded in nanopore spaces of sample EB-GA-02 forming urea loaded nanozeolitic sample EB-GA-02 and pesticide loaded zeolitic sample EB-GA-02 respectfully. XRD, FT-IR, and SEM characterization of the treated samples confirmed the presence of quest molecules. X-Ray diffraction analysis of urea loaded EB-GA-02 indicated 2θ peaks values of 22, 24.5, 29.5, 32, 35.5, 37, 38.5, 40.5, 41.5, 45.5 and 55 corresponding to urea peaks, while the FT-IR spectrum of urea loaded EB-GA-02 contained distinct peaks appearing on the urea spectrum at 3348.42 - 3444.87 cm^{-3}, 1624.06 - 1681.93 cm^{-3} and 1465.90 cm^{-3}, corresponding to N-H, C=O and C-N stretching vibrations for the urea fertilizer functional groups respectively. For the pesticide loaded sample EB-GA-02 in crystalline form indicates the pesticide 2θ values at 28.5º, 33º, 47º, 56º, 58.5º, 68.5º, 76º, 78º and 87º corresponding to lambda cyhalothrin.

Nitrogen sorption studies of BJH pore volume and sizes indicated a 39.844 % and 32.74 % reduction in pore sizes after successful treatment/loading and loading of urea and lambda

cyhalothrin molecules in the nanopore spaces of sample EB-GA-02 respectfully. The optimum nanozeolite formulation for agribusiness was achieved at a 1:60 w/v urea solution of 35 ml having 20.00 g EB-GA-02 incubated for 24 hours for the fertilizer, while for lambda cyhalothrin, 15 g of sample EB-GA-02 was spiked with 25 ml of 100 ppm of the pesticide.

Application of these formulated nanozeolitic smart delivery system was conducted at two levels. The initial level was done to determine the simulated release rate in water and soil over 18 days' duration. For urea loaded nanozeolitic smart delivery system, 82.80% and 74.20% of loaded urea molecules were separately released in water and soil respectfully. While on the other hand, it was determined that for pesticide loaded zeolitic smart delivery system, 34.40% and 40.10% of the loaded Lambda cyhalothrin molecules were separately released in soil and water respectfully. The general rates of desorption recorded an initial rapid discharge, followed by a slow and sustained release for the remaining part of experimental duration.

The second level of application of the formulated nanozeolitic material involved tomato and spinach crop production simulated monitoring experiments conducted over 60 days in which it involved monitoring the concentration of urea and pesticide remaining in the soil over given time intervals. Urea loaded nanozeolitic smart delivery system samples demonstrated a sustained slower but extended release rate when applied to both tomatoes and spinach crops. A difference of 17.00% and 16.00% higher urea concentration in soil was recorded on tomatoes and spinach crops respectfully between the 20^{th} and 35^{th} day as compared to just direct urea application to the soil. Similarly, pesticide loaded nanozeolitic smart delivery system samples gave a difference of 70.00% and 69.00% higher Lambda cyhalothrin pesticide concentration in soil recorded for tomatoes and spinach respectfully around the 20^{th} day for each. It is expected that similar experimental results should be likely observed in different types of soils from other parts of Kenya other than Kiambu, factoring their similarities in soil properties.

These observations demonstrated the application of nanozeolitic sample EB-GA-02 in formulation of nanosmart delivery system that can aid in slow and controlled release and delivery of fertilizer and pesticide to crops. Such formulated systems when actualized would have multiple benefits like enhanced efficiency and effectiveness in application and use of fertilizer and pesticides by plants; this could also translate to green agroeconomy due to reduced environmental pollution and envisaged better developed smart delivery system for agriproduction that could be even modified with biosensors for modern smart farming technologies.

5.2: RECOMMENDATIONS

1.Increased scope in application and awareness of nanoformulated agrichemicals could translate to large-scale demand which could probably rationalize the cost of production which for now tends to be higher compared to conventional inputs.

2.Concerted wider sampling on natural zeolites sampling in Kenya and developed cheaper extraction and purification processes are needed in order to develop wider varieties of nanozeoltic materials of which their diversified applicability in nanotechnology could be explored locally for commercial purposes. This will help minimize the challenge of lack of equipment capacity to sample and purify natural zeolite rocks.

3.Smart Delivery System properties can further be modified with aspects like; improved purification and synthesis processes, intercalation with other nanoparticles and biosensor functionalization for intelligence stimuli response. The recommended formulation of application of the zeolites are 1:60 w/v urea to aqueous medium equilibrated for 24 hours while for lambda cyhalothrin pesticide, 100 ppm 25 ml solution equilibrated with 15 g sample for 24 hours.

REFERENCES

Agrawal, D., Lunkad, S. K., & Malkhed, T. (1999). Diffuse agricultural nitrate pollution of groundwaters in India. *Water Sci Technol* **39**: 67–75.

Al-Amin, S. M. D., & Jayasuriya, H. P. (2007). Nanotechnology prospects in agricultural context: An overview. In: proceedings of the International Agricultural Engineering Conference, **3-6** December 2007, Bangkok, p. 548.

Alan, L. P., Jan, Y., Philip, S., & David, J. S. (2008). Refining search terms for nanotechnology. *J Nanopart Res* **10**:715–728.

Albanbis, T. A., & Hela, D. G. (1993). Multi-residue pesticide analysis in environmental water samples using solid-phase extraction discs and gas chromatography with flame thermionic and mass-selective detection. *Journal of Chromatography* **707**: 283–392.

Aleksiev, B., & Djourova, E. G. (1975). On the origin of zeolitic rocks. C. R. *Acad. Bulg. Sci*. **28**, 517-520.

Ali, M. A., & Baugh, P.J. (2003). Sorption-desorption studies of six pyrethroids and mirex on soils using GC/MS-NICI. *Int J Environ Anal Chem* **83:** 923–933.

Altenbach, J. S., Geluso, K. N., Wilson, D. E., Grnoways, H. H., & Baker, R. J. (1979). Population size of Tadaria brasiliensis at Carlsbad Caverns. In Biological investigations in Guadelupe Mountains National Park. p. 341. *Texas, Natl Park Service Proc Trans Ser No* **4**.

Ammon, O. O. (2013). Resistivity Structure of the Eburru Geothermal Field, Kenya, Depicted Through 1D Joint Inversion of Mt and Tem Data Kenya Electricity Generating Company Ltd. KenGen. Geothermal Resource Development. Geothermal Training Programme. Reports 2013. Number **26.**

Amweg, E. L., Weston, D. P., You, J., & Lydy, M. J. (2006). Pyrethroid insecticides and sediment toxicity in urban creeks from California and Tennessee. *Environ Sci Technol* **40**:1700–1706.

Anderson, D. M., Okaichi, T., Anderson, D. M., & Nemoto, T. (1989). Toxic algal blooms and red tides: a global perspective. In editors. Redtides: biology, environmental science, and toxicology. *Elsevier, New York, USA.* Pages **11-16.**

Andreu, V., & Pico,' Y. (2004). Determination of pesticides and their degradation products in soil: critical review and comparison of methods. *Trends Anal Chemistry* **23** (10–11):772–789.

Anirudhan, T. S., & Suchithra, P. S. (2012). Equilibrium, kinetic and thermodynamic modelling for the adsorption of heavy metals onto chemically modified hydrotactile. *Ind. J. Chem. Technol*, vo1.**17**, pp. 247-259.

Arias, R. N., & Fabra, P. A. (1993). Effects of 2, 4-dichlorophenoxyacetic acid on Rhizobium sp. growth and characterization of its transport. *Toxicol Lett* **68:** 267–273.

Ariga, J. M., Jayne, T. S., Kibaara, B., & Nyoro, J. K. (2008). "Trends and Patterns in Fertilizer Use by Smallholder Farmers in Kenya, (1997–2007)," Working Paper **28**, Tegemeo Institute, Nairobi, Kenya: Egerton University.

Ataman, G., & Beseme, P. (1972). Découverte de l'analcime sédimentaire en Anatolie du nordouest (Turquie): minéralogie, genèse, paragènese. *Chem. Geol* **9,** 203-225.

Ataman, G., & Gündogdu, N. (1982). Analcimic zones in the Tertiary of Anatolia and their geologic positions. *Sediment. Geol* **31**, 89-99.

Awad, N. G. H. (1990). Studies on tomato wilt disease caused by Fusarium Oxysporum F. SP. Lycopersici. Ph. D Thesis, Agricultural Zagazig University, Egypt.

Ayan, S. (2001). Utilization of zeolite as plant growing media. *East Mediterranean Forest Research Institute Journal* **7**: 97-111.

Ayan, S. (2002a). Using of zeolite mineral for seedling production and afforestration practices. *Gazi Unv Faculty of Forestry Journal* **1**: 78-88.

Baden, S. P., Loo, L. O., Pihl, L., & Rosenberg, R. (1990). Effects of eutrophication on benthic communities including fish: Swedish west coast. *Ambio* **19**: 113-122.

Bailey, G. W., & White, J. L. (1964). Soil- pesticides relationships, adsorption and desorption of organic pesticides by soil colloids, with implications concerning pesticides bioactivity. *J. Agri. Food Chem* **12**: 3-4-333.

Bailey, S. E., Olin, T. J., Bricka, R. M., & Adrian, D. D. (1999). *Water Res* **33**. 2469.

Baker, B. H. (1958). Geology of the Magadi Area. Report Geologycal Survey of Kenya **42**.

Bansal, R. C., & Goyal, M. (2005). Activated Carbon Adsorption, Boca Raton, Crc. Press Taylor Francis Group.

Bansiwal, A. K., Rayalu, S. S., Labhasetwar, N. K., Juwarkar, A. A., & Devotta, S. (2006). Surfactant-Modified Zeolite as a Slow Release Fertilizer for Phosphorus. *J. Agric. Food Chem* **54**:4773-4779.

Baptista-Filho, M., Silva, M. G., Polidoro, J. C., Luna, F. J., Monte, M. B. M., Souza-Barros, F., Miklos, A., & Vargas, H. (2008). Detection of Ammonia Released from Zeolite by the Quantum Cascade Laser Based Photoacoustic Set-Up. *The European Physical Journal A*, **153**: 547-555.

Barbarick, K. A., Lai, T. M., & Eberl, D. D. (1990). Exchange fertilizer (phosphate rock plus ammonium-zeolite) effects on sorghum-sudan grass. *Soil Sci. Soc. Am. J* **54**: 911-916.

Barbarick, K. A., & Pirela, H. J. (1984). Agronomic and horticultural uses of zeolites: A review. In: Pond WG and FA.

Barcelo', D., & Hennion, M. C. (1997). Trace Determination of Pesticides and Their Degradation Products in Water. Amsterdam, The Netherlands: *Elsevier* p. 3.

Barnes, D. A., Boles, J. R., Hickey, J., Olson, D., & Bisio, A. (1984). Zeolite occurrences in Triassic-Jurassic sedimentary rocks, Baja California, Mexico. In Proceedings of the Sixth International Zeolite Conference, Reno, USA., Butterworths, 905-913.

Barrett, E. P., Joyner, L. G., & Halenda, P. P., (1951). The determination of pore volume and area distribution in porous substances.1. Computations from nitrogen isotherms. *J. Am. Chem. Soc*. **73**: 373 - 380.

Becker, P. H., Hel, M (1989). Seabirds as monitor organisms of contaminants along the German. *North Sea coast* **43:** 395–403.

Bekkum, V. H., Flanigen, E. M., Jacobs, P. A., & Jansen, J. C. (1991). Introduction to Zeolite Science and Practice, 2nd. Revised Edn., Elsevier, Amsterdam.

Bernardz, J. C., Klem, D., Goodrich, L. J., & Senner, S. E. (1934–1986). Migration counts of raptors at Hawk Mountain, Pennsylvania, as indicators of population trends. *Auk.1990* **107:** 96–109.

Bhaskar, J. S., & Gopalakrishnarao, P. (2010). Fourier Transform Infrared Spectroscopic Characterization of Kaolinite from Assam and Meghalaya, Northeastern India. *J. Mod. Phys* **1**:206-210.

Blanchard, G., Maunaye, M., & Martin, G. (1984). Water Res. **18**. 1501.

Boles, J. R. (1977). Zeolites in deep-sea sediments: In Mineralogy and Geology of Natural Zeolites, Miner. Soc. Amer., Short Course Notes, **4**, 137-163.

Boles, J. R., Wise, W. S., Sand, L. B., & Mumpton, F. A. (1978). Nature and origin of deep-sea clinoptilolite: In Natural Zeolites: Occurrence, Properties, Use, Pergamon Press, Elmsford, New York, 235-244.

Bondarenko, S., Putt, A., Kavanaugh, S., Poletika, N., & Gan, J. Y. (2006). Time dependence of phase distribution of pyrethroid insecticides in sediment. *Environ Toxicol Chem* **25**:3148–3154.

Boopathy, R., Karthikeyan S., Mandal A. B., & Sekaran G. (2013). Adsorption of ammonium ion by coconut shell-activated carbon from aqueous solution: kinetic, isotherm and thermodynamic studies**.** *Environ. Sci. Pollut. Res.,* **20(1)**: 533-542.

Bortleson, G., & Davis, D. (1987–1995). U.S. Geological Survey & Washington State Department of Ecology. Pesticides in selected small streams in the Puget Sound Basin; pp. 1–4.

Boynton, W. R., Kemp, W. M., & Keefe, C. W. (1982). A comparative analysis of nutrients and other factors influencing estuarine phytoplankton production. In V. S. Kennedy, editor. Estuarine comparisons. Academic Press, New York, USA. Pages **69-90.**

Bradbury, S. P., & Coats, J. R. (1989). Toxicokinetics and toxicodynamics of pyrethroid insecticides in fish. *Environ Toxicol Chem* **8**: 373–380.

Breck, D. W. (1974). Zeolite Molecular Sieves: Structure, Chemistry and Use. London: John Wiley and Sons, p.4.

Brock, D. A., Douglas, T.E., Queller, D. C., & Strassmann, J. E. (2011). Primitive agriculture in a social amoeba. *Nature* **469**: 393-396.

Brouwer, A., Longnecker, M. P., Birnbaum, L. S., Cogliano, J., Kostyniak, P., Moore, J., Schantz, S., & Winneke, G. (1999). Characterization of potential endocrine related health effects at lowdose levels of exposure to PCBs. *Environ Health Perspect* **107:** 639.

Browne, P. R. L. (1978). Hydrothermal alteration in active geothermal fields. *Annual Review Earth & Planetary Sciences* **6**: 229-250.

Broxton, D. E., Bish, D. L., & Warren, R. G. (1987). Distribution and chemistry of diagenetic minerals at Yucca Mountain, Nye County, Nevada. *Clays and Clay Minerals* **35**: 89-110.

Bruker, A. X. S., (2001). Introduction to Powder X-ray Diffraction. History and Basic Principles. File 1© 2001.

Brunauer, S., Emmett, P. H., & Teller, E., (1938). Adsorption of gases in multimolecular layers. *J. Am. Chem. Soc*. **60**: 309 - 319.

Brust, M., & Kiely, C. J. (2002). Colloids Surf. A **202** 175.

Burkholder, J. M., Noga, E. J., Hobbs, C. H., & Glasgow, H. B. (1992). New "phantom" dinoflagellate is the causative agent of major estuarine fish kills. *Nature* **358**: 407-410.

Burr, S. A., & Ray, D. E. (2004). Structure-activity and interaction effects of 14 different pyrethroids on voltage-gated chloride ion channels. *Toxicol Sci* **77**: 341–346.

Burton,. (2009) Powder Diffraction in Zeolite Science. *In Zeolite Characterization and Catalysis*, Springer Science Business Media, 1-65.

Cade, T. J., Lincer, J. L., White, C. M., Rosenau, D. G., & Swartz, L. G. (1989). DDE residues and eggshell changes in Alaskan falcons and hawks. *Science* **172:** 955–957.

Calvet, R. (1989). Adsorption of organic chemicals in soils. *Eviron. Health Persp* **83**:145-177.

Campana, M., Moraes, J. P. G., Santos, E., Herling, V., Barioni Junior, W., Bernardi, A. C. C. & Oliveira, P.P.A. (2015). Ammonia Volatilization from Exposed Soil and Tanzania Grass.

Can, L., & Zili, W. (2003). Microporous Materials Characterized by Vibrational Spectroscopies. In Handbook Zeolite Scie. CRC Press, 2003.

Carroll., & Dorothy., (1959). "Ion exchange in clays and other minerals". *Geological Society of America Bulletin* **70** (6): 749-780.

Castillo, L., Thybaud, E., Caquet, T., & Ramade, F. (1994) Organochlorine contaminants in common tern (Sterna hirundo) eggs and young from the Rhine River area (France) Bull. *Environ Contam Toxicol* **53:** 759–764.

Chameides, W. L., Kasibhatla, P. S., Yienger, J., & Levy, H. (1994). The growth of continental-scale metro-agro-plexes, regional ozone pollution, and world food production. *Science* **264**: 74-77.

Chang, H. J. (1997). Method of preparing a slow release fertilizer. US Patent 5695542, Dec 9.1997.

Changdeuck, B., Hyunjun, Y., Sihyeong, K., Kyungeun, L., Jiyoung, K., Myung, M. S., & Hyunjung, S. (2008). Template-Directed Synthesis of Oxide Nanotubes: Fabrication, Characterization, and Applications. *Chem. Mater* **20**: 756–767.

Chantawong, V., Harvey, N. W., & Bashkin, V. N. (2003). Comparison of heavy metal adsorptions by Thai kaolin and ball clay. Water Air Soil Pollut. **148**: 111-125.

Chen, L. Y., Remondetto, G. E., & Subirade, M. (2006). Food protein-based materials as nutraceutical delivery systems. *Trends in Food Science & Technology* **17**: 272-283.

Chesworth, W., Van Straaten, P., Smith, P., & Sadura, S. (1987). Solubility of apatite in clay and zeolite bearing systems: Application to agriculture. *Applied Clay Science* **2**: 291-297.

Chi-Fai, C., Shiuan-Huei, W., & Gow-Chin, Y. (2007). The development of regulations for food nanotechnology. *Trends in Food Science & Technology* **18**: 269-280.

Chilom, G., Kohl, S. D., & Rice, J. A. (2005). "The influence of lipids on the energetics of uptake of polycyclic aromatic hydrocarbon by natural organic matter" *J. Environ. Quality* **34**: 1055-1062.

Chinnamuthu, C. R., & Boopathi, P. M. (2009). Nanotechnology and Agroecosystem. *Madras Agricultural Journal* **96**:17-31.

Chiou, C. T. (1989). Theoretical consideration of the partition uptake of nonionic organic compound by soil organic matter. Soil Science Society of America, Inc:1-29.

Chiou, C. T., Porter, P. E., & Schmeddlng, D. W. (1983). Partition equilibria of nonionic organic compounds between soil organic matter and water. *Environ. Sci. Technol* **17**(4): 227-231.

Chiou, C. T., Schmelddlng, D. W., & Manes, M. (1982). Partitioning of organic compounds in octanol-water systems. *Enviro. Sci. Technol* **16**:4-10.

Chupp, C., & Sherf, A. F. (1960). Vegetable Diseases and Their Control, Ronald Press Company, New York, 534-566 pp.

Chuprova, V. V., Ulyanova, O. A., & Kulebakin, V. G. (2004). The effect of bark–zeolite fertilizers on mobile humus substances of chernozem and on biological productivity of Corn. Poster presented Euro Soil,Freiburg, Germany. 4 - 12p.

Clark, D. R. (1981). Death of bats from DDE, DDT or dieldrin diagnosis via residues in carcass fat. *Bull Environ Contam Toxicol* **26:** 367–371.

Clark, D. R., & Krynitsky, A. J. (1983). DDT: Recent contamination in New Mexico and Arizona. *Environment* **25**: 27–31.

Clark, D. R., & Lamont, T. G. (1976). Organochlorine residues in females and nursing young of the big brown bats. *Bull Environ Contam Toxicol* **15:** 1–8.

Clark, R. N. (2004). Spectroscopy of rocks and minerals, and principles of spectroscopy. In Infrared Spectroscopy in Geochemistry Exploration. Geochemistry and Remote Sensing. Mineral Association Canada, Short course, **33**, 17-35.

Clarke, M. C. G., Woodhall, D. G., Allen, D., & Darling, G. (1990). Geological, volcanological and hydrogeological controls on the occurrence of geothermal activity in the area surrounding Lake Naivasha, Kenya, with coloured 1:100 000 geological maps. Ministry of Energy, Nairobi, **138** pp.

Clifton, R. A. (1987). Natural and synthetic zeolites. US Bureau of Mines Information Circular **9140**.

Colborn, T., & Smolen, M. J. (1996). Epidemiological analysis of persistent organochlorine contaminants in cetaceans. *Rev Environ Contam Toxicol* **146:** 91–172.

Cole, J. J., Findlay, S., & Lovett, G. (1991). Comparative responses of aquatic ecosystems to toxic chemical stress. In editors. Comparative analysis of ecosystems: patterns, mechanisms, and theories. Springer- Verlag, New York, USA. Pages **161-195**

Cosper, E. M., Dennison, W. C., Carpenter, E. J., Bricelj, V. M., Mitchell, J. G., Kuenstner, S. H., Colflesh, D. C., & Dewey, M. (1987). Recurrent and persistent "brown tide" blooms perturb coastal marine ecosystem. *Estuaries* **10**: 284-290.

Crisp, T. M., Clegg, E. D., Cooper, R. L., Wood, W. P., Anderson, D. G., Baeteke, K. P., Hoffmann, J. L., Morrow, M.S., Rodier, D. J., Schaeffer, J. E., Touart, L.W.,

Zeeman, M. G., & Patel, Y. M. (1998). Environmental endocrine disruption: An effects assessment and analysis. *Environ Health Perspect* **106**:11.

Crowley, J. K. (1993). Mapping playa evaporite minerals with AVIRIS data: a first report from Death Valley, California. *Remote Sensing of Environment* **44**: 337–356.

Crowley, J. K., & Hook, S. J. (1996). Mapping playa evaporite minerals and associated sediments in Death Valley, California, with multispectral thermal infrared images. *Journal of Geophysical Research* **101 (B1)**: 643–660.

Cui, H. X., Sun, C. J., Liu, Q., Jiang, J. & Gu, W. (2006) Applications of nanotechnology in agrochemical formulation, perspectives, challenges and strategies. International conference on Nanoagri, Sao pedro, Brazil, 20-25 June 2010.

Cundari, A., & Graziani, G. (1964). Prodotti di alterazione della leucite nelle vulcaniti vicane. Period. *Miner* **33**: 35-52.

Currier, R. H. (1976). Production of zeolite mineral specimens from the Deccan Basalt in India. *Min. Rec.* **7**: 248-264.

Datt, A., Burns, E. A., Dhuna, N. A., & Larsen, S. C. (2013). Loading and release of 5-fluorouracil from HY zeoliteswith varying SiO2/Al2O3 ratios. *Microporous and Mesoporous Materials* **167:** 182–187. doi:10.1016/j.micromeso.2012.09.011.

Datt, A., Fields, D., & Larsen, S. C. (2012). An Experimental and Computational Study of the Loading and Release of Aspirin from Zeolite HY. *J. Phys. Chem. C* **116:** 21382–21390. doi:10.1021/jp3067266.

D'Elia, C. F., Sanders, J. G., & Boynton, W. R. (1986). Nutrient enrichment studies in a coastal plain estuary: phytoplankton growth in large-scale, continuous cultures. *Canadian Journal of Fisheries and Aquatic Sciences* **43**: 397-406.

Denmead, O. T. (1990). An ammonia budget for Australia. *Australian Journal of Soil Research* **28**: 887-900.

DeRosa, M. R., Monreal, C., Schnitzer, M., Walsh, R., & Sultan, Y. (2010). Nanotechnology if fertilizers. *Nat. Nanotechnology . J* **5**: 91.

DeRosa, M. C., Monreal, C., Schnitzer, M., Walshand, R., & Sultan, Y., (2010). Nanotechnology in fertilizers. *Nature Nanotechnol* **5**: *540-547.*

Di Vincenzo, J. P., & Sparks, D. L. (2001). Sorption of the neutral and charged forms of pentachlorophenol on soil: evidence for different mechanisms. *Arch. Environ. Contam. Toxicol.* **40**: 445-450.

Digigrafi Wageningen. (2012). Netherlands ISBN Agromisa: **90**-8573-039-2, ISBN CTA: **92**-9081-299-0, pp. 6-54. (www.prota.org) online date accessed 26/06/2012.

Dimitar, G., Bogdan, B., Krasimira, A., Irena, M., & Yancho, H. (2009). Synthetic Zeolites - Structure, Clasification, Current Trends in Zeolite Synthesis Review. International Science conference 4th - 5th June 2009, Stara Zagora, BULGARIA "Economics and Society development on the Base of Knowledge".Volume **VII**.

Doick, K. J., Klingelmann, E., Burauel, P., Jones, K. C., & Semple, K. T. (2005). "Long-term fate of Polychlorinated Biphenyls and Polycyclic Aromatic Hydrocarbons in agricultural soil." *Environ. Sci. Technol* **39**: 3663-3670.

Drori, Y., Lamc, B., Simpsonc, A., Aizenshtatb, Z., & Chefetz, B. (2006). The Role of Lipids on Sorption characteristics of fresh water-and Wastewater-Irrigated Soils. *J. Environ.Qual* **35**: 2154.

Eberl, D. D., & Lai, T. M. (1992). Slow-release nitrogen fertilizer and soil conditioner. U.S. Patent Appl. US 789,206, 15th Apr. 1992.

Echle, W. (1975). Zusammensetung und Entstehung sedimentärer Analcime in Jungtertiären pyroklastischen Gestein nördlich Mihaliççik, Westanatolien, Türkei. Neues Jahrb. *Miner. Abh.* **124:** 128-146.

Eichner, M. J. (1990). Nitrous oxide emissions from fertilized soils: summary of the available data. *Journal of Environmental Quality* **19**: 272-280.

Eric, O. O., Japheth, O., & Peninah, A. O. (2006). Lake Baringo: Experience and Lessons Learned Brief. UNOPS consultancy reports.

Eugster, H. P. (1969). Inorganic bedded cherts from the Magadi area. Kenya: *Contributions Mineralogy Petrology* **22:**1–31.

European-Commission., (1998). Monitoring of Pesticide Residues in Products of Plant Origin in the European Union. Report **1996**: 15.

European-Commission., (2001). Monitoring of Pesticide Residues in Products of Plant Origin in the European Union, Norway and Iceland. Report **1999**: 46.

Fabra, A., Duffard, R., & Evangelista, D. D. A. (1997). Toxicity of 2, 4-dichlorophenoxyacetic acid in pure culture. *Bull Environ Contam Toxicol* **59**: 645–652.

FAO, WFP & IFAD. (2012). The State of Food Insecurity in the World 2012. Economic growth is necessary but not sufficient to accelerate reduction of hunger and malnutrition. Rome, FAO.

FAO & WHO. (1986). Cyhalothrin: In: 1986 Evaluations of some pesticide residues in food, Part 1: Residues, Rome, Food and Agriculture Organisation of the United Nations. pp 78.

Farmer, D., Hill, I. R., & Maund, S. J. (1995). A comparison of the fate and effects of two pyrethroid insecticides (lambda-cyhalothrin and cypermethrin) in pond mesocosms. *Ecotoxicology* **4**: 219–244.

Fenn, L. B., & Hossner, L. R. (1985). Ammonia volatilization from ammonia or ammonium-forming nitrogen fertilizers. Pages **123-169** in Advances in soil science. Springer Verlag, New York, New York, USA.

Fernandez-Alvarez, M., Sanchez-Prado, L., Lores, M., Llompart, M., Garcia-Jares, C., & Cela, R. (2007). Alternative sample preparation method for photochemical studies based on solid phase microextraction: synthetic pyrethroid photochemistry. *J Chromatogr A Adv Sample Prep* **1152**:156–167.

Folmar, L. C., Sanders, H. O., & Julin, A. M. (1979). Toxicity of the herbicide glyphosate and several of its formulations to fish and aquatic invertebrates. *Arch Environ Contam Toxicol* **8:** 269–278.

Food and Agriculture Organization, (2008). FAOSTAT. http://faostat.fao.org. (Online) Date accessed 10/11/2016.

Forget, G., Goodman, T., & De-Villiers, A. (1993) Balancing the need for pesticides with the risk to human health. In: Impact of Pesticide Use on Health in Developing Countries. IDRC, Ottawa: **2**.

Frankenberger, W.T., Tabatabai, M. A. Jr., & Tabatabai, M. A. (1991). Factors affecting Lasparaginase activity in soils. *Biol. Fert. Soils* **11:** 1-5.

Freundlich, H. Z. (1906). The Adsorption in Solution. *J. Phys. Chem* **57A**: 385-470.

Friedrich, W. (1828). "Ueber künstliche Bildung des Harnstoffs" (On the artificial formation of urea). *Annalen der Physik und Chemie* **88** (2): 253–256

Frumkin, H. (2003). Agent Orange and Cancer: An Overview for Clinicians. CA Cancer J Clin.; **53**: 245.

Gall, Q., & Hyde, R. (1989). Analcime in lake and lake-margin sediments of the Carboniferous Rocky Brook Formation, western Newfoundland, Canada. *Sedimentology* **36**: 875-887

Galli, E., Gottardi, G., Mayer, H., Preisinger, A., & Passaglia, E. (1983). Acta. Crystallogr. Sect. B **39**. 189.

Garbarino, J. R., Snyder-Conn, E., Leiker, T. J., & Hoffman, G. L. (2002). Contaminants in Arctic snow collected over northwest Alaskan sea ice. *Water, Air and Soil Pollution* **139**: 183–214.

Gardiner, D. J. (1989). Practical Raman Spectroscopy. Springer – Verlag; ISBN 978-0-387-50254-0.

G.D.C., (2010): Menengai geothermal prospect; an investigation for its geothermal potential. Geothermal Development Company (GDC); Geothermal resource assessment project, unpubl. Report.

Geluso, K. N., Altenbach, J. S., & Wilson, D. E. (1976). Bat mortality: pesticide poisoning and migratory stress. *Science* **194**: 184–186.

Geselbarcht, J. (1996). Microfiltration/Reverse Osmosis Pilot Trials for Livermore, California, Advanced water Reclamation. AWW P.187.

Gilman, G. P. (2006). A simple device for arsenic removal from drinking water using hydrotalcite. *Sci. Total Environ* **366**: 926-931.

Giovannucci, E. (1999). Tomatoes and tomato-based products, lycopene, and prostate cancer: Review of the epidemiological literature. *Journal of National Cancer Institute* **91**: 317-331.

Gislason, E. A., & Craig, N. C. (2005). Cementing the foundations of thermodynamics: comparison of system-based and surroundings-based definitions of work and heat, J. Chem.*Thermodynamics* **37**: 954-966.

Goble, R. J., Treves, S. B., & Ghazi, A. M. (1993). Comparison of the Rainy ridge analcime phonolite sill and the Crowsnest volcanics, Alberta, Canada. *Can. J. Earth Sci.* **30**: 1644-1649.

GoK. (2010). Agricultural Sector Development Strategy (ASDS) 2010-2020.

Green, S. K., Griggs, T. D., & Mclean, B. T. (1989). Tomato and pepper production in the tropics, Asian Vegetable Research and Development Center. AVRDC Publication, Shanhua,

Thainan, Taiwan. ISBN 92-9058-037-2, 9-27 pp.

Gregory, J. W. (1921). "The Rift Valleys and Geology of East Africa." London. *Quart. Journ. Geol. Soc,* Vol. **LVI**,

Grover, R., & Hance, R. J. (1970). "Effect of ratio of soil to water on adsorption of linuron and atrazine." *Soil Sci* **109**: 136-138.

Gündogdu, M. N., Yalcin, H., Temel, A., & Clauer, N. (1996). Geological, mineralogical and geochemical characteristics of zeolite deposits associated with borates in the Bigadic, Emet and Kirka Neogene lacustrine basins, western Turkey. *Mineral. Deposita* **31**: 492-513.

Gupta, A. K., & Fyfe, W. S. (1975). Leucite survival: The alteration to analcime. *Can. Mineral* **13**: 361-363.

Gupta, S., Handa, S. K., & Sharma, K. K. (1998). A new spray reagent for the detection of synthetic pyrethroids containing a nitrile group on thin-layer plates. *Talanta* **45**: 1111–1114.

Gupta, S. K., Gupta, R. C., & Seth A.K. (2000). Methaemoglobinaemia in areas with high nitrate concentration in drinking water. *Natl Med J. India* **13**: 58–61.

Hadfield, S.T., Sadler, J. K., Bolygo, E., Hill, S., & Hill, I. R. (1993). Pyrethroid residues in sediment and water samples from mesocosm and farm pond studies of simulated accidental aquatic exposure. *Pestic Sci* **38:** 283–294.

Hafez, M. B., Nazmy, A. F., Salem, F., & Eldesoki, M. (1978). *J. Radioanal. Chem.* **47**.115.

Hance, R. J. (1980). Interaction between herbicides and the soils, Academic press.12.

Hance, R. J. (1965). *Weed Res* **5**:108-1149.

Hanson, A. (1995). Natural zeolites — many merits, meagre markets. *Industrial Minerals* **339**: 40–53.

Hansson, S., & Rudstam, L. G. (1990). Eutrophication and Baltic fish communities. *Ambio* **19**: 123-125.

Harker, A. (1954). Petrology for students. Cambridge University Press, Cambridge, England. **283** p.

Harper, S. S. (1994). Sorption-desorption and herbicide behavior in soil. *Rev. Weed Sci* **6**:207

Hassett, J. J., & Banwart, W. L. (1989). The sorption of non-polar organics by soils and sediments. In: Reaction and movement of organic chemicals in soils. SSSA Special publication no.22, (Soil Science Society of America and American Society of Agronomy).

Hay, R. L., Sand, L. B. & Mumpton, F. A. (1978). Geologic occurrence of natural zeolites. In: Natural zeolites—occurrence, properties, use. Pergamon Press, New York. pp. 135–143.

Hay, R. L. & Mumpton, F. A. (1981). Geology of zeolites in sedimentary rocks. In: Mineralogy and geology of natural zeolites. *Reviews in Mineralogy* **4**: 165–175.

Hay, R. L. (1963). Stratigraphy and zeolitic diagenesis of the John Day Formation of Oregon. *Univ. Calif. Pub. In Geol. Sci* **42**(5):199-262.

Hay, R. L. (1970). Silicate reactions in three lithofacies of a semi-arid basin, Olduvai Gorge, Tanzania. *Min. Soc. Amer., Spec. Pa.* **3**: 237-255.

Helfrich, L. A., Weigmann, D. L., Hipkins, P., & Stinson, E. R. (1996). Pesticides and Aquatic Animals: A Guide to Reducing Impacts on Aquatic Systems.

Helle, E., Olsson, M., Jensen, S. (1976). DDT & PCB levels and reproduction in ringed seal from the Bothnian Bay. *Ambio* **5:**188–189.

Hewson, R. D., Cudahy, T. J., Mizuhiko, S., Ueda, K., & Mauger, A. J. (2005). Seamless geological map generation using ASTER in the Broken Hill-Curnamona province of Australia. *Remote Sensing of Environment* **99** (1, 2): 159–172.

Ho, Y. S., & McKay, G. (1999). Pseudo second order model for sorption processes. *Process Biochem* **34**: 451– 465.

Hollister, C. C. (2011). Ammonium, Nitrate and Phosphate sorption to water rinsed and nonrinsed chars. M.Sc. Thesis, Cornell University. pp. 54

Howarth, R. W. (1988). Nutrient limitation of net primary production in marine ecosystems. *Annual Review of Ecology and Systematics* **19**: 89-110.

Howarth, R. W., Jensen, H., Marino, R., & Postma, H. (1995). Transport and processing of phosphorus in near-shore and oceanic waters. In H. Tiessen, editor. Phos-phorus in the global environment: transfers, cycles, and management. John Wiley & Sons, Chichester, England. Pages **323-345.**

Hulscher, T. E., & Cornelissen, G. (1996). "Effect of temperature on sorption equilibrium and sorption kinetics of organic micropollutants- a review." *Chemosphere* **32**(4): 609-626.

Hurley, P. M., Hill, R. N., & Whiting, R. J. (1998). Mode of carcinogenic action of pesticides inducing thyroid follicular cell tumours in rodents. *Environ Health Perspect*.; **106:** 437.

Igbedioh, S. O. (1991). Effects of agricultural pesticides on humans, animals and higher plants in developing countries. *Arch Environ Health* **46:** 218.

Iijima, A., Sand, L. B., & Mumpton, F. A. (1978). Geologic occurrences of zeolite in marine environments. In Natural Zeolites: Occurrence, Properties, Use. *Pergamon Press, Elmsford, New York*, 175-198.

Inglezakis, V. J. (2005). The concept of "capacity" in zeolite ion-exchange systems. *Journal of Colloid and Interface Science* **281**: 68–79.

Inglezakis, V. J., Loizidou, M .D., & Grigoropoulou, H. P. (2003). Journal of Colloid Interface Science **261**:49.

IRPTC data profile, (2016). International Register of Potential Toxic Chemicals http://0-www.worldcat.org.novacat.nova.edu/identities/lccn-n97900852/ (Accessed 2nd Nov. 2016 at 2.31pm).

Jacob, D. J., & Wofsy, S. C. (1990). Budgets of reactive nitrogen, hydrocarbons, and ozone over the Amazon forest during the wet season. *Journal of Geophysical Research* **95**(16): 737-754.

Jan-Åke, P., Mårten, W., & Stephen, O. (2008). Handbook for Kjeldahl Digestion: 11- 42.

Jefferies, D. J., & Zool. J. (1976). Organochlorine insecticide residue in British bats and their significance; **166:** 245–251. (1)

Jeremine, E. (1934). Note sur les zéolites des Monts Lubur et du Mont Elgon, Bull. *Soc. Franc Minéral* **57:** 240-243.

Jeyaratnam, J. (1985). Health problems of pesticide usage in the third world. *B M J* **42**: 505.

Jinghua, G. (2004). Synchrotron radiation, soft X-ray spectroscopy and nano-materials. *J. Nanotechnol* **1**:193-225.

Jiyun, C. H. (2003). Guided molecular self-assembly: a review of recent efforts. *Smart Mater. Struct* **12**: 264–271.

John, W. & Sons Ltd, (2015). Energy Dispersive Spectroscopy. Essential Knowledge Briefings. Second Edition. The Atrium Southern Gate, Chichester, West Sussex, POI985Q.

Jones, J. B., Jones, J. P., Stall, R. E., & Zitter, T. A. (1991). Compendium of Tomato Diseases. Minnesota, American Phytopathological Society.**73** pp.

Joshi, M. S., & Mohan, R. P. (1983). J. Colloid Interface Sci. **95**. 131.

Junrungreang, S., Limtong, P., Wattanaprapat. K., & Patsarayeangyong, T. (2002). Effect of zeolite and chemical fertilizer on the change of physical and chemical properties on Lat Ya soil series for sugar cane. *17th WCSS*, Thailand.

Justic, N., Rabalais, N. N., Turner, R. E., & Dortch, Q. (1995). Changes in nutrient structure of river-dominated coastal waters: stoichiometric nutrient balance and its consequences. *Estuarine, Coastal and Shelf Science* **40**: 339-356.

Kah, M., & Brown, C. D. (2006). Adsorption of ionisable pesticides in soil. *Reviews of Environmental Contamination and Toxicology* **188**:149-218.

Kannan, K., Sinha, R. K., Tanabe, S., Ichihashi, H., & Tatsukawa, R. (1993). Heavy metals and organochlorine residues in Ganges river dolphins from India. *Mar Pollut Bull* **26**: 159–162.

Kannan, K., & Sundaram, M. M. (2001). "Kinetics and mechanism of removal of methylene blue by adsorption on various carbons e a comparative study." *Dyes Pigments* **51**: 25-40.

Karickhoff, S. W., Brown, D. S., & Scott, T. A. (1979). “Sorption of hydrophobic pollutants on natural sediments.” *Waters Res* **13**: 241-248.

Karn, B., Kulken, T., & Otto, M. (2009). Nanotechnology and insitu remediation: A review of benefits and potential risks. *Environmental health Perspective* **117 (12)**:1823-1831.

Kashima, N., & Ogawa, T. (1998). Speleo-minerals in Volcanic Caves of Kenya, East African Rift Zone. *J. Speleol. Soc. Japan* **23**: 46-52.

Kastner, M., Stonecipher, S. A., & Mumpton, F. A. (1978). Zeolites in pelagic sediments of the Atlantic, Pacific, and Indian Oceans. In Natural Zeolites: Occurrence, Properties, Use, Pergamon Press, Elmsford, New York, 199-220.

Kenya Fertilizer Assessment. (2012). IFDC. In support of The African Fertilizer and Agribusiness Partnership, June 2012.

Kenya: Poverty Reduction Strategy Paper (PRSP). IMF Country Report No. 10/224, July 2010.

Kile, D. E., & Modreski, P. J. (1988). Zeolites and related minerals from the Table Mountain lava flows near Golden Colorado. *Min. Rec* **19**:153-184.

Kithure, J. G. N., Murung, J. I., Tum, P. K., Wanjau, R. N., & Thoruwa, C. L. (2017). Fate of Lambda-Cyhalothrin in Kales, Tomatoes and Cabbage from Rural setting in Kenya. International *Journal of Scientific Research and Innovative Technology* ISSN: 2313-3759 Vol. **4** No. 2; February 2017.

Kliewer, (2009). Electron Microscopy and Imaging. *In Zeolite Characterization and Catalysis*, Springer Science Business Media, 169-196.

Koebel, M., Elsener, M., & Kleemann, M. (2000). Urea-SCR: a promising technique to reduce NOx emissions from automotive diesel engines. *Catalysis Today* **59:** 335-345.

Kohl, S. D., & Rice, J. A. (1999). Contribution of lipids to the nonlinear sorption of polycyclic aromatic hydrocarbons to soil organic matter. *Geochem.* **30**: 929-939.

Kokotailo, G. T., & Fyfe, C. A. (1995). Zeolite Structure analysis with powder X-ray diffraction and solid-state NMR techniques. *The RIGAKU Journal*. Vol.**12**, No.1,

Kole, R. K., Banerjee, H., & Bhattacharyya, A., (2001). Monitoring of market fish samples for Endosulfan and Hexachlorocyclohexane residues in and around Calcutta. *Bull Envirron Contam Toxicol* **67:** 554–559.

Komarneni, S. (2009). Potential of Nanotechnology in Environmental Soil Science. Proc. of 9th Int. Conf. East and Southeast Asia Federation of Soil Science Societies, (Korean Society of Soil Science and Fertilizers, Seoul).

Koskinen, W. C., & Harper, S. S. (1990). The retention process: mechanisms. In Pesticides in the soil environment: processes, impacts and modeling. Cheng, H.H. (ed.), Soil Science Society of America (SSSA), Madison, WI, 51-79.

Koyama, J. (1996). Vertebral deformity susceptibilities of marine fishes exposed to herbicide. *Bull Environ Contam Toxicol* **56:** 655–662. [PubMed]

Kramer, M. H., Herwaldt, B. L., & Craun, G. F. (1996). Surveillance of waterborne-disease outbreaks – United States, 1993–1994. CDCP Surveillance Summaries, MMWR **45**: 1–33.

Kuechl, D. E., Benin, A. I., Knight, L. M., Abrevaya, H., Wilson, S. T.J., Sinkler, W., Mezza, T. & Willis, R. R., (2010). Micropor. Mesopor. Mat. **127**, 1-2, 104-118, 1387-1811.

Kulprathipanja, S. (2010). Zeolites in Industrial Separation and Catalysis. Wiley- VCH, Weinham ISBN: 978-3-527-32505-4.

Lagergren, S. (1898). About the theory of so-called adsorption of soluble substances, Kungliga Svenska Vetenskapsakademiens. Handlingar. **24**, 1–39.

Lai, T. M & Eberl, D. D. (1986). Controlled and renewable release of phosphorus in soils from mixture of phosphate rock and NH4-exchanged clinoptilolite. Zeolites **6**:129-132.

Lampert, S. M. (1967). Functional relationship between sorption in soil and chemical structure. J. Agri. Food Chem.**15**:572-576.

Langmuir, I. (1918). The Adsorption of Gases on Plane Surfaces of Glass, Mica, and Platinum. J.A.M. Chem. Soc. **40**, 1361-1403.

Larry, G. B. (2016). Managing Urea-Containing Fertilizers. Department of Soil Science, University of Wisconsin. http://www.soils.wisc.edu/extension/materials/ManagingUrea.pdf (Accessed 2nd Nov. 2016 at 4.48pm).

Larsson, V., Elmgren, R., & Wulff, F. (1985). Eutrophication and the Baltic Sea: causes and consequences. Ambio **14**: 9-14.

Lawrence, M. K., & Kam-biu, L. (2009). Palynological evidence of climate change and land degradation in the Lake Baringo area, Kenya, East Africa, since AD 1650. Palaeogeography, Palaeoclimatology, Palaeoecology **279** (2009) 60–72.

Lee, S., Carr C. S. & Shantz, D. F. (2005). Langmuir, **21, 25,** 12031-12036, 0743-7463.

Lee, S. B., Mitchell, D. T., Trofin, L., Nevanen, T. K., Söderlund, H., & Martin, C. R. (2002). Science, **296**, 2198.

Lee, L. S., & Rao, P. S. C. (1996). "Impact of several water-miscible organic solvents on sorption of benzoic acid by soil." Environ. Sci. Technol. **30**: 1533-1539.

Lein, A. Y., Howarth, R. W., Stewart, J. W. B., & Ivanov, M. V. (1992). Interaction of carbon, sulfur, and oxygen cycles in continental and marginal seas. In editors. Sulphur cycling on the continents: wetlands, terrestrial ecosystems, and associated water bodies. John Wiley & Sons, Chichester, England. Pages **189-213**

Li-Ming, H., John, T., Albert, W., & Kean, G. (2008). Environmental Chemistry, Ecotoxicity, and Fate of Lambda-Cyhalothrin. Reviews of Environmental Contamination and Toxicology. **71** . Springer.

Lin, S. H., Juang, R. S., & Hazard, J. (2002). Mater. B **92**. 315.

Lindsey, J. S. (1991). New J. Chem. **15** 153.

Liu, X., Feng, Z., Zhang, S., Zhang, J., Xiao, Q., & Wang, Y. (2006). Preparation and testing of cementing nano-subnano composites of slow or controlled release of fertilizers. Sci. Agr. Sin. J **39**:1598-1604.

Liu, M., Liang, R., Liu, F., & Niu, A. (2006). Synthesis of a slow release and superabsorbent nitrogen fertilizer and its properties. *Polym Adv Tech* **17**: 430-438.

Liu, (2009). Infrared and Raman Spectroscopy. *In Zeolite Characterization and Catalysis*, Springer Science Business Media, 197-222.

Logan, J. A. (1985). Tropospheric ozone: seasonal behavior, trends, and anthropogenic influence. Journal of Geophysical Research **90**: 10, 463-10, 482.

Lu, Y., & Pignatello, J. J. (2002). "Demonstration of the 'Conditioning effect' in soil organic matter in support of pore deformation mechanism for sorption hysteresis." Environ. Sci. Technol. **36**: 4553-4561.

Luhr, J., & Giannetti, B. (1987). The Brown Leucitic Tuff of Roccamonfina Volcano (Roman Region, Italy). Cont. Mineral. Petrol. **95**, 420-436.

Macdonald, R., Baginski, B., Leat, P. T., White, J. C., & Dzierzanowski. (2011): Mineral stability in peralkaline silicic rocks: Information from trachytes of the Menengai volcano, Kenya.

Majewski, M., Capel, P. (1995). Pesticides in the atmosphere: distribution, trends, and governing factors. In: Volume one, Pesticides in the Hydrologic System. Ann Arbor Press Inc; p. 118.

Mallin, M. A. (2000). Impacts of industrial animal production on rivers and estuaries. Am Sci **88**: 2–13.

Manikandan, A., & Subramanian, K. S. (2014). Fabrication and characterisation of nanoporous zeolite based N fertilizer. African Journal of Agricultural Research. Vol. 9(2), pp. 276-284, 9 January.

Martens, D. A., & Bremner, J. M. (1993). Influence of herbicides on transformations of urea nitrogen in soil. J. Environ Sci Health B.; **28:** 377–395.

Martin, C. R., & Kohli P (2003). Nat. ReV. Drug DiscoVery, **2**, 29.

Martin, C. R. (1996). Chem. Mater. **8**,1739.

Martin, C. R. (1995). Acc. Chem. Res.**28**, 61.

Martineau, D., Be′land, P., Desjardins, C., & Lagace′, A. (1987). Levels of organochlorine chemicals in tissues of beluga whales (Delphinapterusleucas) from the St. Lawrence Estuary, Que′bec, Canada. Arch Environ Contam Toxicol.;**16**: 137–147.

Martyn, V. T. (2006). Progress and future challenges in controlling automotive exhaust gas emissions, Applied Catalysis B: Environmental **70:** 2-15.

Matheson, F. J. (1966). Geology of the Kajiado Area. Ministry of Natural Resources and Wildlife Geological Survey of Kenya. Report no. **70**. Degree sheet 51, S.E. Quarter

Maynard, A. D. (2006). Nanotechnology: assessing the risks. Nanotoday, **1**, 22-33.

McCall, G. J. H., Baker, B. H. & Walsh, J. (1965). "Late Tertiary and Quaternary Sediments of the Kenya Rift Valley." Wenner-Gren Foundation for Anthropological Research, Vienna. Paper read at Symposium No. **29.**

Mccall, G. J. H. (1967). Geology of the Nakuru, Thomson's falls, Lake Hannington Area. Ministry of Natural Resources Geological Survey of Kenya. Report No. **78**. Degree sheet no. 35 S.W. Quarter and 43 n.w. Quarter.

Meessen, J. H. & Petersen, H. (2005). "Urea", Ullmann's Encyclopedia of Industrial Chemistry, Weinheim: Wiley-VCH, doi:10.1002/14356007.a27_333.

Mehlich, A. (1953). Determination of P, Ca, Mg, K, Na, and NH4. North Carolina Soil Test Division, 23-89.

Ming, D. W., & Mumpton, F. A. (2003). Zeolites in Soil. In: Dixon, J.B. and Weed, S.B., Eds., Minerals and Soil Environments, Soil Science Society of America, Madison, 873-911.

Mohanraj, J. (2013). Effect of nano-zeolite on nitrogen dynamics and greenhouse gas emission in rice soil eco system M.Tech. Thesis, Tamil Nadu Agricultural University, Coimbatore.

Mondale, K. D., Carland, R. M., & Aplan, F. F. (1995). Miner. Eng. **8**. 535.

Mora M. A. (1996). Conger-specific polychlorinated biphenyl patterns in eggs of aquatic birds from the Lower Laguna, Madre, Texas. Environ. Toxicol. Chem.; **15:** 1003–1010.

Mora, M. A. (1997). Transboundary pollution: Persistent organochlorine pesticides in migrant birds of the southeastern United States and Mexico. Environ Toxicol Chem; **16:** 3–11.

Mozgawa, W., Jastrzebski, W., & Handke, M. (2005). Vibration Spectra of D4R and D6R Structural Units. Journal of Molecular Structures. 744-747, 663-670.

Mumpton, F. A. (1984). Natural zeolites. In: Pond WG and FA Mumpton (eds.) Zeo-agriculture: Use of natural zeolites in agriculture and aquaculture. Westview Press Boulder, Colorado, pp. 247-254.

Murray, C. J. L., & Lopez, A. D. (1996). The global burden of disease: a comprehensive assessment of mortality and disability from diseases, injuries and risk factors in 1990 and projected to 2020 [Volume **1 of 10** in the Global Burden of Disease and Injury Series] Cambridge, MA: Harvard School of Public Health;.

Murray, J., & Renard, A. F. (1891). Report on Scientific Results of the Voyage of "H.M.S. Challenger" during the years 1873-1876; Deep Sea Deposits. Johnson Reprint Co., London, **525** pp.

Naderi, M. R., & Danesh-Shahraki, A. (2013). Nanofertilizers and their role in sustainable agriculture. International Journal of Agriculture and Crop Sciences, vol **5 (19)**: 2229-2232.

Naik, S. P., Chen, J. C., & Chiang, A. S. T. (2002). Micropor, Mesopor. Mater, **54, 3**, 293-303, 1387-1811.

National Council for Population and Development (NCPD), July 2013. Ministry of Devolution and Planning. Report of 2013 on Kenya Population Situation Analysis.

Nixon, S. W. (1995). Coastal marine eutrophication: a definition, social causes, and future concerns. Ophelia **41**:199-219.

Nixon, S. W., Ammerman, J. W., Atkinson, L. P., Berounsky, V. M., Billen, G., Boicourt, W. C., Boyton, W. R., Church, T. M., Ditoro, D. M., Elmgren, R., Garber, J. H., Giblin, A. E., Jahnke, R. A., Owens, N. P. J., Pilson, M. E. Q., & Seitzinger, S. P. (1996). The fate of nitrogen and phosphorus at the land-sea margin of the North Atlantic Ocean. Biogeochemistry **35**: 141-180.

N. R. C. (1993). [National Research Council Committee on Wastewater Management for Coastal Urban Areas, Water Science and Technology Board]. Managing wastewater in coastal urban areas. National Research Council, Washington, D.C., USA.

Nyoro, J., Ayieko, M., & Muyanga, M. (2007). "The Compatibility of Trade Policy with Domestic Policy Interventions Affecting the Grains Sector in Kenya," Paper presented at the FAO's workshop on Trade and Policy for Food Products Conducive to Development in Eastern Africa, March 1-2, Rome, Italy.

Oenema, O., Boers, P. C. M., & van Eerdt, M. M. (1998). Leaching of nitrate from agriculture to groundwater: the effect of policies and measures in the Netherlands. Environ Pollut **102**: 471–78.

Officer, C. B., Biggs, R. B., Taft, J., Cronin, L. E.; Tyler, M. A., & Boynton, W. R. (1984). Chesapeake Bay anoxia: origin, development, and significance. Science **223:** 22-27.

Ohrman, O. (2000). Synthesis and Characterization of Zeolite Coatings on Monoliths Support, MSc Thesis, Lulea University of Technology.

Oudo, H., & Hansen, H.C. (2002). Sorption of lambda-cyhalothrin, cypermethrin, deltamethrin and fenvalerate to quartz, corundum, kaolinite and montmorillonite. Chemosphere **49:** 1285–1294.

Paolo, F., Ermanno, G., & Antonio, R. (2003). Minerogenesis of Volcanic Caves of Kenya. Int. J. Speleol., **32** (1/4): 3-18

Parham, W. (1989). Natural zeolites: Some potential agricultural application for developing countries. Natural Resources Forum, May 1989:107-115.

Park, J., Kim, H. S., & Bard, A. (2006). J. Nano. Lett. **6**, 24.

Parker, C. A., & O'Reilly, J. E. (1991). Oxygen depletion in Long Island Sound: a historical perspective. Estuaries **14**: 248-264.

Pauling, L. XXII (1930). The Structure of Sodalite and Helvite. *Z. Kristallogr.* **74**, 213–225 .

PCAST, (2005). The National Nanotechnology Initiative at 5 years Washington, DC: President's council of Advisors on Science and Technology, Executive Office of the president.

Pearce, T. H. (1970). The analcite-bearing volcanic rocks of the Crowsnest Formation, Alberta. Can. J. Earth Sci., 7, 46-66.

Pearce, T. H. (1993). Analcime phenocrysts in igneous rocks: Primary or secondary? Discussion. Am. Mineral. **78,** 225-229.

Pell, M., Stenberg, B., & Torstensson, L. (1998). Potential denitrification and nitrification tests for evaluation of pesticide effects in soil. Ambio. **27**: 24–28.

Peng, G. (2016). Structure Determination and Prediction of Zeolites. Accombined study by Electron Diffraction, Powder X-ray Diffraction and Database Mining. Doctoral Thesis ©PengGuo, Stockholm University 2016. ISBN 978-91-7649-384-7.

Pereira, E. I., Minussi, F. B., Cruz, C. C. T., Bernardi, A. C. C., & Ribeiro, C. (2012). Urea−Montmorillonite-Extruded Nanocomposites: A Novel Slow-Release Material. *J. Agric. Food Chem.,* **60**: 5267−5272.

Perrin, W. F., Brownell, R. L., Kaiya, Z., & Jiankang, L. (1989). Biology and Conservation of the river Dolphins. In Proceedings of the Workshop on Biology and Conservation of the Platanistoid Dolphins; Wuhan, China, October **28–30**, 1986.

Peter, B. (2003). Theory of XRF. Getting acquainted with the principles. ©2003 by PANalytical BV, The Netherlands. ISBN: 90-9016758-7. 3rd edition.

Pickering, H. W., Menzies, N. W., & Hunter, M. N. (2002). Zeolite/rock phosphate–A novel slow release phosphorus fertilizer for potted plant production. *Sci Hort* **94**: 333-343.

Priyanka, A. (2014). Applications of Iron Oxide Based Nanoadsorbents in Water Remediations. International Journal of Modern Engineering and Research Technology.Vol.**1**, Issue 1.

Rahmat, H., Ganjar, F., Uswatul, C., Sayekti, W., & Ari, H. R. (2015). Effectiveness of urea nanofertilizer based aminopropyltrimethoxysilane zeolite as slow release fertilizer system. *African Journal of Agricultural Research. Vol*. **10**(14):1785-1788.

Rai, V., Acharya, S. & Dey, N. (2012). Implication s of Nanobiosensors in Agriculture. Journal of Biomaterials and Nanotechnology **3**: 315-324.

Ramesh, K., Biswas, A. K., Somasundaram, J., & Subbarao, A. (2010). Nanoporous zeolites in farming: Current status and issues ahead. Curr. Sci. **99**:760-764.

Rao, C. N. R., & Cheetham, A. K. (2001). Science and technology of nanomaterials: current status and future propects. J. Matter. Chem, 11, 2887-2894.

Rao, P. S., Hornsby, C. A. G., Kilcrease, D. P., & Nkedi-Kizza, P. (1985). "Sorption and transport of hydrophobic organic chemicals in aqueous and mixed solvent systems; model development and preliminary evaluation." J. Environ. Qual. **14**: 376-383.

Redlich, O., & Peterson, D. L. (1959). A useful adsorption isotherm. J. Phys. Chem. **63**, 1024–1029.

Reeves, R. R.., & Chaudhry, A. A. (1998). Status of the Indus river dolphin, Platanista minor. Oryx.; **32**: 35–44.

Reeves, R. R., Chaudhry, A. A., & Khalid, U. (1991). Competing for water on the Indus plain: Is there a future for Pakistan river dolphins? Environ Conserv.; **18:** 341–350.

Reich, P. B., & Amundson, R. B. (1985). Ambient levels of ozone reduce net photosynthesis in tree and crop species. Science **230**: 566-570.

Reid, B. J., Jones, K. C., & Semple, K. T. (2000). " Bioavailability of persistent organic pollutants in soil and sediments – a perspective on mechanisms, consequences and assessment." Environ. Poll. **108**: 103-112.

Reijnders, P. J. H. (1986). Reproductive failure in common seals feeding on fish from polluted coastal waters. Nature; **324**: 456–457. [PubMed]

Remy, R. R.., & Ferrell, R. E. (1989). Distribution and origin of analcime in marginal lacustrine mudstones of the Green River Formation, south-central Uintsa Basin, Utah. Clays and Clay Miner. **37**, 419-432.

Renaut, R. W. (1993). Zeolitic diagenesis of late Quarternary fluviolacustrine sediments and associated calcrete formation in the Lake Bogoria Basin, Kenya Rift Valley. Sedimentology, **40**, 271-301.

Rice, C. P., & Cherniak, S. M. (1997). Marine arctic fog: an accumulator of currently used pesticide. Chemosphere; **35:** 867–878.

Rice, R. D., Rice, L. W., & Tindall, H. D. (1993): Fruit and vegetable production in warm climates, MacMillan press, London, 486pp.

Roberts, T. R. (1998). Herbicides and Plant Growth Regulators; The Royal Soc Chem. Cambridge, UK: Metabolic Pathway of Agrochemicals. Part I.

Roberts, T. R., & Hutson, D. H. (1999). Insecticides and Fungicides. The Royal Soc Chem. Cambridge, UK: Metabolic Pathway of Agrochemicals Part II.

Robson, M. J., & Crosby, J. (1984). Insecticidal product and preparation thereof. European Patent Office. Patent Number EU 106469. UK.

Robson, H. (2001). Verified synthesis of Zeolitic Materials, 2nd Revised Edition, Elsevier Science, Amsterdam.

Roco, M. C., & Bainbridge, W. S. (2005). Societal implications of nanoscience and nanotechnology: Maximizing human benefit. Journal of Nanoparticle Research, **7**: 1–13.

Roessink, I., Arts, G. H. P., Belgers, J. D. M., Bransen, F., Maund, S. J., & Brock, T. C. M. (2005). Effects of lambdacyhalothrin in two ditch microcosm systems of different trophic status. Environ Toxicol Chem **24**: 1684–1696.

Ross, P. S., De-Swart, R. L., Reijnders, P. J. H., Loveren, H. V., Vos J. G., & Osterhaus, A. D. M. E. (1995). Contaminant-related suppression of delayed-type hypersensitivity and antibody responses in harbor seals fed herring from the Baltic Sea. Environ Health Perspect.; **103**: 162–167. [PMC free article] [PubMed]

Ross, C. S. (1928). Sedimentary analcite. Am. Mineral. **13**, 195-197.

Roux, J., Hamilton, D. L., & Petrol, J. (1976). Primary igneous analcite--an experimental study. **17**, 244-257.

Ruren, X., Wenqin, P., Jihong, Y., Qishen, H., & Jiesheng, C. (2007). Chemistry of Zeolites and Related Porous Materials: Synthesis and Structure.. ISBN 978-0-470-82233-3 (HB) Copyright © 2007. www.wiley.com

Saha, P. (1959). Geochemical and X-ray investigation of natural and synthetic analcites. Am. Mineral. **44**, 300-313.

Sakami, W., & Harrington, H. (1963). "Amino acid metabolism". Annual Review of Biochemistry. **32** (1): 355–98

Santos, A., & Flores, M. (1995). Effects of glyphosate on nitrogen fixation of free-living heterotrophic bacteria. Lett Appl Microbiol.; **20**: 349–352.

Schaber, P. M., Colson, J., Higgins, S., Thielen, D., Anspach, B., & Brauer, J. (2004). Thermal decomposition (pyrolysis) of urea in an open reaction vessel, Thermochimica Acta **424**: 131-142.

Schlesinger, W. H., & Hartley, A. E. (1992). A global budget for atmospheric NH_3. Biogeochemistry **15**: 191-211.

Schnoor, J. L. (1997). Phytoremedition: Ground water Remediation Technologies, Analysis Centre, Pittsburgh TE97:01.

Schwarzenbach, R. P., Gschwed, P. M., & Imboden, D. M. (1993). Environmental Organic Chemistry. New York, Wiley.

Scribner, S. L., Benzing, T. R., Sun, S. B., & Boyd, S. A. (1992). Desorption and bioavailability of aged simazine residues in soil from a continuous corn field. J. Environ. Qual. **21**:115-120.

Semmens, M. J., & Seyfarth, M. (1976). In: An International Conference on the Occurrence, Properties and Utilization of Natural Senilities, Tucson, AZ, p. 517.

Semple, K. T., Morris., & Paton, G. I. (2003). "Bioavailability of hydrophobic organic contamination in soil: Fundamental concepts and techniques for analysis" Eur.J. Soil Science **54**:809-818.

Senesi, N. (1992). Binding mechanisms of pesticides to soil humic substances. Sci. Total Environ. 123-124:63-76.

Sengupta, A. K., & Clifford, D. (1986). Environ. Sci. Technol. **20**. 149.

Senthilkumar, K., Kannan, K., Subramanian, A., & Tanabe, S. (2000). Accumulation of Organochlorine Pesticides and Polychlorinated Biphenylsin Sediments, Aquatic Organisms, Birds, Bird Eggs and Bat Collected from South India. Environ Sci Pollut Res.; **7:** 1–13. [PubMed]

Shafer, T. J., & Meyer, D. A., (2004). Effects of pyrethroids on voltage-sensitive calcium channels: a critical evaluation of strengths, weaknesses, data needs, and relationship to assessment of cumulative neurotoxicity. Toxicol Appl Pharmacol **196**: 303–318.

Shafiei, T. M. (1990). Costa H.H. The susceptibility and resistance of fry and fingerlings of Oreochromis mossambicus Peters to some pesticides commonly used in Sri Lanka. J Appl Ichthyol; **6:** 73–80.

Shahmohammadi, K., Babazadeh, H., Nazemi, H. A., & Manshouri, M. (2011). Isotherm and Kinetic Studies on Adsorption of Pb, Zn and Cu by Kaolinite. Caspian J. Env. Sci., Vol. **9** No.2 pp. 243-255.

Shakeel, A., Mudasir, A., Babu, L. S., & Saiqa, I. (2015). A review on plants extract mediated synthesis of silver nanoparticles for antimicrobial applications: A green expertise. Journal of Advanced Research (2015) xxx, xxx–xxx.

Shankara, N., Joep-Van, L. de J., Marja, de G., Martin, H., Barbara., & Van Dam: (2005). © Agromisa Foundation and CTA, Wageningen; Agrodok 17

Sharmila, R. C. (2010). Nutrient release pattern of nano-fertilizer formulations. Ph D Thesis, Tamil Nadu Agricultural University, Coimbatore, Tamil Nadu, India.

Sharmila, R. (2011). Nutrient release pattern of nanofertilizer formulation. Ph.D (Agri.) Thesis. Tamilnadu Agricultural University, Coimbatore.

Shaviv, A. (2000). Advances in Controlled Release of Fertlizers. Advanced Agronomy Journal **71**: 1-49.

Shenbagavalli, S. (2011). Development and evaluation of biochar for mitigation of greenhouse gaseous emission by carbon sequestration in agricultural field. Ph.D. Thesis, Tamil Nadu Agricultural University, Coimbatore.

Sheppard, R. A., & Gude, A. J. (1969). Diagenesis of tuffs in the Barstow Formation, Mud Hills San Bernardino County, California. U.S. Geol. Surv., Prof. Paper 634, 35 pp.

Simons, J. W. E. (1974). The lava caves of the northern Chyuly Hill, Kenya, Studies in Speleology, **2** (6), 238-255.

Simons, J. W. E., (1976). Leviathan Cave, a Major Lava Tube in Kenya, BCRA Bull., **14**, p.23-25.

Simons, J. W. E. (1998). Volcanic Caves of Kenya. A guide for the8th Int. Symp, on Vulcanospeleology. Nairobi, Kenya, February 1998, **37** pp.

Sing, K. S. W., Everett, D. H., Haul, R. A. W., Moscou, L., Pierotti, R. A., Rouquerol, J., & Siemieniewska, T. (1985). Reporting physisorption data for gas/solid systems with special reference to the determination of surface area and porosity. *Pure Appl. Chem*. **57**: 603 - 619.

Singh, J. B., & Singh, S. (1989). Effect of 2, 4-dichlorophenoxyacetic acid and maleic hydrazide on growth of bluegreen algae (cyanobacteria) Anabaena doliolum and Anacystis nidulans. Sci. Cult.; **55**: 459–460.

Sitarz, M., Mozgawa, W., & Handke, M. (1997). Vibration spectra of complex ring silicate anions method of recognition. Journal of molecular structure. Vol. **404**: 193-197.

Slow- and Controlled-Release and Stabilized Fertilizers: An Option for Enhancing Nutrient Efficiency in Agriculture. Second edition, IFA, Paris, France, October 2010 Copyright 2010 IFA. All rights reserved. ISBN 978-2-9523139-7-1

Smayda, T. J., Cosper, E. M., Carpenter, E. J., and Bricelj, V. M., (1989). Primary production and the global epidemic of phytoplankton blooms in the sea: a linkage? In Novel phytoplankton blooms: causes and impacts of recurrent brown tides and other unusual blooms. Springer Verlag, Berlin, Germany. Pages **29-40**

Spanakis, M., Bouropoulos, N., Theodoropoulos, D., Sygellou, L., Ewart, S., & Moschovi, A. M. (2014). Controlled release of 5-fluorouracil from microporous zeolites, Nanomedicine: *Nanotechnology, Biology and Medicine.* **10**:197–205. doi:10.1016/j.nano.2013.06.016.

Sparks, D. L. & Suarez, D. L. (1991). Rates of soil chemical processes. SSSA Spec Publ. No. **27**, Soil Sci. Soc.Am., Madison,Wl.

Sparks, D. L. (1989). Kinetics of soil chemical processes. Academic Press, San Diego, CA.

Sprynskyy, M., Lebedynets, M., Terzyk, A. P., Kowalczyk, P., & Namiesnik, J. (2005) Ammonium sorption from aqueous solutions by the natural zeolite transcarpathian clinoptilolite studied under dynamic conditions. *J. Colloid Interface Sci.* **284**: 408-415.

Sri Lankan Ministry of Health, Colombo: Ministry of Health, (1995). Annual health bulletin, Sri Lanka. 1997.

Srinivasan, R. (2010). Safer tomato production methods: A field guide for soil fertility and pest management. AVRDC-The world vegetable center, Shanhau, Taiwan. AVRDC Publication No.**10** - 740. 97p.

Stevenson, F. J. (1994). Humus chemistry: Genesis, composition, reactions. NewYork, John wiley and sons.

Stevenson, F. J. (1972). Organic matter reactions involving herbicides in soil. J. Environ. Qual. **1**:333-343.

Stone, J. K., Bacon, C.W., & White, J. F. (2006). An overview of endophytic microbes*:* endophytism defined In: Microbial Endophytes Macel Dekker, Incorporated, New York., pp. 3-29.

Stuart, B., (2004). Infrared Spectroscopy: Fundamentals and Applications © 2004 John Wiley & Sons, Ltd. ISBN: 0-470-85427-8 (HB); 0-470-85428-6 (PB).

Subramanian, K. S., Paulraj, C., & Natarajan, S. (2008). Nanotechnological approaches in Nutrient Management. In: *Nanotechnology Applications in Agriculture* 37-42.

Sutcliffe, A. J. (1973). Caves of the East African Rift Valley, Trans. Cave Res. Group of G.B., **15** (1), 41-65.

Tago, T., Aoki D., Iwakai, K. & Masuda, T. (2009). Top. Catal., **52**, 6-7, 865-871, 1022-5528.

Tago, T., Iwakai, K., Nishi, N., & Masuda, T. (2009). J. NanoSci. Nanotchnol., **9, 1**, 612-617, 1533-4880.

Tago, T., Nishi M., Kono, Y., & Masuda, T. (2004). Chem. Lett., **33, 8,** 1040- 1041, 0366 - 70221, 176-183, 1387-1811.

Tanabe, S., Senthilkumar, K., Kannan, K., & Subramanian, A. N. (1998). Accumulation features of polychlorinated biphenyls and organochlorine pesticides in resident and migratory birds from south India. Arch Environ Contam Toxicol; **34:** 387–397. [PubMed]

Tariq, M. Y., Afzal, S., & Hussain, I. (2006). Degradation and persistence of cotton pesticides in sandy loam soils from Punjab, Pakistan. Environ Res **100**:184–196.

Temkin, M. J., & Pyzhev, V. (1940). Kinetics of ammonia synthesis on promoted iron catalysts. Acta Physiochim. Urs. **12**, 217-222.

Thies, M. L., & Mc Bee, K. (1994). Cross-placental transfer of organochlorine pesticides in Mexican free-tailed bats from Oklahoma and New Mexico. Arch. Environ. Contam. Toxicol; **27**: 239–242. [PubMed]

Toraya, H. (1986). Whole-powder-pattern fitting without reference to a structural model: Application to X-ray powder diffraction data. J. Appl. Crystallogr. **19**: 440.

Tözüm-Çalgan, S.R.D., & Sivaci-Güner, S. (1993). Effects of 2, 4-D and methylparathion on growth and nitrogen fixation in cyanobacterium, Gloeocapsa. Intern J Environ Stud.; **23**: 307–311.

Treacy, M. J., & Higgins, J. B. (2001). Collections of Simulated XRD Powder Patterns for Zeolites, **4**th ed. Elsevier, Amsterdam, The Netherlands, **379** p.

Tremblay, L., Kohl, S. D., Rice, J. A., & Gagne, J. P. (2005a). "Effects of temperature, salinity, anddissolved humic substances on the sorption of polycyclic aromatic hydrocarbons to estuarine particles." Mar. Chem. **96**: 21-34.

Tremblay, L., Kohls, S. D., Rice, J. A., & Gagne, J. P. (2005b). "Effects of lipids on the sorption of hydrophobic organic compounds on geosorbents: a case study using phenanthrene" Chemosphere **58**: 1609-1620.

Trends in Analytical Chemistry (2004). Vol. **23**, No. 10–11.

Truong, C. D., Takehito, N., & Yasuo, N. (2007). Magnetic and Optical Properties of Rb and Cs Clusters Incorporated into Zeolite A. Conference Paper -Handai Nano 2006 (http://www.sssj.org/ejssnt/titleauthors-Vol5.html-1100Hrs, 10th January 2016).

Trunschke, A. (2015). Surface Area and Pore Size Determination. Modern Methods in Heterogeneous Catalysis Research 30 Oct.

Turner, R. C., & Clark, J. S. (1966). Lime potential in acid clay and soil suspensions. Trans. Comm. II & IV Int. Soc. Soil Science, pp. 208-215.

Uchida, S., Chiba, R., Tomiha, M., Masaki, N., & Shirai, M. (2002). Electrochem. **70**, 418.

Udluft, H. (1928). Zeolithe als Fossilisationsmaterial, Arrkiv Kemi Min. Geol., **9** (33), 15 pp., 2pls.

U.S. E.P.A., (1996). Office of Prevention, Pesticides, and Toxic Substances. Reregistration eligibility decision (RED): trifluralin. Washington, D.C., April.

U.S. E.P.A., (2001). Water protection practices bulletin. Washington, DC: Office of Water; Jul, Managing small-scale application of pesticides to prevent contamination of drinking water. EPA 816-F-01-031.

UVan Houten, F. B. (1960). Composition of Upper Triassic Lockatong argillite, west-central New Jersey. Jour. Geol. **68**, 666-669.

Van Houten, F. B. (1962). Cyclic sedimentation and the origin of analcime-rich Upper Triassic Lockatong Formation, west-central New Jersey and adjacent Pennsylvania. Am. Jour. Sci. **260**, 561-576.

Van Houten, F. B. (1965). Composition of Triassic Lockatong and associated formations of Newark Group, central New Jersey and adjacent Pennsylvania. Am. Jour. Sci. **263**, 825-863.

Van-Lanen, H. A. J., & Dijksma, R. (1999). Water flow and nitrate transport to a groundwater-fed stream in the Belgian–Dutch chalk region. Hydrol Process **13**: 295–307.

Van-Maanen, J. M. S., Welle, I. J., & Hageman, G. (1996). Nitrate contamination of drinking water: relationship with HPRT variant frequency in lymphocyte DNA and urinary excretion of Nnitrosamines. Environ Health Persp **104**: 522–28.

Vanev, Y., Cochemé, J. J., Ivanova, R., Grauby, O., Burlet, E., & Pravchanska, R. (2006). Zeolites and zeolitization of acid pyroclastic rocks from paroxysmal Paleogene volcanism, Eastern Rhodopes, Bulgaria. Neues. Jahrb. Miner. Abh., **182/3**, p. 265–283.

Vaughan, R. G., Hook, S. J., Calvin, W. M., & Taranik, J. V. (2005). Surface mineral mapping at Steamboat Springs, Nevada, USA, with multi-wavelength thermal infrared images. Remote

Sensing of Environment **99** (1–2), 140–158.

Vilaça, N., Amorim, R., Machado, A.F., Parpot, P., Pereira, M.F.R., & Sardo, M. (2013). Potentiation of 5-fluorouracil encapsulated in zeolites as drug delivery systems for in vitro models of colorectal carcinoma, Colloids and Surfaces B: Biointerfaces. 112: 237–244. doi:10.1016/j.colsurfb.2013.07.042.

Walker, G. P. L. (1960). Zeolite zones and dike distribution in relation to the structure of the basalts of eastern Iceland. *Jour. Geol*. **68**: 515-528.

Wang, S., Kimber, S. W. L., & Kennedy, I. R. (1997). The dissipation of lambda-cyhalothrin from cotton production systems. *J Environ Sci Health B* **32**: 335–352.

Wang, X., & Xing, B. (2007). "Roles of acetone-conditioning and lipid in sorption of organic contaminants." Environ. *Sci. Technol*. **41**: 5731-5737.

Ward, M. H., Mark, S. D., & Cantor, K. P. (1996). Drinking water nitrate and the risk of Non-Hodgkin's Lymphoma. *Epidemiology* 7: 465–71.

Warren, J. K. (2006). Evaporites: Sediments, Resources and Hydrocarbons. *Springer, p.* 1032.

Wauchope, R. D., Slinders, J. B. H. J., Kloskowski, R., Tanaka, K., & Unsworth, B. (2002). Pesticides soil sorption parameter: theory, measurement, uses, limitations and reliability. *Pest Manag. Sci*. **58**: 419-445.

Wener, J. N. (2000). Guide to tomato production in home gardens, available www.agrisupportonline.com Date accessed 10/11/2016

Weston, D. P., You, J. C., Lydy, M. J. (2004). Distribution and toxicity of sediment-associated pesticides in agriculture-dominated water bodies of California's Central Valley. *Environ Sci Technol* **38**: 2752–2759.

Weyer, P. J., Cerhan, J., & Kross, B. C. (2001). Municipal drinking water nitrate level and cancer risk in older women: the Iowa Women's Health Study. *Epidemiology* **12**: 327–38.

Whateley, M. K. G., Querol, X., Fernández-Turiel, J. L., & Tuncali, E. (1996). Zeolites in Teriary coal from the Cayirhan mine, Beypazari, Turkey. *Mineral. Deposita* **31:** 529-538.

Whitesides, G. M., & Grzybowski, B. (2002). *Science* **295:** 2418.

Whitesides, G. M., Mathias, J. P., & Seto, C. T. (1991). *Science* **254:** 1312.

W.H.O., (2001). The world health report. Geneva: World Health Organization; Mental health: new understanding, new hope.

Wieslaw, J. R., Petr, N., Russell, E. M., & Jiří, Č. (2014). Two-Dimensional Zeolites: Current Status and Perspectives. *Chem. Rev*.,**114 (9)**: 4807–4837.

Wilkinson, J. F. G. (1968). Analcimes from some potassic igneous rocks and aspects of analcimerich igneous assemblages. *Contr. Min. Petr*. **18**: 252-269.

Wilkinson, J. F. G., Nundle, N. S. W., & Petrol, J. (1965). Some feldspars, nephelines and analcimes from the Square Top Intrusion, **6**: 420-444.

Williams, E. J., Hutchinson, G. L., & Fehsenfeld, F. C. (1992). NO_2 and N_2O emissions from soil. *Global Biogeochemical Cycles* **6**: 351-388.

Wlodzimier, M., Magdalena, K., & Kataryzana, B. (2011). FT-IR of zeolites from different structural groups. *CHEMIK* **65** (7): 667-674.

Wolters, A., Kleinb, M., & Vereecken, H. (2004). An improved description of pesticide.

Xia, G., & Pignatello, J. J. (2001). "Detailed sorption isotherms of polar and a polar compound in a high-organic soil." *Environ. Sci.* **35**: 84-94.

Young, H., Thomas, M. H., Seong-Jae, K., & Carl, E. C. (2005). Adsorption and Clay –Catalized Degradation of Erythromycin A on Homoionic Clays. *J. Environ. Qual*., **33**: 257-264.

Zamzow, M. J., & Murphy, J. E. (1992). Sep. *Sci. Technol*. **27**: 1969.

Zaranyika, M. F., & Mandihza, N. T. (1999). Adsorption of Amitraz by a river sediment: Apparent thermodynamic properties. Journal of environmental science and health part B –pesticides food contaminants and agricultural wastes **33 (3)**: 235-251.

Zhou, J. L., Rowland, S., & Mantoura, R. F. C. (1995). Partition of synthetic pyrethroid insecticides between dissolved and particulate phases. *Water Res* **29**:1023–1031.

INTERNET REFRENCES

Barros, M. A. S. D., Zola, A. S., Arroyo, P. A., Sousa-Aguiar, E. F., & Tavares, C. R. G. (2003). Binary Ion Exchange of Metal Ions in Y and X Zeolites. *Brazilian Journal of Chemical Engineering* **20**: 413-421. http://dx.doi.org/10.1590/S0104-66322003000400008. Link valid on 5th March 2016.

Bartz, J. K., & Jones, R. L., (1983). Availability of Nitrogen to Sudangrass from Ammonium-Saturated Clinoptilolite. *Soil Science Society of America Journal* **47**: 259-262. http://dx.doi.org/10.2136/sssaj1983.03615995004700020017x Link valid on 16th June 2019.

Bernardi, A. C. C., Souza, G. B., Polidoro, J. C., Monte, M. B. M. & Paiva, P. R. P. (2011). Yield, Quality Components, and Nitrogen Levels of Silage Corn Fertilized with Urea and Zeolite. *Communication in Soil Science and Plant Analysis* **42**: 1266 - 1275. http://dx.doi.org/10.1080/00103624.2011.571980 .Link valid on 12th December 2017.

Bernardi, A. C. C., Oliveira, P. P. A., Monte, M. B. M. & Souza-Barros, F. (2013). Brazilian Sedimentary Zeolite Use in Agriculture. Microporous and Mesoporous Materials **167**: 16-21. http://dx.doi.org/10.1016/j.micromeso. Link valid on 16th July 2018

Pasture Fertilized with Urea and Zeolite Mixture. *Communication in Soil Science and Plant Analysis* , **46**:101 - 109. http://dx.doi.org/10.1080/00103624.2015.1019080 Link valid on 8th April 2016.

Clain, J., Brad, D. B., Rick, E., Don, H., & Kathrin, O. R**.** (2013). Factors Affecting Nitrogen Fertilizer Volatilization .EB0208 new February

http://landresources.montana.edu/soilfertility/ documents/PDF/pub/UvolfactEB0208.pdf Link valid on 2nd November 2016.

Dan, D. (2010). Spinach in the Garden. Home gardening. Utah State University. Cooperative Extention. http://ultimatepreparednesslibrary.com/wpcontent/ uploads/2012/04/spinach.pdf . Link valid on 16th June 2016.

European-Commission., (2001). Review report for the active substance lambda-cyhalothrin. 7572/VI/97 final. http://ec.europa.eu/food/plant/protection/evaluation/existactive/list1-24_en.pdf. Link valid on 18th December 2017.

Filippone, P. T. (2006). Tomato and Health, From: (Heinz Institute of Nutritional Sciences, 1998). http://homecooking.about.com/od/foodhealthinformation/a/tomatohealth.htm. Link valid on 11th November 2016.

Fergunson, G., & Pepper, I. (1987). Ammonium Retention in Soils Amended with Clinoptilolite. *Soil Science Society of America Journal* 51:231-234. http://dx.doi.org/10.2136/sssaj1987.03615995005100010047x\ Link valid on 16th June 2017.

John, N., & Micaela, C. (2007). Principles and Practices of Organic Spinach Seed Production in the Pacific Northwest. Organic Seed Alliance. https://www.seedalliance.org/uploads/pdf/ SpinachSeedManual.pdf Link valid on 16th June 2019.

Kenya Vision (2030), July-August 2007 http://www.vision2030.go.ke/ . Link valid on 26th October 2016.

Martin, E. T. (1997). Improving Fertilizer use Efficiency Controlled-Release and Stabilised Fertilizer in Agriculture. ISBN: 2-9506299-0-3. (http://www.fertilizer.org). Link valid on 4th February 2016.

Mumpton, F. A. (1999). La roca magica: Uses of Natural Previous Zeolites in Agriculture and Industry. Proceedings of the National Academy of Sciences of the United States of America, **96**: 3463-3470. http://dx.doi.org/10.1073/pnas.96.7.346. Link valid on 27th June 2017.

O'Neil, W., Raucher, R., & Wayzata, M. N. (1998). Groundwater Policy Education Project; Aug, Groundwater public policy leaflet series #**4**: The costs of groundwater contamination. http://www.dnr.state.wi.us/org/water/dwg/gw/costofgw.htm. Link valid on 27th July 2016.

Savonen, C. (1997). Soil microorganisms object of new OSU service. Good Fruit Grower. http://www.goodfruit.com/archive/1995/6other.html. Link valid on 16th June 2019.

Selva Preetha, P., & Balakrishnan, N. (2017). A Review of Nano Fertilizers and Their Use and Functions in Soil. *Int.J.Curr.Microbiol.App.Sci.* 6(12): 3117-3133. doi: https://doi.org/10.20546/ijcmas.2017.612.364. Link valid on 1st July 2019.

Spurlock, F. (2006). Synthetic pyrethroids and California surface water: use patterns, properties, and unique aspects. http://wwwcdprcagov/docs/sw/swposters/spurlock_acs06pdf. Link valid on 16th June 2017.

Spurlock, F. (2006). Synthetic pyrethroids and California surface water: use patterns, properties, and unique aspects. http://wwwcdprcagov/docs/sw/swposters/spurlock_acs06pdf. Link valid on 25thth June 2018

Steven, T. K., Michael, C., Marita, C., Steve, F., Michelle, L., Erick, N., Richard, F. S., & Etaferahu, T., (2011). Spinach production in Califonia. Universityb of California Agricultural and Natural resources. Publication **7212**. http://anrcatalog.ucdavis.edu. Link valid on 29th September 2019

Syngenta, (2007). Karate. http://wwwsyngentacom/en/products_services/karate_pageaspx. Link valid on 16th June 2019

Teruoki, T., & Takao, M. (2010). Zeolite Nanocrystals- Synthesis and Applications, Nanocrystals, Yoshitake Masuda (Ed.), ISBN: 978-953-307-126-8, InTech, Available from: http://www.intechopen.com/books/nanocrystals/zeolite-nanocrystals-synthesisand-applications. Link valid on 22nd June 2019.

Townsend, A. R., Howarth, R. W., Bazzaz, F. A., Booth, M. S., Cleveland, C. C., Collinge, S. K., Dobson, A. P., Epstein, P. R.; Holland, Elisabeth, A.; Keeney D. R.; Mallin M. A.; Rogers C. A.; Wayne P., & Wolfe A. H., (2003). "Human Health Effects of a Changing Global Nitrogen Cycle" Ecosystem and Conservation Sciences Faculty Publications. Paper **9**. http://scholarworks.umt.edu/decs_pubs/9. Link valid on 6th June 2019.

USDA (2007). USDA-ARS Pesticide Properties Database: http://www.ars.usda.gov/Services/docs.htm?docid=14199. Link valid on 1st June 2018.

U.S. E.P.A., (2000). Reregistration eligibility science chapter for chlorpyrifos. Fate and environmental risk assessment chapter (Revised June).

http://www.epa.gov/pesticides/op/chlorpyrifos/efedrra1.pdf. Link valid on 22nd June 2018.

.S. E.P.A. (2007). ECOTOX database. http://cfpubepagov/ecotox/quick_queryhtm. Link valid on 3rd June 2019.

U.S. Geological Survey., (1999). Reston, VA: USGS; The quality of our nation'swaters – nutrients and pesticides. http://water.usgs.gov/pubs/circ/circ1225/ Circular **1225.** Link valid on 6th June 2018.

USGS. (2013) US Geological Survey Minerals Yearbook. Volume I, Metals and Minerals, Zeolites Statistics and Information. http://minerals.usgs.gov/minerals/pubs/commodity/zeolites/myb1-2013-zeoli.pdf Link valid on 10th July 2017.

Waskom, R. (1994). Best management practices for private well protection. Colorado State Univ. Cooperative Extension (August). http://hermes.ecn.purdue.edu:8001/cgi/convertwq?7488. Link valid on 25th January 2016.

APPENDICES

A. SAMPLING SITES

Figure A 1: Section of Lake Magadi showing surface trona minerals

Figure A 2: Terrain and vegetation cover of Lake Magadi basin

Figure A 3: Section of seasonal rivers (River Ol Arabel) draining to Lake Baringo

Figure A 4: Erosion gulley developed by seasonal river flash floods

Figure A 5: Quarry excavation site at Ebul bul

Figure A 6: Kitum caves: (a) The “mouth” of caves and (b) Waterfalls

B. FIELD STATIONS

Figure B 2: Field Demonstration 1

Figure B 1: Field Demonstration 4

Figure B 4: Field Demonstration 2

Figure B 3: Field Demonstration 5

Figure B 6: Field Demonstration 3

Figure B 5: Field Demonstration 6

Figure B 7: Field Demonstration 7

Figure B 8: Field Demonstration 8

C. ADDITIONAL DATA AND FIGURES

Table T4. 1: X-ray diffraction parameter data for ZT-GA-01

2θ	*h*	*k*	*l*	*d*	*M*	I_{rel}
7.18	2	0	0	12.305	6	100.0
10.17	2	2	0	8.701	12	51.3
12.46	2	2	2	7.104	8	31.8
16.11	4	2	0	5.503	24	20.3
20.41	4	4	0	4.350	12	3.6
21.67	6	0	0	4.102	6	10.6
22.85	6	2	0	3.891	24	1.2
23.99	6	2	2	3.710	24	44.3
26.11	6	4	0	3.413	24	10.1
27.11	6	4	2	3.289	48	41.0
30.83	8	2	2	2.900	24	5.4
31.70	6	6	2	2.823	24	0.2
32.54	8	4	0	2.751	24	9.3
33.37	8	4	2	2.685	48	3.0
34.77	9	3	1	2.580	48	0.1
35.75	8	4	4	2.512	24	4.7
36.51	8	6	0	2.461	24	0.4
38.00	10	2	2	2.368	24	1.6
40.14	10	4	2	2.247	48	2.2
41.51	8	8	0	2.175	12	4.3
42.19	10	4	4	2.142	24	3.4
42.85	8	6	6	2.110	24	2.3
43.51	10	6	2	2.080	48	1.8
47.30	10	8	0	1.922	24	2.3
47.91	10	8	2	1.899	48	5.1
49.70	10	8	4	1.834	48	1.8

Table T4. 2: Variation of absorbance with concentration of urea

Concentration (w/v)	Concentration (mol/dm^3)	Absorbance
1 (1:200)	0.08332	1.26881
2 (1:100)	0.16664	2.92937
3 (1:80)	0.20830	3.66448
4 (1:60)	0.27773	4.72319
5 (1:40)	0.41660	5.12990
6 (1:20)	0.83320	5.31555
7 (1:10)	1.66640	5.59000
8 (1:2)	8.33200	7.24100

Table T4. 3: Absorbance of Urea analysis with varying concentrations

C	a_1	a_2	a_3
1:100	2.868	2.700	2.776
1:80	2.892	2.951	2.756
1:60	2.914	2.818	2.839
1:40	3.096	2.977	3.012
1:20	3.451	3.297	3.288
1:10	3.858	3.732	3.748
1:8	4.603	4.609	4.704
1:6	4.996	4.799	4.721
1:4	5.343	4.947	5.003
1:2	5.495	5.145	5.537

Where:

C - is the sample concentration of urea in water w/v

a_1 -is the 1st absorbance reading

a_2 -is the 2nd absorbance reading

a_3 -is the 3rd absorbance reading

Table T4. 4: Corresponding concentrations of Urea

C (w/v)	C (mol/dm^3)	[Ce_1]	[Ce_2]	[Ce_3]	[Ce_{av}]	SD	q_e	$R_{\%}$
1:100	0.16664	0.16833	0.15891	0.16317	0.16347	0.004718	0.003166	1.90
1:80	0.20830	0.16968	0.17299	0.16205	0.16824	0.005609	0.040059	19.2
1:60	0.27773	0.17091	0.16553	0.16671	0.16772	0.002831	0.110013	39.6
1:40	0.41660	0.18112	0.17445	0.17641	0.17733	0.00343	0.239273	57.4
1:20	0.83320	0.20103	0.19189	0.19189	0.19494	0.005278	0.638263	76.6
1:10	1.66640	0.32931	0.33522	0.34422	0.33625	0.003847	1.330152	79.9
1:8	2.08300	0.65022	0.64122	0.64022	0.64388	0.12447	1.442783	80.3
1:6	2.77730	1.07206	0.97206	0.99205	1.01205	0.311349	1.765247	80.3
1:4	4.16600	1.56794	1.64698	1.66695	1.62729	0.470786	2.538711	80.3
1:2	8.33200	3.72144	2.95255	3.81371	3.49590	0.472812	4.836101	80.3

Where:

C - is the sample concentration in w/v

[C_{e1}] - is the 1st scan equilibrium concentration in w/v of the fertilizer after shaking with the samples.

[C_{e2}] - is the 2nd scan equilibrium concentration in w/v of the fertilizer after shaking with the samples.

[C_{e3}] - is the 3rd scan equilibrium concentration in w/v of the fertilizer after shaking with the samples.

[C_{av}] - is the average scan equilibrium concentration w/v of the fertilizer after shaking with the samples.

SD - is the standard deviations of scans for equilibrium concentrations of the fertilizer after shaking with the samples.

q_e -is the amount of equilibrium adsorbed fertilizer in mg/L

$R_{\%}$ - is the percentage fertilizer adsorbed

Table T4. 5: Variation of shaking time for Urea analysis (absorbance readings)

T	a_1	a_2	a_3
0	2.185	2.099	2.085
15	2.045	2.114	2.106
30	1.861	1.892	1.897
45	1.854	1.859	1.897
60	1.852	1.855	1.899
75	1.848	1.806	1.804
90	1.844	1.855	1.874
100	1.833	1.838	1.840
120	1.820	1.906	1.900
140	1.814	1.865	1.877
160	1.807	1.867	1.881

Where:

T - is the shaking time in minutes

a_1 -is the 1st absorbance reading

a_2 -is the 2nd absorbance reading

a_3 -is the 3rd absorbance reading

Table T4. 6: Corresponding concentrations for varying shaking time of Urea analysis

T	$[Ce_1]$	$[Ce_2]$	$[Ce_3]$	$[Ce_{av}]$	SD	qe	R%
0	0.130028	0.1252047	0.1244195	0.126551	0.003037	0.0422205	25.3
15	0.12217610	0.12604598	0.1255973	0.124606	0.002117	0.042034	25.2
30	0.1118564	0.11359506	0.11387549	0.113109	0.001094	0.053531	32.1
45	0.11146382	0.11174425	0.1138755	0.112361	0.001319	0.054279	32.6
60	0.111351654	0.1115199	0.113987661	0.112286	0.001476	0.054354	32.6
75	0.11112731	0.10877173	0.10865956	0.10952	0.001394	0.057120	34.3
90	0.11090297	0.1115199	0.1125855	0.111669	0.000851	0.055971	33.9
100	0.110286034	0.110566461	0.1106786	0.11051	0.000202	0.05613	33.7
120	0.109556926	0.11438025	0.11404374	0.11266	0.002693	0.05398	32.4
140	0.10922041	0.1120807627	0.11275378	0.111352	0.001876	0.055288	33.2
160	0.10882781	0.112192933	0.1129781267	0.111333	0.002205	0.055307	33.2

Where:

T - is the shaking time in minutes.

$[C_{e1}]$ - is the 1st scan equilibrium concentration in w/v of the fertilizer after shaking with the samples.

$[C_{e2}]$ - is the 2nd scan equilibrium concentration in w/v of the fertilizer after shaking with the samples.

$[C_{e3}]$ - is the 3rd scan equilibrium concentration in w/v of the fertilizer after shaking with the samples.

$[C_{av}]$ - is the average scan equilibrium concentration w/v of the fertilizer after shaking with the samples.

SD - is the standard deviations of scans for equilibrium concentrations of the fertilizer after shaking with the samples.

qe -is the amount of equilibrium adsorbed fertilizer in mg/L

R% - is the percentage fertilizer adsorbed

Table T4. 7: Absorbance readings for quantitative urea adsorbed at varying times

T	a_1	a_2	a_3
3	3.214	3.196	3.197
10	3.166	3.150	3.157
20	3.118	3.100	3.131
24	3.080	3.084	3.103
40	3.180	3.174	3.179
48	3.231	3.246	3.220
96	3.317	3.364	3.307

Where:

T - is the shaking time in hours.

a_1 -is the 1st absorbance reading

a_2 -is the 2nd absorbance reading

a_3 -is the 3rd absorbance reading

Table T4. 8: Corresponding concentration readings for quantitative urea adsorbed

T	$[Ce_1]$	$[Ce_2]$	$[Ce_3]$	$[Ce_{av}]$	SD	qe	R%
3	0.18774548	0.18675521	0.18678381	0.187095	0.000564	0.090635	32.6
10	0.1850447	0.1841349	0.1845247	0.184568	0.000456	0.093162	33.5
20	0.1823473	0.18135769	0.18305701	0.182254	0.000853	0.095476	34.3
24	0.1802249	0.1804247	0.1815257	0.180725	0.000701	0.097005	34.9
40	0.1858328	0.18549635	0.18577678	0.185702	0.00018	0.091953	33.1
48	0.1886932	0.18953449	0.1880762	0.188768	0.000732	0.088962	32.0
96	0.19351654	0.19615255	0.19295569	0.194208	0.001707	0.083522	30.1

Where:

T - is the shaking time in hours.

$[C_{e1}]$ - is the 1st scan equilibrium concentration in w/v of the fertilizer after shaking with

the samples.

[C_{e2}] - is the 2nd scan equilibrium concentration in w/v of the fertilizer after shaking with the samples.

[C_{e3}] - is the 3rd scan equilibrium concentration in w/v of the fertilizer after shaking with the samples.

qe -is the amount of equilibrium adsorbed fertilizer in mg/L

R% - is the percentage fertilizer adsorbed

Table T4. 9: Absorbance readings for amount of loaded urea

T	Trial 1	Trial 2	Trial 3
24	2.837755	2.48277807	2.6605075

Table T4. 10: Corresponding concentrations for amount of loaded urea

T	[Ce_1]	[Ce_2]	[Ce_3]	[Ce_{av}]	SD	qe	R%
24	0.166638	0.146729	0.156697	0.156688	0.009955	0.121042	43.5

Where:

T - is the shaking time in hours.

[C_{e1}] - is the 1st scan equilibrium concentration in w/v of the fertilizer after shaking with the samples.

[C_{e2}] - is the 2nd scan equilibrium concentration in w/v of the fertilizer after shaking with the samples.

[C_{e3}] - is the 3rd scan equilibrium concentration in w/v of the fertilizer after shaking with the samples.

qe -is the amount of equilibrium adsorbed fertilizer in mg/L

R% - is the percentage fertilizer adsorbed

Table T4. 11: Corresponding concentrations for released fertilizer in water

T	$[Ce_1]$	$[Ce_2]$	$[Ce_3]$	$[Ce_{av}]$	SD	%D
1	0.0403876	0.04024446	0.0400369068	0.040222989	0.00017633	33.2
2	0.021083193	0.02057436	0.02084432	0.020833958	0.000254575	17.2
3	0.0104668536	0.01046461	0.010607319	0.010512928	8.17531E-05	8.7
4	0.005044475	0.0074669	0.00604458	0.006185318	0.00121733	5.1
5	0.004108721	0.0051131127	0.005012806	0.00474488	0.000553208	3.9
6	0.002041298	0.00340157	0.003057655	0.002833508	0.000707295	2.3
7	0.002125473	0.0031351093	0.002207178	0.002489253	0.000560818	2.1
8	0.0020151155	0.0021254514	0.002201547	0.002114038	9.37383E-05	1.7
9	0.001617498	0.0021095681	0.001589455	0.001772174	0.000292528	1.5
10	0.0013258553	0.001269770	0.0012529444	0.001282857	3.81765E-05	1.1
11	0.001045429	0.00107908	0.0010173864	0.001047298	3.08893E-05	0.86
12	0.001034212	0.00103982	0.0010566461	0.001043559	1.16752E-05	0.86
13	0.0010229949	0.000909343	0.0010117779	0.000981372	6.26305E-05	0.81
14	0.0009220415	0.00091643297	0.0009444756	0.00092765	1.48388E-05	0.77
15	0.0009108244	0.00089399887	0.00087156477	0.000892129	1.96965E-05	0.74
16	0.0008883903	0.0000507692	0.0008659563	0.000601705	0.000477256	0.50
17	0.0009108244	0.0008883903	0.0008659562	0.00088839	2.24341E-05	0.72
18	0.0008827818	0.0008883903	0.00087156477	0.000880912	8.56714E-06	0.73

Where:

T - is the time in days

$[C_{e1}]$ - is the 1st scan equilibrium concentration in w/v of the fertilizer after shaking with the samples.

$[C_{e2}]$ - is the 2nd scan equilibrium concentration in w/v of the fertilizer after shaking with

the samples.

$[C_{e3}]$ - is the 3rd scan equilibrium concentration in w/v of the fertilizer after shaking with the samples.

$[C_{av}]$ - is the average scan equilibrium concentration w/v of the fertilizer after shaking with the samples.

SD - is the standard deviations of scans for equilibrium concentrations of the fertilizer after shaking with the samples.

Table T4. 12: Corresponding concentration readings for released fertilizer in soil

T	$[C_{e1}]$	$[Ce_2]$	$[Ce_3]$	$[Ce_{av}]$	SD	%D
1	0.03273144	0.03624192	0.031031171	0.033335	0.002657263	27.5
2	0.019033001	0.015637155	0.017188721	0.017286	0.001700024	14.3
3	0.009178913	0.008979914	0.009067519	0.009075	9.97362E-05	7.5
4	0.007147513	0.007325872	0.007213210	0.007229	9.02042E-05	6.0
5	0.005911651	0.006921441	0.005713102	0.006182	0.000647969	5.1
6	0.004001813	0.004881317	0.004151301	0.004345	0.000470602	3.6
7	0.003126115	0.003218100	0.003201101	0.003182	4.8944E-05	2.6
8	0.001906172	0.001684131	0.001705817	0.001765	0.000122416	1.5
9	0.001401621	0.001321301	0.001330311	0.001351	4.4003E-05	1.1
10	0.001114115	0.001210100	0.001030121	0.001118	9.0056E-05	0.9
11	0.001045429	0.001051116	0.001021145	0.001039	1.59181E-05	0.9
12	0.000937446	0.000951213	0.000940117	0.000943	7.30052E-06	0.7
13	0.000921789	0.000912214	0.000881016	0.000905	2.13207E-05	0.7
14	0.000718634	0.000700143	0.000705116	0.000708	9.56891E-06	0.5
15	0.000588113	0.000491305	0.000499010	0.000526	5.3806E-05	0.4
16	0.0003115385	0.000321741	0.0003012111	0.000311	1.0265E-05	0.3
17	0.000264774	0.000254417	0.0002215501	0.000247	2.25677E-05	0.2
18	0.000277349	0.00019664	0.0002110991	0.000228	4.3035E-05	0.2

Where:

T - is the time in days

[C_{e1}] - is the 1st scan equilibrium concentration in w/v of the fertilizer after shaking with the samples.

[C_{e2}] - is the 2nd scan equilibrium concentration in w/v of the fertilizer after shaking with the samples.

[C_{e3}] - is the 3rd scan equilibrium concentration in w/v of the fertilizer after shaking with the samples.

[C_{eav}] - is the average scan equilibrium concentration w/v of the fertilizer after shaking with the samples.

SD - is the standard deviations of scans for equilibrium concentrations of the fertilizer after shaking with the samples.

Table T4. 13: Concentrations for released fertilizer by sample KIK-GA-01 in water

T	$[Ce_1]$	$[Ce_2]$	$[Ce_3]$	$[Ce_{av}]$	SD	%D
1	0.02927327	0.02383139	0.02611911	0.026408	0.002732412	21.8
2	0.01511720	0.01601310	0.01505611	0.015395	0.000535755	12.7
3	0.00803613	0.00783312	0.00791132	0.007927	0.000102393	6.5
4	0.00614218	0.00512035	0.00623113	0.005831	0.000617236	4.8
5	0.004200231	0.00441834	0.00419137	0.00427	0.00012856	3.5
6	0.003302001	0.00351832	0.00326613	0.003362	0.000136431	2.8
7	0.002413013	0.00234211	0.00251141	0.002422	8.50213E-05	2.0
8	0.001313170	0.00121401	0.00121731	0.001248	5.63216E-05	1.0
9	0.001201211	0.001104281	0.00131109	0.001206	0.000103472	1.0
10	0.000912071	0.00087518	0.000901076	0.000896	1.89404E-05	0.7
11	0.000648190	0.000682150	0.000625132	0.000652	2.86822E-05	0.5
12	0.000519231	0.000499451	0.000504243	0.000508	1.03187E-05	0.4
13	0.000351172	0.000341323	0.000330145	0.000341	1.05205E-05	0.3
14	0.000210741	0.000221051	0.000200331	0.000211	1.036E-05	0.2
15	0.000207281	0.0002032001	0.000203252	0.000205	2.34127E-06	0.2
16	0.000163171	0.000152014	0.000155124	0.000157	5.75768E-06	0.1
17	0.00014316	0.00011021	0.00013413	0.000129	1.70265E-05	0.1
18	0.00014167	0.000140011	0.000142415	0.000141	1.23062E-06	0.1

Where:

T - is the time in days

$[C_{e1}]$ - is the 1st scan equilibrium concentration in w/v of the fertilizer after shaking with the samples.

$[C_{e2}]$ - is the 2nd scan equilibrium concentration in w/v of the fertilizer after shaking with the samples.

$[C_{e3}]$ - is the 3rd scan equilibrium concentration in w/v of the fertilizer after shaking with the samples.

$[C_{av}]$ - is the average scan equilibrium concentration w/v of the fertilizer after shaking with the samples.

SD - is the standard deviations of scans for equilibrium concentrations of the fertilizer after shaking with the samples.

Table T4. 14: Efficiency of fertilizer loaded zeolitic materials

T	C	BT	BS	UST	USS	UKT	UKS
5	[C_{e1}]	0.000110	0.000107	0.033294	0.034153	0.040090	0.041085
	[C_{e2}]	0.000111	0.000109	0.033299	0.034181	0.040101	0.041176
	[C_{e3}]	0.000109	0.000106	0.033309	0.034907	0.040110	0.049257
	[C_{eav}]	0.000110	0.000107	0.033301	0.034414	0.040100	0.043839
	SD	0.000001	0.000002	0.000008	0.000427	0.000010	0.004692
20	[C_{e1}]	0.000105	0.000101	0.009822	0.008920	0.009180	0.009650
	[C_{e2}]	0.000100	0.000100	0.009826	0.008922	0.009150	0.009640
	[C_{e3}]	0.000107	0.000099	0.009825	0.008921	0.009190	0.009670
	[C_{eav}]	0.000104	0.000100	0.009824	0.008921	0.009173	0.009653
	SD	0.000004	0.000002	0.000004	0.000003	0.000002	0.000015
30	[C_{e1}]	0.000100	0.000095	0.001915	0.001906	0.000103	0.000105
	[C_{e2}]	0.000101	0.000093	0.001917	0.001909	0.000104	0.000104
	[C_{e3}]	0.000100	0.000096	0.001914	0.001904	0.000105	0.000105
	[C_{eav}]	0.000100	0.000095	0.001916	0.001905	0.000104	0.000105
	SD	0.0000005	0.0000015	0.000003	0.000002	0.000001	0.0000005
45	[C_{e1}]	0.000093	0.000096	0.000706	0.000718	0.000067	0.000060
	[C_{e2}]	0.000095	0.000095	0.000705	0.000717	0.000068	0.000061
	[C_{e3}]	0.000090	0.000097	0.000707	0.000719	0.000066	0.000063
	[C_{eav}]	0.000093	0.000096	0.000706	0.000718	0.000067	0.000061
	SD	0.000003	0.000001	0.000001	0.000001	0.000001	0.000001
60	[C_{e1}]	0.000090	0.000095	0.000102	0.000200	0.000045	0.000040
	[C_{e2}]	0.000091	0.000093	0.000101	0.000205	0.000044	0.000041
	[C_{e3}]	0.000093	0.000094	0.000102	0.000201	0.000047	0.000042
	[C_{eav}]	0.000091	0.000094	0.000102	0.000202	0.000045	0.000041
	SD	0.000002	0.000001	0.0000005	0.000003	0.000002	0.000001

Where:

BT - Samples taken from a setup of tomatoes grown on blank soil

BS - Samples taken from a setup of spinach grown on blank soil

UST - Samples taken from a setup of tomatoes grown using urea loaded sample EB-GA-02

USS - Samples taken from a setup of spinach grown using urea loaded sample EB-GA-02

UKT - Samples taken from a setup of tomatoes grown using commercial urea fertilizer

UKS - Samples taken from a setup of spinach grown using commercial urea fertilizer

T - time in days

[C]- is the sample concentration in ppm

$[C_{e1}]$ - is the first scan equilibrium concentration in ppm

$[C_{e2}]$ - is the second scan equilibrium concentration in ppm

$[C_{e3}]$ - is the third scan equilibrium concentration in ppm

$[C_{av}]$ - is the average scan equilibrium concentration in ppm

SD - is the standard deviations of scans for equilibrium concentrations

Table T4. 15: Concentration versus absorbance for Lambda cyhalothrin standards

Concentration (ppm)	Absorbance
0.000	0.0000
2.000	1.3053
4.000	2.6265
6.000	3.9095
8.000	4.8965
10.00	5.7654
20.00	5.9739
40.00	6.0965
60.00	7.7986
80.00	8.6365
100.0	9.9652

Table T4. 16: Pesticide on EB-GA-02 for varying concentrations and shaking time

T_s	$[C_{in}]$	a_1	a_2	a_3
15	10.000	1.6430	1.6420	1.6420
	20.000	3.0520	3.0550	3.0570
	30.000	4.1020	3.874	4.0050
	40.000	4.2260	4.0670	4.3900
	50.000	4.1490	4.1630	4.1750
30	10.000	1.4790	1.4810	1.4800
	20.000	3.1170	3.1210	3.1110
	30.000	3.8640	3.3910	3.8220
	40.000	4.1830	4.2130	4.0020
	50.000	4.5120	4.3060	4.2230
45	10.000	1.5120	1.5130	1.5130
	20.000	3.0770	3.0650	3.0890
	30.000	3.8270	3.9220	3.8800
	40.000	4.0590	4.0330	4.0120
	50.000	3.9860	3.9150	3.9900
60	10.000	1.4860	1.4850	1.4840
	20.000	3.0780	3.0630	3.0660
	30.000	3.9020	3.8510	3.9890
	40.000	3.9860	4.0790	4.0590
	50.000	4.0550	3.9650	3.9580

Where:

T_s - is the shaking time in minutes.

$[C_{in}]$ - is the initial concentration in ppm of the pesticide before shaking with the samples.

a_1 -is the 1st absorbance reading

a_2 -is the 2nd absorbance reading

a_3 -is the 3rd absorbance reading

Table T4. 17: Pesticide on EB-GA-02 for varying concentrations and shaking time

T_s	$[C_{in}]$	$[Ce_1]$	$[Ce_2]$	$[Ce_3]$	$[Ce_{av}]$	SD	q_e	$R_{\%}$
15	10.000	2.5328	2.5321	2.5311	2.5320	0.0009	7.4280	74.680
	20.000	4.9450	4.9502	4.9536	4.9496	0.0043	15.050	75.250
	30.000	15.928	12.948	14.660	14.512	1.4957	15.488	51.620
	40.000	17.549	15.471	19.693	17.571	2.1112	22.429	56.070
	50.000	16.543	16.726	16.882	16.712	0.1702	33.288	66.570
30	10.000	2.2520	2.2554	2.2537	2.2537	0.0017	7.7463	77.460
	20.000	5.0563	5.0632	5.0460	5.0552	0.0087	14.945	74.720
	30.000	12.817	6.3398	12.268	10.475	3.5916	19.525	65.080
	40.000	16.987	17.379	14.621	16.329	1.4922	23.671	59.180
	50.000	21.987	18.595	17.509	19.364	2.3356	30.636	61.270
45	10.000	2.3085	2.3102	2.3102	2.3096	0.0009	7.6904	76.900
	20.000	4.9878	4.9673	5.0083	4.9878	0.0205	15.012	75.060
	30.000	12.333	13.575	13.026	12.978	0.6223	17.022	56.740
	40.000	15.366	15.026	14.752	15.048	0.3078	24.952	62.380
	50.000	14.412	13.484	14.464	14.119	0.5515	35.881	71.760
60	10.000	2.2640	2.2623	2.2606	2.2623	0.0017	7.7377	77.370
	20.000	4.9896	4.9639	4.9690	4.9742	0.0136	15.026	75.130
	30.000	13.314	12.647	14.451	13.471	0.9121	16.529	55.100
	40.000	14.412	15.627	15.366	15.135	0.6397	24.865	62.160
	50.000	15.314	14.137	14.046	14.499	0.7071	35.501	71.000

Where:

T_s - is the shaking time in minutes.

$[C_{in}]$ - is the initial concentration in ppm of the pesticide before shaking with the samples.

$[C_{e1}]$ - is the 1st scan equilibrium concentration in mg/L of the pesticide after shaking with the samples.

$[C_{e2}]$ - is the 2nd scan equilibrium concentration in mg/L of the pesticide after shaking with

the samples.

[C_{e3}] - is the 3rd scan equilibrium concentration in mg/L of the pesticide after shaking with the samples.

[C_{av}] - is the average scan equilibrium concentration in mg/L of the pesticide after shaking with the samples.

SD - is the standard deviations of scans for equilibrium concentrations of the pesticide after shaking with the samples.

q_e -is the amount of equilibrium adsorbed pesticide in mg/L

$R_{\%}$ - is the percentage pesticide removed

Table T4. 18: Pesticide on the varying masses of samples EB-GA-02

m	a_1	a_2	a_3
0.1	4.1490	4.0790	4.4660
0.2	4.2160	4.2240	4.1000
0.5	4.3820	4.1620	4.0620
1.0	4.1330	4.3000	4.0790
1.5	4.0540	4.1170	4.2070
2.0	3.9830	3.9720	4.0020

Where:

m – is the mass in grams of the samples used.

a_1 -is the 1st absorbance reading

a_2 -is the 2nd absorbance reading

a_3 -is the 3rd absorbance reading

Table T4. 19: Pesticide on the varying masses of samples EB-GA-02 (concentrations)

m	$[Ce_1]$	$[Ce_2]$	$[Ce_3]$	$[Ce_{av}]$	SD	q_e	$R_{\%}$
0.1	16.5425	15.6270	20.6863	17.6186	2.6959	32.381	64.760
0.2	17.4183	17.5229	15.9000	16.9471	0.9083	33.053	65.110
0.5	19.5882	16.7124	15.4052	17.2353	2.1399	32.765	65.530
1.0	16.3333	18.5163	15.6270	16.8255	1.5062	33.175	66.350
1.5	15.3007	16.1242	17.3007	16.2419	1.0052	33.758	67.520
2.0	14.3725	14.2287	14.6209	14.4074	0.1984	35.593	71.120

Where:

m – is the mass in grams of the samples used.

$[C_{e1}]$ - is the first scan equilibrium concentration in ppm of the pesticide after shaking with the samples.

$[C_{e2}]$ - is the second scan equilibrium concentration in ppm of the pesticide after shaking with the samples.

$[C_{e3}]$ - is the third scan equilibrium concentration in ppm of the pesticide after shaking with the samples.

$[C_{av}]$ - is the average scan equilibrium concentration in ppm of the pesticide after shaking with the samples.

SD - is the standard deviations of scans for equilibrium concentrations of the pesticide

after shaking with the samples.

q_e -is the amount of equilibrium adsorbed pesticide in mg/L

$R_{\%}$ - is the percentage pesticide removed

Table T4. 20: Pesticide loading on samples EB-GA-02

Time (Hours)	a_1	a_2	a_3
24	4.474	4.306	4.509

Where:

a_1 -is the 1st absorbance reading

a_2 -is the 2nd absorbance reading

a_3 -is the 3rd absorbance reading

Table T4. 21: Concentrations for pesticide loading on samples EB-GA-02

Time (Hours)	$[Ce_1]$	$[Ce_2]$	$[Ce_3]$	$[Ce_{av}]$	SD	q_e	$R_{\%}$
24	20.8340	20.056	21.003	20.631	0.505083	79.369	79.4

Where:

$[C_{e1}]$ - is the first scan equilibrium concentration in ppm of the pesticide after shaking with the samples.

$[C_{e2}]$ - is the second scan equilibrium concentration in ppm of the pesticide after shaking with the samples.

$[C_{e3}]$ - is the third scan equilibrium concentration in ppm of the pesticide after shaking with the samples.

$[C_{av}]$ - is the average scan equilibrium concentration in ppm of the pesticide after shaking with the samples.

SD - is the standard deviations of scans for equilibrium concentrations of the pesticide after shaking with the samples.

q_e -is the amount of equilibrium adsorbed pesticide in mg/L

$R_{\%}$ - is the percentage pesticide removed from the solution

Table T4. 22: Pesticide loaded sample EB-GA-02 release in water

Day	a_1	a_2	a_3
1	4.0980	4.1100	3.9930
2	1.4670	1.5640	1.4800
3	0.0820	0.0820	0.0820
4	0.0580	0.0590	0.0590
5	0.0390	0.0390	0.0390
6	0.0430	0.0440	0.0440
7	0.0360	0.0390	0.0400
8	0.0290	0.0330	0.0350
9	0.0300	0.0370	0.0290
10	0.0250	0.0200	0.0230
11	0.0130	0.0190	0.0160
12	0.0100	0.0110	0.0090
13	0.0070	0.0090	0.0080
14	0.0060	0.0080	0.0090
15	0.0070	0.0080	0.0070
16	0.0060	0.0050	0.0040
17	0.0040	0.0040	0.0050
18	0.0030	0.0020	0.0050

Where:

a_1 -is the 1st absorbance reading

a_2 -is the 2nd absorbance reading

a_3 -is the 3rd absorbance reading

a_{av} -is the average of absorbance reading

a_{SD} -is the standard deviation of the absorbance readings

Table T4. 23: Concentrations of pesticide loaded sample EB-GA-02 release in water

Day	$[Ce_1]$	$[Ce_2]$	$[Ce_3]$	$[Ce_{av}]$	SD
1	19.085	19.141	18.595	18.940	0.3004
2	6.8082	7.1022	6.4955	6.8019	0.3034
3	0.8586	0.3738	0.3313	0.5212	0.2929
4	0.2331	0.2286	0.2473	0.2363	0.0098
5	0.1447	0.1167	0.1307	0.1307	0.0140
6	0.1633	0.1679	0.1726	0.1679	0.0047
7	0.1307	0.1446	0.1493	0.1415	0.0097
8	0.0979	0.1166	0.1259	0.1135	0.0143
9	0.1026	0.1353	0.0979	0.1119	0.0204
10	0.0793	0.0559	0.0699	0.0684	0.0118
11	0.0233	0.0513	0.0373	0.0373	0.0140
12	0.0093	0.0139	0.0046	0.0093	0.0046
13	0.0046	0.0046	0.0046	0.0046	0.0000
14	0.0044	0.0046	0.0047	0.0046	0.0002
15	0.0045	0.0046	0.0045	0.0045	0.0002
16	0.0043	0.0042	0.0040	0.0042	0.0002
17	0.0004	0.0040	0.0043	0.0029	0.0021
18	0.0003	0.0035	0.0043	0.0027	0.0021

Where:

$[C_{e1}]$ - is the first scan equilibrium concentration in ppm of the pesticide after shaking with the samples.

$[C_{e2}]$ - is the second scan equilibrium concentration in ppm of the pesticide after shaking with the samples.

$[C_{e3}]$ - is the third scan equilibrium concentration in ppm of the pesticide after shaking with the samples.

[C_{av}] - is the average scan equilibrium concentration in ppm of the pesticide after shaking with the samples.

SD - is the standard deviations of scans for equilibrium concentrations of the pesticide after shaking with the samples.

Table T4. 24: Pesticide loaded sample EB-GA-02 release in soil

Day	a_1	a_2	a_3
1	4.0847	4.0952	4.0917
2	1.4920	1.5047	0.0119
3	0.5062	0.5042	0.5052
4	0.2548	0.2458	0.2397
5	0.1783	0.1667	0.1757
6	0.1201	0.1203	0.1202
7	0.0714	0.0465	0.0500
8	0.0686	0.0686	0.0682
9	0.0581	0.0582	0.0583
10	0.0403	0.0358	0.0413
11	0.0278	0.0286	0.0258
12	0.0272	0.0291	0.0204
13	0.0095	0.0095	0.0095
14	0.0093	0.0094	0.0094
15	0.0090	0.0090	0.0090
16	0.0089	0.0089	0.0089
17	0.0086	0.0086	0.0086
18	0.0086	0.0086	0.0027

Where:

a_1 -is the 1st absorbance reading

a_2 -is the 2nd absorbance reading

a_3 -is the 3rd absorbance reading

a_{av} -is the average of absorbance reading

a_{SD} -is the standard deviation of the absorbance readings

Table T4. 25: Concentrations of pesticide loaded sample EB-GA-02 release in soil

Day	$[Ce_1]$	$[Ce_2]$	$[Ce_3]$	$[Ce_{av}]$	SD
1	19.023	19.072	19.056	19.050	0.0250
2	6.9620	6.9841	6.9529	6.9663	0.0160
3	2.3248	2.3154	2.3201	2.3201	0.0047
4	1.1516	1.1096	1.0756	1.1123	0.0380
5	0.7943	0.7403	0.7823	0.7723	0.0284
6	0.5231	0.5240	0.5236	0.5236	0.0005
7	0.2957	0.1797	0.1957	0.2237	0.0629
8	0.2828	0.2828	0.2809	0.2823	0.0011
9	0.2338	0.2343	0.2347	0.2343	0.0005
10	0.1506	0.1296	0.1553	0.1451	0.0137
11	0.0923	0.0960	0.0829	0.0904	0.0067
12	0.0895	0.0983	0.0579	0.0819	0.0213
13	0.0069	0.0068	0.0069	0.0069	0.0030
14	0.0059	0.0063	0.0062	0.0061	0.0003
15	0.0046	0.0047	0.0045	0.0046	0.0001
16	0.0042	0.0041	0.0044	0.0042	0.0001
17	0.0028	0.0029	0.0029	0.0029	0.0004
18	0.0027	0.0028	0.0027	0.0027	0.0002

Where:

$[C_{e1}]$ - is the first scan equilibrium concentration in ppm of the pesticide after shaking with the samples.

$[C_{e2}]$ - is the second scan equilibrium concentration in ppm of the pesticide after shaking with the samples.

$[C_{e3}]$ - is the third scan equilibrium concentration in ppm of the pesticide after shaking with the samples.

$[C_{av}]$ - is the average scan equilibrium concentration in ppm of the pesticide after shaking with

the samples.

SD - is the standard deviations of scans for equilibrium concentrations of the pesticide after shaking with the samples.

Table T4. 26: Pesticide loaded sample KIK-GA-01 release in water

Day	a_1	a_2	a_3
1	4.1770	4.2740	4.1730
2	1.5667	1.6657	1.5687
3	0.7638	0.7338	0.8238
4	0.2812	0.4355	0.3885
5	0.2732	0.2528	0.2428
6	0.2222	0.1958	0.1958
7	0.1835	0.1835	0.1913
8	0.1594	0.1723	0.1479
9	0.1181	0.1170	0.1213
10	0.0785	0.0735	0.0834
11	0.0605	0.0699	0.0719
12	0.0471	0.0461	0.0340
13	0.0261	0.0280	0.0284
14	0.0173	0.0284	0.0249
15	0.0091	0.0091	0.0092
16	0.0089	0.0089	0.0090
17	0.0088	0.0087	0.0088
18	0.0087	0.0088	0.0087

Where:

a_1 -is the 1st absorbance reading

a_2 -is the 2nd absorbance reading

a_3 -is the 3rd absorbance reading

a_{av} -is the average of absorbance reading

Table T4. 27: Concentrations of pesticide loaded sample KIK-GA-01 release in water

Day	$[Ce_1]$	$[Ce_2]$	$[Ce_3]$	$[Ce_{av}]$	SD
1	19.454	19.907	19.435	19.599	0.2669
2	7.2734	7.7354	7.2828	7.4305	0.2641
3	3.5268	3.3868	3.8068	3.5735	0.2139
4	1.2748	1.9948	1.7755	1.6817	0.3690
5	1.2375	1.1423	1.0957	1.1585	0.0723
6	0.9995	0.8765	0.8765	0.9175	0.0710
7	0.8189	0.8189	0.8555	0.8311	0.0211
8	0.7063	0.7663	0.6529	0.7085	0.0567
9	0.5136	0.5089	0.5289	0.5171	0.0105
10	0.3289	0.3056	0.3523	0.3289	0.0234
11	0.2449	0.2889	0.2983	0.2774	0.0285
12	0.1824	0.1777	0.1217	0.1606	0.0338
13	0.0844	0.0935	0.0950	0.0910	0.0057
14	0.0431	0.0952	0.0792	0.0725	0.0267
15	0.0051	0.0050	0.0053	0.0051	0.0002
16	0.0045	0.0041	0.0046	0.0044	0.0003
17	0.0035	0.0037	0.0034	0.0035	0.0002
18	0.0032	0.0035	0.0031	0.0033	0.0002

Where:

$[C_{e1}]$ - is the first scan equilibrium concentration in ppm of the pesticide after shaking with the samples.

$[C_{e2}]$ - is the second scan equilibrium concentration in ppm of the pesticide after shaking with the samples.

$[C_{e3}]$ - is the third scan equilibrium concentration in ppm of the pesticide after shaking with

the samples.

[C_{av}] - is the average scan equilibrium concentration in ppm of the pesticide after shaking with the samples.

SD - is the standard deviations of scans for equilibrium concentrations of the pesticide after shaking with the samples.

Table T4. 28: Pesticide loaded zeolitic materials in crop production

T	[C]	BT	BS	PST	PSS	PKT	PKS
5	[C_{e1}]	0.0005	0.0006	19.638	19.709	20.104	20.506
	[C_{e2}]	0.0005	0.0006	19.636	19.705	20.109	20.500
	[C_{e3}]	0.0004	0.0005	19.639	19.710	20.100	20.509
	[C_{eav}]	0.0005	0.0006	19.638	19.708	20.104	20.505
	SD	0.00006	0.00005	0.0015	0.0026	0.0045	0.0046
20	[C_{e1}]	0.0004	0.0005	1.6936	0.0954	0.9953	0.0983
	[C_{e2}]	0.0003	0.0005	1.6935	0.0950	0.9956	0.0980
	[C_{e3}]	0.0004	0.0004	1.6937	0.0957	0.9952	0.0984
	[C_{eav}]	0.0004	0.0005	1.6936	0.0954	0.9954	0.0982
	SD	0.00006	0.00006	0.0003	0.0004	0.0002	0.0002
30	[C_{e1}]	0.00025	0.0003	0.0932	0.0039	0.0024	0.0022
	[C_{e2}]	0.00022	0.0004	0.0931	0.0040	0.0025	0.0024
	[C_{e3}]	0.00025	0.0003	0.0933	0.0037	0.0024	0.0023
	[C_{eav}]	0.00024	0.0003	0.0932	0.0039	0.0024	0.0023
	SD	0.00002	0.00006	0.0001	0.0002	0.00006	0.0001
45	[C_{e1}]	0.0003	0.0003	0.0028	0.0025	0.0023	0.0020
	[C_{e2}]	0.0003	0.0002	0.0026	0.0024	0.0024	0.0021
	[C_{e3}]	0.0002	0.0003	0.0029	0.0026	0.0022	0.0020
	[C_{eav}]	0.0003	0.0003	0.0028	0.0025	0.0023	0.0020
	SD	0.00006	0.00006	0.0002	0.0001	0.0001	0.00006
60	[C_{e1}]	0.0002	0.0002	0.0015	0.0016	0.0010	0.0011
	[C_{e2}]	0.0002	0.0001	0.0013	0.0017	0.0011	0.0013
	[C_{e3}]	0.0001	0.0002	0.0016	0.0016	0.0015	0.0010
	[C_{eav}]	0.0002	0.0002	0.0015	0.0016	0.0012	0.0011
	SD	0.00006	0.00006	0.0002	0.00006	0.0003	0.0002

Where:

BT - Samples taken from a setup of tomatoes grown on blank soil

BS - Samples taken from a setup of spinach grown on blank soil

PST - Samples taken from a setup of tomatoes grown using pesticide loaded sample EB-GA-02

PSS - Samples taken from a setup of spinach grown using pesticide loaded sample EB-GA-02

PKT - Samples taken from a setup of tomatoes grown using commercial pesticide

PKS - Samples taken from a setup of spinach grown using commercial pesticide

T - time in days

[C]- is the sample concentration in ppm

$[C_{e1}]$ - is the first scan equilibrium concentration in ppm

$[C_{e2}]$ - is the second scan equilibrium concentration in ppm

$[C_{e3}]$ - is the third scan equilibrium concentration in ppm

$[C_{av}]$ - is the average scan equilibrium concentration in ppm

SD - is the standard deviations of scans for equilibrium concentrations

Table T4. 29: Comparative studies for urea and pesticide applications

T	C	UPST	UPSS	PUST	PUSS
5	$[C_{e1}]$	0.036692	0.037619	19.8710	20.1075
	$[C_{e2}]$	0.036700	0.037679	19.8725	20.1025
	$[C_{e3}]$	0.036710	0.042082	19.8695	20.1095
	$[C_{eav}]$	0.036701	0.039127	19.8710	20.1065
	SD	0.000009	0.002560	0.00300	0.00360
20	$[C_{e1}]$	0.009501	0.009285	1.34445	0.09685
	$[C_{e2}]$	0.009488	0.009281	1.34455	0.09650
	$[C_{e3}]$	0.009508	0.009296	1.34445	0.09705
	$[C_{eav}]$	0.009499	0.009287	1.34450	0.09680
	SD	0.000003	0.000009	0.00025	0.00030
30	$[C_{e1}]$	0.001009	0.001006	0.04780	0.00305
	$[C_{e2}]$	0.001011	0.001007	0.04780	0.00320
	$[C_{e3}]$	0.001010	0.001005	0.04785	0.00300
	$[C_{eav}]$	0.001010	0.001005	0.04780	0.00310
	SD	0.000002	0.000001	0.00008	0.00015
45	$[C_{e1}]$	0.0003865	0.000389	0.00255	0.00225
	$[C_{e2}]$	0.0003865	0.000389	0.00250	0.00225
	$[C_{e3}]$	0.0003865	0.000391	0.00255	0.00230
	$[C_{eav}]$	0.0003865	0.000390	0.00255	0.00225
	SD	0.0000010	0.000001	0.00015	0.00008
60	$[C_{e1}]$	0.0000735	0.000120	0.00125	0.00135
	$[C_{e2}]$	0.0000725	0.000123	0.00120	0.00150
	$[C_{e3}]$	0.0000745	0.000122	0.00155	0.00130
	$[C_{eav}]$	0.0000735	0.000122	0.00135	0.00135
	SD	0.00000125	0.000002	0.00025	0.00013

Where:

BT - Samples taken from a setup of tomatoes grown on blank soil

BS - Samples taken from a setup of spinach grown on blank soil

UPST – Fertilizer samples taken from a setup of tomatoes grown using urea loaded sample EB-GA-02 and pesticide loaded sample EB-GA-02

UPSS - Fertilizer samples taken from a setup of spinach grown using urea loaded sample EB-GA-02 and pesticide loaded sample EB-GA-02

PUST - Pesticide samples taken from a setup of tomatoes grown using urea loaded sample EB-GA-02 and pesticide loaded sample EB-GA-02

PUSS - Fertilizer samples taken from a setup of spinach grown using urea loaded sample EB-GA-02 and pesticide loaded sample EB-GA-02

T - time in days

[C]- is the sample concentration in ppm

$[C_{e1}]$ - is the first scan equilibrium concentration in ppm

$[C_{e2}]$ - is the second scan equilibrium concentration in ppm

$[C_{e3}]$ - is the third scan equilibrium concentration in ppm

$[C_{av}]$ - is the average scan equilibrium concentration in ppm

SD - is the standard deviations of scans for equilibrium concentrations

Table T4. 30: Summary of analysis of variance (ANOVA) data.

TABLE	Analysis of Variance						Means								
	Source	DF	Adj SS	Adj MS	F-Value	P-Value	Factor	N	Mean	StDev	95% CI	S	R-sq	R-sq(adj)	R-sq (pred)
T4.4	Factor	2	0.0500	0.02500	0.02	0.978	[Ce1]	10	0.823	1.124	(0.128, 1.518)	1.07138	0.16%	0.00%	0.00%
	Error	27	30.9923	1.14786			[Ce2]	10	0.741	0.916	(0.046, 1.436)				
	Total	29	31.0423				[Ce3]	10	0.832	1.158	(0.137, 1.527)				
T4.6	Factor	2	0.000013	0.000006	0.19	0.832	[Ce1]	11	0.11335	0.00662	(0.10970, 0.11699)	0.0059172	1.22%	0.00%	0.00%
	Error	30	0.001050	0.000035			[Ce2]	11	0.11433	0.00577	(0.11069, 0.11797)				
	Total	32	0.001063				[Ce3]	11	0.11486	0.00528	(0.11122, 0.11850)				
T4.8	Factor	2	0.000000	0.000000	0.00	0.998	[Ce1]	7	0.18620	0.00436	(0.18260, 0.18980)	0.0045357	0.03%	0.00%	0.00%
	Error	18	0.000370	0.000021			[Ce2]	7	0.18627	0.00535	(0.18266, 0.18987)				
	Total	20	0.000370				[Ce3]	7	0.18610	0.00374	(0.18250, 0.18970)				
T4.11	Factor	2	0.000001	0.000000	0.00	0.997	[Ce1]	18	0.00544	0.01006	(0.00071, 0.01016)	0.0099908	0.01%	0.00%	0.00%
	Error	51	0.005091	0.000100			[Ce2]	18	0.00570	0.00996	(0.00097, 0.01043)				
	Total	53	0.005091				[Ce3]	18	0.00558	0.00995	(0.00085, 0.01030)				
T4.12	Factor	2	0.000001	0.000001	0.01	0.993	[Ce1]	18	0.00503	0.00835	(0.00109, 0.00898)	0.0083343	0.03%	0.00%	0.00%

	Error	51	0.003542	0.000069			[Ce2]	18	0.00513	0.00878	(0.00118, 0.00907)				
	Total	53	0.003543				[Ce3]	18	0.00480	0.00785	(0.00086, 0.00874)				
T4.13	Factor	2	0.000001	0.000000	0.01	0.990	[Ce1]	18	0.00413	0.00736	(0.00089, 0.00736)	0.0068345	0.04%	0.00%	0.00%
	Error	51	0.002382	0.000047			[Ce2]	18	0.00381	0.00638	(0.00058, 0.00705)				
	Total	53	0.002383				[Ce3]	18	0.00395	0.00673	(0.00071, 0.00718)				
T4.14	Factor	2	0.000298	0.000149	0.90	0.433	BT	5	0.000099	0.000007	(-0.012454, 0.012651)	0.0128825	13.0%	0.00%	0.00%
	Error	12	0.001992	0.000166			UST	5	0.00917	0.01405	(-0.00338, 0.02172)				
	Total	14	0.002290				UKT	5	0.00990	0.01734	(-0.00266, 0.02245)				
T4.14	Factor	2	0.000332	0.000166	0.87	0.443	BS	5	0.000099	0.000007	(-0.013332, 0.013530)	0.0137840	12.70%	0.00%	0.00%
	Error	12	0.002280	0.000190			USS	5	0.00923	0.01451	(-0.00420, 0.02266)				
	Total	14	0.002612				UKS	5	0.01074	0.01896	(-0.00269, 0.02417)				
T4.17	Factor	4	1565.84	391.459	191.88	0.000	10ppm	4	7.6506	0.1504	(6.1284, 9.1728)	1.42833	98.08%	97.57%	96.59%
	Error	15	30.60	2.040			20ppm	4	15.0083	0.0450	(13.4860, 16.5305)				
	Total	19	1596.44				30ppm	4	17.141	1.713	(15.619, 18.663)				
							40ppm	4	23.979	1.187	(22.457, 25.501)				
							50ppm	4	33.83	2.41	(32.30, 35.35)				
T4.19	Factor	2	0.0741	0.03703	0.01	0.989	[Ce1]	6	16.593	1.807	(14.980, 18.205)	1.85291	0.14%	0.00%	0.00%
	Error	15	51.4994	3.43329			[Ce2]	6	16.455	1.497	(14.843, 18.068)				

T4.23	Factor	2	0.06	0.0281	0.00	0.999	[Ce1]	18	1.54	4.66	(-0.65, 3.73)	4.62838	0.01%	0.00%	0.00%
	Error	51	1092.52	21.4219			[Ce2]	18	1.54	4.69	(-0.65, 3.73)				
	Total	53	1092.57				[Ce3]	18	1.47	4.53	(-0.72, 3.66)				
T4.25	Factor	2	0.00	0.0006	0.00	1.000	[Ce1]	18	1.78	4.61	(-0.41, 3.96)	4.62013	0.00%	0.00%	0.00%
	Error	51	1088.63	21.3456			[Ce2]	18	1.77	4.63	(-0.42, 3.95)				
	Total	53	1088.63				[Ce3]	18	1.76	4.62	(-0.42, 3.95)				
T4.27	Factor	2	0.06	0.0279	0.00	0.999	[Ce1]	18	2.04	4.70	(-0.20, 4.28)	4.73682	0.00%	0.00%	0.00%
	Error	51	1144.31	22.4375			[Ce2]	18	2.12	4.82	(-0.12, 4.36)				
	Total	53	1144.37				[Ce3]	18	2.07	4.70	(-0.17, 4.31)				
T4.28	Factor	2	60.31	30.15	0.59	0.569	BT	5	0.000328	0.000122	(-6.962571, 6.963227)	7.14587	8.96%	0.00%	0.00%
	Error	12	612.76	51.06			PST	5	4.29	8.61	(-2.68, 11.25)				
	Total	14	673.07				PKT	5	4.22	8.89	(-2.74, 11.18)				
T4.28	Factor	2	54.52	27.26	0.51	0.615	BS	5	0.000380	0.000164	(-7.145934, 7.146694)	7.33411	7.79%	0.00%	0.00%
	Error	12	645.47	53.79			PSS	5	3.96	8.80	(-3.18, 11.11)				
	Total	14	699.98				PKS	5	4.12	9.16	(-3.02, 11.27)				
T4.29	Factor	1	0.000001	0.000001	0.00	0.966	UPST	5	0.00953	0.01568	(-0.00719, 0.02626)	0.0162157	0.02%	0.00%	0.00%
	Error	8	0.002104	0.000263			UPSS	5	0.00999	0.01673	(-0.00673, 0.02671)				
	Total	9	0.002104												
T4.29	Factor	1	0.112	0.1118	0.00	0.971	PUST	5	4.25	8.75	(-4.89, 13.40)	8.86566	0.02%	0.00%	0.00%
	Error	8	628.800	78.6000			PUSS	5	4.04	8.98	(-5.10, 13.18)				
	Total	9	628.912												

Where: DF is the Degree of Freedom; Adj SS is the Adjusted Sum of Square; Adj MS is the Adjusted mean of Square; StDev is the Standard Deviations; CI is the Confidence Interval; S is the response variable; R-sq is the percentage of fit in the response; R-sq(adj) is the adjusted percentage of fit in the response; R-sq (pred) is the predicted percentage of fit in the response.

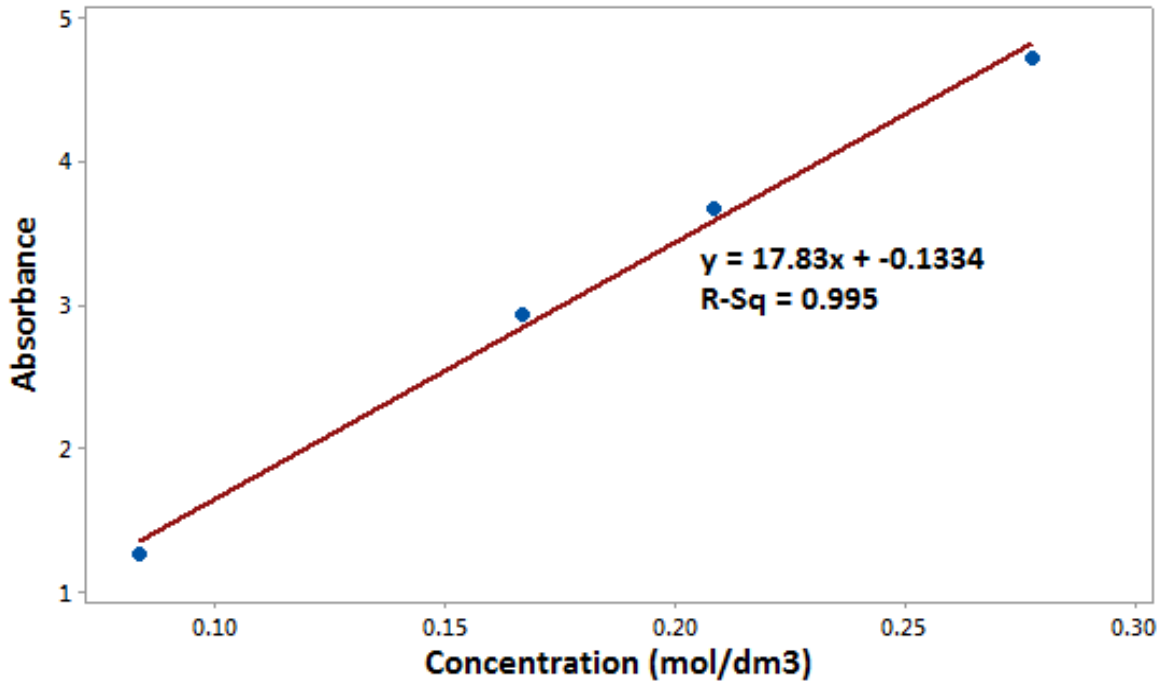

Figure F4. 1: Calibration line for Urea

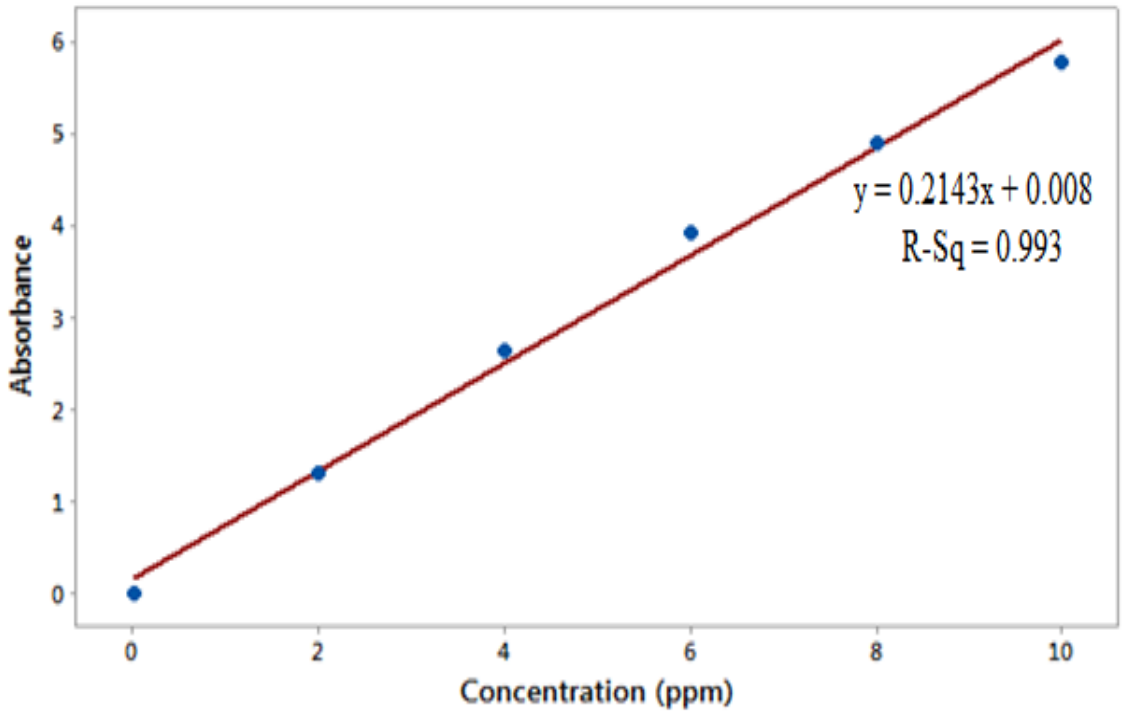

Figure F4. 2: Absorbance curves for Lambda-cyhalothrin

D. MAPS

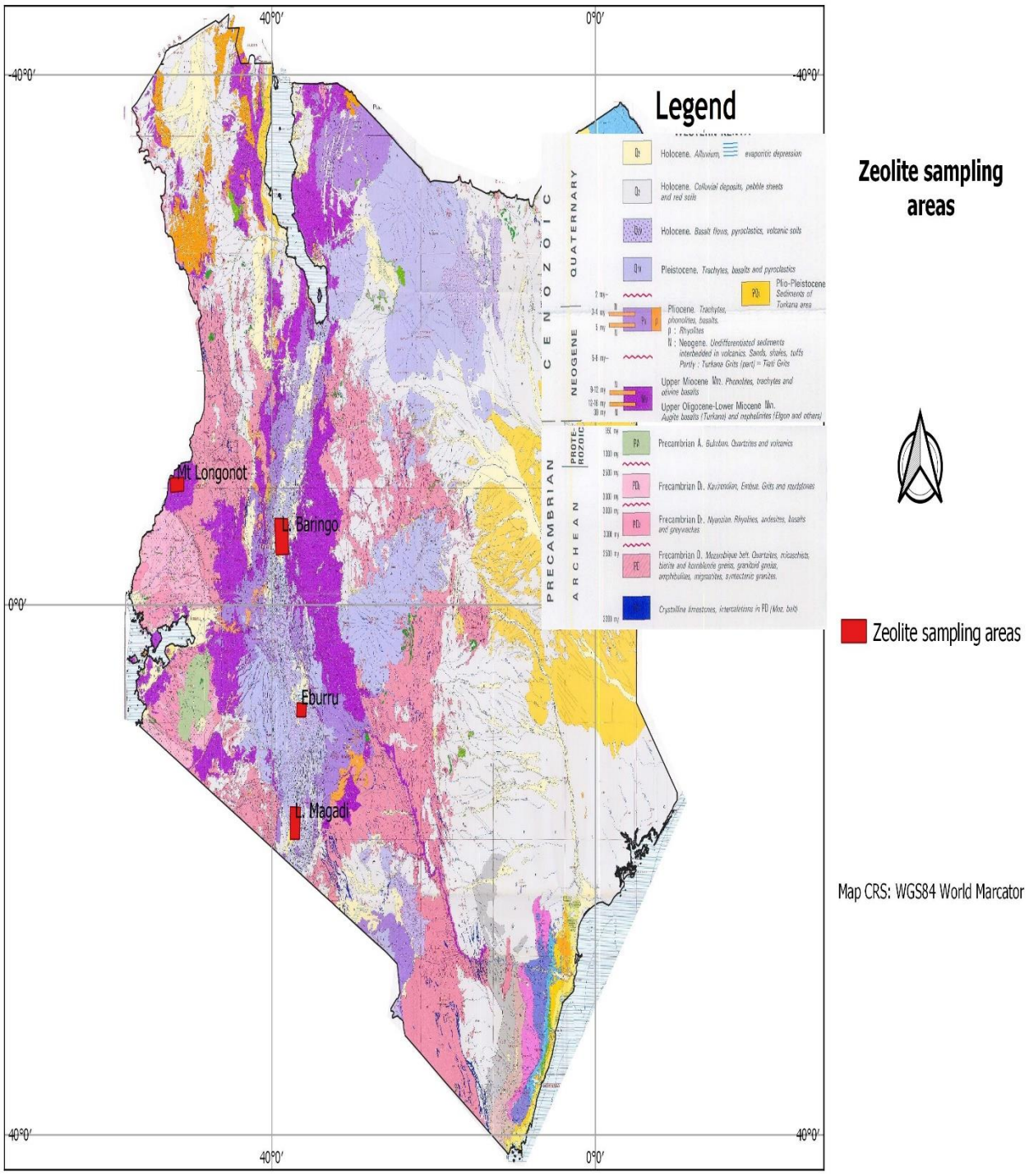

Figure D 1: Map of the Republic of Kenya showing the sampling sites

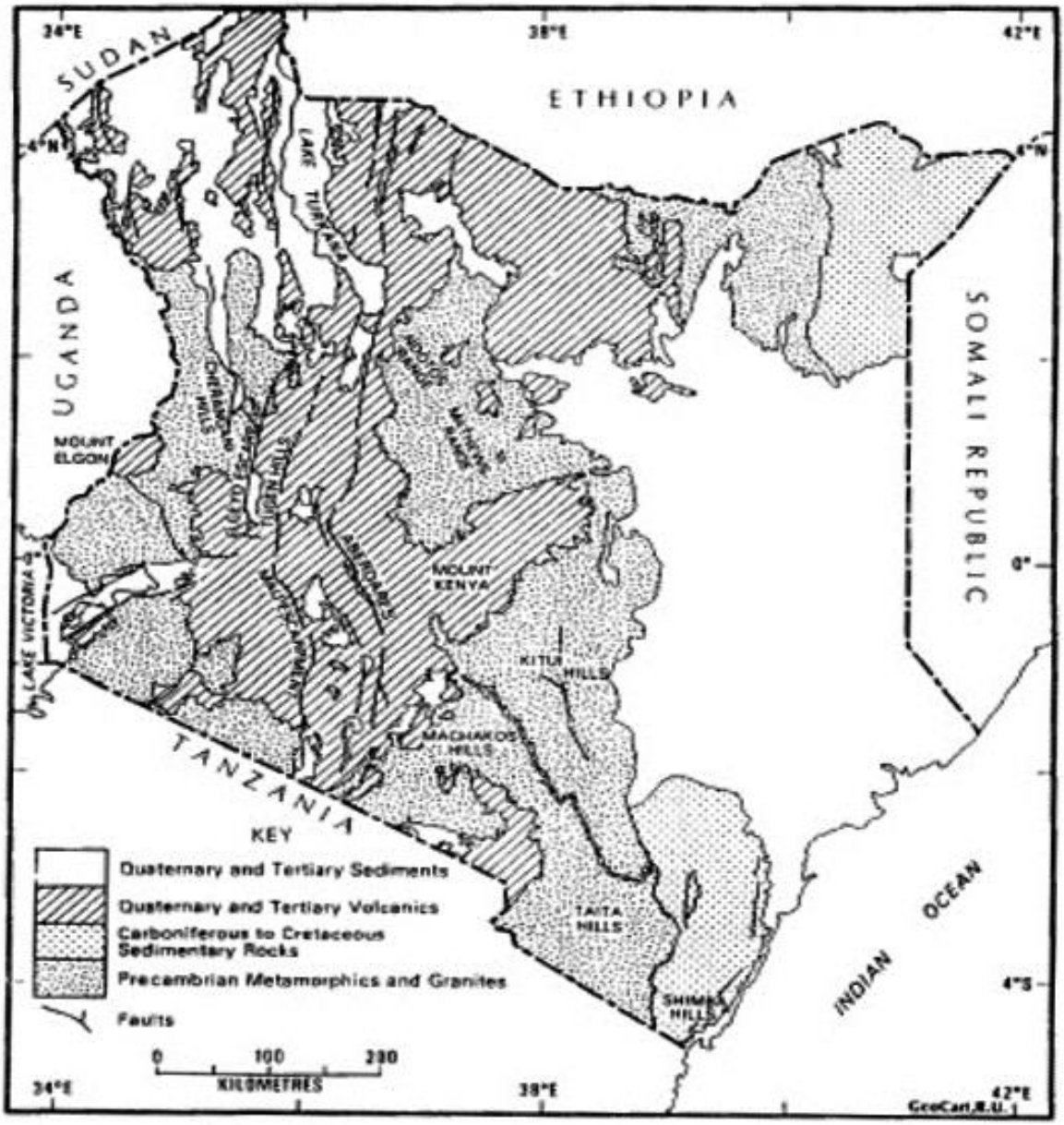

Figure D 2: Simplified geology of Kenya

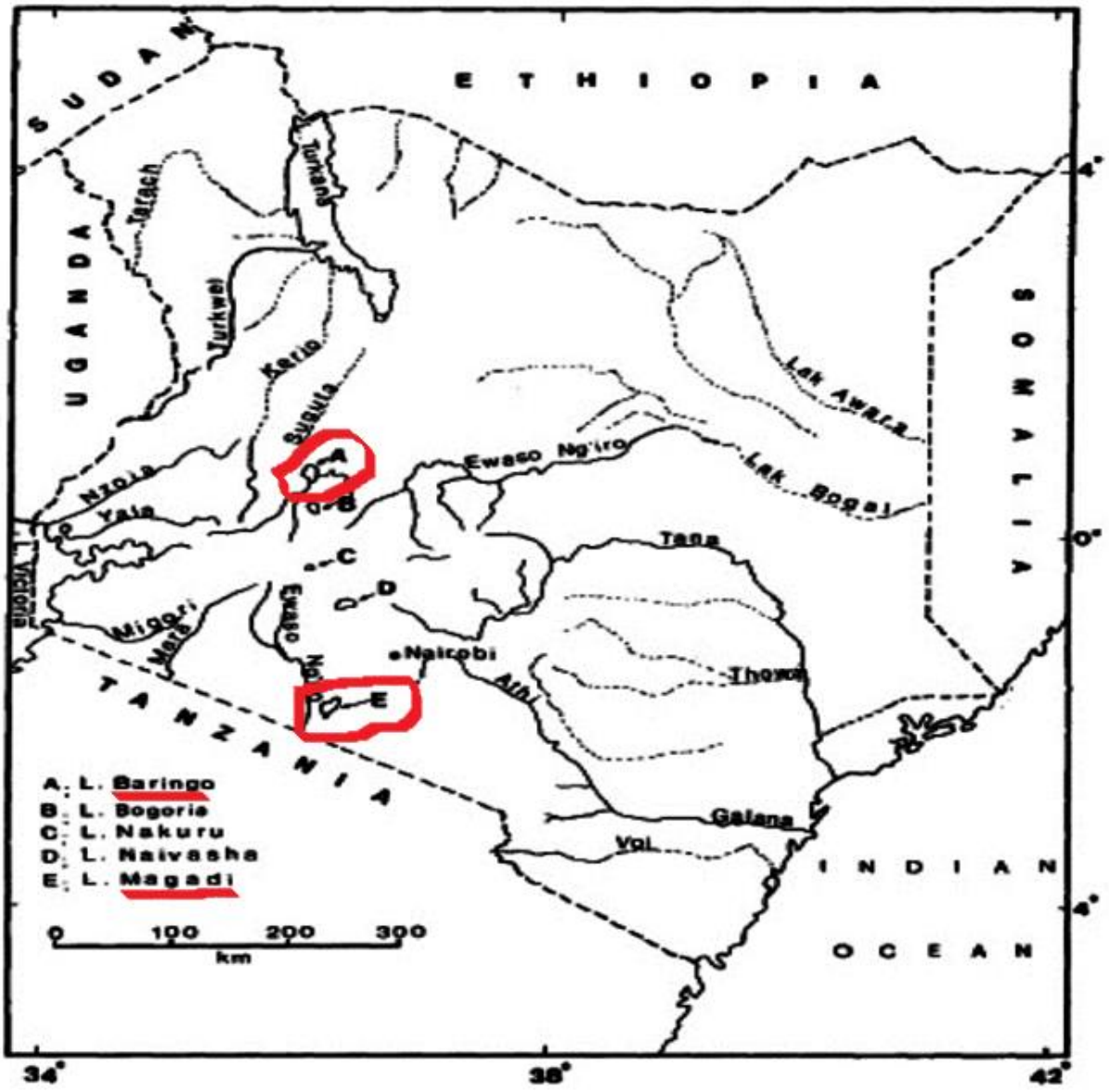

Figure D 3: Lakes and major drainage networks of Kenya

Available online at www.kenchemsoc.org

Journal of the Kenya Chemical Society 10-1 (2017), 24-34

JOURNAL OF THE KENYA CHEMICAL SOCIETY

Kinetics and Isothermal studies of Lambda Cyhalothrin sorption on Eburru soil in Kenya

G. A. Waswa[a], D. Andala[b] , A. O. Aluoch[c], G. N. Kamau[a],I. Michira[a] and J. K. Mbugua[a]

[a]Department of Chemistry, University of Nairobi, P.O. Box 30197-00100, Nairobi, Kenya

[b]Department of Chemistry, Multimedia University of Kenya,P.O. Box 15653- 00503, Nairobi, Kenya

[c]Department of Chemical Scienceand Technology, Technical University of Kenya, P.O. Box 52428 - 00200Nairobi-Kenya

Corresponding author's E-mail address: waswagabriel@gmail.com

Abstract

A kinetic and mechanistic study on adsorption of Lambda cyhalothrin on Eburru soils in Kenya was carried out using adsorption isothermal model. The study was carried out to predict adsorption mechanisms on Kenya soil. In this paper, Freundlich, Langmuir, Quasi-Langmuir and Temkin isotherm models were employed to correlate data from the batch mode experiments. Kinetic investigation was done under pseudo first-order conditions and fitted to second-order and intrapartical diffusion models. The results show a linearized good fit to the employed models with correlation coefficient (r^2) in the range of 0.984 – 0.999

Keywords: *Lambda-cyhalothrin, sorption, equilibrium constant, free energ*.

1. Introduction

Lambda-cyhalothrin is a pyrethroid insecticide active ingredient found in several brand name products like scimitar, warrior, matador and icon, applied in agriculture to aphids, coleopterous and lepidopterous pests, as well as in public health to control cockroaches, mosquitoes, flies and ticks. This compound,was first reported by Robson and Crosby [1], is synthesized from pyrethrum chrysanthemum flowers and photostabilized bysubstitution reactions [2,3].

The structure of Lambda-cyhalothrin shown in (Figure 1) is a 1:1 mixture of two isomers: (*S*)-α-cyano-3-phenoxybenzyl-(*Z*)-(1*R*, 3R)-3-(2-chloro-3,3,3-trifluoroprop-1-enyl)-2,2-dimethyl cyclopropanecarboxylate ('a')and (*R*)-α-cyano-3-phenoxybenzyl-(*Z*) -(1*S*,3*S*)- 3-(2-chloro-3, 3,3-trifluoroprop-1-enyl)-2,2-dimethylcyclopropanecarboxylate ('b') [4].
The compound acts as a pesticide by binding to a protein that regulates the voltage-gated sodium channel of the nervous system, preventing them from closing normally which results in continuous nerve stimulation and tremors leading to paralysis and death [5,6,7,8].

When introduced into the environment, like many other organic compounds, Lambda-cyhalothrinundergoes a number of processes, including adsorption on soils and dissipation in water, which contribute to its pollution effect. Studies on ecotoxicity of Lambda-cyhalothrin reveals it has slight to high toxicity levels to terrestrial and aquatic animals [9]. It is highly toxic to a number of fish and shellfish, the LC_{50} (96 hrs) is 210ng/L for bluegill sunfish and 0.8ng/L for sheepshead minnow [10, 11]. Weston et al., [12] studied Lambda-cyhalothrin sediment toxicity, with the median lethal concentration LC_{50} residue being 0.45µg/g which corresponds to 1.4 ng/L for pore water concentration [13].

Hence, there is need to mitigate the environmental contamination associated with the wide range use of this pesticide. The main significance of this study is to analyze the sorption properties of Eburru soils on Lambda-cyhalothrin, which could be applied as carrier materials for smart delivery of the pesticide to minimize the related environmental contamination effects.

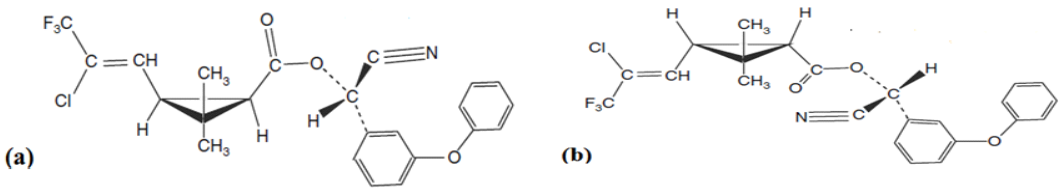

Figure 1: Structures of Lambda-cyhalothrin; (a) (S)-alcohol(Z)-(1R)-*cis*-acid, (b) (R) - alcohol (Z) - (1S) - *cis*– acid.

Sorption models

Freundlich, Langmuir, Quasi-Langmuir and Temkin models were used to assess the adsorption of Lambda-cyhalothrin onto the Eburru soils of Kenya.

Freundlich Equation

The Freundlich [14] equation is an empirical equation based on adsorption on a heterogeneous surface. The equation is commonly represented as shown in equation (1).

$$q_e = K_F C_e^{1/n} 1) \quad \text{.....(1)}$$

This can be rearranged linearly by equation 2.

$$\ln q_e = \ln K_F + \frac{1}{n} \ln C_e \quad \text{.....(2)}$$

Where C_e(mg/L) is the equilibrium concentration and q_e(mg/g) is the amount of adsorbed pesticide per unit mass of the adsorbent. The constant n is the Freundlich equation exponent that represents the parameter characterizing quasi-Gaussian energetic heterogeneity of the adsorption surface [15].K_F (L/g) is the Freundlich constant indicative of the relative adsorption capacity of the adsorbent.

Langmuir model

This model assumes that adsorption of sorbate molecules occurs on a homogeneous surface to form a monolayer with no interactions between the adsorbed molecules [16].

The Langmuir equation is representedby equation 3 as:

$$q_e = \frac{q_m K_L C_e}{1+K_L C_e} \quad \text{.....(3)}$$

Which can be expressed in a linear form as:

$$\frac{C_e}{q_e} = \frac{1}{q_m K_L} + \frac{C_e}{q_m} \quad \text{.....(4)}$$

Where: q_e (mg/g) is the amount adsorbed, C_e (mg/L) is the concentration of sorbate molecules, q_m (mg/g) is the maximum amount of adsorbed sorbate molecules per unit mass of sorbent corresponding to complete coverage of the adsorptive sites and K_L(L/mg) is the Langmuir constant related to the energy of adsorption.

Quasi-Langmuir Model

Quasi-Langmuir model is used as a compromise between Langmuir and Freundlichmodels, which is givenin equation (5) [17]:

$$q_e = \frac{K_c C_e}{1+ \alpha_c C_e^{\beta}} \quad \text{.....(5)}$$

This can be expressed in its linear form as:

$$\frac{1}{q_e} = \frac{1}{K_c C_e} + \frac{\alpha_c}{K_c} \quad \text{.....(6)}$$

Where K_c(L/g), α_c(L/mol) and β are Quasi-Langmuir constants. The value of β lies between 0 and 1. Hence plots of $1/q_e$ versus $1/C_e$from equation 6 are linear.

Temkin Isotherm Equation

The Temkin isotherm equation assumes that the heat of adsorption of all the molecules in layer decreases linearly with coverage due to adsorbent-adsorbate interactions, and that the adsorption is characterized by a uniform distribution of the bonding energies, up to some maximum binding energy [18]. The Temkin isotherm is represented by equation (7).

$$q_e = \frac{RT}{b} \ln(K_T C_e) \quad \text{.....(7)}$$

Taking $B_T = RT/b$, this can be rearranged linearly as:

$$q_e = B_T \ln K_T + B_T \ln C_e \quad \text{.....(8)}$$

Where T is the absolute temperature (K), R is the universal gas constant (8.314J/mol. K), K_T is the equilibrium binding constant (L/mg), $b$is the variation of adsorption energy (kJ/mol) and $B_T$is Temkin constant, which is related to the heat of adsorption (kJ/mol).

Therefore, plots of q_e against ln$C_e$from equation 8 should be linear.

2. Materials and methods

The following instruments, materials and reagents were used: UV-Visible spectrometer (UV-1700 model, Shimadzu Corporation, Kyoto, Japan), Analytical balance (Fischer A-160), Orbital shaker (fitted with timer), Lambda cyhalothrin pesticide (analytical standard 99% pure from IOBA Chemie), distilled water and soil samples from Eburru crater, Rift valley, Kenya (0.63S, 36.23E).

The soil samples were prepared for analysis by air drying in natural sunlight at room temperature for four days to prevent nutrient transformation, crashing, sieved using 0.85mm sieve size and stored in plastic sampling bags.

The dried soil samples were analyzed for Na, Ca and K using a flame photometer while P, Mg and Mn were analyzed calorimetrically, using theMehlich Double Acid Method [19,20].

Other trace elements Fe, Zn, and Cu and exchangeableCa and Mgwere determined by Atomic Absorbance Spectrophotometer [21].

Total organic carbon (C) was determined by calorimetric method [22]. Total nitrogen was determined by Kjeldahl method [23]. Soil pH was determined using a pH meter on a 1:1 (w/v) soil-water suspension. Exchangeable Na and K were determined by flame photometer after leaching with 1M KCl. Cation Exchange Capacity (CEC) was determined on the leachate at pH 7.0 by distillation followed by titration with 0.01 M HCl [24,25].

To carry out sorption studies, standard concentrations of Lambda-cyhalothrin pesticide were prepared by varying concentrations from 2.0, 4.0, 6.0, 8.0, 10.0, 20.0, 40.0, 60.0, 80.0 and 100.0 ppm in aqueous medium. They were scanned between 200-900nm wavelengths on the UV-Visible Spectrophotometer to determine the maximum absorption wavelength of the pesticide, which was obtained at 218 nm. Calibration curves at218nm were used to determine concentrations of other pesticide solutions. Studies on variation of time and concentrations were done by treating 1.00g of the soil with 10ml aqueous solutions each containing 10.0, 20.0, 30.0, 40.0 and 50.0ppm concentrations of Lambda-cyhalothrin pesticide. The media were shaken at room temperature for 15, 30, 45 and 60 minutes each, and then centrifuged at 10,000rpm for 10 minutes. The supernatants were then filtered using 0.22µm what-man papers and equilibrium concentration determined. Varying masses was conducted using 0.10, 0.20, 0.50, 1.0, 1.5, and 2.0 g of soil suspended in 10ml pesticide solution of concentration 50ppm, shaken for 24 hours and equilibrium concentration determined. Procedures modified from Manikandan and Subramanian (2014) [26].

To load the pesticide into the soil pores, 15g of soil was spiked with 25ml of 100ppm Lambda- cyhalothrin pesticide solution, shaken at room temperature for 24 hours, then equilibrium concentration of the remaining pesticide determined .The difference between initial concentration and equilibrium concentration gave the amount loaded in the samples. The resulting soil was dried at 100^0C for 24 hours to obtain the pesticide loaded soil samples. Desorption studies were conducted by placing 15g of pesticide loaded soil samples in 250ml separating funnels and 50ml distilled water infiltrated through at an approximate flow rate of 0.1667ml/min. 50ml distilled water was refilled every 24 hours to infiltrate the same samples for 18 days. Modified from Bansiwal*et. al.*, (2006) [27].The filtrates/elutes were collected on a daily basis prior to refilling, filtered using 0.22 µm what- man papers and equilibrium concentration determined.

The amount of Lambda-cyhalothrin pesticide adsorbed (mg/g) was calculated using equation (9)reported by Vanderborght and van Greikenm [28].

$$q_e = \frac{v(C_i - C_e)}{W} \quad \text{.....(9)}$$

Where $q_e$is the amount of solute adsorbed from the solution, v is the volume of the adsorbate, $C_i$is the concentration before adsorption, C_e is the concentration after adsorption, and w is the weight in grams of the adsorbent.

3. Results and discussion

Soil analysis

The nature of the soil greatly influences its adsorption characteristics. Table 1 shows the pH (8.38) of the soil being basic, while the low percentage of organic carbon (0.94%) supports the low degree of adsorption of Lambda-cyhalothrin onto the soil.

Table 1: Properties of the soils used in adsorption experiment

Properties	**Description**
Soil pH	8.38
Total Nitrogen %	0.10
Total Org. Carbon %	0.94
Phosphorus (Olsen) ppm	3.40
Potassium me%	0.62
Calcium me%	4.70
Magnesium me%	0.59
Manganese me%	0.20
Copper ppm	1.36
Iron ppm	13.34
Zinc ppm	10.22
Sodium me%	0.84
Electrical conductivity (mS/cm)	0.23

Absorbance curves

The absorbance curves at 218 nm for Lambda-cyhalothrin obeyed Beer's law at lower concentrations (2-10ppm) as shown in Figure 2.

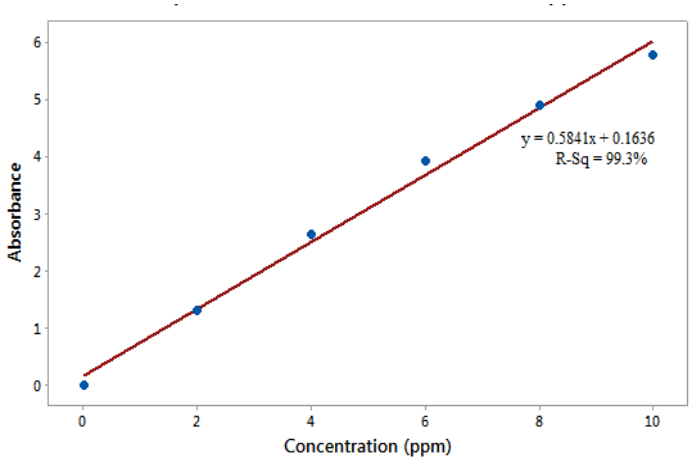

Sorption studies

Figure 3 shows the plots of Lambda-cyhalothrin varying concentration versus different shaking time.

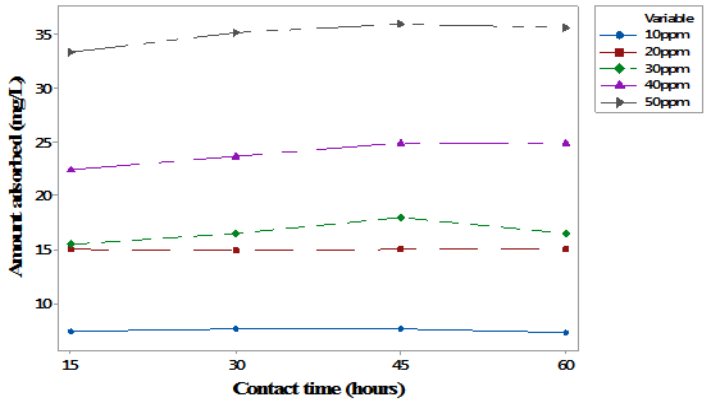

Figure 3: Concentration versus time on Lambda-cyhalothrin adsorption.

The amount of pesticide adsorbed on the soil surface increases with increase in spiking levels. This is due to the presence of the high number of vacant adsorption sites, leading to increase in concentration gradient between adsorbate in solution and the adsorbent surface. The equilibration time depends on the initial concentration of the pesticide. The lower the concentration, the shorter the time to equilibrate due to higher adsorbent surface site ratio to pesticide molecules per unit volume. Therefore increasing the initial pesticide concentration increases the amount of pesticide molecules uptake per unit mass of the soil. Variation in masses of soil reported overall positive gradient on amounts of Lambda-cyhalothrin molecules adsorbed, as shown in Figure 4.Increase in amount of soil decreased the concentration of the pesticide.

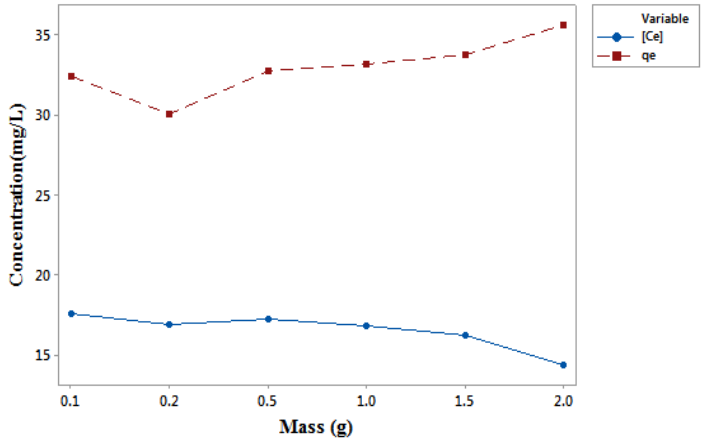

Figure 4: Effect of varying mass of soil with concentrationon Lambda-cyhalothrin adsorption

Similarly, percentage of pesticide removed from aqueous medium increased from 65 – 70% when the mass of the soil increased from about 0.2 – 2.0g (Figure 5). Increasing amounts of soil relates to increasing number of adsorption sites which generates higher adsorption gradient.

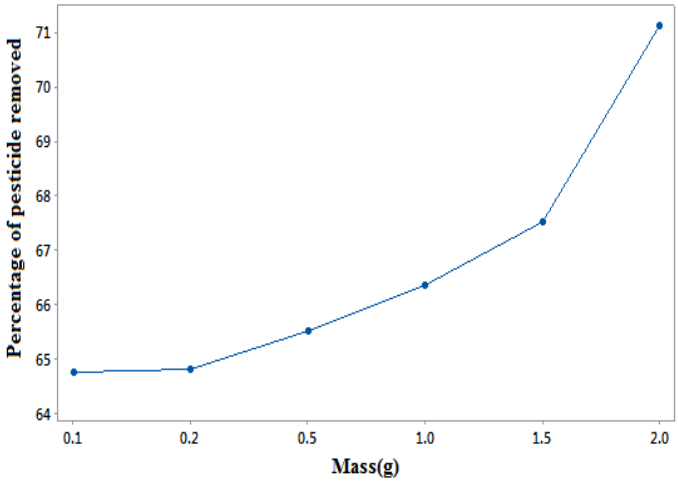

Figure 5: Percentage of pesticide removed by varying the mass of the soil

Desorption studies of Lambda cyhalothrin indicated a rapid discharge of pesticide molecules into the aqueous medium (Figure 6), with more than half of the loaded amounts desorbed within the first four days. Although the literature reported soil adsorption (Koc) for Lambdacyhalothrin (247,000 – 330,000 cm3g-1)(Table 6) is a high value, which is indicative of high preferential affinity to organic matter, only 0.94% of the soil used was the total organic content. This low organic

composition could be strongly attributed to the high initial desorption rates.

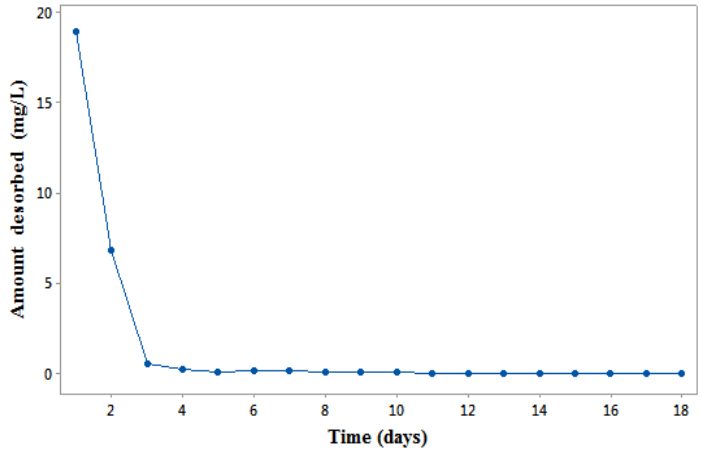

Figure 6: Variation ofamount of pesticidedesorbed with time

Adsorption isotherms

Freundlich isotherms

The Freundlich model was chosen to estimate the adsorption intensity of the sorbate on the sorbent surface. The experimental data from the batch sorption study of the Lambda-cyhalothrin pesticide on Eburru soils of Kenya were plotted logarithmically using the linear Freundlich isotherm equation as shown in Figure7 below.

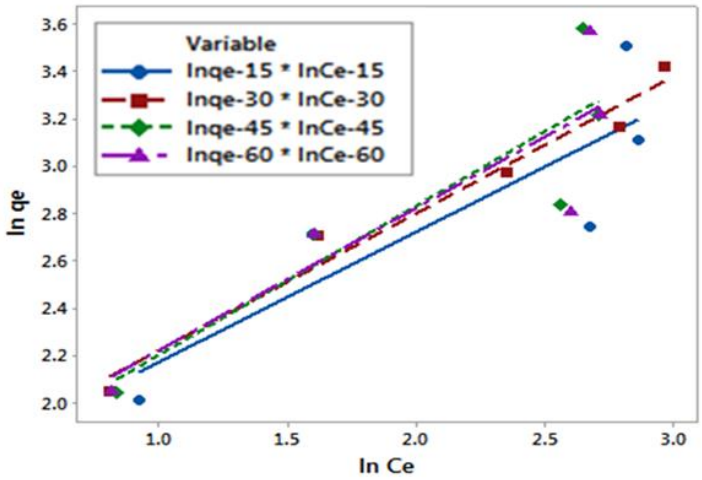

Figure 7: Linear Freundlich isotherm plot

The linear Freundlich isotherm constants for Lambda-cyhalothrin pesticide on Eburrusoils are presented in Table 2. The average Gibb's free energy of -3.9864 kJmol^{-1}indicates spontaneity in the adsorption process. Adsorption non-linearity parameter (n), which also indicates the quasi-Guassian energetic heterogeneity obtained was an average of 1.6949, while R^2 values ranged from 0.753 to 0.970, comparatively making Freundlich isotherm better definitive of lambda-cyhalothrin adsorption on Eburru soils.

Table 2: Freundlich isotherm parameters for Lambda-cyhalothrin

Time (min.)	n	K_F (L/g)	R^2	ΔG (kJmol^{-1})
15	1.8089	5.0128	0.753	-3.9938
30	1.7209	5.1397	0.970	-4.0559
45	1.5893	4.8163	0.804	-3.8947
60	1.6606	5.0279	0.786	-4.0013

Langmuir isotherms

The Langmuir model was used for a homogenous monolayer adsorption without any interaction between adsorbed molecules and uniform energies of adsorption, whose plots generated Figure 8 below.

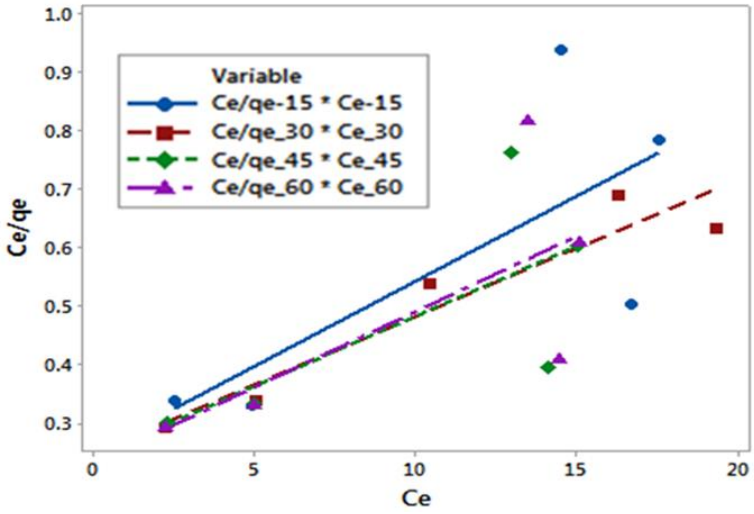

Figure 8: Linear Langmuir isotherm plots

The assumption made is that the adsorbed chemical species do not react with one another. From figure 8 above, the following constants were calculated.

Table 3 Langmuir isotherm parameters for Lambda-cyhalothrin

Time (min.)	$1/q_m$	$1/q_mK_L$	K_L(L/mg)	R^2
15	0.02910	0.2506	0.11610	0.5611
30	0.02325	0.2488	0.09344	0.9110
45	0.02490	0.2475	0.10061	0.9313
60	0.02572	0.2321	0.11081	0.4990

R^2 values ranged from 0.4990 to 0.9313, while the average value of K_L constant was 0.1052, as obtained from Table 3 above.

Quasi Langmuir isotherms

This was used as a compromise between Langmuir and Freundlich models, whose linear plots of $1/q_e$ versus $1/C_e$obtained are shown below.

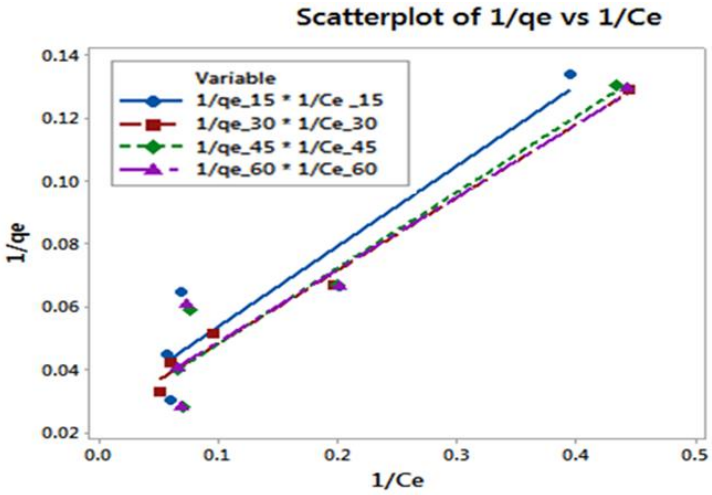

Table 4 shows the Quasi-Langmuir equilibrium constant values from the plots.

Table 4: Quasi-Langmuir isotherm parameters for Lambda-cyhalothrin

Time	$1/K_cc_e$	$1/c_e$	K_{RP} (L/g)	R^2
15	0.02910	0.2506	8.6117	0.5611
30	0.02325	0.2488	10.7011	0.9110
45	0.02697	0.2387	8.8506	0.8910
60	0.02572	0.2321	9.0241	0.4990

Quasi-Langmuir average K_c value was 9.2969, while the R^2 values ranged from 0.4990 to 0.9110 as obtained from Table 4 above.

Temkin isotherms

This was used to assume the linear decrease in the heat of adsorption of all the molecules with layer coverage, and that the adsorption is characterized by a uniform distribution of the bondingenergies.Plots of q_e against $\ln C_e$were linear.

The data in table 5 shows the Temkin equilibrium constant values from the plots.

The average equilibrium binding constant,K_T, obtained was 1.0815Lmg^{-1}, while the average Temkin constant,B_T, related to heat of adsorption was9.6253k$Jmol^{-1}$.

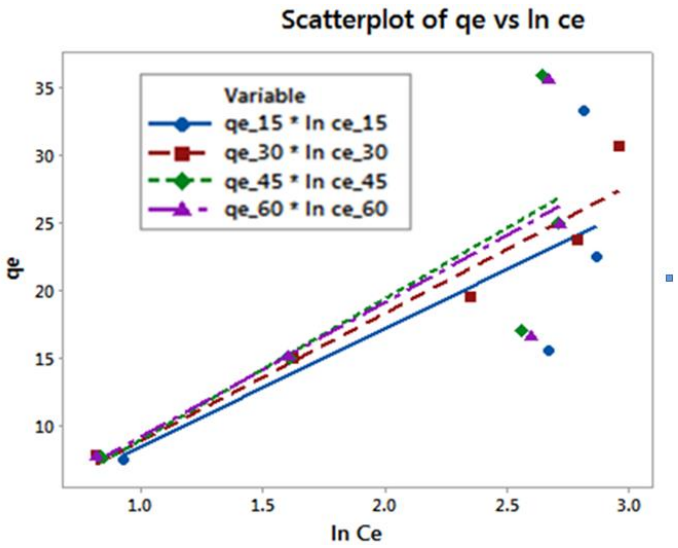

Figure 10: Linear Temkin isotherm plots

Table 5: Temkin isotherm parameters for Lambda-cyhalothrin

Time in minutes	B_T(kJ/mol)	B_TInK_T	K_T(L/mg)	R^2
15	8.740	0.284	1.033	0.614
30	9.398	0.502	1.059	0.934
45	10.42	1.487	1.153	0.640
60	9.943	0.774	1.081	0.625

Physicochemical properties

Table 6 below gives a summary of the physical, chemical and environmental properties of Lambda-cyhalothrin.

Table 6: Physicochemical properties of Lambda-cyhalothrin [4]

Properties	Description
Molecular formula	$C_{23}H_{19}ClF_3NO_3$
Molecular weight (g/mol)	449.9
Density (g/mL at 25°C)	1.33
Melting point (°C)	49.2
Boiling point (°C at 0.2 mmHg)	187–190
Water solubility (mg/L at 20°C)	0.005
Octanol–water partitioning (log *K*ow at 20°C)	7.00
Hydrolysis half-life (d): pH 5 pH 7 pH 9	 Stable Stable 8.66
Photolysis half-life (d): Water at pH 5 and 25°C Soil	 24.5 53.7
Bioconcentration factor (BCF) (fish)	2,240
Soil adsorption *K*oc (cm^3/g)	247,000–330,000
Soil degradation half-life (d)	

Aerobic soil	42.6
Aquatic degradation half-life (d) aerobic aquatic 21.9	 21.9
State at room temperature	solid
Colour: Solid solution	 Colourless yellow
CAS number	91465-08-6
US EPA PC Code	128897

Thelow water solubility and relative stability at neutral conditionscould contribute to its persistence , the high octanol-water partition coefficient (K_{ow}) indicates greater lipid partitions, while the high mean water-soil organic carbon partition coefficient (K_{oc}) indicates preferential affinity to organic matter and higher adsorption rates to particles (sediments), an aspect that may reduce its degradation rate due to unavailability to micro-organisms and sunlight when introduced in streams and rivers; but also may form the mechanisms of sediment sorption removal and mitigation of toxicity in water. A number of studies have been reported on adsorption of Lambda-cyhalothrin on different types of soils, sediments and varied contact time. Most of these data was found to fit theFreundlich isotherm. The extent of adsorption was dependent on the amount of organic matter in these soils, contact time and soil type [29,30,31,32,33,34,35].

Adsorption Kinetics

Kinetic studies was used to analyze sorption dynamics and mechanisms while pseudo-first and secondorders were used to determine the rate constants and orders of sorption processes.

Pseudo-First-Order Model

Pseudo-first-order Kinetic model of Lagergren [36] is based on the solid capacity forsorption analysis and is expressed as given in equation 10.

$$\frac{dq_t}{dt} = kf(q_e - q_t) \quad \text{.....(10)}$$

where qt is the amount of adsorbate adsorbed at time t (mg/g), kfis the rate constant ofpseudo-first-order kinetics (min) and t is the time (min). The integration of equation 10 withthe initial condition, qt =0 at t = 0 leads to the pseudo-first-order rate equation:

$$\ln(q_e - q_t) = lnq_e - kft \quad \text{.....(11)}$$

A straight line of ln(qe −qt) versus t suggests the applicability of this kinetic model.Pseudo-first-order rate constant (kf) (1/min) can be determined from the slope of the plot.Figure 11and Table 7shows plotsfrom experimental data.

Table 7: *Pseudo*-first order kinetic parameter

Concentration(ppm)	$\ln q_e$	K_f	R^2
100	0.3872	0.02939	0.996
200	1.240	0.03338	0.831
300	1.828	0.03652	0.746
400	2.162	0.07138	0.957
500	2.929	0.07230	0.980

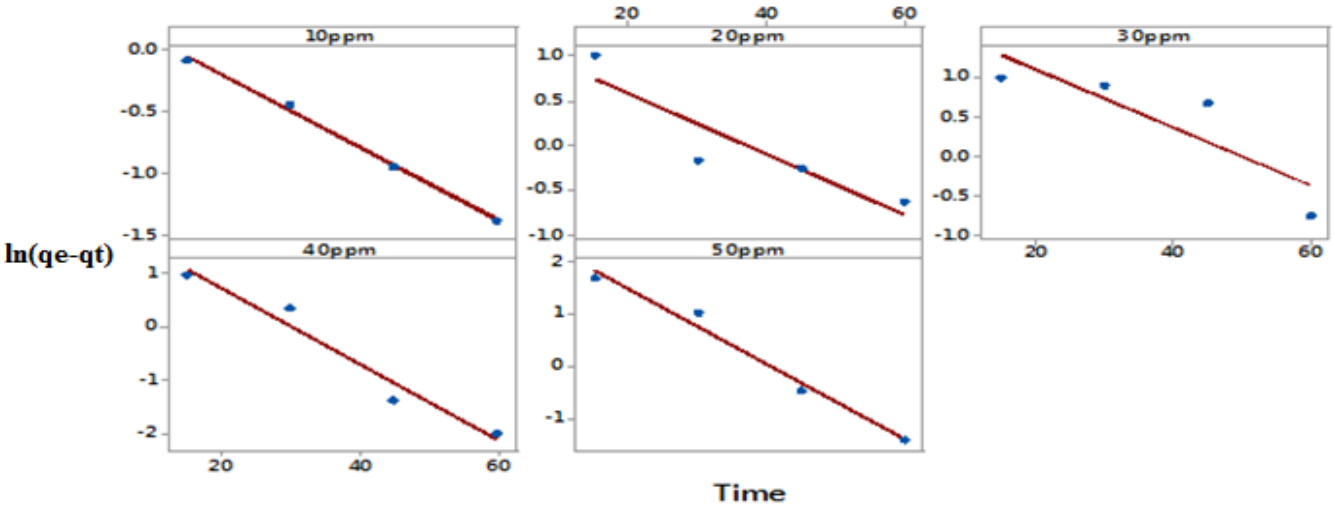

Figure 11: *Pseudo*-first order model plot

Pseudo-second-Order Model

The pseudo-second order reaction kinetic model based on the sorption equilibriumcapacity can be expressed by equation 12[37],

$$\frac{dq_t}{d_t} = ks(q_e - q_t) \quad \text{.....(12)}$$

where k_S is the pseudo-second-order rate constant (g/mg min). Integrating equation 12 andnoting that q_t =0 at t = 0, the following equation is obtained:

$$\frac{t}{q_t} = \frac{1}{ksq_e} + \frac{1}{q_e t} \quad \text{.....(13)}$$

The plot t/qt versus t gives a straight line if second-order kinetics are applicable,whereqe and ks can be determined from the slope and intercept of the plot, respectively. Theinitial sorption rate, h (mg/g min), as $t \rightarrow 0$ can be defined as

$$h = ksq_e^2 \quad \text{.....(14)}$$

The straight line plot for the *pseudo*-first-order sorption kinetic model betweenln($q_e - q_t$) vs. t was plotted (Figure11) for sorption of Lambda cyhalothrin. The value of the rate constantcalculated from the slope of plotsranged from 0.02939 to 0.07230 min^{-1}. The linear plots of *pseudo*-second-order kinetic model was also plotted between t/qt. vs. t, and sorption capacity and *pseudo*-second-order rate constants q_e and $k_s$werecalculated from the slope and intercept of the plot (Figure 12).

Table 8: *Pseudo*-second-order kinetic parameter

Conc.(ppm)	$1/k_sq_e$	$1/q_e$	k_s(g/mg min)	h(mg/g min)	R^2
100	0.06786	0.1281	1.8877	115.0363	0.999
200	0.03781	0.0665	1.7588	397.7161	0.997
300	0.0782	0.06061	0.7751	210.9935	0.984
400	0.09594	0.03846	0.4009	271.0301	0.999
500	0.09525	0.026682	0.2801	393.4380	0.987

The *pseudo*-second-orderkinetic constant $k_s$and sorption capacity $q_e$ranged from1.8877 to 0.280 $gmg^{-1}min^{-1}$ and 7.8064 to 37.47845 mgg^{-1} between 100 to 500ppm respectively. Coefficient of determination values ranged from 0.984 to0.999, a good illustration of the pesticide adsorption having followed *pseudo*-second-orderrate expression. Additionally, initial sorption rates, h,increased from 115.0363 – 393.438 $mgg^{-1}min^{-1}$between 100 to 500ppm respectively, as shown in Table 8.

Intraparticle Diffusion Model

Theintra-particle diffusion was determinedusing the intra-particlediffusion modelgiven in equation (15).

$$q_t = k_{id}t^{\frac{1}{2}} + I \quad \text{.....(15)}$$

where k_{id} is the intra-particle diffusion rate constant. According to equation 15, a plot of $q_t$versus $t^{1/2}$should be a straight line with a slope k_{id} and intercept I when adsorptionmechanism follows the intra-particle diffusion process as shown in Figure 13.

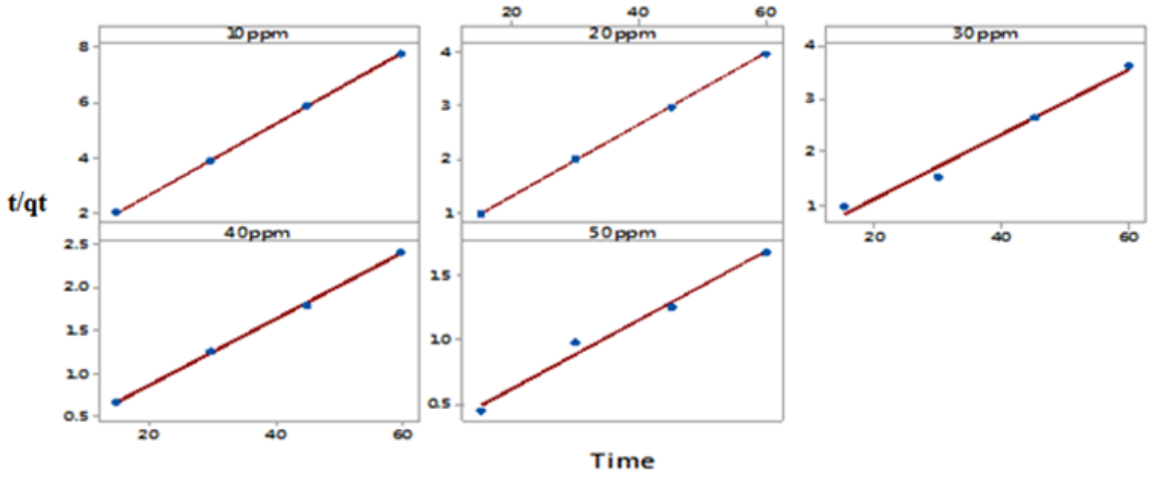

Figure 12: Pseudo second order model plot

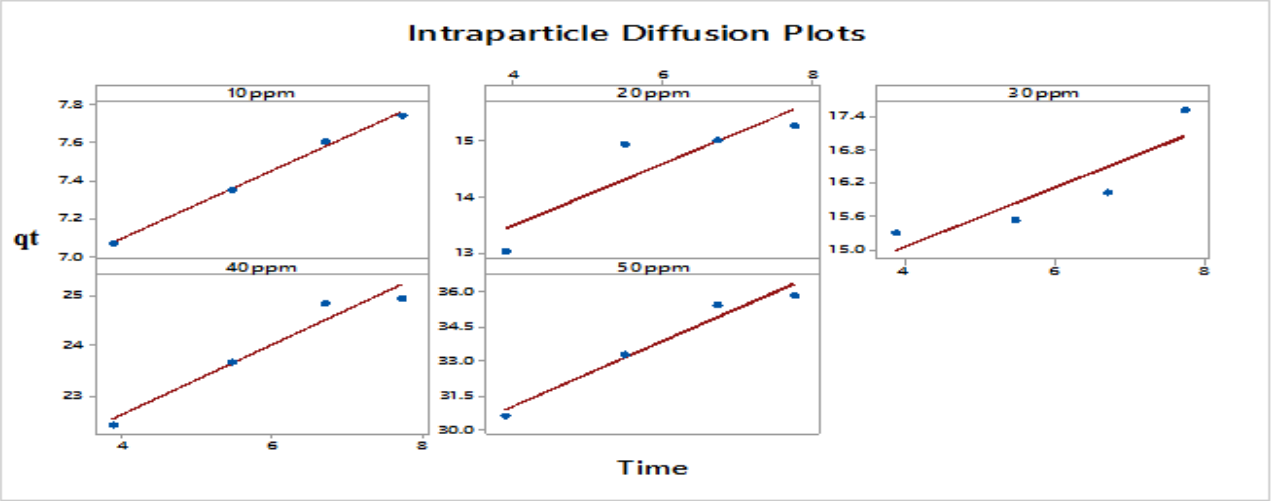

Figure 13: intra-particle diffusion model

The data obtained from the plots in Figure 13 above are summarized in Table 9.

Table 9: Intra-particle diffusion model parameters

Concentration(ppm)	I	k_{id}	R^2
100	6.386	0.1770	0.995
200	11.32	0.5458	0.796
300	12.90	0.5357	0.787
400	19.84	0.6953	0.953
500	25.37	1.4200	0.961

Lower regression values were obtained with the plots not passing the origin. The values for k_{id} and *I* were in a range of 0.177 – 1.42 and 6.386 – 25.37 respectively. *'I'*values are usually directly proportional to the thickness of the boundary layer[38]. Deviation of the lines from the origin is attributed tothe differences in the rate of mass transfer in the initial and final stages of adsorption, indicating that pore diffusion may not be the only rate controlling step [39].

4. Conclusion

The present study has shown that Lambda-cyhalothrin has a moderateadsorption capacity on Eburrusoils. This weak adsorption capacity is due to its low organic content. Also this adsorption behavior of Lambda-cyhalothrin depends significantly on the properties of the soil; like organic carbon, clay contents, organic matter and pH.The negativefree energydemonstrated by the Freundlich isotherm illustrates that the pesticide adsorbs onto Eburru soils spontaneously, althoughit's also shown to be affected by the solute concentration. In conclusion, the study recommends Eburru soil to be used for carrier materials in smart delivery of Lambda-cyhalothrin pesticide for improved agronomic practice.

Acknowledgement

The authors thank Kenya Bureau of Standards for availing the Lambda-cyhalothrin standard, Kenya Agricultural and Livestock Research Organization for soil analysis and the University of Nairobi, where this analysis was conducted.

References

1.Robson M. J and Crosby J., (1984). Insecticidal product and preparation thereof.European Patent Office.Patent Number EU 106469. UK.

2.Spurlock F., (2006). Synthetic pyrethroids and California surface water: use patterns, properties, and unique aspects. http://wwwcdprcagov/docs/sw/swposters/spurlock_acs06pdf.

3.Syngenta (2007). KARATE. http://wwwsyngentacom/en/products_services/karate_pageaspx .

4.Li-Ming H., John T., Albert W and Kean G., (2008). Environmental Chemistry, Ecotoxicity, and Fate of Lambda-Cyhalothrin.*Reviews of Environmental Contamination and Toxicology*.71 .Springer.

5.Bradbury S. P and Coats J. R., (1989). Toxicokinetics and toxicodynamics of pyrethroid insecticides in fish. Environ ToxicolChem 8:373–380.

6.Shafer T. J and Meyer D. A., (2004). Effects of pyrethroids on voltage-sensitive calcium channels: a critical evaluation of

strengths, weaknesses, data needs, and relationship to assessment of cumulative neurotoxicity. ToxicolApplPharmacol 196:303–318.

7.Burr S. A and Ray D. E., (2004).Structure-activity and interaction effects of 14 different pyrethroids on voltage-gated chloride ion channels.ToxicolSci 77:341–346.

8.Fernandez-Alvarez M, Sanchez-Prado L, Lores M, Llompart M., Garcia-Jares C, Cela R., (2007).Alternative sample preparation method for photochemical studies based on solid phase microextraction: synthetic pyrethroid photochemistry. J Chromatogr A Adv Sample Prep 1152:156–167.

9.Roessink I, Arts G. H. P, Belgers J. D. M, Bransen F, Maund S. J, Brock T. C. M., (2005). Effects of lambdacyhalothrin in two ditch microcosm systems of different trophic status. Environ ToxicolChem 24:1684–1696.

10.USDA, (2007). USDA-ARS Pesticide Properties Database: http://www.ars.usda.gov/Services/docs. htm?docid=14199.

11.USEPA, (2007). ECOTOX database.http://cfpubepagov/ecotox/quick_queryhtm.

12.Weston D. P, You J. C and Lydy M. J., (2004). Distribution and toxicity of sediment-associated pesticides in agriculture-dominated water bodies of California's Central Valley. Environ Sci Technol. 38:2752–2759.

13.Amweg E. L, Weston D. P, You J and Lydy M. J., (2006). Pyrethroid insecticides and sediment toxicity in urban creeks from California and Tennessee. Environ SciTechnol 40:1700–1706.

14.Freundlich H.M.F., (1906). Over the adsorption in solution. J. Phys. Chem. 57, 385–470.

15.Bansal R.C and Goyal M., (2005). Activated Carbon Adsorption, Boca Raton, Crc Press Taylor Francis Group.

16.Langmuir I (1918). The Adsorption of Gases on Plane Surfaces of Glass, Mica, and Platinum. J.A.M. Chem. Soc. 40, 1361-1403.

17.Redlich O. and Peterson D.L., (1959). A useful adsorption isotherm. J. Phys. Chem. 63, 1024–1029.

18.Temkin M. J and Pyzhev V., (1940). Kinetics of ammonia synthesis on promoted iron catalysts. ActaPhysiochim.Urs. 12, 217-222.

19.Mehlich A., (1953). Determination of P, Ca, Mg, K, Na, and NH4. North Carolina Soil Test Division (Mimeo 1953); 23-89.

20.Tran T. S and Simard R. R., (1993). Mehlich III-Extractable Elements. In: M. R. Carter, Ed. Soil Sampling and Methods of Analysis: 43-49.

21.Yang S.Y and Chang W.L., (2005). Soil Sci., 170, 55.

22.Gislason E.A and Craig N.C., (2005). Cementing the foundations of thermodynamics:comparison of system-based and surroundings-based definitions of work and heat, J. Chem.Thermodynamics 37: 954-966.

23.Jan-Åke P, Mårten W and Stephen O., (2008). Handbook for Kjeldahl Digestion:11- 42.

24.Carrolland Dorothy "Ion exchange in clays and other minerals". Geological Society of America Bulletin 70 (6): 749-780 (1959).

25.Turner R. C and Clark J. S., (1966). Lime potential in acid clay and soil suspensions. Trans. Comm. II & IV Int. Soc. Soil Science, pp. 208-215.

26.Manikandan A and Subramanian K. S. (2014). Fabrication and characterization of nanoporous zeolite based N fertilizer. African Journal of Agricultural Researc. Vol. 9(2): 276-284.

27.Bansiwal A. K; Rayalu S. S; Labhasetwar N. K; Juwarkar A. A and Devotta S (2006).Surfactant-modified zeolites as slow release fertilizer for phosphorus. J. Agri. Food Chem. 54:4773-4779.

28.Vanderborght M and Van Grieken E., (1997). "Enrichment of trace metals in water by adsorption on activated carbon," *Analytical Chemistry*, vol. 49, no. 2, pp. 311–316.

29.Gupta S, Handa S. K and Sharma K. K., (1998). A new spray reagent for the detection of synthetic pyrethroids containing a nitrile group on thin-layer plates.Talanta 45:1111–1114.

30.Wang S, Kimber L, and Kennedy I. R., (1997). The dissipation of lambda-cyhalothrin from cotton production systems. J Environ Sci Health B B32:335–352.

31.European-Commission, (2001). Review report for the active substance lambda-cyhalothrin. 7572/VI/97-final.http://ec.europa.eu/food/plant/protection/evaluation/existactive/list1-24_en.pdf.

32.Ali M. A and Baugh P. J., (2003). Sorption-desorption studies of six pyrethroids and mirex on soils using GC/MS-NICI. Int J Environ Anal Chem 83:923–933.

33.Oudo H, Hansen H. C., (2002). Sorption of lambda-cyhalothrin, cypermethrin, deltamethrin and fenvalerate to quartz, corundum, kaolinite and montmorillonite. Chemosphere 49:1285–1294.

34.Zhou J. L, Rowland S and Mantoura C., (1995). Partition of synthetic pyrethroid insecticides between dissolved and particulate phases. Water Res 29:1023–1031.

35.Bondarenko S, Putt A, Kavanaugh S, Poletika N and Gan J. Y., (2006). Time dependence of phase distribution of pyrethroid insecticides in sediment. Environ ToxicolChem 25:3148–3154.

36.Lagergren S., "ZurTheorie der sogenannten Adsorption gelosterStoffe," KungligaSvenskaVetenkapsakademiens, Handlingar 24, 1-39 (1898).

37.Ho Y. S., (2006). "Review of second order models for adsorption systems," *J. Hazard.Mater*. 136, 681-689.

38.Anirudhan T.S and Suchithra P.S., (2012). "equilibrium, kinetic and thermodynamic modelling for the adsorption of heavy metals onto chemically modified hydrotactile', Ind. J. Chem. Technol, vol.17, pp.247-259.

39.Kannan K, and Sundaram M. M., (2001). "Kinetics and mechanism of removal ofmethylene blue by adsorption on various carbons e a comparative study," *DyesPigments* 51, 25

International Journal of Scientific Research in Science, Engineering and Technology (www.ijsrset.com)
© 2020 IJSRSET | Volume 7 | Issue 3 | Print ISSN: 2395-1990 | Online ISSN : 2394-4099
DOI : https://doi.org/10.32628/IJSRSET207349

Characterization; Formulation and Application of Natural Nano Zeolitic Materials from Kenya as Smart Delivery Systems for Fertilizers and Pesticides

*Gabriel A. Waswa[1], Immaculate N. Michira[1], Debora A. Abong'o[1], Dickson Andala[2], Austin O. Aluoch[3]
[1]Department of Chemistry, University of Nairobi, Nairobi, Kenya
[2]Department of Chemistry, Multimedia University of Kenya, Nairobi, Kenya
[3]Department of Chemical Science and Technology, Technical University of Kenya, Nairobi, Kenya
*Corresponding author's E-mail address: waswagabriel@gmail.com[1]

ABSTRACT

This study aimed at using natural zeolitic materials sampled form different places and characterized as nano porous smart delivery systems for storage and controlled release of fertilizer and pesticide molecules. XRD characterization of sample ZT-GA-01 showed that it was zeolite A artificial, abbreviated as Linde Type A (LTA), sample EL-GA-06 was Phillipsite natural zeolites. IR Spectroscopy for ZT-GA-01 and EB-GA-02 showed similar peaks between 3420 – 3480 cm-1, 2350 – 2360 cm-1 and 1630 – 1660 cm-1 indicating H-O-H stretching and bending, while 440 – 670 cm-1 representing Si-O-Si bending for internal tetrahedral. Besides comparable EDX characterized silica to alumina composition of sample EB-GA-02 and the artificial zeolite A applied as the standard, determined as 37.4 % to 18.8 % and 43.6 % to 56.4 % respectfully. Physical properties of samples ZT-GA-01 and EB-GA-02 in terms of BET surface area, BJH pore volume and pore sizes were obtained as; 0.6716 m2/g, 0.002333 cm3/g, 151.519 Å and 0.7099 m2/g, 0.006767 cm3/g, 389.846 Å respectively. Urea loaded samples EB-GA-02 indicated a 39.844 % reduction in pore sizes after successful loading of urea fertilizer into the nano-spaces, while pesticide loading indicated a reduction in pore volumes and pore sizes by 19.15 % and 32.74 % respectively. The simulated release shoed about 82.8 % of stacked urea fertilizer discharged in water and 74.2 % loaded urea released in soil, while 34.4 % and 40.1 % lambda cyhalothrin pesticide amounts were released by pesticide loaded zeolitic sample EB-GA-02 in water and soil respectively. Application of zeolitic sample EB-GA-02 as smart delivery systems demonstrated a sustained slow release of both urea and Lambda cyhalothrin pesticide on tomato and spinach growing and monitoring experiments for the 60 days' period. In conclusion, our study showed that there exist zeolites and zeolitic materials in some selected parts in Kenya. As well, identified zeolitic sample EB-GA-02 can be used to successfully store agrochemical molecules and significantly delay their release in soil hence applied as nanozeolitic smart delivery systems.

Keywords : Zeolites, Nanopores, fabrication, Smart Delivery Systems

I. INTRODUCTION

To enhance productivity for many decades, uses of fertilizer and pesticides have been applied in the agricultural sector as a measure for sustainable livelihood. Of concern now however, are the counter effects of sustained addition of these chemical components to the environment. Aspects like imbalanced fertilization, decreasing soil organic matter, increasing environmental pollution through processes like leaching, eutrophication, bioaccumulation or otherwise, have a direct correlation to the type and amount of fertilizer and pesticides introduced to the environment, factors that

could hamper the intended increased productivity in the long ran. Besides, a number of researchers (Shaviv, 2000; Chinnamuthu and Boopathi, 2009; Brock *et al*., 2011), have indicated that averagely only 35 % for nitrogen and 20 % for phosphorous fertilizers are actually utilized efficiently by plants. This raises concerns, because it seems that a significant percentage of fertilizer applied is actually not utilized by plants. Meaning, the increased production is not achieved as anticipated and also more chemical pollutant components are continuously added to the environment. To mitigate these dynamics, modern practices are being adopted, many of which integrate the latest line of technological innovations such as the use of Nanotechnology in agriculture, where a great focus on nanostructured formulations of fertilizer and pesticides, through new mechanisms such as target delivery or slow/controlled release, employing carrier agents such as zeolitic materials (materials which contain some percentage of zeolites or having zeolite like properties) could be applied. Usually, they contain crystalline aluminosilicates (Manikandan and Subramanian, 2013) with a series of microporous, mesoporous and nanoporous structures in which ions or molecules can be immobilized through processes like ion exchange and chemisorption mechanisms as a way of loading or encapsulating fertilizer or pesticides to be delivered to plants, while acting as slow/ controlled release process (Chinnamuthu and Boopathi, 2009; Naderi *et al*., (2013). This research focused on formulation of nanozeolitic materials from sampled rocks in selected places within Kenya, characterization and exploration of their applicability on selected fertilizer and pesticide as carrier agents for target delivery or slow/controlled release on selected vegetable production with the intention of enhanced productivity alongside reduced environmental pollution.

II. MATERIALS AND METHODS

Commercial Purchased zeolites (CPZ, from Sigma-Aldrich, P-Code: 101554254, Lot # BCBM 9330V and CAS:1318-02-1.) labeled as sample ZT-GA-01, natural zeolitic rock samples labeled EB-GA-02, MG-GA-03, BG-GA-04, NG-GA-05, EL-GA-06, Urea (analytical standard 99 % pure from IOBA Chemie), Lambda cyhalothrin (analytical standard 99 % pure from IOBA Chemie), Acidified dichromate, Barium chloride, Concentrated Sulfuric acid, Potassium sulfate, Copper sulfate, Selenium sulfate, Concentrated hydrochloric acid, Ammonium acetate, Potassium chloride, Potassium bromide (all analytical standards 99 % pure from IOBA Chemie) and soil sample KIK-GA-01. UV-Visible spectrometer, X-ray diffractometer (XRD, D2 Phaser SSD160 A26-X1-A2DOB2B1, 2nd Gen. from Bruker), Fourier Transform Infrared (FTIR, IR Tracer-100 from Shimadzu), Energy dispersive spectrophotometer (EDS, Shimadzu EDX-720), Analytical balance (Fischer A-160), Orbital shaker (Fischer G-18), Atomic absorbance spectrophotometer (AAS, Perkin Elmer 2100), XRay fluorescence spectrometer (XRF, TITAN 600), Scanning Electron Microscope (SEM, Hitachi S4800), ASAP 2020 Micromeritics equipment, Flame photometer (Sherwood scientific 410), Calcinator (N3A Simon Muller 220V Berlin). Sample EB-GA-02 was collected from Eburru volcanic crater (0.63S, 36.23E), which is located about 8 Km North-West of Lake Naivasha within the Kenyan Rift Valley. Sample MG-GA-03 were collected along the shores of Lake Magadi, as relatively homogeneous bare surface deposits spatially extending 200 m by 10 m. Sample BG-GA-04 were collected on Ol Arabel and Endao seasonal riverbeds near their entry to Lake Baringo. Sample NG-GA-05 was collected from a quarry at Ebul bul (1^0 22'S and $36^0$38'E) near Ngong town in Kajiado County. Sample EL-GA-06 was collected from Kitum caves found at the foot of Mt. Elgon. Sample KIK-GA-01 was collected in Kikuyu area, Kiambu County, at a depth not exceeding 40 cm in arable land, previously having maize and vegetables intergrown,

while sample ZT-GA-01 was commercial zeolitic material samples purchased from Sigma Aldrich. The preparation of the natural zeolitic rock material samples labeled as EB-GA-02, MG-GA-03, BG-GA-04, NG-GA-05 and EL-GA-06 involved mechanical grinding, sieving using 0.85 mm and calcination at 550 °C for 2 hours. KIK-GA-01 and ZT-GA-0 were used as received in all the experiments, without further preparation. Characterization methods included X-Ray Diffraction (XRD), Energy Dispersive X-Ray Spectroscopy (EDX), Fourier-Transform Infrared Spectroscopy (FT-IR), X- Ray Fluorescence Spectroscopy (XRF), Scanning Electron Microscopy (SEM); all followed standard procedures. Soil content analysis and kinetics of fertilizer and pesticide adsorption on zeolitic materials was as reported in our previous publications Waswa *et al.,* 2017(a), Waswa *et al.,* 2017(b), Waswa GA *et al.*, 2018. Modelling efficiency of fertilizer loaded zeolitic materials in crop production procedures involved "pot-set-ups" studied in the form of blank experiments, control experiments and actual monitoring experiments with the crops grown under uniform environmental conditions and crop husbandry practice. Data collection involved determination of the concentration of urea in the soil at a depth of 30 cm over a two months' period, at 5, 20, 30, 45 and 60 days' intervals. Concentration determinations in triplicates were conducted using UV-Spectrophotometry studies. Additional data collection was also done on the physical comparisons of the respective crops in regard to vigor index, size, colour and yield over the entire crop cycle. Efficiency of pesticide loaded zeolitic materials in crop production followed a similar model adopted for fertilizer studies.

III. RESULTS AND DISCUSSION

X-ray diffraction analysis of sample ZT-GA-01(Figure 1) show distinct peaks similar to the ones reported by Treacy *et al.*, (2001), having 2θ values of characteristic artificial zeolite A at 7.2°, 10.3°, 12.6°, 16.2°, 21.8°, 24°, 26.2°, 27.2°, 30°, 30.9°, 31.1°, 32.6°, 33.4° and 34.3°.

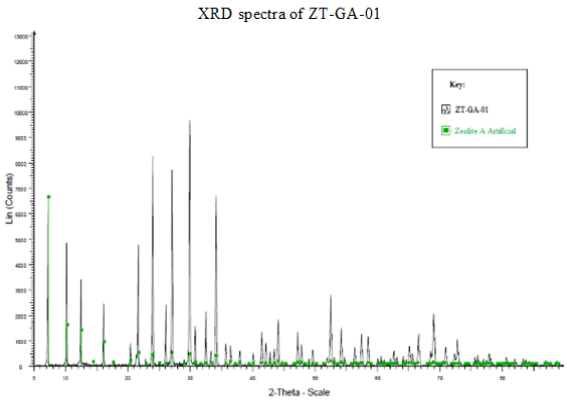

Figure 1: XRD spectra of ZT-GA-01

According to Treacy and Higgins (2001), in their collection of simulated XRD powder patterns for zeolites, zeolite A Artificial is abbreviated as Linde Type A (LTA), having a chemical composition of $[Na_{96}(H_2O)_{216}][Si_{96}Al_{96}O_{384}]$, crystal data of: a = 24.61Å, b = 24.61Å, c = 24.61Å, α=90°, β=90°, γ=90° and X-ray single refinement (Rw) = 0.04, hence the commercial zeolite sample ZT-GA-01 were classified as Zeolite A. Other natural rock samples EB-GA-02, MG-GA-03, BG-GA-04 and NG-GA-05 were analyzed to determine their similarity with sample ZT-GA-01 above. These rocks were characterized while in their natural state after calcination, without any advanced purification process, hence this explains the presence of non-uniform peaks and additional mineral peaks detected.

XRD characterization of zeolitic sample EB-GA-02 gave the characteristic spectrum shown by figure 2.

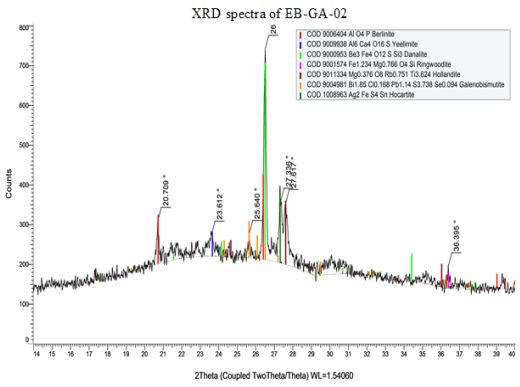

Figure 2: XRD spectra of EB-GA-02

Donalite, Hollandite and Berlinite minerals were found to be the most predominant in this sample at 41.2%, 21.6% and 14.3% respectively.

Figure 3 indicates XRD information generated by sample MG-GA-03.

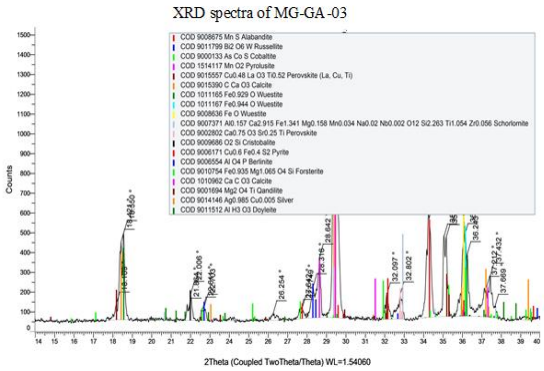

Figure 3: XRD spectra of MG-GA-03

This sample was mainly of trona origin composed of mineral salt calcite. For zeolitic sample BG-GA-04, it's XRD characterization spectrum is shown by figure 4.

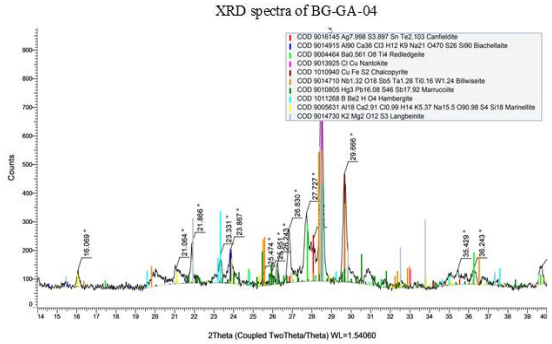

Figure 4: XRD spectra of BG-GA-04

This sample was mainly found to contain Hambergite and Langbeinite minerals at 42.5% and 12.3% respectfully, which are accessory minerals in granite pegmatites.

Analysis of zeolitic sample NG-GA-05 gave the spectrum in figure 5.

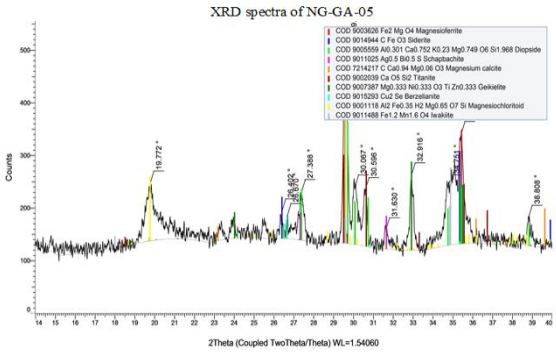

Figure 5: XRD spectra of NG-GA-05

This sample was found to contain Diopside and Titanite minerals in greater quantities.

XRD characterization of zeolitic sample EL-GA-06 generated the spectrum and diffraction parameters recorded in figure 6.

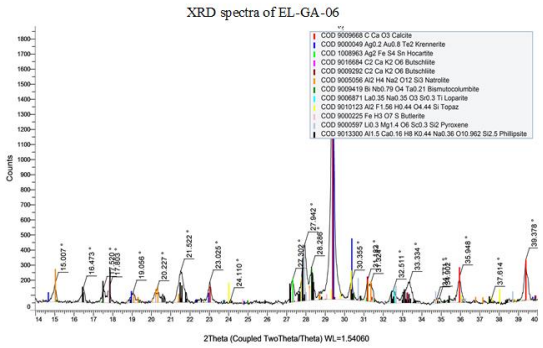

Figure 6: XRD spectra of EL-GA-06

Mineral composition of this sample indicated presence of natural zeolites like Phillipsite, Natrolite and Krennerite. Sample EL-GA-06 was found to be natural zeolites of Phillipsite nature.

Energy Dispersive X-Ray Spectroscopy (EDX) was done to characterize the samples in terms of elemental oxides composition. Zeolite A which was commercially acquired contained mainly oxides of Aluminium and Silicon at 56.000% and 44.000% respectively, as shown by table 1, with its corresponding spectrum (figure 7) below. This was used as standard reference in Energy Dispersive characterization of the other samples.

TABLE I. EDX QUANTITATIVE RESULTS OF SAMPLE ZT-GA-01

Analyte	Result %	Standard Deviation	Intensity (cps/uA)
Al_2O_3	56.368	1.335	0.0721
SiO_2	43.632	0.398	0.4315

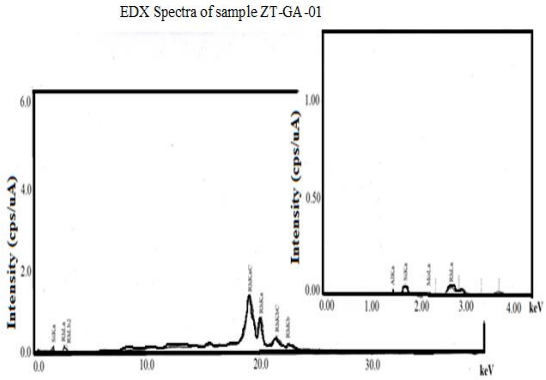

Figure 7: EDX Spectra of sample ZT-GA-01

Characterization of sample EB-GA-02 indicated oxides of Aluminium and Silicon at 18.8 % and 37.4 % respectively, alongside other oxides like of Fe and K. Multiple peaks corresponding to the present elements are illustrated by the spectrum in figure 8 below.

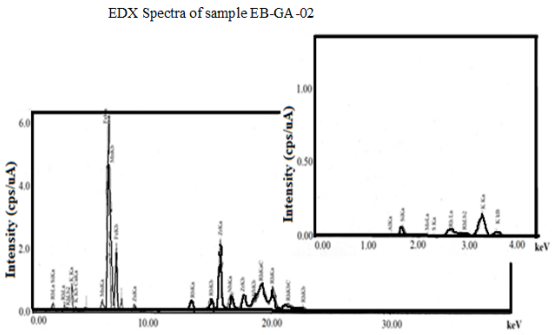

Figure 8: EDX Spectra of sample EB-GA-02

Fourier-Transform Infrared spectra of the zeolitic samples ZT-GA-01, EB-GA-02, MG-GA-03, BG-GA-04 and NG-GA-05 were scanned in the mid and far (4000-400cm^{-1}) infrared regions to generate distinct peaks as assigned in table 2 below. According to Clark *et al.*, 2004, strong fundamental vibrations of the alumino silicate framework of minerals and glasses, as well as the principal vibration modes of most molecular species like Si-O, C-O, S=O and P-O are located in the mid IR-region. (Can *et al.*, 2003, Wlodzimier *et al.*, 2011, Sitarz *et al.*, 1997, Mozgawa *et al.*, 2005).

TABLE II. AN OVERVIEW OF INFRARED BAND POSITIONS OF STUDIED ZEOLITIC MATERIALS

Wavenumbers (cm^{-1})					Assignments
ZT-GA-01	EB-GA-02	MG-GA-03	BG-GA-04	NG-GA-05	
3471.87	3421.72	3421.72	3421.72	3444.87	H-O-H Stretching of absorbed water (Mozgawa *et al.*, 2005)
-	-	2924.09	2924.09	2924.09	C-H Stretching
2357.01	2360.87	2360.87	2360.87	2360.87	-
1654.92	1635.64	1774.51	1774.54	-	H-O-H Bending of water
-	-	1438.90	1438.90	1435.04	C-H Stretching
-	-	1033.85	1033.85	1037.70	Si-O Assymetric stretch for internal tetrahedral (Sitarz *et al.*, 1997)
-	-	875.68	875.68	-	OH Deformation linked to $2Al^{3-}$ (Wlodzimier *et al.*, 2011)
-	786.96	702.09	702.09	775.38	Si-O quartz (Wlodzimier *et al.*, 2011)
663.51	-	-	-	-	Si-O-Si Bending (Can *et al.*, 2003)
-	447.49	-	-	-	Si-O-Si Bending for internal tetrahedral (Can *et al.*, 2003)

X-Ray Fluorescence spectroscopy (XRF) summary of data for all the analysed indicated that sample ZT-GA-01, which was used as the standard, being zeolite A obtained commercially had very low concentration units of the listed elements. Cu at 148 ppm was detected as the highest concentration of impurities, followed by Ti at 127 ppm and Mn at 82.1 ppm. Most of the other impurities like Pb, Nb, Y and Rb were below 5ppm. Additionally, this sample had percent by weight of less than 0.08 of K, Ca and Fe elements, which indicates a high level of purity of the commercial zeolites. Comparatively, sample EB-GA-02 had the highest composition of Ti impurities at 2478ppm, Mn at 2358ppm, Zr at 2111 ppm and Cu at 1901 ppm, while the other impurities like Pb, Nb, Y and Rb mostly being below 300ppm. This sample had percent by weight between 0.3 – 7.00 of K, Ca and Fe elements. Hence, effective purification process could improve the extent of zeolitic comparability to sample ZT-GA-01, if carried out, process that was beyond the scope of this current research work.

Scanning Electron Microscopy (SEM) images provided information on sample surface morphology and particle sizes. Sample ZT-GA-01 which was artificial commercial zeolite A showed aggregated cubical particles of uniform sizes (Figure 9).

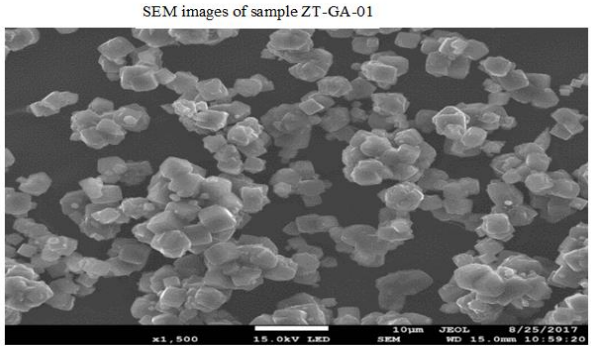

Figure 9: SEM images of sample ZT-GA-01

They had better defined crystals with regular shapes, which seemed to have well-developed structures on surface and converged particles. These are similar observations made by Pereira *et al.* (2012) and Mohanraj (2013). This could probably be due to high levels of crystal purity. The rest of the samples had non uniform surface morphologies and particle sizes (Figure 10). These SEM images were from raw natural zeolitic materials which would have probably given more elaborate images on purification and particle reduction processes.

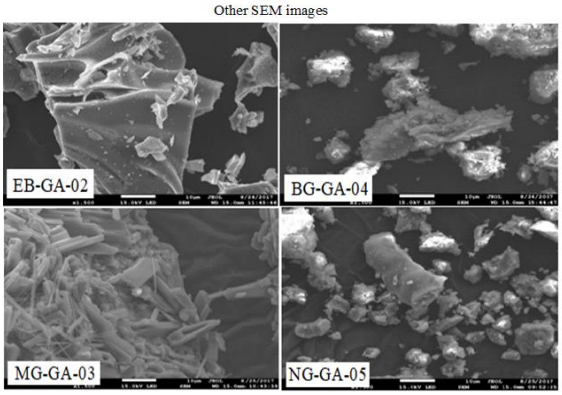

Figure 10: Other SEM images

Nitrogen adsorption-desorption isotherm of commercial zeolite sample ZT-GA-01 and natural zeolitic rock sample EB-GA-02 are presented in figure 11 below. These isotherms show variation in adsorption between pressures below 0.2, 0.3 - 0.6 and above 0.8, giving a similarity to type IV isotherm commonly shown by mesoporous materials (Sing *et al.,* 1985). At relatively higher pressure desorption levels, there is formation of narrow hysteresis loops which could be associated with mesopore capillary condensation. Pressure zon 0.3 – 0.6 could represent completion of monolayer coverage and formation of multilayer process. Physical properties of samples ZT-GA-01 and EB-GA-02 in terms of BET surface area, BJH pore volume and pore sizes were obtained as; 0.6716 m^2/g, 0.002333 cm^3/g, 151.519 Å and 0.7099 m^2/g, 0.006767 cm^3/g, 389.846 Å respectively. Urea loaded samples EB-GA-02 indicated a 39.844 % reduction in pore sizes after successful loading of urea fertilizer into the nano-spaces, while pesticide loading indicated a reduction in pore volumes and pore sizes by 19.15 % and 32.74 % respectively.

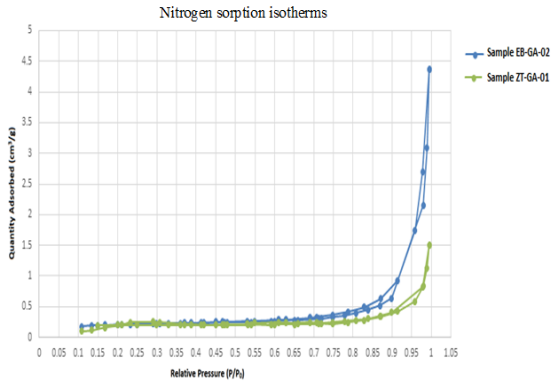

Figure 11. Nitrogen sorption isotherms of samples ZT-GA-01 and EB-GA-02.

The results and discussions on kinetics of fertilizer and pesticide sorption on zeolitic materials were as reported in our initial work Waswa *et al.,* 2017(a) and Waswa *et al.,* 2017(b). Results of Loading of fertilizer into zeolitic materials showed X-Ray diffraction analysis of urea loaded sample EB-GA-02 (Figure 12) indicated 2θ peaks values of 22, 24.5, 29.5, 32, 35.5, 37, 38.5, 40.5, 41.5, 45.5 and 55 corresponding to urea peaks.

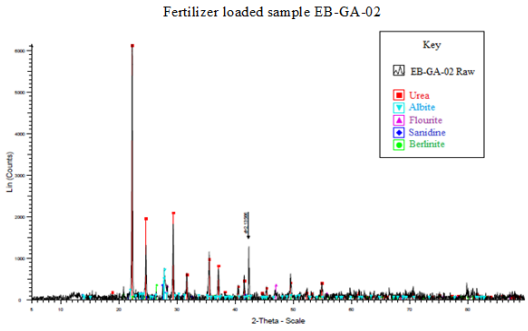

Figure 12: Fertilizer loaded sample EB-GA-02

Fourier Transform Infrared analysis of urea fertilizer showed major peaks at 3348.42-3444.87cm^{-3}, 1624.06-1681.93cm^{-3} and 1465.90cm^{-3} corresponding to N-H, C=O and C-N functional groups respectively (Stuart, 2004). The spectrum of Urea loaded sample EB-GA-02 below (figure 13) contained distinct peaks appearing on the urea spectrum at 3348.42-3444.87cm^{-3}, 1624.06-1681.93cm^{-3} and 1465.90cm^{-3}, corresponding to N-H, C=O and C-N stretching vibrations for the urea fertilizer functional groups respectively. The SEM image obtain are shown by figure 14.

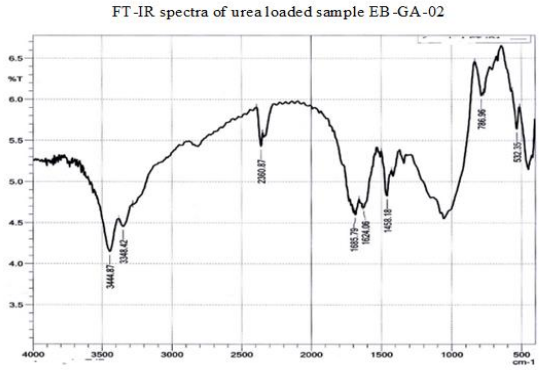

Figure 13: FT-IR spectra of urea loaded sample EB-GA-02

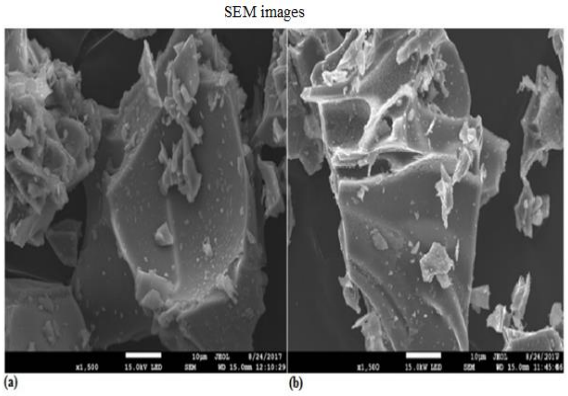

Figure 14: SEM images of (a) urea loaded sample EB-GA-02 (b) blank sample EB-GA-02

Controlled release behavior of fertilizer loaded zeolitic materials EB-GA-02 in water had 82.8 % and 74.2% in soil. Urea loaded sample KIK-GA-01 had 0.071309 moldm^{-3} at 58.9% desorption discharge rate, a low percentage likely due to high organic carbon content with stronger binding forces, all with a rapid initial and then steady sustainable rate. These comparative discharge for urea loaded sample EB-GA-02 in aqueous medium, in Kikuyu soil and in aqueous medium was presented by 'a', 'b' and 'c' respectively in the 'key' for figure 15 where urea loaded sample KIK-GA-01 had the least discharge amount of urea in aqueous medium. Beyond the 12 days, the bars of discharge of urea loaded sample EB-GA-02 in aqueous medium was higher proportionally than the others. This implies that loading urea fertilizer into sample EB-GA-02 and applying the same as carrier agents had a better sustained release rate, which could still

avail the minimum remaining fertilizer to the crops for slightly longer duration than the direct application.

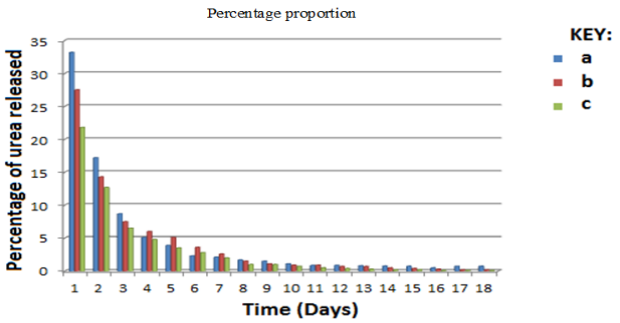

Figure 15: Percentage proportion variation of urea release

Efficiency of fertilizer loaded zeolitic materials in crop production showed urea loaded zeolitic sample EB-GA-02 having a sustained slower but extended releases rate when applied for tomato monitoring (Figure 16) and spinach monitoring (Figure 17). In both of these figures, it was observed that the graph of urea loaded zeolitic sample EB-GA-02 initially had a lower concentration, but beyond the 25th day, they recorded slightly higher concentration compared to concentration determined by direct fertilizer application. For tomato studies, urea loaded zeolitic sample EB-GA-02 gave a difference of almost 17.00% higher concentration, while a difference of about 16.00% higher concentration was recorded on spinach between the 25th and 35th.

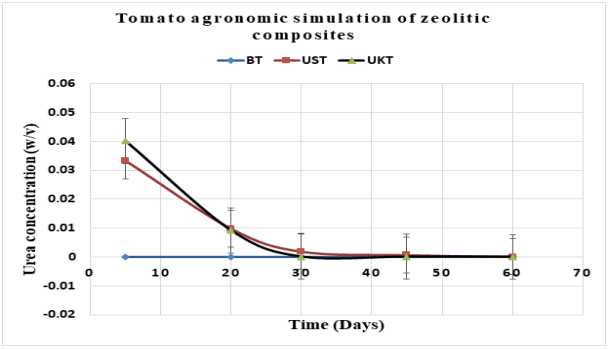

Figure 16: Comparative slow release rates for urea loaded zeolitic materials in tomatoes studies

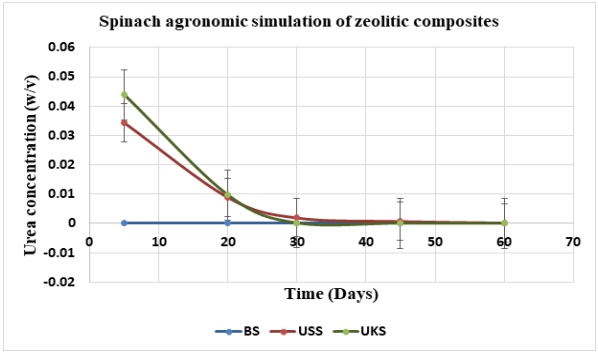

Figure 17: Comparative slow release rates for urea loaded zeolitic materials in spinach studies

Therefore, these observations indicate that it is possible to apply urea loaded zeolitic sample EB-GA-02 as carrier agent for urea fertilizer in which the rate of delivery of urea molecules to both tomato and spinach can be monitored. The sustained concentration of urea in the soil over the entire monitoring duration indicated slow delivery process which helps avail the urea nutrients to the plant over a longer duration.

Loading of pesticides into the zeolitic materials indicated that, 79.4% of Lambda cyhalothrin pesticide was loaded in the weighed mass of the sample EB-GA-02. Confirmation of loading the pesticide molecules into the samples was done using X-Ray diffraction and Fourier Transform Infrared analysis. X-ray diffraction analysis of Lambda cyhalothrin pesticide loaded sample EB-GA-02 (figure 18) indicated the pesticide 2θ values at 28.5, 33, 47, 56, 58.5, 68.5, 76, 78 and 87 degrees.

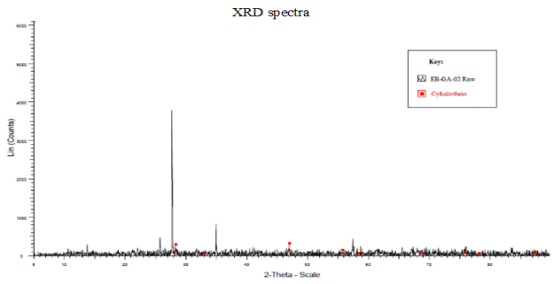

Figure 18: XRD spectra of pesticide loaded sample EB-GA-02

While FT-IR analysis gave the spectrum shown in figure 19 below, with peaks corresponding to some of the functional groups present in Lambda cyhalothrin molecule. The corresponding SEM images are shown by figure 20.

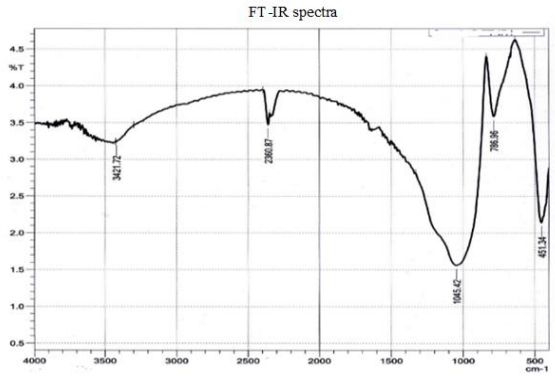

Figure 19: FT-IR spectra of pesticide loaded sample EB-GA-02

From the Infrared spectrum, some specific peaks associated with some functional groups present in Lambda cyhalothrin structure can be identified. These includes 3695.61cm^{-1} associated with C-H stretching in heterocyclic compounds,1635.64cm^{-1} for esters, 1037.7 cm^{-1} for C-O stretching in ethers and 794.67 cm^{-1} that could be associated with C-F stretching for halogen substituted organic compounds (Stuart, 2004).

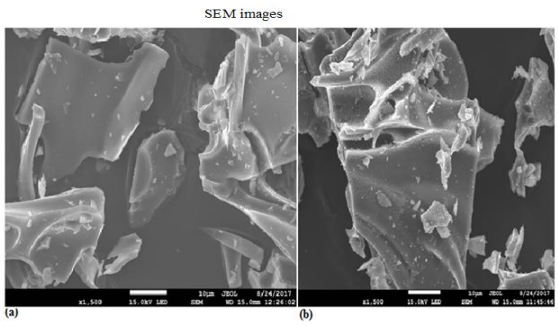

Figure 20: SEM images of (a) pesticide loaded sample EB-GA-02 (b) blank sample EB-GA-02

Comparative discharge studies were conducted between the pesticide loaded sample EB-GA-02 in aqueous medium, pesticide loaded sample EB-GA-02 in Kikuyu soil and finally pesticide loaded sample KIK-GA-01 in aqueous medium. The results obtained were represented in figure 21. The rate of discharge of the pesticide loaded zeolitic materials in aqueous medium was the highest as seen by graph x having the steepest initial gradient. This could be attributes to very low organic matter content present in these natural rock materials, hence exhibiting low physicochemical interaction between the Lambda cyhalothrin molecules and the sorption sites of the rock.

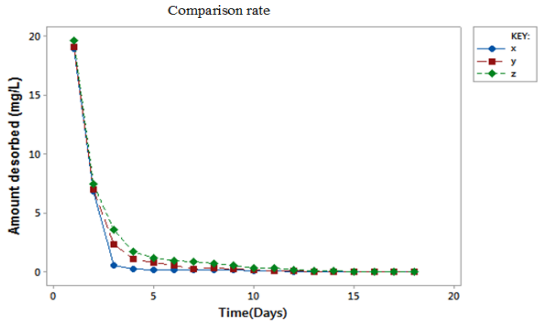

Figure 21: Comparison rate of pesticide release (Where x represents pesticide loaded

EB-GA-02 release in aqueous medium, y represents pesticide loaded sample EB-GA-02 mixed with soil from Kikuyu and z represents pesticide loaded sample KIK-GA-01release in aqueous medium. Pesticide loaded Kikuyu soil (sample KIK-GA-01) had the least discharge of the loaded pesticide in aqueous medium as represented by 'z' illustrated by plots and the bar chart in figure 22. This soil had higher carbon content at 2.7%, with more silt and clay medium in it, which could imply a relatively higher physicochemical interaction between the Lambda cyhalothrin molecules and the soil particles. This implies that more pesticide molecules were retained by the soil molecules and matrix.

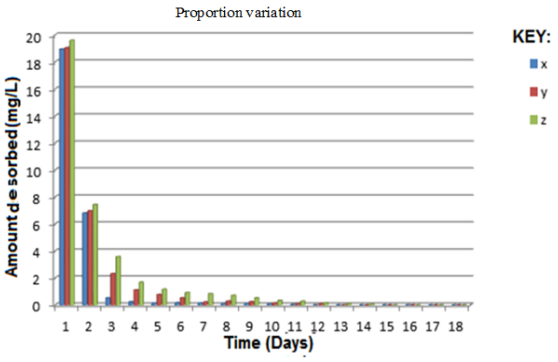

Figure 22: Proportion variation of pesticide release (Where x represents pesticide loaded sample EB-GA-02 release in aqueous medium, y represents pesticide loaded sample EB-GA-02 mixed with soil from

Kikuyu and z represents pesticide loaded sample KIK-GA-01 release in aqueous medium).

Efficiency of pesticide loaded zeolitic materials in crop production for tomatoes monitoring studies indicated a sustained slow decrease when pesticide loaded zeolitic sample EB-GA-02 were applied as compared to direct application of the pesticide (Figure 23).

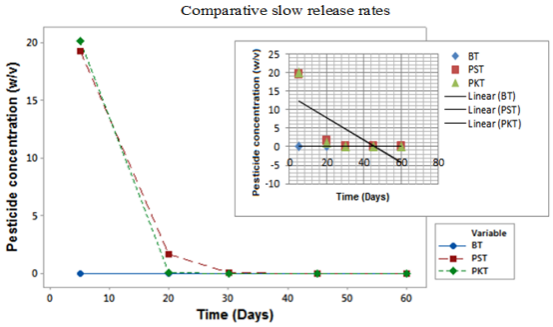

Figure 23: Comparative slow release rates for pesticide loaded zeolitic materials in tomatoes studies

Initially, there was more pesticide in the soil where direct application was done, mainly over the first 10 days, but around the 20th day, a higher concentration of Lambda cyhalothrin which was more than fivefold, was recorded for the soils in the experiments done using pesticide loaded zeolitic sample EB-GA-02 at almost 70% difference.

Similar trends were observed when it came to spinach studies. Generally, over the 60 days duration, there was a more sustained release of Lambda cyhalothrin pesticide into the soil by the pesticide loaded sample EB-GA-02 (Figure 24). Higher concentration amounts were noted in the soil, particularly from the 15th day to the 35th day, with a 69% highest value recorded around the 30th day. These findings reinforced the idea of sustained and controlled release of pesticide molecules by the zeolitic loaded samples. Hence, zeolitic samples EB-GA-02 were successfully used as smart delivery systems for lambda cyhalothrin pesticide when applied to both tomatoes and spinach studies.

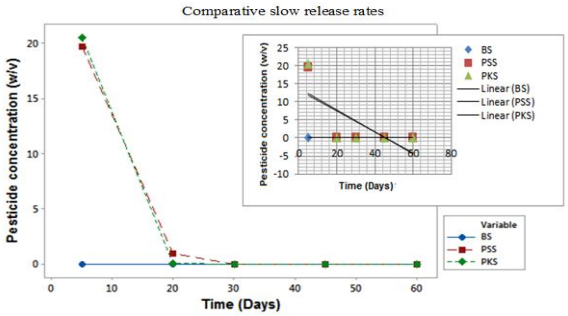

Figure 24: Comparative slow release rates for pesticide loaded zeolitic materials in spinach studies

IV. CONCLUSION

Zeolitic materials labeled EB-GA-02, MG-GA-03, BG-GA-04, NG-GA-05 and EL-GA-06 were explored from five different sites in Kenya and characterized using XRD, XRF, EDX and FT-IR compared to artificial zeolite A (sample ZT-GA-01) as the standard. Sample EL-GA-06 was found to be mainly natural zeolite Phillipsite with some Nitrolite deposits; sample EB-GA-02 had a higher favourable similarity in silica and alumina ratio to the standard, besides it's morphological properties like porosity and large quantity deposits that made it preferred for nanozeolitic formulation for smart delivery system. Formulation nanozeolitic smart delivery system indicated that 35.00 % of urea fertilizer and 79.40 % of Lambda cyhalothrin pesticide were loaded separately in the nonopore spaces of the sample EB-GA-02 forming urea loaded nanozeolitic sample EB-GA-02 and pesticide loaded nanozeolitic sample EB-GA-02 smart delivery systems. Simulation studies showed 82.80% and 74.20% of loaded urea molecules were separately released in water and soil respectfully, while 34.40% and 40.10% of the loaded Lambda cyhalothrin molecules were separately released in soil and water respectfully. Urea loaded nanozeolitic smart delivery system samples demonstrated a sustained slower but extended release rate when applied to both tomatoes and spinach crops. A difference of 17.00% and 16.00% higher urea concentration in soil was recorded on tomatoes and spinach crops respectfully between the 20th and 35th day as compared to just direct urea application to the

soil. Similarly, pesticide loaded nanozeolitic smart delivery system samples gave a difference of 70.00% and 69.00% higher Lambda cyhalothrin pesticide concentration in soil recorded for tomatoes and spinach respectfully around the 20th day for each. These observations demonstrated the application of nanozeolitic sample EB-GA-02 in formulation of nanosmart delivery system that can aid in slow and controlled release and delivery of fertilizer and pesticide to crops.

IV. ACKNOWLEDGEMENT

I would like to acknowledge the National Commission for Science, Technology and Innovation (NACOSTI) and the National Research Fund (NRF) for their Endowment Funds for this Project. The following institutions availed instruments for various analysis: State Department of Infrastructure Material Testing and Research Division in Kenya, Mines and Geology Department in Kenya, Kenya Agricultural and Livestock Research Organization, University of Nairobi College of Biological and Physical Sciences and St. Austin's Academy Chemistry Laboratory. The following people provided their special support that helped to obtain project objectives: Dr. A. K. Waswa from Department of Geology, UoN for your insights on zeolites, Mr. J. K. Mbugua PhD student from Chemistry Department UoN for being part of my research team and hosting my field work studies, Mr. J. Njoroge from Infrastructure Material Testing and Research Division for facilitating some of our laboratory works.

V. REFERENCES

[1]. Brock, D. A., Douglas, T.E., Queller, D. C. & Strassmann, J. E. (2011). Primitive agriculture in a social amoeba. Nature 469: 393-396.

[2]. Can, L. & Zili, W. (2003). Microporous Materials Characterized by Vibrational Spectroscopies. In Handbook Zeolite Scie. CRC Press, 2003.

[3]. Chinnamuthu, C. R. & Boopathi, P. M. (2009). Nanotechnology and Agroecosystem. Madras Agricultural Journal 96:17-31.

[4]. Clark, R. N. (2004). Spectroscopy of rocks and minerals, and principles of spectroscopy. In Infrared Spectroscopy in Geochemistry Exploration. Geochemistry and Remote Sensing. Mineral Association Canada, Short course, 33, 17-35.

[5]. Manikandan, A. & Subramanian, K. S. (2014). Fabrication and characterisation of nanoporous zeolite-based N fertilizer. African Journal of Agricultural Research. Vol. 9(2), pp. 276-284, 9 January.

[6]. Mohanraj, J. (2013). Effect of nano-zeolite on nitrogen dynamics and greenhouse gas emission in rice soil eco system M.Tech. Thesis, Tamil Nadu Agricultural University, Coimbatore.

[7]. Mozgawa, W., Jastrzebski, W. & Handke, M. (2005). Vibration Spectra of D4R and D6R Structural Units. Journal of Molecular Structures. 744-747, 663-670.

[8]. Naderi, M. R. & Danesh-Shahraki, A. (2013). Nanofertilizers and their role in sustainable agriculture. International Journal of Agriculture and Crop Sciences: vol 5 (19): 2229-2232.

[9]. Pereira, E. I., Minussi, F. B., Cruz, C. C. T., Bernardi, A. C. C., & Ribeiro, C. (2012). Urea–Montmorillonite-Extruded Nanocomposites: A Novel Slow-Release Material. J. Agric. Food Chem., 60: 5267–5272.

[10]. Shaviv, A. (2000). Advances in Controlled Release of Fertlizers. Advanced Agronomy Journal 71: 1-49.

[11]. Sitarz, M., Mozgawa, W. & Handke, M. (1997). Vibration spectra of complex ring silicate anions method of recognition. Journal of molecular structure. Vol. 404: 193-197.

[12]. Sing, K. S. W., Everett, D. H., Haul, R. A. W., Moscou, L., Pierotti, R. A., Rouquerol, J. & Siemieniewska T. (1985). Reporting

[13]. physisorption data for gas/solid systems with special reference to the determination of surface

area and porosity. Pure Appl. Chem. 57: 603 - 619.

[14]. Stuart, B. (2004). Infrared Spectroscopy: Fundamentals and Applications © 2004 John Wiley & Sons, Ltd. ISBN: 0-470-85427-8 (HB); 0-470-85428-6 (PB).

[15]. Treacy, M. J. & Higgins, J. B. (2001). Collections of Simulated XRD Powder Patterns for Zeolites, 4th ed. Elsevier, Amsterdam, The Netherlands, 379 p.

[16]. Waswa, G. A., Andala, D., Aluoch, A. O., Kamau, G. N. & Michira, I. (2017). APPLICATION OF EBURRU ROCKS FROM KENYA AS UREA CARRIER AGENTS. International Journal of Recent Advances in Multidisciplinary Research: Vol. 04, Issue 04, pp.2532-254.

[17]. Waswa, G. A., D. Andala, A. O. Aluoch, G. N. Kamau, I. Michira & J. K. Mbugua (2017).

[18]. Kinetics and Isothermal studies of Lambda Cyhalothrin sorption on Eburru soil in Kenya. Journal of the Kenya Chemical Society: 10-1, 24-34.

[19]. Waswa, G. A., Michira I, Abong O, Mbugua J. K. & Andala, D. (2018). Dissipation and Sorption of Urea on Eburru Soils in Kenya. J Phys Chem Biophys 7: 271.

[20]. Wlodzimier, M., Magdalena K. & Kataryzana, B. (2011). FT-IR of zeolites from different structural groups. CHEMIK 65 (7): 667-674.

Cite this article as :

Gabriel A. Waswa, Immaculate N. Michira, Debora A. Abong'o, Dickson Andala, Austin O. Aluoch, "Characterization; formulation and application of Natural Nano zeolitic materials from Kenya as Smart Delivery Systems for fertilizers and pesticides", International Journal of Scientific Research in Science, Engineering and Technology (IJSRSET), Online ISSN : 2394-4099, Print ISSN : 2395-1990, Volume 7 Issue 3, pp. 338-349, May-June 2020. Available at doi : https://doi.org/10.32628/IJSRSET207349
Journal URL : http://ijsrset.com/IJSRSET207349

Journal of Physical Chemistry & Biophysics
ISSN: 2161-0398
Waswa et al., J Phys Chem Biophys 2018, 8:3
DOI: 10.4172/2161-0398.1000271
Research Article
OMICS International

Dissipation and Sorption of Urea on Eburru Soils in Kenya

Waswa GA[1]*, Michira I[1], Abong O[1], Mbugua JK[1], Andala D[2] and Aluoch AO[3]

[1]Department of Chemistry, University of Nairobi, Nairobi, Kenya

[2]Department of Chemistry, Multimedia University of Kenya, Nairobi, Kenya

[3]Department of Chemical Science and Technology, Technical University of Kenya, Nairobi, Kenya

Abstract

Dissipation and sorption of urea on Eburru soils in Kenya was done using kinetic studies which indicated that 35.00% of urea was adsorbed in the Eburru soil matrix nanopores within an equilibration of 24 hours. The presence of urea molecules in the loaded soil samples was further confirmed by XRD, FTIR and SEM characterization. Controlled urea release behavior of Eburru loaded soil samples was also determined to be 82.8% in water and 74.2% in Kikuyu soil.

Keywords: Dissipation; Degradation; Sorption

Introduction

Urea (Figure 1) is an organic compound that is mainly applied in agricultural production as a nitrogenous fertilizer. Beside, urea which is also called carbamide, is applied in many industrial sectors for functions like binders and analytical reagents. Manufacture of urea from inorganic starting materials (ammonia and carbon dioxide) was discovered as early as 1828 [1], processes which were modified subsequently leading to industrial production, with almost 90% of the produce meant for agricultural consumption [2]. In living organisms, urea is synthesized as part of the urea cycle, mainly as an oxidant of amino acids or from ammonia [3-5]. Urea is usually a colorless, odorless and highly soluble organic compound.

Urea degradation processes

Hydrolysis is soil: On studying reactions of urea in soil (IRPTC data profile) [6]. Bund [7] from University of Wisconsin indicates that when applied to soil, urea decomposes in the presence of water and urease to ammonium carbonate that further forms ammonium ions. Presence of hydroxide ions in the soil could lead to ammonia being discharged through reactions (volatization), as shown by the equations below:

$$(NH_2)_2CO+2H_2O \rightarrow (NH_4)_2CO_3 \quad (1)$$

$$(NH_4)_2CO_3+2H^+ \rightarrow 2NH_4^++CO_2+H_2O \quad (2)$$

$$NH_4^++OH^- \rightarrow NH_3+H_2O \quad (3)$$

He argues that the rate of ammonia loss in this process is favored by high temperature, high pH and low soil CEC.

Volatization of ammonia from soil: Ammonia formed when NH_4^+ reacts with OH^- ions in soil could be lost by volatization process, as illustrated by the nitrogen cycled below Figure 2. As already mentioned, high temperature, high pH and low CEC value of soil favors this process, which in turn accelerates the nitrogen cycle [4].

Materials and Methods

The following instruments, materials and reagents were used: UV-Visible spectrometer (UV-1700 model, Shimadzu Corporation, Kyoto, Japan), Analytical balance (Fischer A-160), Orbital shaker (fitted with timer), Urea, distilled water and soil samples from Eburru crater, Rift valley, Kenya (0.63 S, 36.23 E). The soil samples were prepared for analysis by air drying in natural sunlight at room temperature for four days to prevent nutrient transformation, crashed, sieved using 0.85 mm sieve size and stored in plastic sampling bags. The soil analysis method and results were as recorded in our previous work done by Waswa et al. [5]. Kinetics of fertilizer adsorption on zeolitic materials was done by preparing Standard concentrations of urea fertilizer from 1:2, 1:4, 1:10, 1:20, 1:40, 1:60, 1:80, 1:100 and 1:200 w/v in aqueous medium. The varying concentrations were scanned between 200-900 nm wavelength on the UV-Visible Spectrophotometer to determine the maximum wavelength of urea and subsequently generate the calibration curves at obtained wavelength of 203 nm which was subsequently used to determine concentrations of urea in the current studies. Sorption studies on effect of concentration variation was done by treating 5.0036 g of the zeolitic materials with 10 ml aqueous solutions each containing 1:2, 1:4, 1:6, 1:8, 1:10, 1:20, 1:40, 1:60, 1:80 and 1:100 w/v concentrations of urea solutions. The mediums were shaken at room temperature for 24 hours each, then centrifuged at 10,000 rpm for 10 minutes. The supernatants were then filtered using

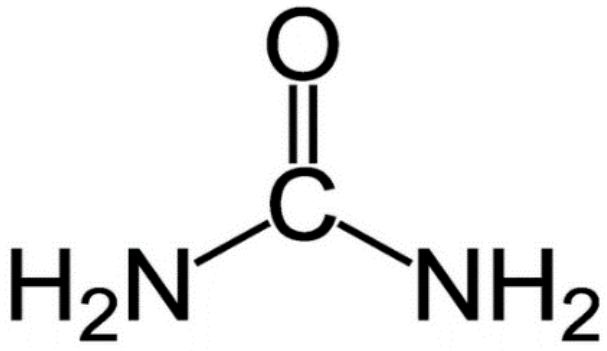

Figure 1: Structure of Urea.

***Corresponding author:** Waswa GA, Department of Chemistry, University of Nairobi, Nairobi, Kenya, Tel: +254723851462; E-mail: waswagabriel@gmail.com

Received May 16, 2018; **Accepted** May 29, 2018; **Published** Jun 01, 2018

Citation: Waswa GA, Michira I, Abong O, Mbugua JK, Andala D, et al. (2018) Dissipation and Sorption of Urea on Eburru Soils in Kenya. J Phys Chem Biophys 7: 271. doi: 10.4172/2161-0398.1000271

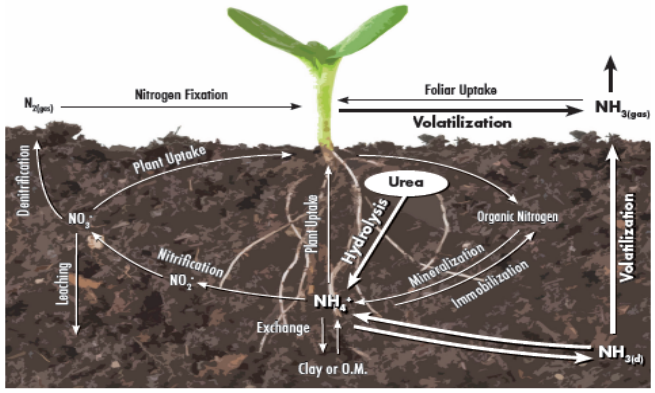

Figure 2: The nitrogen cycle, with emphasis on ammonia volatization.

0.22 um whatman papers and equilibrium concentration determined by UV-Visible Spectrophotometer at 203 nm. Sorption studies on varying shaking times were conducted using 1.00 g of zeolitic material suspended in 10 ml urea solution of concentration 1:100 w/v. The mediums were shaken at room temperature for 15, 30, 45, 60, 75, 90, 100, 120, 140 and 160 minutes each, then centrifuged at 10,000 rpm for 10 minutes. The supernatants were then filtered using 0.22 um whatman papers and equilibrium concentration determined by UV-Visible Spectrophotometer at 203 nm. Quantitative determination of equilibrium amount of loaded urea was done by spiking 1.00 g of zeolitic materials with 10 ml of 1:60 w/v urea solutions. The mediums was shaken at room temperature for varied timings of 3, 10, 20, 24, 40, 48 and 96 hours, and then centrifuged at 10,000 rpm for 10 minutes. The supernatant was then filtered using 0.22 um whatman papers and equilibrium concentration of the remaining urea determined by UV-Visible Spectrophotometer at 203 nm. The difference between initial concentration and equilibrium concentration gave the amount loaded in the samples used in determination of equilibration time. Loading of fertilizer into zeolitic materials was done by spiking 20.00 g of zeolitic material with 35 ml of 1:60 w/v urea solution. The mediums was shaken at room temperature for 24 hours, then centrifuged at 10,000 rpm for 10 minutes. The supernatant was then filtered using 0.22 um Whatman papers and equilibrium concentration of the remaining urea determined by UV-Visible Spectrophotometer at 203 nm. The difference between initial concentration and equilibrium concentration gave the amount loaded in the samples. The resulting urea loaded samples were dried at 100°C for 24 hours. Similar procedures were repeated for soils samples obtained from Kikuyu area, applied as control experiment. Controlled release behavior of fertilizer loaded zeolitic materials in water was done by placing 20.00 g of urea loaded zeolitic materials in 250 ml separating funnels and 50 ml distilled water infiltrated through at an approximate flow rate of 0.1667 ml/min. 50 ml distilled water was refilled every 24 hours to infiltrate the same samples for 18 days. The filtrates/elutes were collected on a daily basis prior to refilling, filtered using 0.22 um Whatman papers and equilibrium concentration determined by UV-Visible Spectrophotometer at 203 nm. Blank experiment was conducted using 20.00 g of zeolitic material following similar procedures. Controlled release behavior of fertilizer loaded zeolitic materials in soil was done by homogenizing 20.00 g of urea loaded zeolitic materials with 20.00 g of soil samples from Kikuyu, placed in 250 ml separating funnels and 50 ml distilled water infiltrated through at an approximate flow rate of 0.1667 ml/min. 50 ml distilled water was refilled every 24 hours to infiltrate the same samples for 18 days. The filtrates/elutes were collected on a daily basis prior to refilling, filtered using 0.22 um Whatman papers and equilibrium concentration determined by UV-Visible Spectrophotometer at 203 nm. Control experiment was done using 20.00 g of urea loaded Kikuyu soil placed in 250 ml separating funnel, followed by similar procedures above.

Results and Discussion

Kinetics of fertilizer adsorption on zeolitic materials

Generally, there is an increase in amount of urea adsorbed as the spiking concentration increases as illustrated by Figure 3. This may be attributed to gradual increase in adsorbate molecules in solution as compared to higher initial adsorption active sites of the adsorbent surface. The highest percentage de-sorbed was determined to be 80.0%, preceded by an initial rapid adsorption from 1.90% and then proceeded by final gradual adsorption to 58.00% as represented by Figure 4. The initial rapid phase could be due to a high initial sorption gradient between adsorbate in solution and the adsorbent surface of sample EB-GA-02, resultant of initial high number of vacant adsorption sites. Equilibrium sorption rate was attained at the recorded highest percentage above, beyond which desorption also started occurring. Significantly, more amount of urea was adsorbed from the solution initially till equilibration, after which more of the urea molecules could be desorbed back in the solution as illustrated by Figure 5. Keeping the spiking concentration constant while increasing the shaking time enhances solute sorbate contact that represents more stable equilibration timing with dismal change in amount adsorbed beyond the 30-60 minutes as represented by Figure 6. Better equilibration was recorded at a slightly higher shaking time, though once the most of the sorption active sites were used up, further increase in contact time between the urea molecules and sample EB-GA-02 had no significant change of rate of adsorption. Determination of the percentage of amount of urea adsorbed with increasing shaking time indicated that adsorption rate tend to equilibrate at approximately 33% for the amount adsorbed, giving near zero gradient at higher shaking time as demonstrated by Figure 7 below.

Quantitative determination of adsorbed fertilizer

Relatively, a higher concentration and longer shaking intervals were used in this study for quantitative determination of adsorbed urea. Higher concentration of sorption solutes exposed to sorption sites for longer durations generated better equilibrations as indicated by Figure 8, of which the highest column represented maximum desorbed amounts shaken at 24 hours duration starting with a solution of concentration 0.278 moldm^{-3} corresponding to 1:60 m/v. Similarly, at maximum equilibration, there is an almost equivalent sorption rate on amount of urea molecules binding the sample EB-GA-2 sorption active site as to those released in the aqueous medium. The positive gradient to the maximum could be attributed to more sorption sites and gradual increase in physicochemical binding, while the subsequent decline could be a factor of reverse process of desorption. Further analysis of variation of percentage of urea adsorption with time as represented by Figures 9 and 10 below gives the highest index at approximately 35% when contact shaking time is done for 24 hours. Hence, this experimental finding gave the optimum parameters for loading urea fertilizer in the nanopores of sample EB-GA-02, as will be was done in the subsequent procedure.

Loading of fertilizer into zeolitic materials

Confirmation of the loaded urea into the samples was determined by characterization of the urea loaded samples using X-ray diffraction spectroscopy and Fourier transform infra-red spectroscopy. X-Ray

Citation: Waswa GA, Michira I, Abong O, Mbugua JK, Andala D, et al. (2018) Dissipation and Sorption of Urea on Eburru Soils in Kenya. J Phys Chem Biophys 7: 271. doi: 10.4172/2161-0398.1000271

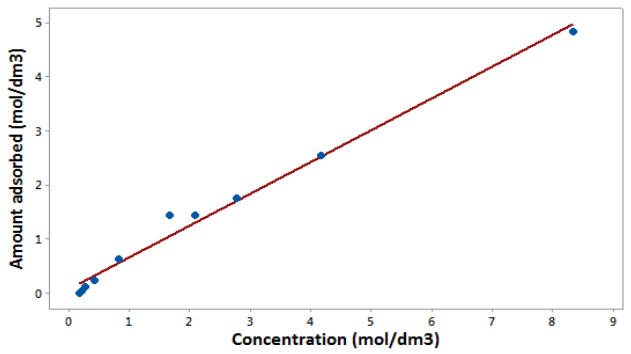

Figure 3: Varying concentration of urea with constant amount of adsorbent.

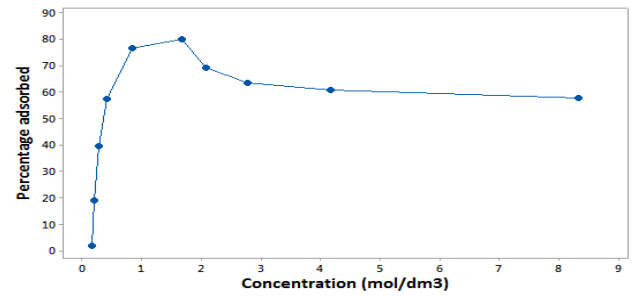

Figure 4: Percentage of urea adsorbed with varying concentration and constant mass of adsorbent.

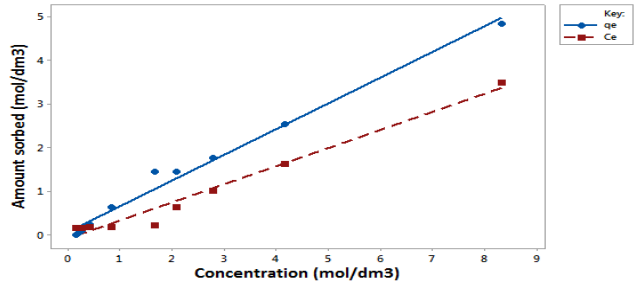

Figure 5: Variation of amount adsorbed (qe) with solution remaining amount (Ce) at equilibrium.

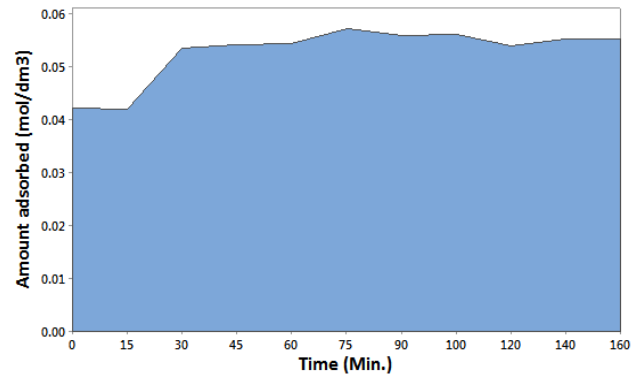

Figure 6: Proportion area on amount adsorbed with varying time.

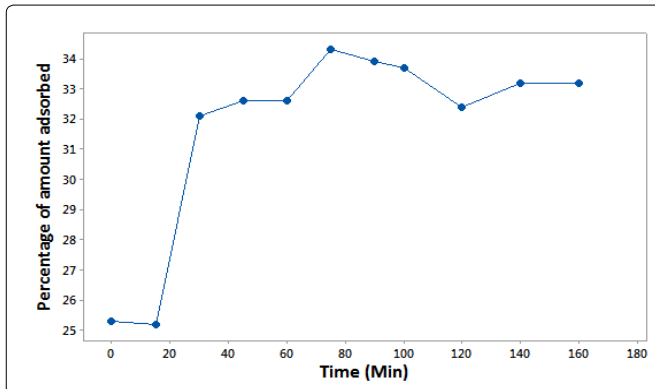

Figure 7: Percentage of urea adsorbed with time.

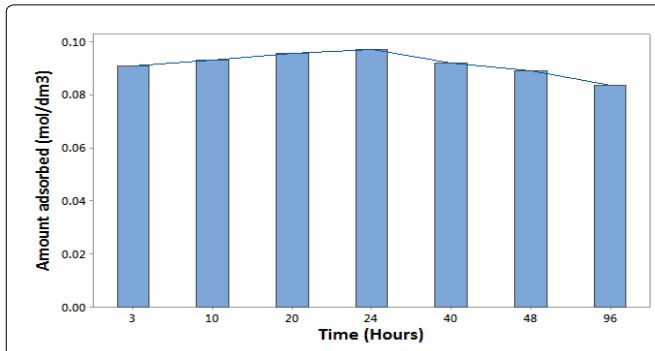

Figure 8: Comparison of urea amount adsorbed with time.

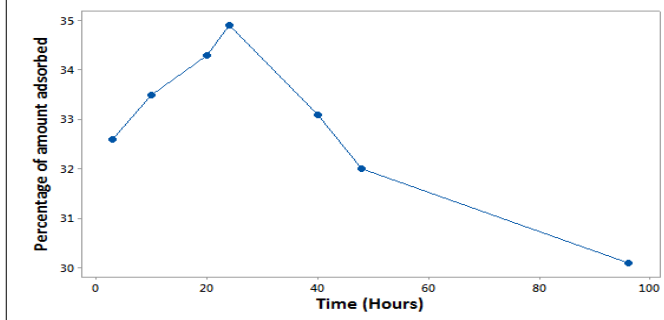

Figure 9: Variation of percentage absorption of urea with time.

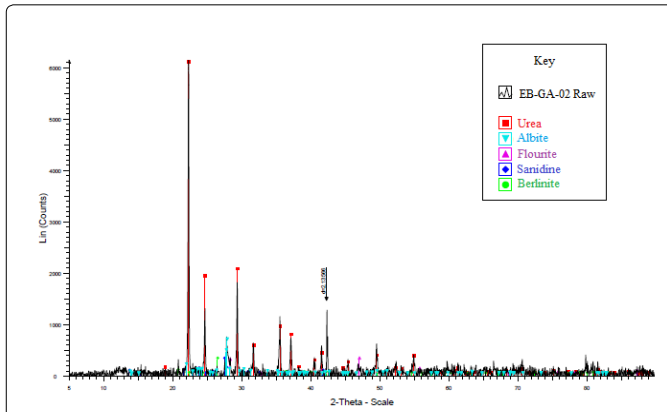

Figure 10: Fertilizer loaded sample EB-GA-02.

diffraction analysis (Figure 10) indicated 2θ peaks values of 22, 24.5, 29.5, 32, 35.5, 37, 38.5, 40.5, 41.5, 45.5 and 55 corresponding to urea peaks. Fourier Transform Infrared analysis of urea fertilizer (Figure 11) showed major peaks at 3348.42-3444.87 cm^{-3}, 1624.06-1681.93 cm^{-3} and 1465.90 cm^{-3} corresponding to N-H, C=O and C-N functional groups respectively [8]. On the other hand, the spectrum of Urea loaded sample EB-GA-02 below (Figure 12) contained distinct peaks appearing on the urea spectrum at 3348.42-3444.87 cm^{-3}, 1624.06-1681.93 cm^{-3} and 1465.90 cm^{-3}, corresponding to N-H, C=O and C-N stretching vibrations for the urea fertilizer functional groups respectively, as appeared in the previous. The SEM images obtained for the urea loaded sample EB-GA-02 were as recorded in Figure 13. Comparative studies were also conducted on Kikuyu soil (sample KIKI-GA-01) for urea loading procedures. The urea loaded soil was also analyzed to confirm the presence urea molecules in their matrix as represented below. For the X-Ray diffraction analysis of urea loaded Kikuyu soil, indications of urea fertilizer peaks at 2θ values of 22.5, 24.5, 26.5, 29.5, 35.5, 37.0, 41.5, 45.4 and 49.5 degrees were noted as shown in Figures 14 and 15 below. Furthermore, the corresponding Infra-red analysis (Figure 14) of the urea loaded kikuyu soil showed conspicuous peaks of N-H stretching at 3444.87 cm^{-1}, with tiny shoulders at 3618.46 cm^{-1} and 3699.47 cm^{-1}. The C=O stretching peak appears at 1624.06 cm^{-1}, while the C-N stretching peak shifted to 1458.18 cm^{-1}. The obtained SEM images were also recorded in Figure 16.

Controlled release behavior of fertilizer loaded zeolitic materials in water

The total amount of desorbed fertilizer was determined to be 0.100254919 mol/dm^3. From this study, it was found that a total of 82.8% of loaded urea fertilizer was released in water from the carrier material sample EB-GA-02. The rate of discharge was rapid initially, but gradually declined beyond the fifth day till the end of the monitoring period, with steady sustainable release of the fertilizer as represented by Figure 17.

Controlled release behavior of fertilizer loaded zeolitic materials in soil

The total amount of desorbed fertilizer was determined to be 0.089776702 mol/dm^3, giving a percentage desorption of 74.2% on the initial amount loaded. Graphical representation on the rate of percentage of urea released in Kikuyu soil medium was represented by Figure 18. Comparatively, a higher percentage was determined for the discharge of urea loaded sample EB-GA-02 in aqueous medium as compared to discharge on Kikuyu soil medium. As already discussed, natural rock samples of EB-GA-02 had a lower organic carbon content compared to the Kikuyu soil sample KIK-GA-01, a factor that could contribute to low attraction of urea molecules to the sample matrix. The total amount of desorbed fertilizer from urea loaded sample KIK-GA-01 was 0.071309 $moldm^{-3}$ giving a 58.9% percentage desorption. Previous discussions on this sample KIK-GA-01 which essentially was soil from Kikuyu area indicated a higher organic matter content and proportion of clay. The lower release of loaded urea could then be alluded to stronger binding forces between the urea molecules and the soil matrix, which could be of physicochemical aspect. Graphical representation of the release process indicates lower percentage changes with a relatively much lower desorption percentage rates as represented by Figure 19. Comparative analysis studies on the urea release for the loaded carrier materials was also conducted for urea loaded sample EB-GA-02 in aqueous medium, urea loaded sample EB-GA-02 in Kikuyu soil and urea loaded sample KIK-GA-01 in

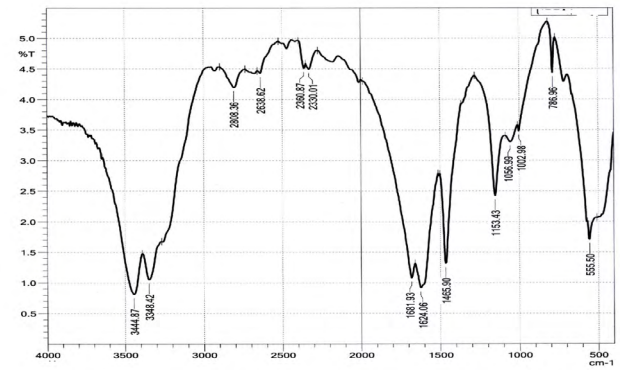

Figure 11: FT-IR spectra of urea.

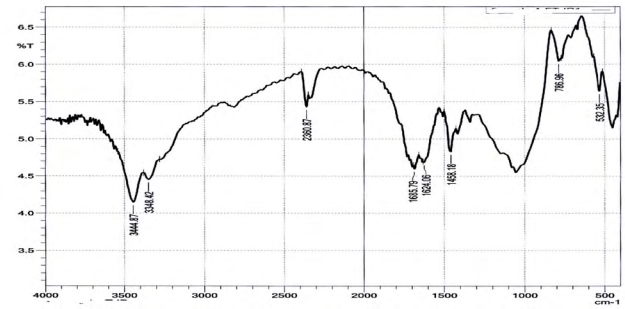

Figure 12: FT-IR spectra of urea loaded sample EB-GA-02.

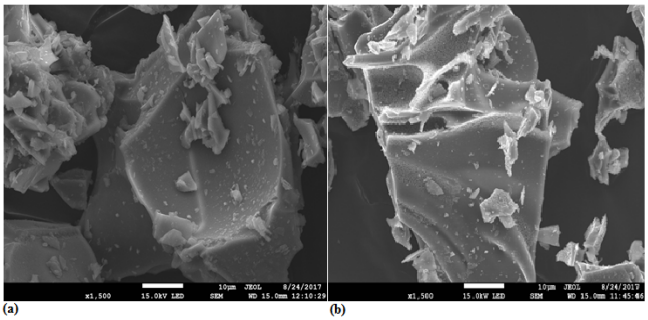

Figure 13: SEM images of (a) urea loaded sample EB-GA-02 (b) blank sample EB-GA-02.

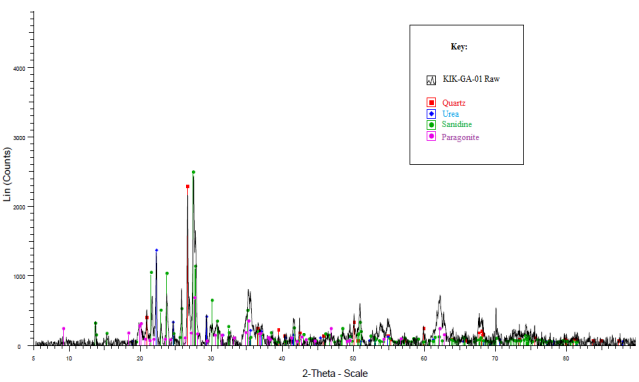

Figure 14: Fertilizer loaded sample KIK-GA-01.

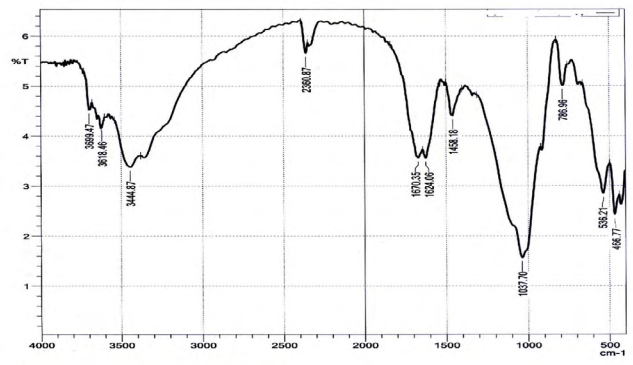

Figure 15: FT-IR spectra of urea loaded sample KIK-GA-01.

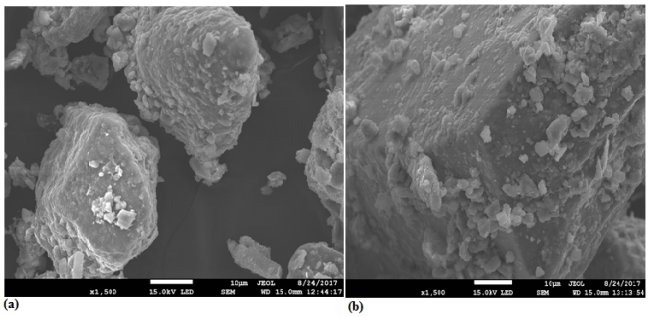

Figure 16: SEM images of (a) urea loaded sample KIK-GA-01 (b) blank sample KIK-GA-01.

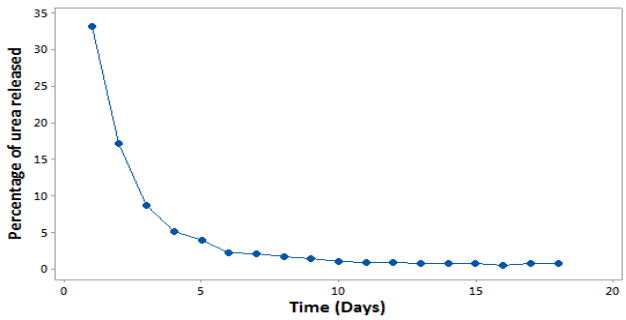

Figure 17: Percentage of urea release in water.

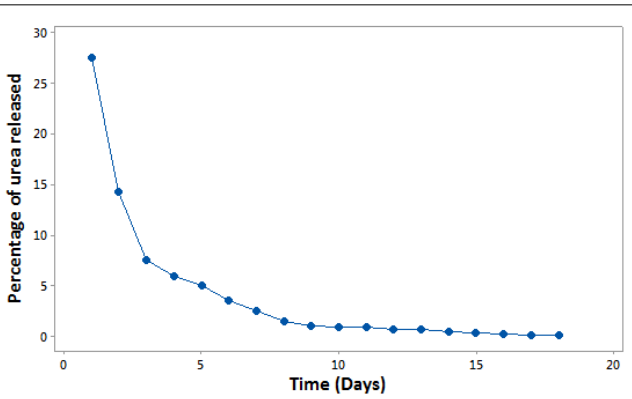

Figure 18: Percentage of urea release in soil.

aqueous medium represented by 'a', 'b' and 'c' respectively in the 'key' for Figures 20 and 21. Significantly, a higher percentage of urea was discharged in the aqueous medium by the urea loaded sample EB-GA-02 at slower rate on evaluation of the starting point and initial gradient of the three curves in the figure above. Furthermore, this is clearly illustrated by Figure 4. 62 that represents relative heights of the bars in the graph. Evidently, urea loaded sample KIK-GA-01 had the least discharge amount of urea in aqueous medium as shown by both figures. Beyond the 12 days, it can be seen again from Figure 21 below that the curve and bars respectively of discharge of urea loaded sample EB-GA-02 in aqueous medium was higher proportionally than the others. This implies that loading urea fertilizer into sample EB-GA-02 and applying the same as carrier agents had a better sustained release rate, which could still avail the minimum remaining fertilizer to the crops for slightly longer duration than the direct application.

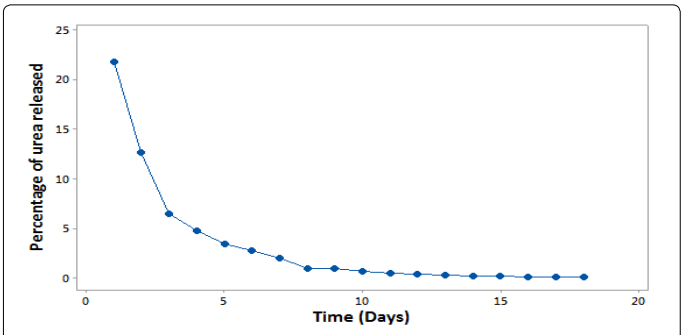

Figure 19: Percentage of urea release in by sample KIK-GA-01.

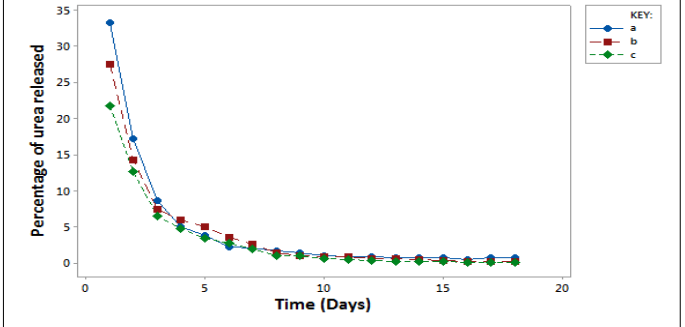

Figure 20: Comparison rate of urea release.

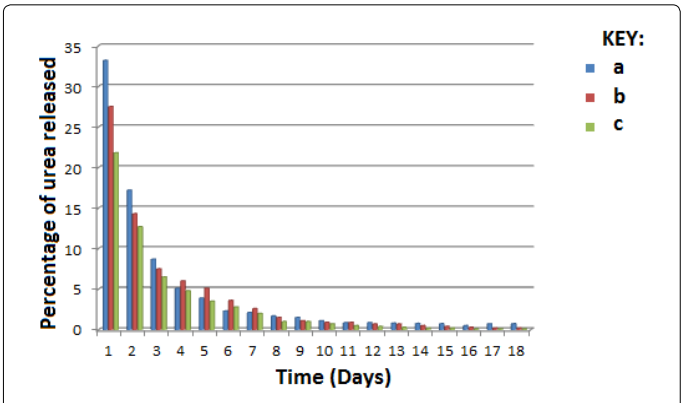

Figure 21: Percentage proportion variation of urea release.

The study shows that Eburru soil samples can effectively adsorb urea fertilizer molecules, a method that can be applied on loading urea into the nanopores of these soil samples. Rate and amount of urea adsorbed was depended on the equilibration time and initial concentrations of the solutions. Desorption studies carried out indicated that most of the adsorbed urea molecules could be released into the water or soil medium. In conclusion, the study found that urea molecules can be loaded and released from Eburru soil materials, an aspect that can be applied as fertilizer carrier agent.

Acknowledgements

The authors thank NACOSTI for providing the funds for the project work through NCST Grant No: NACOSTI/RCD/ST&I 7TH CALL/ PhD/096.

References

1. Friedrich W (1828) On the artificial formation of urea. Annals of Physics and Chemistry 88: 253-256.
2. Meessen JH, Petersen H (2000) Urea ullmann's encyclopedia of industrial chemistry.
3. Sakami W, Harrington H (1963) Amino acid metabolism. Annual Review of Biochemistry 32: 355-398.
4. Clain J, Brad DB, Rick E (2013) Factors affecting nitrogen fertilizer volatilization.
5. Waswa GA, Andalab D, Aluochc AO (2017) Kinetics and isothermal studies of lambda cyhalothrin sorption on eburru soil in Kenya. Journal of the Kenya Chemical Society 10: 24-34.
6. Larry GB (2016) Managing urea-containing fertilizers.
7. IRPTC Data Profile (2016) International register of potential toxic chemicals.
8. Stuart B (2004) Infrared Spectroscopy: Fundamentals and Applications.

ISSN : 2350-0743

www.ijramr.com

International Journal of Recent Advances in Multidisciplinary Research
Vol. 04, Issue 04, pp.2532-2541, April, 2017

RESEARCH ARTICLE

APPLICATION OF EBURRU ROCKS FROM KENYA AS UREA CARRIER AGENTS

[1,*]Waswa G. A., [2]Andala D., [3]Aluoch A. O., [1]Kamau G. N. and [1]Michira I.

[1]Department of Chemistry, University of Nairobi, P.O. Box 30197-00100, Nairobi, Kenya
[2]Department of Chemistry, Multimedia University of Kenya, P.O. Box 15653- 00503, Nairobi, Kenya
[3]Department of Chemical Science and Technology, Technical University of Kenya, P.O. Box 52428 - 00200Nairobi- Kenya

ARTICLE INFO

Article History:
Received 19th January, 2017
Received in revised form
28th February, 2017
Accepted 15th March, 2017
Published online 30th April, 2017

Keywords:
Urea,
Zeolites,
Sorption Kinetics,
Slow Release.

ABSTRACT

Application of Eburru rock samples as urea fertilizer carrier agents was conducted using sorption studies. Characterization by EDS, FT-IR and XRD was done on the samples to determine their zeolite comparativeness. Urea loading and release studies were done through simple aqueous immersion techniques or wet chemistry techniques. The results from these studies indicated that close to 33% of urea could be loaded into the Eburru rock samples within 24 hours equilibration duration, of which 74% net loaded urea could be released in aqueous medium within the 18 experimental days.

INTRODUCTION

Urea (Figure 1) is an organic compound that is mainly applied in agricultural production as a nitrogenous fertilizer. It also finds applicationin many industrial sectors for functions like binders and analytical reagents (www.worldcat.org. novacat.nova.edu/identities/lccn-n97900852/ (Accessed 2nd Nov. 2016 at 2.31pm)). It is a colorless, odorless and highly soluble in both aqueous and organic media with its solubility in the two media being 1080 g/L at 20^{0}C and 500 g/L in glycerol respectively. Urea is mainly synthesized industrially using ammonia and carbon dioxide precursors and this supplies almost 90% of all the urea consumed in the agricultural sector (Friedrich, 1828; Meessen, 2005). In living organisms, urea is synthesized as part of the urea cycle, mainly as an oxidant of amino acids or from ammonia (Sakami, 1963). As a chemical compound, urea undergoes a number of degradation processes which includes hydrolysis and thermal decomposition. In soil, in the presence of the urease enzyme, urea hydrolysis to ammonium carbonate. Further protonation of this carbonate yields ammonium ions, that could further react with hydroxide ions with consequential release of ammonia gas (http://www.soils.wisc.edu/extension/materials/ManagingUrea.pdf (Accessed 2nd Nov. 2016 at 4.48pm).) (Scheme 1 below).

Corresponding author: Waswa G. A.,
Department of Chemistry, University of Nairobi, P.O. Box 30197-00100, Nairobi, Kenya.

$$(NH_2)_2CO + 2H_2O \rightarrow (NH_4)_2CO_3$$
$$(NH_4)_2CO_3 + 2H^+ \rightarrow 2NH_4^+ + CO_2 + H_2O$$
$$NH_4^+ + OH^- \rightarrow NH_3 + H_2O$$

Scheme 1: Release of ammonia from urea

Thermolysis studies on urea indicate its initial vaporization occurs between 133 ^{0}C – 250 ^{0}C, followed by decomposition as shown by the equation below:

$$(NH_2)_2CO \rightarrow NH_3 + HNCO$$

Much higher temperatures could cause production of biuret, isocyanic acid or formation of ammelide or melanine (Koebel *et al*., 2000; Schaber*et al*., 2004). The HNCO formed could still decompose further in presence of water as shown below (Martyn, 2006).

$$HNCO + H_2O \rightarrow CO_2 + NH_3$$

The ammonia formed when NH_4^+ reacts with OH^- ions in soil could be lost by volatilization process, whose rate is increased by high temperature, high pH and low cation exchange capacity value of soil, as illustrated by the nitrogen cycle below (Figure 2) (Clain *et al*., 2019). The major concern about urea is that, owing to its high water solubility like all nitrogeneous fertilizers, urea tends to cause great ground water pollution, fertilization and eutrophication of water bodies (Howarth, 1988; Boynton *et al*., 1982).

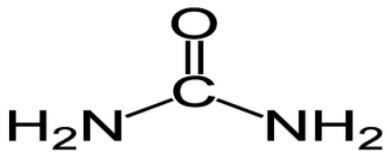

Figure 1. Structure of Urea

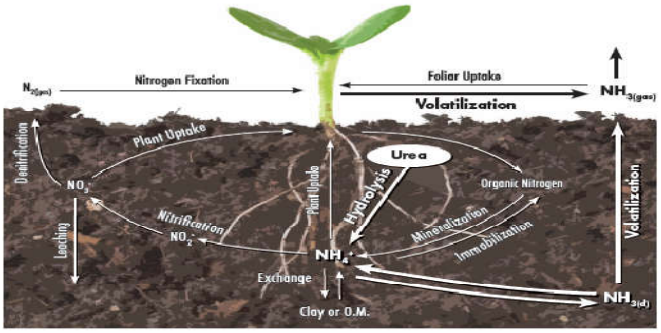

Figure 2: Illustration of the nitrogen cycle (Clain et al., 2013)

Therefore, the main objective of this work was to study and characterize Eburru rock samples as possible urea carrier materials that could be applied as smart delivery system as a way of mitigating urea environmental pollution effects.

MATERIALS AND METHODS

The following instruments, materials and reagents were used: UV-Visible spectrometer, X-ray diffractometer(XRD, D2 Phaser 2nd Gen. from Bruker), Fourier Transform Infrared (FTIR, IR Tracer-100 from Shimadzu), Energy dispersive spectrophotometer (EDS, Shimadzu EDX-720),Analytical balance (Fischer A-160), Orbital shaker (Ratek OM6), Atomic absorbance spectrophotometer (AAS, Perkin Elmer 2100), X-Ray fluorescence spectrometer (XRF Oxford Instruments MDX 1080), Flame photometer (Sherwood scientific 410), Calcinator (N3A Simon Muller 220V Berlin), Commercial Purchased zeolites (CPZ, from Sigma-Aldrich in South Africa,P-Code: 101554254, Lot # BCBM 9330V and CAS: 1318-02-1.), Urea (analytical standard 99% pure from IOBA Chemie), distilled water, rock samples from Eburru crater, Rift valley, Kenya (0.63S, 36.23E) and soil from Kikuyu area(Kiambu County, Kenya), applied as the normal for comparative purposes.

The rock samples were prepared for analysis by air drying in natural sunlight for four days to prevent nutrient transformation, crashed, calcined, sieved using 0.85mm sieve size and stored in plastic sampling bags labeled as Eburru Rock Samples (ERS). The soil from Kikuyu area was also air dried in natural sunlight for four days, sieved using 0.85mm and stored in plastic sampling bags labeled as Kikuyu Soil Sample (KSS). Elemental composition ofERS and CPZ was done using EDS,XRD was used to verify the crystallinity of the samples, FTIR was used in identification of functional groups, while all the Urea quantitation and calibration studies were done on UV-Vis spectrophotometer. A flame photometer was used to monitor levels of Na, Ca and K in the ERS and KSS samples, while at the same time P, Mg and Mncontent were determined calorimetrically. Other trace elements like Fe, Zn, and Cu and exchangeable Ca and Mg were determined by AAS. The total organic carbons were analyzed calorimetrically, based on the Mehlich Double Acid Method (Mehlich, 1953; Tran, 1993; Yang, 2005; Gislason, 2005). Total nitrogen was determined by Kjeldahl method (Jan-Åke, 2008). Soil pH was determined using a pH meter on a 1:1 (w/v) soil-water suspension. Exchangeable Na and K were determined by flame photometer after leaching with 1M KCl. Cation Exchange Capacity (CEC) was determined on the leachate at pH 7.0 by distillation followed by titration with 0.01 M HCl (Carrolland Dorothy, 1959; Turner, 1966). Other instruments used in the study were similar to those found in an ordinary laboratory set-up, including Orbital shaker (fitted with timer). To carry out sorption studies, standard concentrations of urea were prepared by varying concentrations from 1:2, 1:4, 1:10, 1:20, 1:40, 1:60, 1:80, 1:100 ad 1:200 w/v in aqueous medium. They were scanned between 200-900nm wavelengths on the UV-Visible Spectrophotometer to determine the maximum absorption wavelength of urea, which was obtained at 203 nm. Calibration curves at 203 nm were used to determine concentrations of other urea solutions.

Studies on variation of concentrations were done by treating 5.0036g of ERS with 10ml aqueous solutions each containing 1:2, 1:4, 1:6, 1:8, 1:10, 1:20, 1:40, 1:60, 1:80 and 1:100 w/v concentrations of urea. The media were shaken at room temperature for 24 hours each, and then centrifuged at 10,000 rpm for 10 minutes. The supernatants were then filtered using 0.22µm what-man papers and equilibrium concentration determined. Varying shaking time was conducted using 1.0 g of ERS suspended in 10ml urea solution of concentration 1:100 w/v, shaken for 15, 30, 45, 60, 75, 90, 100, 120, 140 and 160 minutes each and equilibrium concentration determined. Procedures modified from Manikandan andSubramanian (2014) (Manikandan, 2014). To load urea into the pores, 20 g of ERS were spiked with 35ml of 1:60w/v urea solution, shaken at room temperature for 24 hours, then equilibrium concentration of the remaining urea determined .The difference between initial concentration and equilibrium concentration gave the amount of fertilizer loaded in the samples. The resulting samples were dried at 100 ^{0}C for 24 hours and stored in air tight plastic bags labeled as Urea loaded Eburru Rock Samples (UBRS).

Controlled release behavior of fertilizer in water was conducted by placing 20 g of UBRS in 250 ml separating funnels and 50 ml distilled water infiltrated through at an approximate flow rate of 0.1667 ml/min. 50 ml distilled water was refilled every 24 hours to infiltrate the same samples for 18 days. This was repeated using a homogenized mixture of 20 g UBRS and 20 g Kikuyu Soil (KS). Modified from Bansiwal*et. al*., (2006)).The filtrates/elutes were collected on a daily basis prior to refilling, filtered using 0.22 µm what- man papers and equilibrium concentration determined.

The amount of urea loaded (mg/g) was calculated using the equation shown below, as reported by Vanderborght and van Greikenm (Vanderborght, 1997).

$$q_e = \frac{v(C_i - C_e)}{w} \quad (1)$$

Where $q_e$is the amount of solute adsorbed from the solution, v is the volume of the adsorbate, $C_i$is the concentration before

adsorption, C_e is the concentration after adsorption, and w is the weight in grams of the adsorbent.

RESULTS AND DISCUSSION

Soil analysis

The nature of the soil greatly influences its sorption characteristics. Figure 3 below shows aERS. Both ERS andKSS wereanalysedfor their properties.

Figure 3. Rock samples from Eburru crater, Rift valley, Kenya (Sample ERS)

According to table 2 below, elemental composition comparison of these samples indicates higher mineral content in KSS. Calcination of ERS lowered its contents of volatile components.

Table 2. Soil analysis

Property	Value	
Soil depth cm	ERS	KSS
Soil pH-H_2O (1:2.5)	8.38	6.50
Elect. Cond. mS/cm	0.23	0.3
Carbon %	0.94	2.7
Sand %	-	40
Silt %	-	40
Clay %	-	20
Zinc ppm	10.22	62.9
Copper ppm	1.36	1.22
Calcium milliequivalent(me)%	4.7	44.4
Magnesium me%	0.59	3.1
Potassium me%	0.62	1.5
Sodium me%	0.84	3.6
Total nitrogen %	0.25	0.25
Phosphorus ppm	3.4	44
Iron ppm	13.34	96.2

Further characterization of ERS was donein comparison to CPZ due to their common application as carrier molecules in development of smart delivery systems (Chinnamuthu, 2009), enabled by their high porosity (Mumpton, 1984). Energy Dispersive Spectroscopy (EDS) of ERS indicates 18.8% Al_2O_3 and 37.4% SiO_2 compared to 56.4% and 43.6%respectively of the commercially purchased zeolites (tables 3 and 4). Besides, ERS had other mineral compositions like 21% Fe_2O_3 and similar amount for K_2O, implying that purification of the raw rocks could increase zeolite mineral composition. Their respective spectrums as illustrated by figures 4 and 5 indicate common peaks near the regions of 20 keV and 1-4 keV, indicating some similarity in mineral composition. Fourier Transform Infra-Red (FTIR) Spectroscopy analysis of ERS (figure 6) and CPZ (Figure 7) indicate some common peaks corresponding to their transmittance spectrums.

Table 3. EDS quantitative results of ERS

Analyte	Result %	Standard Deviation	Line	Intensity (cps/ uA)
SiO_2	37.410	0.433	SiKa	0.7178
Fe_2O_3	21.389	0.069	FeKa	116.996
K_2O	20.671	0.149	K Ka	1.8806
Al_2O_3	18.764	1.649	AlKa	0.0294
ZrO_2	0.609	0.004	ZrKa	29.8216
MnO	0.585	0.014	MnKa	2.8732
CaO	0.194	0.033	CaKa	0.2792
NbO	0.100	0.002	NbKa	5.9555
SO_3	0.075	0.004	S Ka	0.0746
Y_2O_3	0.074	0.002	Y Ka	3.6852
ZnO	0.074	0.003	ZnKa	1.6514
Rb_2O	0.057	0.002	RbKa	2.8905

Peaks in the region of 3400-3700cm^{-1} could correspond to the stretching of the –OH bridging groups such as –Al(OH)Si-. In addition, peaks between 600-800cm^{-1} are associated with asymmetrical stretching of the zeolites, while those of 300-450cm^{-1} could be of ring vibrations, which are commonly affected by the type of structure due to overlap of internal and external tetrahedral vibrations of the secondary building units, alongside the effects of dehydration cation movements (Perego *et al*., 1984).

X-Ray Diffraction (XRD) characterization of ERS gives distinct peaks in the region of 2θ (20^0-40^0) as indicated by figure 8 below, with the highest peak at 22^0. Impurities in the sample could have contributed to peak masking, since the XRD spectrum CPZ (figure 9) gave additional peaks to the distinct in the region of 2θ (20^0-40^0).

Absorbance curves

Urea absorbance curves at 203 nm obeyed Beer's law at lower concentrations as shown in figure 10.

Kinetics of fertilizer adsorption ERS

Generally, the amount of urea adsorbed by ERS increased with increase in spiking levels (Figure 11), a factor largely attributed to the presence of high number of vacant adsorption sites, resulting to high sorption gradient between adsorbate in solution and the adsorbent surface or nano pore spaces. Equilibrium sorption rate was highly dependent on the spiking concentration of urea. Initial lower concentration recorded rapid increase in percentage of urea adsorbed, highest amount being 80% of amount spiked (as shown by figure 12 below) at 1:10w/v corresponding to 1.67$moldm^{-3}$. Highest adsorption amounts were recorded at higher concentrations of fertilizer. From figure 13 below, increasing amounts adsorbed (qe) varies more with solution retained amount (Ce) as concentration increases. Sorption studies of urea on variation of shaking time with constant concentration and amount of ERS used indicated slight proportional increase in amount adsorbed, of which on equilibration almost attained constant amounts of urea (figure 14). Better equilibration could be attained by increased shaking time, in which solute sorbate contact is enhanced. The low organic content (less than 1%) ERS could be attributed for the lower overall percentage amounts adsorbed, as indicated by figure 15 below. Similarly, sorption rates tend to equilibrate at around 33% for the amount adsorbed, giving near zero gradient, at higher shaking minutes.

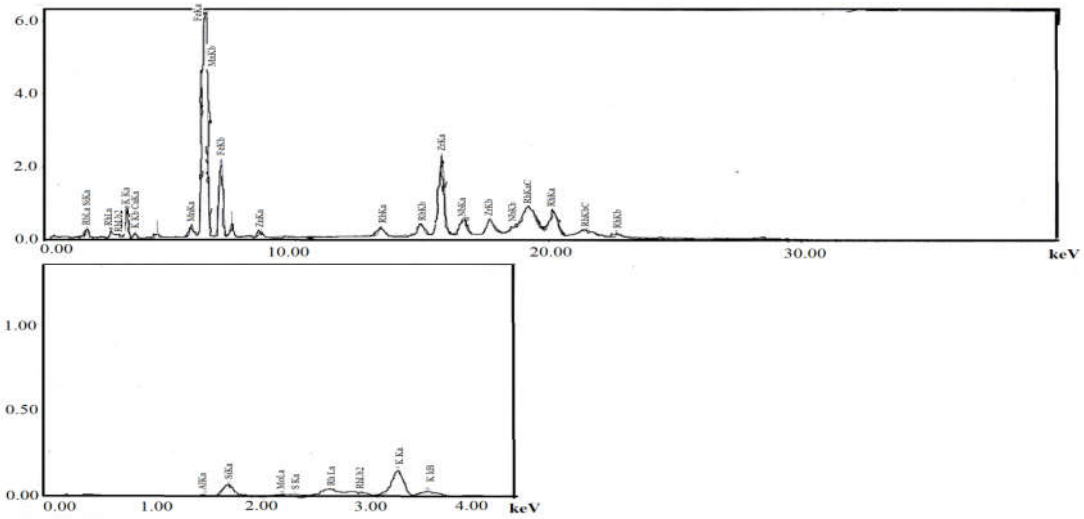

Figure 4. EDS Spectra of ERS

Table 4. EDS quantitative results CPZ

Analyte	Result %	Standard Deviation	Line	Intensity(cps/uA)
Al_2O_3	56.368	1.335	AlKa	0.0721
SiO_2	43.632	0.398	SiKa	0.4315

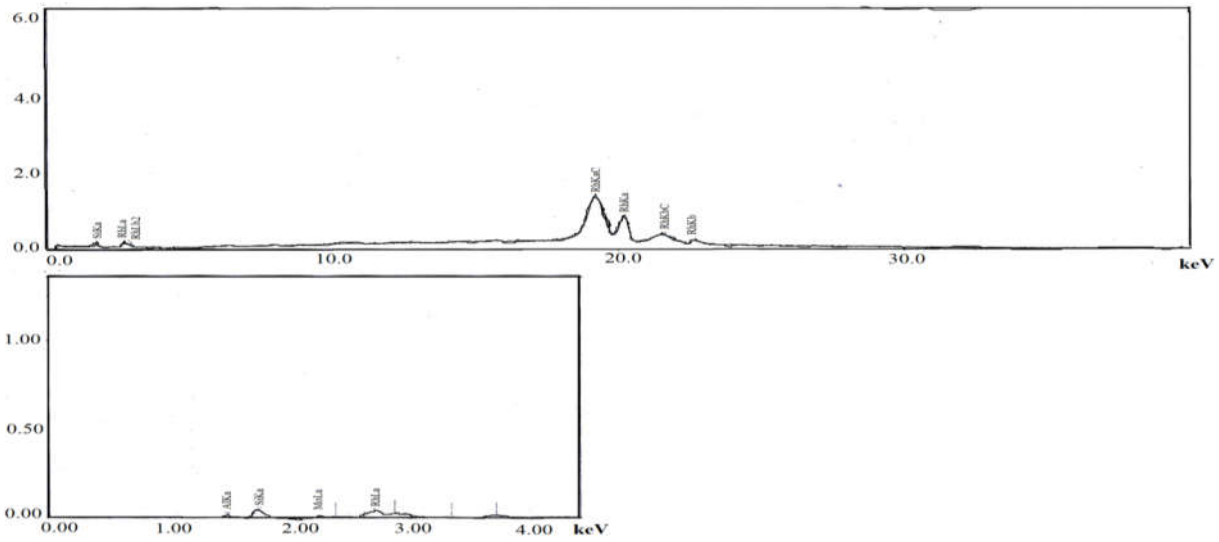

Figure 5. EDS Spectra of CPZ

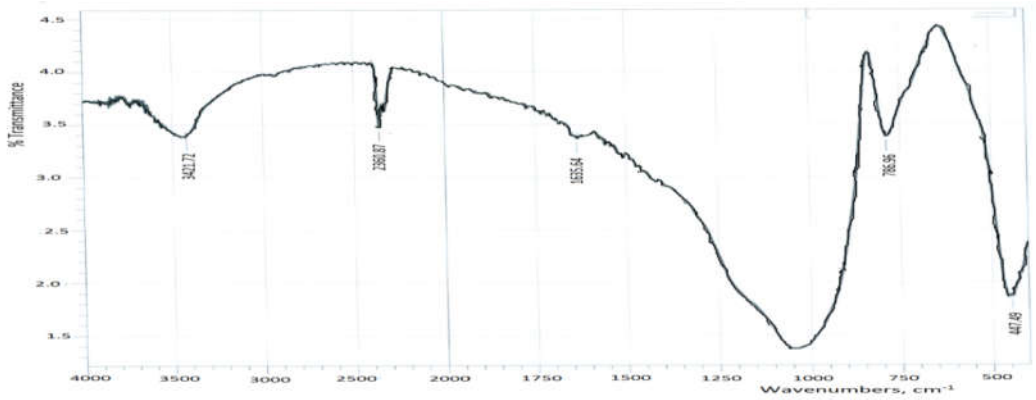

Figure 6. FT-IR spectra of ERS

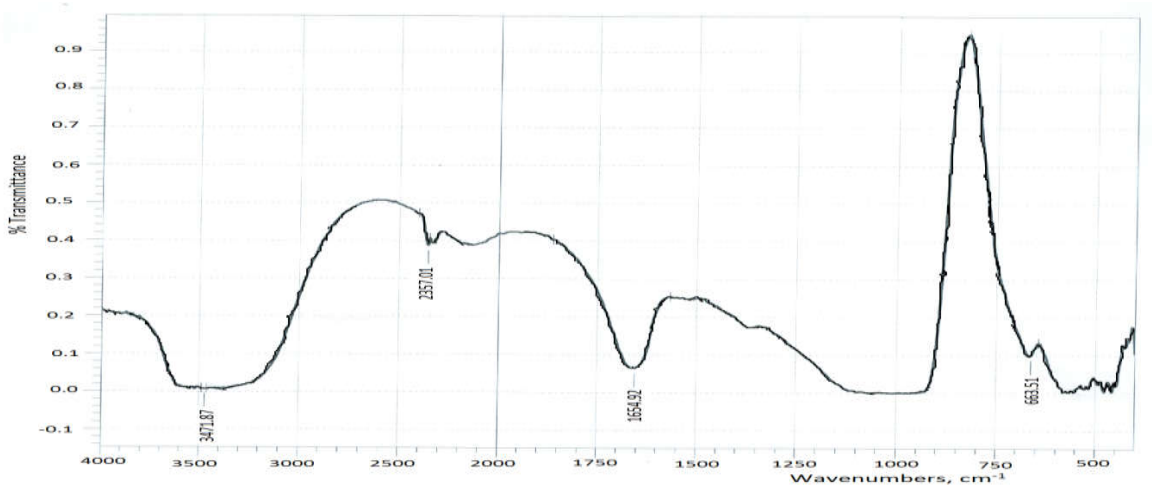

Figure 7. FT-IR spectra of CPZ

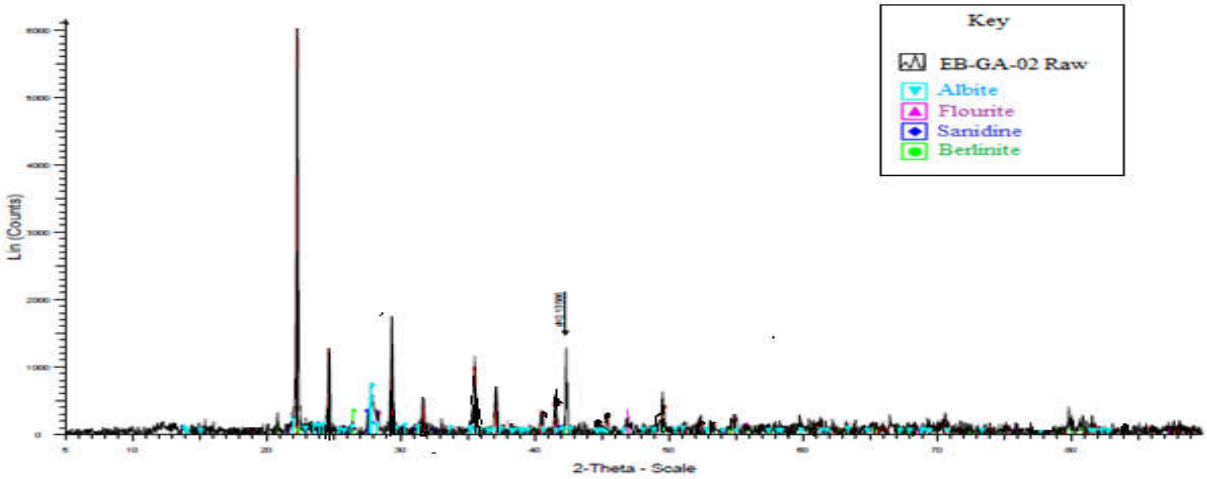

Figure 8. XRD spectra of ERS

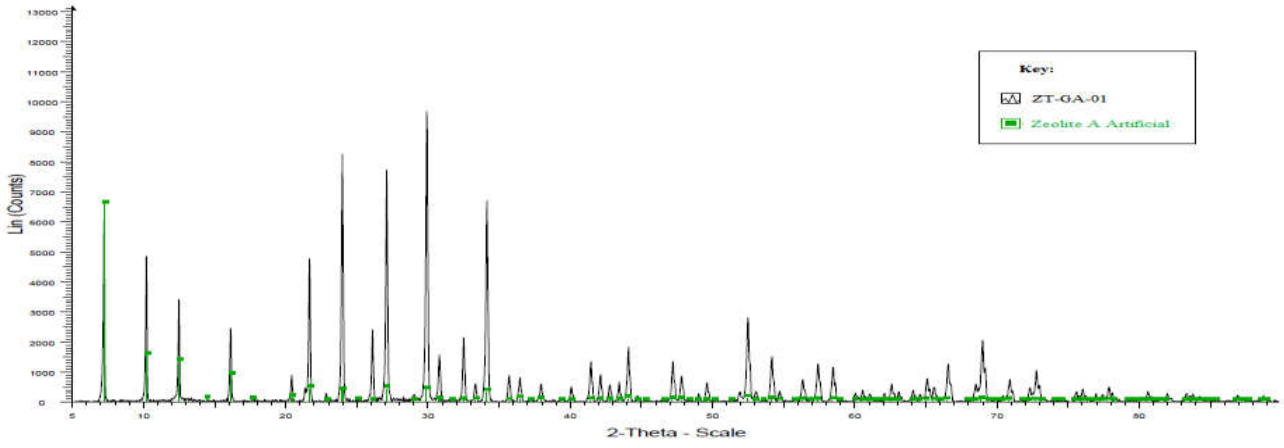

Figure 9. XRD spectra CPZ

Quantitative determination of adsorbed fertilizer

Relatively higher concentration with longer shaking durations were applied for quantitative determination of adsorbed urea. Higher concentration of sorption solutes exposed to sorption sites for longer durations, generates better equilibrations, as indicated by figure 16 below, of which the highest column represents maximum sorbed amounts shaken at 24 hours, starting with a solution of concentration 0.278 moldm^{-3} corresponding to 1:60m/v.The plot of percentage amount of urea adsorbed with longer shaking time as indicated by figure 17 below, shows that with an equilibration time of 24 hours, almost 35% of urea could be adsorbed by ERS.Hence, loading of the fertilizer into ERS as carrier material was based on the highest percentage determined above.Confirmation of the loaded urea molecules in the ERS nanopores was done using

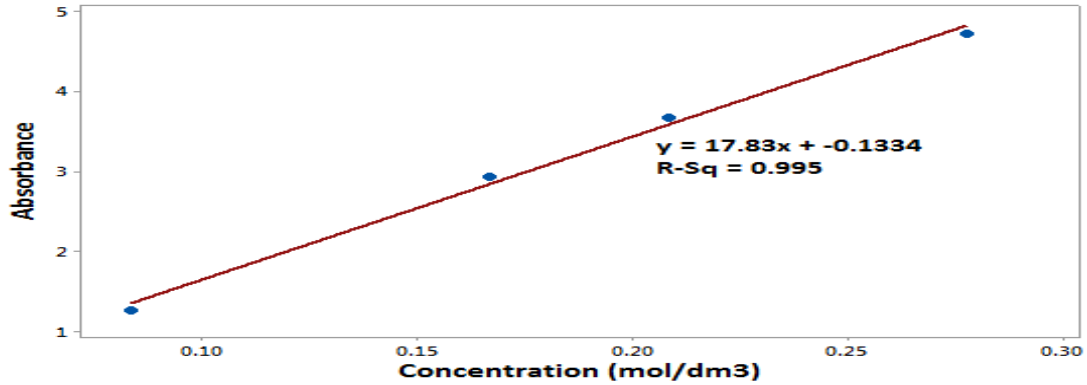

Figure 10: Calibration plot for urea between 0-0.28 M measured at λmax 203nm

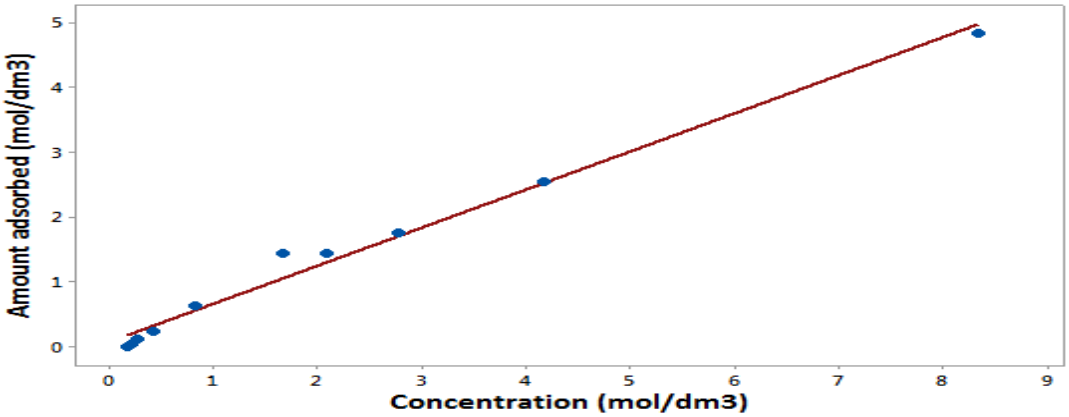

Figure 11. Changes in urea adsorption with varying spiking levels of ERS

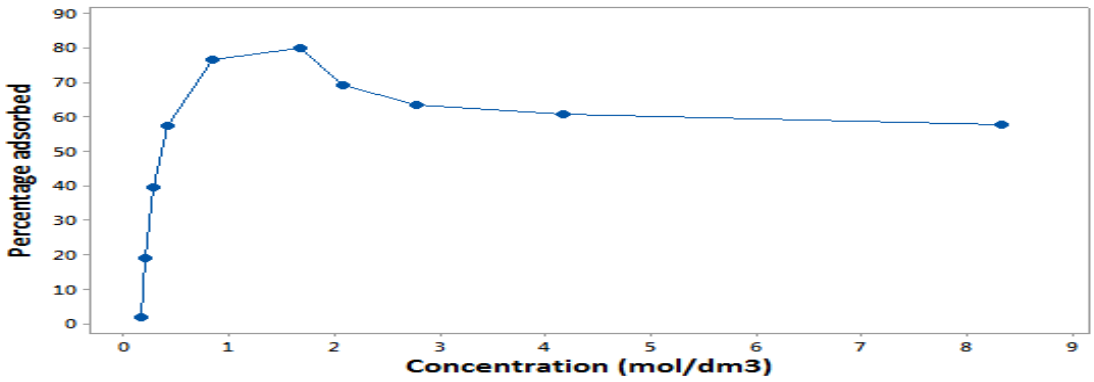

Figure 12: Percentage of urea adsorbed with varying concentration.

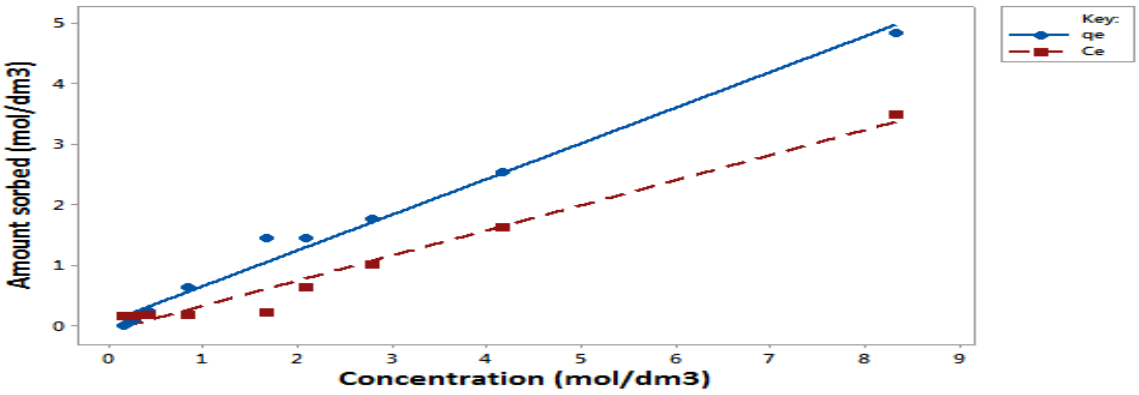

Figure 13: Variation of urea amount adsorbed (qe) with that remaining in solution (Ce) at equilibrium

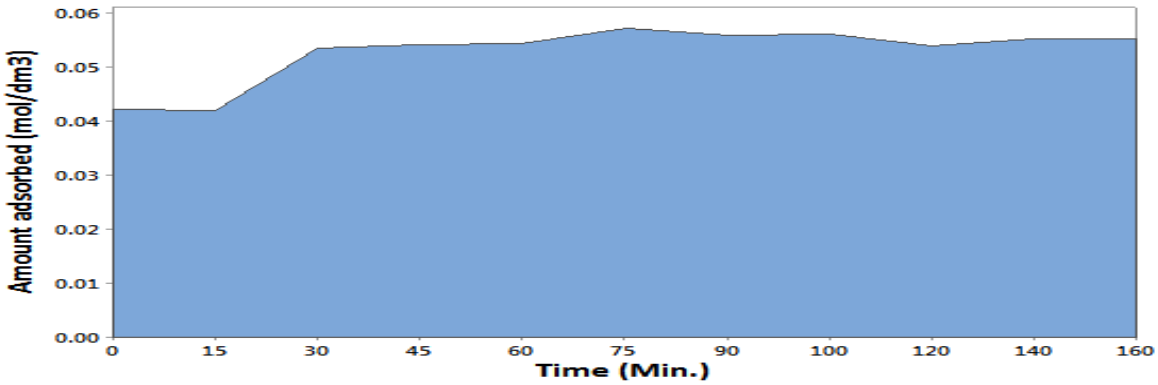

Figure 14. Proportion area on amount adsorbed with varying time

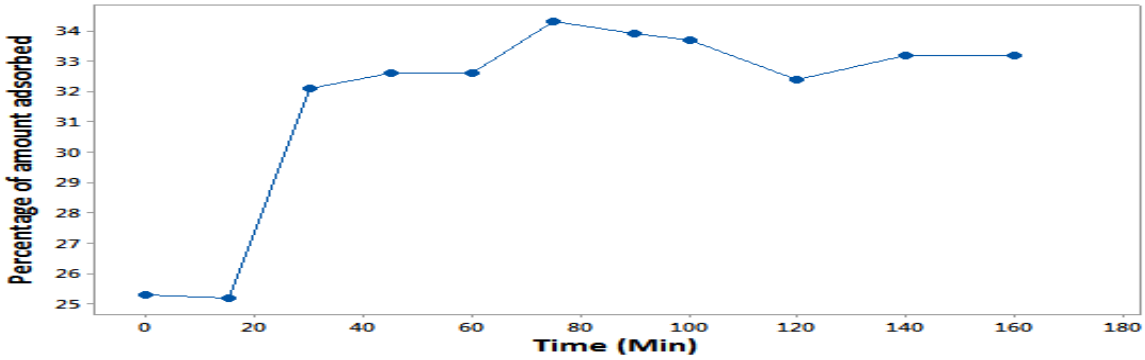

Figure15. Percentage of urea adsorbed with time

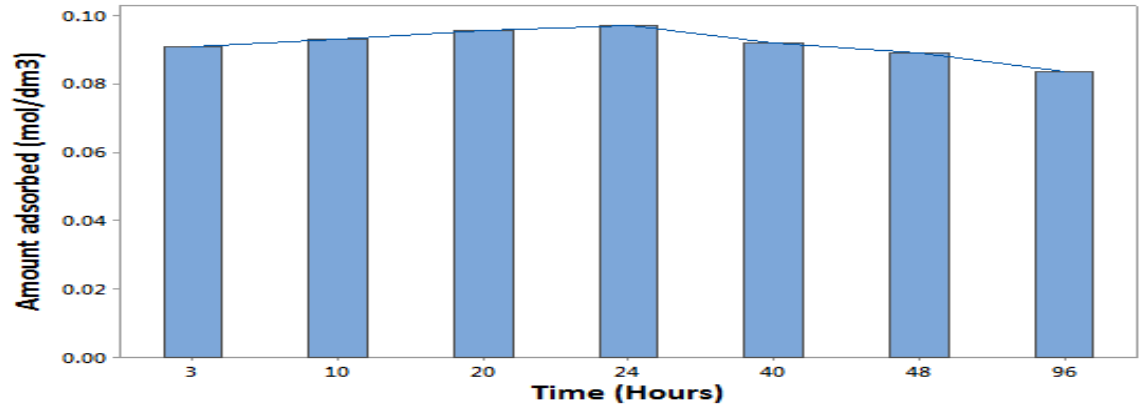

Figure16. Comparison of urea amount adsorbed on ERS with time

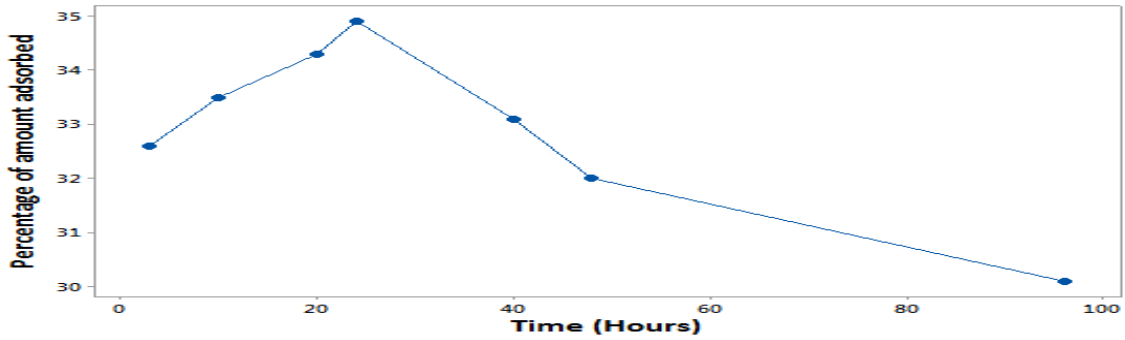

Figure 17. Variation of percentage absorption of urea with time

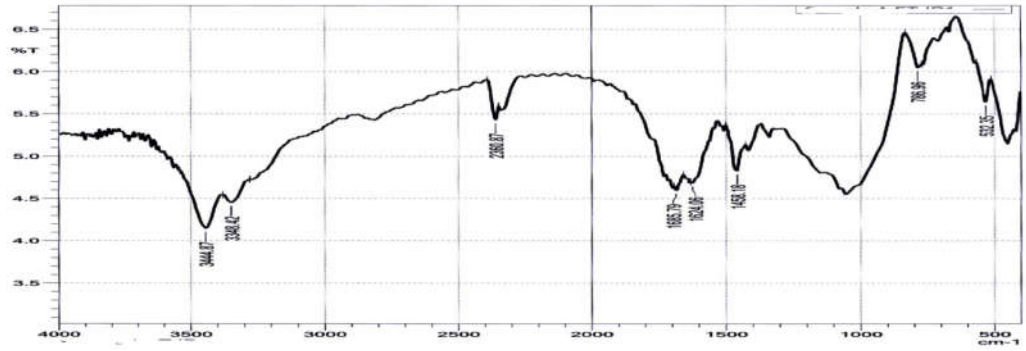

Figure 18: FTIR spectrum of UERS

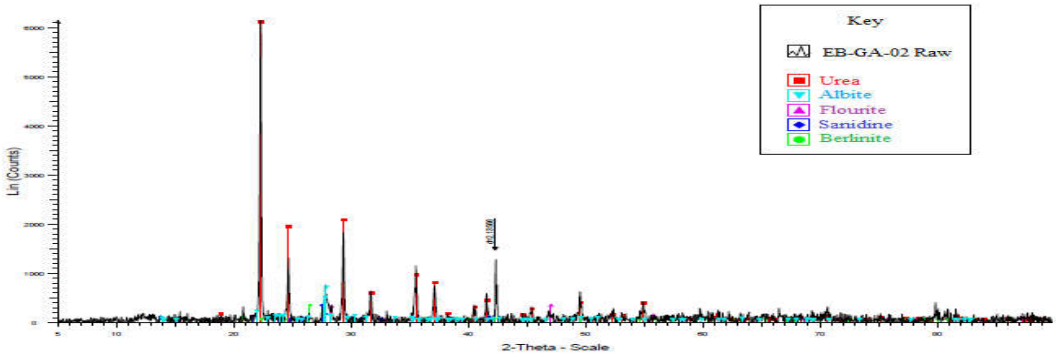

Figure 19. XRD patterns of UERS

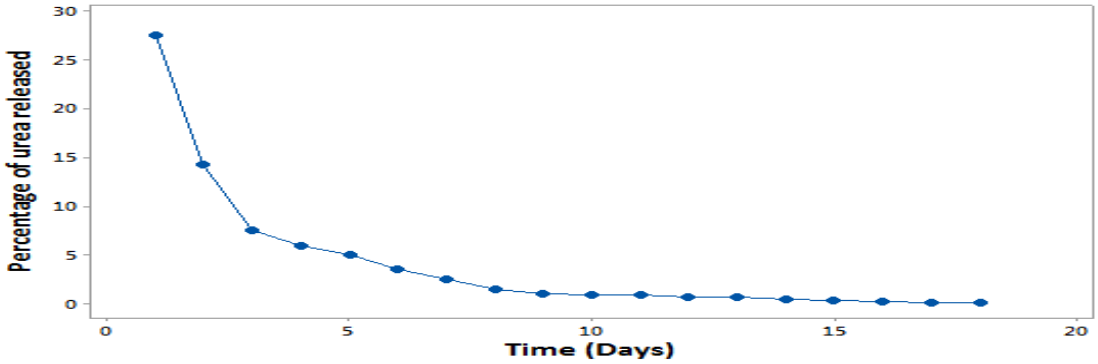

Figure 20. Variation of amount of urea released by UERS with time in water

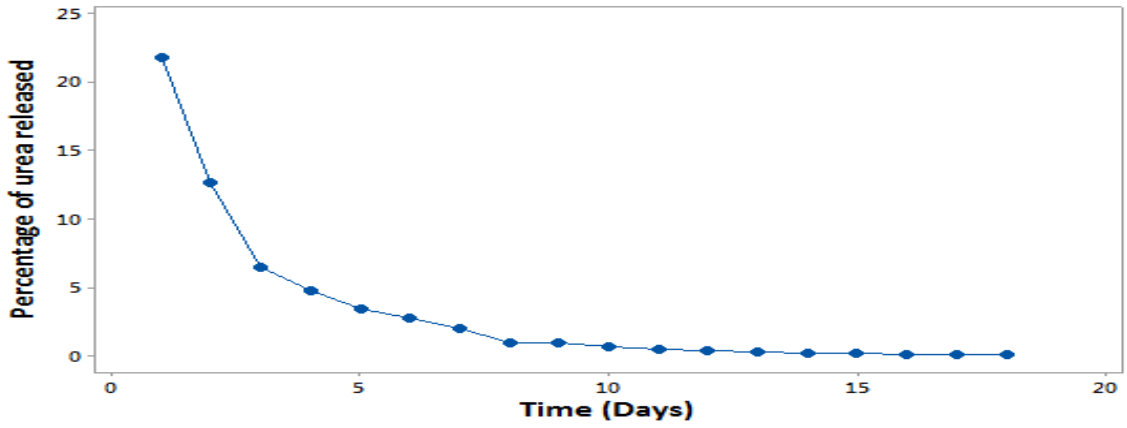

Figure 21. Variation of amount of urea released with timeby UERS mixed with KS

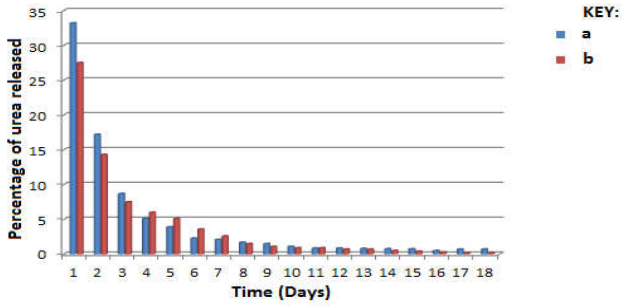

Figure 22: Comparative release of urea by UERS in water (a) and UERS mixed with KS (b)

FTIR and XRD. The mid-IR-Spectrum of UERS (Figure 18) indicates distinct peaks associated with various functional groups vibrations. The peak at 1458.18 cm^{-1} is characteristic of C-N stretching vibration, C=O stretching vibration is associated with the peak at 1685.79cm-1, while the two peaks at 3348.42 and 3444.87 are characteristic of N-H stretching vibrations (Stuart, 2004). X-ray diffraction patterns (figure 19) of UERS indicates urea composition at well-defined peaks of 2θ (22^0, 25^0, 29^0, 33^0, 36^0, 38^0).

Controlled release behavior of UERS

Nearly 74% of net loaded urea fertilizer was discharged in water within 18 days of the experimental duration. Release rate decreased with time as illustrated by figure 20 below, sustainably for the first 9 day and near zero rate for the last 5 days. Higher sorption gradient for the partitioned medium and weaker physicochemical attraction effects could be attributed for the gradual release of the urea molecules. Mixing of UERS with KS gave a percentage urea release of around 60% within the 18 experimental days (figure 21).Higher soil organic content could be attributed to the increased retention of urea in the soil, though the sustained release rate within the first 9 days was still observed. Comparatively, urea release process was better in aqueous medium than in the homogenized samples as illustrated by figure 22 below.

Conclusion

This study has shown that Eburru rock samples compares favourably to the zeolitic material, though purification processes are needed for improved properties. Kinetics of fertilizer adsorption on these samples gave good equilibration rates, with about 33% attained in 24 hours, which also corresponded to the proportion of fertilizer loaded in the samples. This was depended on spiking concentration, contact time and sample composition. From thecontrolled release determinations, it was found that 74% of the net loaded fertilizer was discharged in aqueous medium by the rock samples, having a sustained rate over the first 9 days of the total 18 days of experimental duration. This implies that UERS could potentially extend urea availability duration to plants due to this slowed release aspect. Homogenizing of UERS with typical farming soil such as KS gave 60%urea released over the total experimental duration. An aspect that could further extend duration of urea availability to plants, since the soil organic matter serves to increase urea retention, which could minimize leaching due to its high solubility. Subsequently, these findings indicate that Eburru rock samples could be positively applied in an attempt to develop urea fertilizer carrier agent from local materials for smart delivery systems.

Acknowledgement

The authors thank Kenya Bureau of Standards for availing the urea standard, Kenya Agricultural and Livestock Research Organization for soil analysis and the University of Nairobi, where this analysis was conducted.

REFERENCES

Bansiwal A. K., Rayalu S. S; Labhasetwar N. K., Juwarkar A. A and Devotta S 2006).Surfactant-modified zeolites as slow release fertilizer for phosphorus. J. Agri. Food Chem. 54:4773-4779.

Boynton W. R., Kemp W. M., and Keefe C. W., (1982). A comparative analysis of nutrients and other factors influencing estuarine phytoplankton production.In V. S. Kennedy, editor.Estuarine comparisons.Academic Press, New York, New York, USA. Pages 69-90

Carrolland Dorothy "Ion exchange in clays and other minerals". Geological Society of America Bulletin 70 (6): 749-780 (1959).

Chinnamuthu C.R and Boopathi P.M (2009). Nanotechnology and Agroecosystem. *Madras Agricultural Journal* 96:17-31.

Clain J., Brad D. B., Rick E., Don H., Kathrin O-R**.** 2013. Factors Affecting Nitrogen Fertilizer Volatilization .EB0208 new February http://landresources. montana.edu/soilfertility/ documents/PDF/ pub/ UvolfactEB0208.pdf (Accessed 2nd Nov. 2016 at 5.26pm).

Friedrich W.1828. "UeberkünstlicheBildung des Harnstoffs" (On the artificial formation of urea), Annalen der Physik und Chemie, **88** (2): 253–256

Gislason E.A and Craig N.C. 2005. Cementing the foundations of thermodynamics: comparison of system-based and surroundings-based definitions of work and heat, J. Chem. Thermodynamics 37: 954-966.

Howarth R. W. 1988. Nutrient limitation of net primary production in marine ecosystems. Annual Review of Ecology and Systematics 19: 89-110.

IRPTC data profile, (2016). International Register of Potential Toxic Chemicals http://0-www.worldcat.org. novacat.nova.edu/identities/lccn-n97900852/ (Accessed 2nd Nov. 2016 at 2.31pm).

Jan-Åke P, Mårten W and Stephen O. 2008. Handbook for Kjeldahl Digestion:11- 42.

Koebel M., Elsener M., Kleemann M. 2000. Urea-SCR: a promising technique to reduce NOx emissions from automotive diesel engines, Catalysis Today **59:** 335-345.

Larry G. B. 2016. Managing Urea-Containing Fertilizers. Department of Soil Science, University of Wisconsin. http://www.soils.wisc.edu/extension/materials/ManagingUrea.pdf (Accessed 2nd Nov. 2016 at 4.48pm).

Manikandan A and Subramanian K. S. 2014. Fabrication and characterization of nanoporous zeolite based N fertilizer. African Journal of Agricultural Researc. Vol. 9(2): 276-284.

Martyn V. T. 2006. Progress and future challenges in controlling automotive exhaust gas emissions, Applied Catalysis B: Environmental **70:** 2-15.

Meessen J. H., Petersen H. 2005. "Urea", Ullmann's Encyclopedia of Industrial Chemistry,

Mehlich A. 1953. Determination of P, Ca, Mg, K, Na, and NH4. North Carolina Soil Test Division (Mimeo 1953); 23-89.

Mumpton F. A. 1984.Natural zeolites. In: Pond WG and FA Mumpton (eds.) Zeo-agriculture: Use of natural zeolites in agriculture and aquaculture. Westview Press Boulder, Colorado, pp. 247-254.

Perego G, G. Bellussi, G. Corno, M. Taramasso, F. Buonomo, A. Esposito, in Stud. Surf. Sci. Catalysis 28, Y. Murakanii, A. lijima, J. W. Ward (eds.), Elsevier, Amsterdam, 1986, pp. 129-136

Sakami W., Harrington H. 1963. "Amino acid metabolism".Annual Review of Biochemistry.32 (1): 355–98

Schaber P. M., Colson J., Higgins S., Thielen D., Anspach B., Brauer J., (2004). Thermal decomposition (pyrolysis) of urea in an open reaction vessel, ThermochimicaActa424: 131-142.

Stuart B. 2004. Infrared Spectroscopy: Fundamentals and Applications ©2004 John Wiley & Sons, Ltd. ISBN; 0-470-85427-8, (HB); 0-470-85428-6 (PB)

Tran T. S and Simard R. R. 1993. Mehlich III-Extractable Elements. In: M. R. Carter, Ed. Soil Sampling and Methods of Analysis: 43-49.

Turner R. C and Clark J. S. 1966. Lime potential in acid clay and soil suspensions. Trans. Comm. II & IV Int. Soc. Soil Science, pp. 208-215.

Vanderborght M and Van Grieken E. 1997. "Enrichment of trace metals in water by adsorption on activated carbon," *Analytical Chemistry*, vol. 49, no. 2, pp. 311–316.

Weinheim: Wiley-VCH, doi:10.1002/14356007.a27_333

Yang S.Y and Chang W.L. 2005. Soil Sci., 170, 55.

****